Hydrochemistry and Isotopic Analysis of Deep (Partly Thermal) Wells and Springs in NW-Slovenia

Master thesis by

Sven Philipp, Matr.-Nr.: 1416062

Institute for Applied Geosciences
Darmstadt, February 2015

Hydrochemistry and Isotopic Analysis of Deep (Partly Thermal) Wells and Springs in NW-Slovenia

Master thesis
submitted to the
Department 11
Institute of Applied Geosciences
TU Darmstadt

by Sven Philipp
Matriculation number: 1416062

Supervisors:
Prof. Dr. Kempe
Bojan Otoničar, PhD

First reviewer:
Prof. Dr. Kempe

Second reviewers:
Bojan Otoničar, PhD
Prof. Dr. Schüth

12. Februar 2015

TECHNISCHE
UNIVERSITÄT
DARMSTADT

Zdravljica
by France Prešeren

Žive naj vsi narodi
ki hrepene dočakat' dan,
da koder sonce hodi,
prepir iz sveta bo pregnan,
da rojak
prost bo vsak,
ne vrag, le sosed bo mejak!

Das Trinklied
von France Prešeren
übersetzt von Klaus Detlef Olof

Es leben alle Völker,
die sehnend warten auf den Tag,
dass unter dieser Sonne
die Welt dem alten Streit entsag!
Frei sei dann
jedermann,
nicht Feind, nur Nachbar mehr fortan!

A Toast
by France Prešeren
translated by Janko Lavrin

God's blessing on all nations,
Who long and work for that bright day,
When o'er earth's habitations
No war, no strife shall hold its sway;
Who long to see
That all men free
No more shall foes, but neighbours be.

Eidesstattliche Erklärung

Hiermit erkläre ich, Sven Philipp (Matrikel-Nr. 1416062), dass ich die vorliegende Masterarbeit

"Hydrochemistry and Isotopic Analysis of deep (partly thermal) wells and springs in NW-Slovenia"

ohne Hilfe Dritter und ohne Benutzung anderer als der angegebenen Hilfsmittel angefertigt habe; die aus fremden Quellen direkt oder indirekt übernommenen Gedanken sind als solche kenntlich gemacht. Die Arbeit wurde bisher in gleicher oder ähnlicher Form keiner anderen Prüfungsbehörde vorgelegt und nicht veröffentlicht.

....
Ort, Datum Unterschrift

Erstberichterstatter: Prof. Dr. Stephan Kempe

Zweitberichterstatter: Prof. Dr. Christoph Schüth

Declaration of Authorship

Hereby I certify, Sven Philipp (Matrikel No. 1416062) that the complete work of this master thesis

"Hydrochemistry and Isotopic Analysis of Deep (Partly Thermal) Wells and Springs in NW-Slovenia"

was done by myself and only by using the referenced literature and the described methods. This thesis was not submitted in identical or similar form to another examination authority and it was not published before.

....
Place, Date Signature

First supervisor: Prof. Dr. Stephan Kempe

Second supervisor: Prof. Dr. Christoph Schüth

Zusammenfassung (German)

Die Ziele dieser Masterarbeit sind zum einen abzuschätzen, ob Dedolomitisierung ein derzeit ablaufender Prozess im Untergrund von *Rovte* (W Slowenien) ist und zum anderen die Hydrochemie der Thermalbrunnen und subthermalen Quellen in NW-Slowenien zu charakterisieren.

Um diese Ziele zu erreichen, wurden Wässer aus tiefen Brunnen und Quellen im Gebiet *Rovte* und Wässer aus Thermalbrunnen und subthermalen Quellen im Gebiet *Cerkno/Kranj* analysiert. Die hydrochemischen Analysen wurden mit Spektrophotometrie, Ionenchromatographie und Atomabsorptionsspektrometrie und die Isotopen-Analysen (δ^2H und $\delta^{18}O$) mit dem automatischen Analysegerät Picarro L2130-i vorgenommen.

Die Brunnen Z (Zavčan), R (Rodofov Mlin) und B (Bizjakov Mlin) durchteufen Schichten von Gips in einer Tiefe von mehreren hundert Metern. Daher zeigen die Wasserproben der Brunnen Z und R hohe SO_4^{2-}-Konzentrationen und molare Mg^{2+}/Ca^{2+}-Verhältnisse kleiner als 1. Die Wasserproben von den oberflächennahen Quellen zeigen sehr geringe SO_4^{2-}-, aber im Gegensatz dazu hohe NO_3^-- and Cl^--Konzentrationen. Diese sind eindeutig durch anthropogene Einflüsse beeinflusst. Die Isotope (δ^2H and $\delta^{18}O$) der Brunnen Z und R befinden sich im gleichen Bereich. Dies läßt darauf schließen, dass die Wässer von Z und R dem gleichen Aquifersystem entstammen. Berechnungen der Saturationsindizes mit PHREEQC zeigen, dass die meisten Proben der Brunnen mit Calcit übersättigt und meistens mit Dolomit untersättigt sind. Außerdem zeigt das Diagramm pH vs. SO_4^{2-}-Konzentration eine negative Korrelation. Dies und die präferentielle Abfuhr von Mg^{2+} aufgrund der molaren Mg^{2+}/Ca^{2+}-Verhältnisse kleiner als 1, deutet auf eine derzeit ablaufende Dedolomitisierung hin.

Hydrochemische Analysen der Wässer von den Thermalbrunnen und subthermalen Quellen zeigten, dass eine Tiefenzirkulationsmuster in NW-Slowenien existiert. Vermutlich werden die Bohrlöcher durch das tiefe Aquifersystem (nämlich die grau geschichteten Dolomite in der Oberen Trias, Norian) gespeist.

Abstract (English)

The purposees of this master thesis are on the one hand to assess if dedolomitisation is still an ongoing process in the underground of the *Rovte* area (W Slovenia) and on the other hand to characterise the hydrochemistry of thermal wells and subthermal springs in NW-Slovenia.

To achieve these purposes, waters from deep wells and springs in the *Rovte* area and waters from thermal wells and subthermal springs in the *Cerkno/Kranj* area were analysed. Hydrochemical analysis was done by spectrophotometry, ion chromatography and atom absorption spectrometry. Isotope analysis ($\delta^{2}H$ and $\delta^{18}O$) was done with the automated Picarro L2130-i analyser.

The wells Z (Zavčan), R (Rodofov Mlin) and B (Bizjakov Mlin) penetrate gypsum strata at a depth of several hundred meters. Thus, samples from wells Z and R show high SO_4^{2-} concentrations and molar-Mg^{2+}/Ca^{2+}-ratios lower than 1. In contrast, water samples from surface springs show very low SO_4^{2-} but high NO_3^- and Cl^- concentrations. These samples are clearly impacted anthropogenically. The isotopes ($\delta^{2}H$ and $\delta^{18}O$) of the wells Z and R are in the same range suggesting that the waters from Z and R derive from the same aquifer system. The Calculation of saturation indices with PHREEQC shows that most samples from the wells were supersaturated with respect to calcite and mostly undersaturated with respect to dolomite. Furthermore, the diagram of pH vs. SO_4^{2-} concentration from Z and R show a negative correlation. This and the preferential removal of Mg^{2+}, as suggested by the molar-Mg^{2+}/Ca^{2+}-ratios lower than 1, indicates that dedolomitisation might still be occurring.

The hydrochemical analysis of the waters from thermal wells and subthermal springs revealed that a deep flow pattern exists in NW-Slovenia. The boreholes probably drain the deep aquifer system (namely the *Upper Triassic Norian stage* grey stratified dolomite).

Table of contents

1. Introduction

The presented master thesis deals with the „Hydrochemistry and Isotopic Analysis of Deep (Partly Thermal) Wells and Springs in NW-Slovenia“. During two sampling periods in the years 2013 and 2014, water samples (n = 92) were taken from karstic and non-karstic springs, deep and thermal wells, and surface streams in NW-*Slovenia*, namely in the *Rovte*, *Cerkno* and *Kranj* area. In the field, temperature, pH, electrical conductivity, discharge and alkalinity were measured. The main cations, anions and isotopes (δ^2H and $\delta^{18}O$) of water samples were measured in the lab.

The motivation for this master thesis arose during a visit of the cave *Mravljetovo brezno v Gošarjevih rupah*, which is developed in dedolomite and the visit of the deep well *Rodofov Mlin*, which contains high amounts of H_2S as noticed by an olfactory test.

The main topic of this master thesis is to investigate if dedolomitisation is still an ongoing process in the underground in the *Rovte* area. This topic will be approached by the hydrochemical analysis of deep wells and springs in the *Rovte* area. Additionally, thermal springs and wells were analysed to get a first view on the hydrochemistry of deep waters in the carbonate aquifers of NW-Slovenia.

In the following first chapter the general information about the geography and geology of Slovenia and main sampling areas is given. Furthermore, the theoretical background concerning the hydro- and the isotope geochemistry with detailed information about dolomitisation, dedolomitisation and isotopic fractionation is presented. In the second chapter a description of the used methods in the field and in the laboratory and possible errors are displayed. The third chapter presents the main results for the process of dedolomitisation and the hydrochemistry of waters from thermal wells and springs. Also the relations between the measured thermal springs and wells are illuminated. In the fourth chapter almost all samplings points are compared with data from literature. In the fifth chapter (conclusions), a discussion, whether dedolomitisation is an ongoing process in the underground in the *Rovte* area or not, is presented.

1.1. Geography of Slovenia and areas of interest

Slovenia is located at the *Adriatic sea* southeast of the Alps. Neighboring states are *Austria* in the north, *Hungary* in the east, *Croatia* in the south and *Italy* in the west. The highest mountain ranges (Julian Alps, Karawanks and Kamnik-Savinja Alps) are located in the northwest of *Slovenia* which are part or foothills of the Alps with the highest mountain of *Slovenia* called '*Triglav*' with an altitude of 2 864 m above sea level (a. s. l.).

Two sampling campaigns were done in the year 2013 and 2014 in the ***Rovte***, ***Cerkno*** and ***Kranj*** area (see Appendix 1).

The ***Rovte*** area is located east of Ljubljana and north of Logatec. *Rovte* can be reached from the highway E61, following the country road 408 to the north. The river *Rovatarska Sora* is flowing through the *Rovte* area from southwest to northeast. The *Rovatarska Sora* flows into the *Sovra* river near the settlement *Hleviše*. The highest point in the *Rovte* area is the mountain *Three Kings* (*Vrh Trh*) with the settlement *Vrh Sv. Treh Kraljev* upon it at an altitude of 826 m a. s. l. Lowest altitudes of around 500 m a. s. l. are in the valleys where the rivers flow. In the *Rovte* area the sampling points Z, R, B, BW, P, PG, V, D, F and J are located (compare Fig. 1 and Appendix 1).

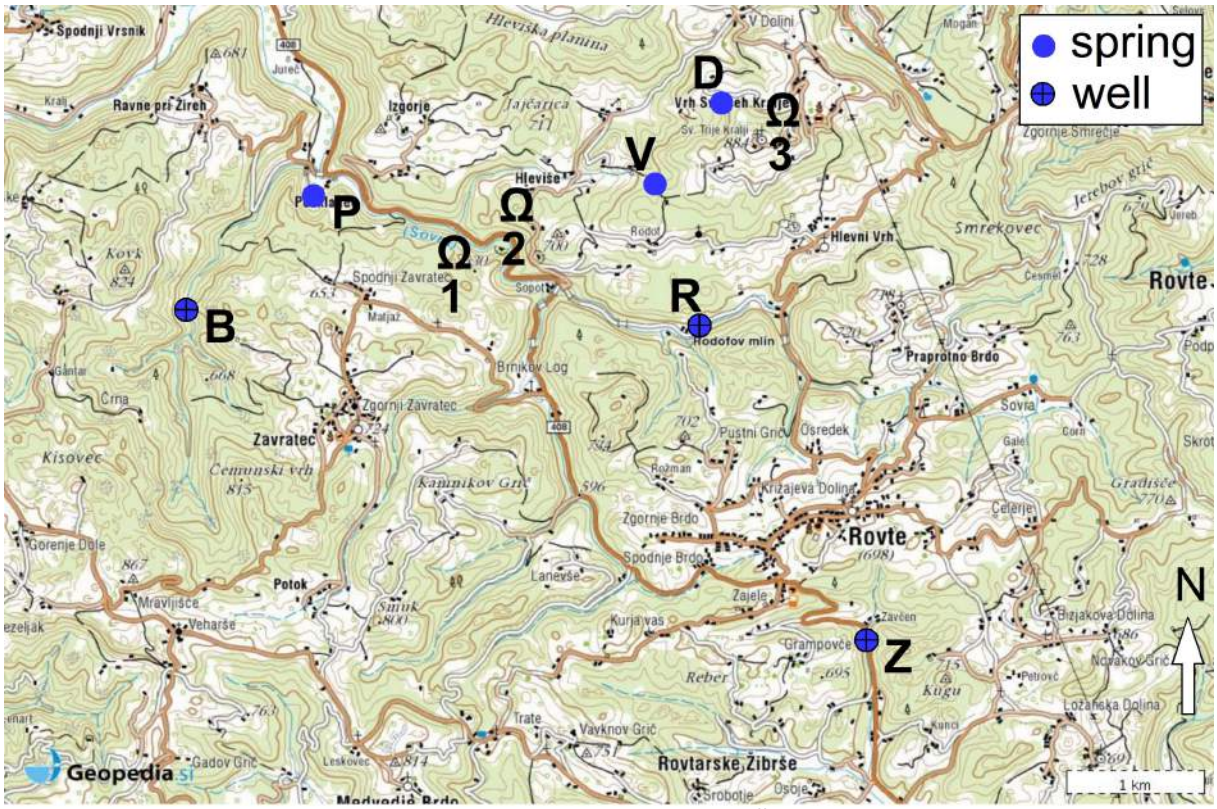

Fig. 1: Overview map of the *Rovte* area with the wells Z: Zavčan , R: Rodofov Mlin and B: Bizjakov Mlin, the springs P: Podklanec, V: Vrh and D: Dolenja and the caves 1: Matjaževe kamre, 2: Mravljetovo brezno v Gošarjevih rupah, 3: Jama pri Sv. Treh kraljih, www.geopedia.si

The ***Cerkno*** area is located north of Idrija in the west of *Slovenia*. *Cerkno* can be reached from the highway E61 at the exit *Logatec*, following the main road 102 to the northwest. One of the main rivers of *Slovenia* flowing from southeast to northwest through the area is *Idrijca*, which is flowing into the *Soča* river at the village *Most Na Soči*. The highest mountains in the area rise up to 1000 m a. s. l. and the valleys have an altitude of around 200 m a. s. l. In the *Cerkno* area the sampling points S, SR, ZE, T and C are located (compare Appendix 1).

The ***Kranj*** area is located in the northern part of Slovenia, northwest of the city *Kranj*. *Kranj* can be reached from the highway E61. The city *Bled* can be reached by the highway E61 and the main road 209 to the west. In the Ljubljana basin the river *Sava* is flowing, drained by the *Sava Bohinjka* from the west. The Ljubljana basin is on the altitude of around 400 m a. s. l. and the highest mountains have an altitude of around 1300 m a. s. l. In the *Kranj* area, the sampling points are oriented along the Ljubljana basin from southeast to northwest: BA, BAA, K, M, L and BH (compare Appendix 1).

1.2. Paleogeography of Slovenia

Paleogeographically, *Slovenia* belongs to the Adriatic continental microplate and is located at the junction between four major Alpine structural units: the Dinarides (S), the Southern Alps (W), the Eastern Alps (N) and the Pannonian Basin (E) (Fig. 2). These geological structures were mainly formed during the *Neogene* (23.8 to 2.6 ma ago).

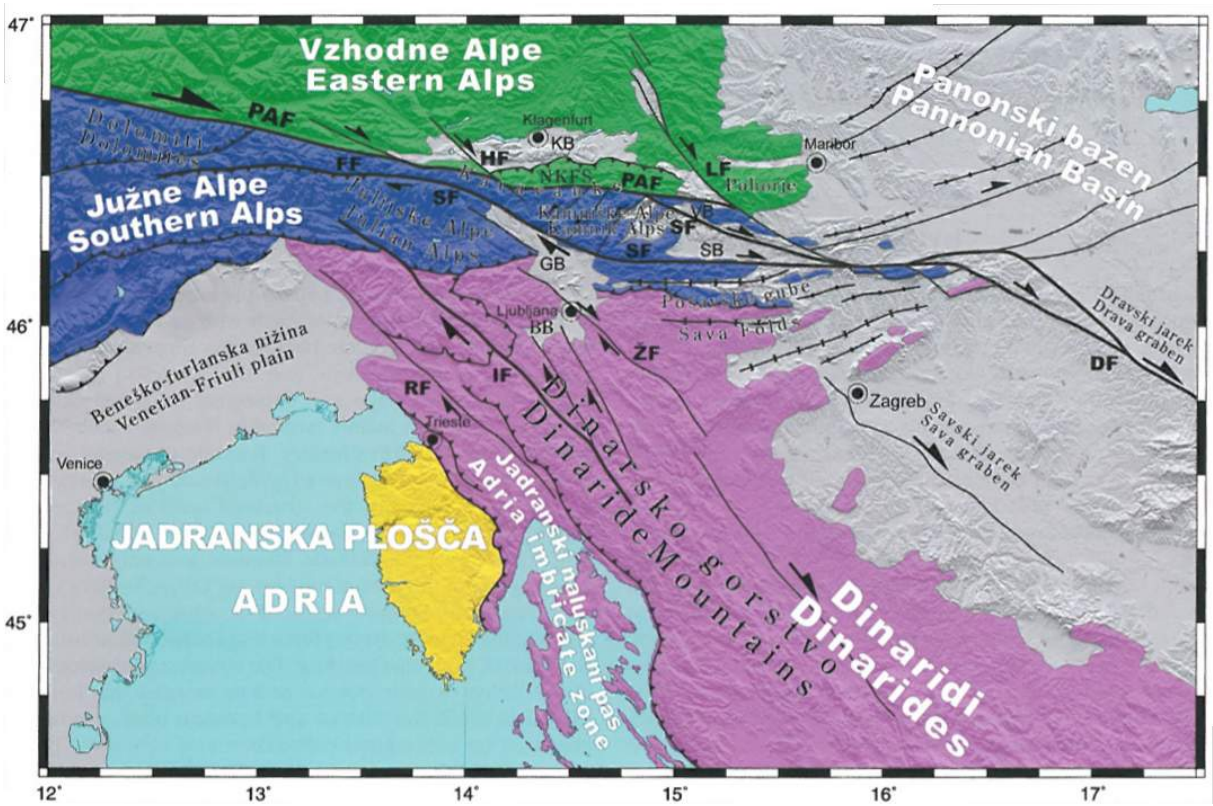

Fig. 2: Simplified tectonic map of the north-eastern corner of the Adria-Europe collision zone with principal geographic features, Explanation: KB – Klagenfurt basin, HF – Hochstuhl fault, PAF – Periadriatic fault, FF – Fella fault, SF – Sava fault, ŠF – Šoštanj fault, VB -Velenej basin, SB- Savinja basin, GB – Gorenjska basin, LF – Lavanttal fault, BB – Barje basin, ŽF – Želimlje fault, IF – Idrija fault, RF – Raša fault, DF – Drava fault (Vrabec et al., 2009).

Pre-Perm, older than 299 ma (Cohen et al., 2014)

In the east of *Slovenia* the oldest known sedimentary rocks are found as pebbles in *Permo-Carboniferous* conglomerates, whereas *Devonian* limestones

occur in the Southern *Karavanke* mountains. In the end of the *Devonian*, a drop in sea level can be attributed to a global eustatic lowstand. This lowstand subaerially exposed the carbonate platform, causing erosion and karstification. The deepening of the depositional environment in the *Early Carboniferous* reflects the onset of the Variscan orogeny. The presence of porphyritic volcanic breccias and tuffs indicates a short-lived volcanic event (Vrabec et al., 2009).

Perm, 299 to 252 ma ago (Cohen et al., 2014)

A mixed carbonate-siliciclastic sedimentation continued on a coastal shelf in the *Early Permian*. Beds of black limestones were being deposited in associated back-reef lagoons. In the *Middle Permian,* the so called Tarvis breccia and Val Gardena beds, comprised of conglomerates, sandstones, siltstones and mudstones were deposited. A reddish coloration of these breccias and Val Gardena beds indicates an arid climate during their sedimentation. In the *late Permian*, the entire proto-Slovenia territory drowned by a shallow sea. This marks the beginning of the Slovenian Carbonate Platform. The *Upper Permian* is characterised by the deposition of evaporites (gypsum) (Vrabec et al., 2009).

The most abundant rocks in *Slovenia* are of Mesozoic age. They belong to the northern margin of the Adria. Slovenia was linked by the Alpine Tethys (Piemont-Liguria ocean) to the north and the west, and by the Vardar ocean to the east (Fig. 3, Vrabec et al., 2009).

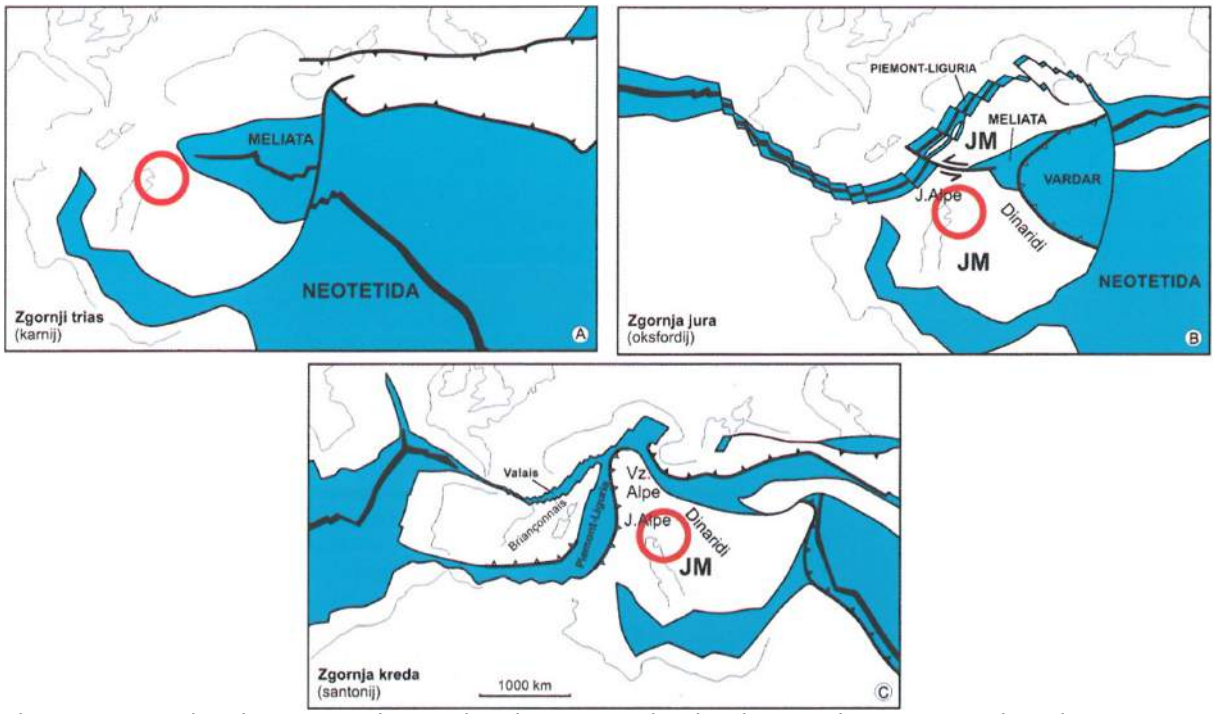

Fig. 3: Mesozoic plate tectonics and paleogeography in the south-European domain, A - Late Triassic (Carnian), B - Late Jurassic (Oxfordian), C - Late Cretaceous (Santonian). Circles marks the approximate position of present-day territory of Slovenia. JM - Adriatic (Apulian) microplate, J. Alpe - Southern Alps, Vz. Alpe - Eastern Alps, Dinaridi - Dinarides, Neotetida – Neothethys (Schmid et al., 2004) and (Vrabec et al., 2009).

Triassic, 252 to 201 ma ago (Cohen et al., 2014)

The Slovenian Carbonate Platform is characterised by a shallow-marine and continuous sedimentation during the *Late Permian* into the *Early Triassic*. The deposition of mixed siliciclastic-carbonate sediments of the *Werfen-Formation* presisted in the *Early Triassic.* The *Werfen-Formation* includes sandstones, micaceous marls with abundant fossils, and various carbonates, including diagnostic red oolithic limestones. In the *Anisian* the input of terrigenous material terminated, and shallow-water limestones were deposited, which were subsequently dolomitised. In the *Middle Triassic* the Carbonate Platform was fragmented into separate tectonic units with a different subsidence history, due to the opening of the Meliata Ocean along the Eurasian margin. In the *Middle Triassic* the famous Idrija mercury deposit was produced by volcanism. In the *Middle Carnian*, a tectonic event generated intraplatform grabens on the Julian Carbonate Platform. Concurrent, bedded limestones were deposited on the

platform and subsequently dolomitised to a large extent. In the *Norian* and *Rhaetian* the Dachstein limestone were deposited on the Julian Carbonate Platform. On the Dinaric Carbonate Platform, shallow water limestones were deposited and later changed into the *Hauptdolomit*-Formation. A major rifting episode began in the *Late Triassic*, initiating the break-up of the supercontinent Pangea and the opening of the Atlantic Ocean (Vrabec et al., 2009).

In Slovenia, three paleogeographic units can be considered: 1) the **Julian Carbonate Platform** in the north (comprising rocks of the present-day Southern Karavanke mountains, the Julian Alps and the Kamnik-Savinja Alps), 2) the **Dinaric Carbonate Platform** in the south and 3) the **Slovenian Basin**, which was a deep-water domain between the two platforms (comprising rocks of the present-day foreland of the Julian Alps and central Slovenia) (Vrabec et al., 2009).

Jurassic, 201 to 145 ma ago (Cohen et al., 2014)

The *Jurassic* produced extensive deep-water basins and submarine plateaus, which existed up to the end of the *Mesozoic*. Two major subsidence phases can be considered: 1) At the *Triassic/Jurassic* transition, related to initial rifting of the Alpine Tethys and Vardar, causing a deepening of the Slovenian Basin and an increase in water level above the Julian and Dinaric Carbonate Platform, 2) thermal subsidence with further deepening of the Slovenian Basin. The thermal subsidence phase did not affect the sedimentation on the Dinaric Carbonate Platform. In the *Late Jurassic* a barrier reef formed along the northern margin of the platform (Vrabec et al., 2009).

Cretaceous, 145 to 66 ma ago (Cohen et al., 2014)

In the *Early Cretaceous* the subduction and closure of the Meliata Ocean led to orogeny in the eastern part of the Alpine orogen. After the extension in the *Late Cretaceous,* a compression followed. The compression is interpreted as an orogenic collapse of the Austroalpine orogen. On the Dinaric Carbonate Platform shallow water sedimentation persisted throughout most of the *Cretaceous*. In the *Late Cretaceous* the Dinaric Carbonate Platform was drowned due to the eustatic sea level rise. In this time, the northeastern margin of the Adria collided with the

continental lithosphere. In the end of the *Cretaceous*, flysch was deposited in the northern margin of the Dinaric Carbonate Platform. The rocks of the Dinaric Carbonate Platform were subaerially exposed and karstified with bauxites and breccias deposited locally (Vrabec et al., 2009).

Tertiary, 66 to 2.6 ma ago (Cohen et al., 2014)

In the Slovenian Dinarides, flysch sedimentation prevailed in the advancing foreland basin during the *Late Cretaceous* and into the *Paleocene.* Carbonate sedimentation ended with the deposition of *Lower- to Mid-Eocene* limestones. flysch sedimentation was terminated by thrusts and flysch basins were deformed and partially overthrusted. The *Tertiary* collision of Adria with Eurasia produced the Alpine orogenic chain. This was the tectonic driving force that shaped the present-day structure of Slovenian territory. At the beginning of the *Oligocene*, the rising mountain chains of the Alps, Dinarides and Carpathians isolated the shallow marine domain of the Paratethys sea. The subduction of Alpine Tethys ended in the *Paleogene*, which resulted in the continental collision of Adria and Eurasia. The *Neogene* shortening in the Adria-Eurasia collision zone produced top-to-the south thrusting of the Alps south of the Periadriatic fault system. Thrusting began in the *Middle Miocene* and mostly ended by the *Pliocene* but appears to be still active in the Julian Alps and their foreland. In the *Neogene*, the underthrusting of Adria under the Dinarides began (Vrabec et al., 2009).

Quarternary, 2.6 ma ago to present (Cohen et al., 2014)

In the *Pleistocene*, the Alpine glaciers from the Julian Alps, Kamnik-Savinja Alps, and Karavanke mountains expanded into the foreland. Partly tectonically controlled depressions were filled with fluvial and lacustrine sediments, which are up to 120 m thick. The compressional tectonic regime continued from the *Pliocene* into the *Quaternary*. The ongoing tectonic deformation is evidenced by significant earthquake activity. A northward push of Adria relative to Eurasia drives the southward thrusting into the Slovenian Alps. Due to reverse and dextral motion, faults north of Istria are oriented WNW-ESE to NW-SE (Fig. 2, Vrabec et al., 2009).

1.3. Geology of NW-Slovenia

Nearly all *Triassic* horizons, *Cretaceous* and *Eocene* beds are found in the Idrija area, whereas *Jurassic* rocks do not occur. The *Permo-Carboniferous* beds are built up of black and dark grey clayey shale with lenses of grey siltstone and quartz sandstone, which represent the oldest rocks in the Idrija area.

The *Permian* beds are built up of grey and red shale, siltstone, quartz sandstone and conglomerate. These rocks form the footwall of the paleontologically well defined *Upper Permian* dolomite and limestone. The *Upper Permian* dolomite abounds with gypsum in the surroundings of *Rovte* (Mlakar, 1969).

The *Upper Permian* beds are overlain by *Lower Scythian* dolomite with stylolites on bedding planes. In the middle of the lower portion of *Lower Scythian* beds, a rhytmic variations of grey granular and sandy micaceous dolomite occur. This dolomite is overlain by greyish green and reddish calcareous micaceous shale and sandstone, including lenses of oolithic limestone. In the lower part of *Upper Scythian* beds grey granular dolomite and rarely bedded dolomite occur. In the upper part alternating grey marly shale and limestone occur. *Anisian* dolomite extends over a relatively small part of the area, removed partly or entirely by *Middle Triassic* erosion. This dolomite is grey and brittle. The basal sediment of *Langobardian* strata is composed of quartz sandstone, in some places of bauxite or black clayey shale and sandstone. The older beds are directly overlain by *Langobardian* conglomerate, which is composed of gravel originated from *Anisian*, *Scythian* and even *Upper Permian* rocks. The conglomerate is overlain by reddish calcareous sandstone and shale. The youngest *Langobardian* stratigraphic unit is built up of tuff and tuffite with chert. The *Cordevol* beds are composed of white granular dolomite, light grey reef limestone and platy limestone with chert. *Cordevol* and *Carnian* limestones join without interbedded dolomite in *Rovte*. Only the lower part of *Norian* dolomite occurs in the Idrija area. This dolomite is light grey, crushable and usually bedded (Mlakar, 1969).

The *Lower Cretaceous* is represented by dark grey bedded bituminous limestone with thin layers of grey granulated dolomite. The geosynclinal sedimentation terminates with *Eocene* beds, which overlie unconformably the

Upper Cretaceous beds and consist of greyish-green flysch marl, more rarely sandstone. *Quarternary* sediments are found along the Idrijca and some larger creeks (Mlakar, 1969).

1.3.1. Structural units of NW-Slovenia

Mlakar (1969) proposed five structural units that are considered as nappes (Appendix 2) in following order: (1) Autochthonous Basement, (2) Koševnik Nappe, (3) Čekovnik Nappe, (4) Idrija Nappe and (5) Žiri-Trnovo Nappe. Placer et al. (2000) tapped thermal water by hydrogeologic-exploration and exploitation of the 2000 m deep borehole Ce-2/95 (C) in *Cerkno*. This borehole confirms the model of the nappe structures of the NW margin of the External Dinarides (Fig. 5 and Appendix 2, Placer et al., 2000). Detailed information about the borehole can be found in the chapter 1.3.4. Geology at the (thermal) springs and wells .

1) The Autochtonous Basement is composed of *Upper Cretaceous* and *Eocene* rocks. In the southwest, south and southeast of Idrija the autochthonous basement is built up of different tectonic units (Appendix 2). The Trst-Komen, Hrušica and Logatec plain are parts of a large *Mesozoic* plateau. This plateau is syncline-shaped in the Vipava region and cut by the Predjama and Idrija faults. The main characteristics of this plateau are the *Mesozoic* age of the rocks, their great thickness, simple tectonic structure and in the north the onlap of *Eocene* beds over the *Upper Cretaceous* limestone (Mlakar, 1969).

2) The Koševnik Nappe lies over the *Eocene* flysch and consists in the northeast of *Lower Cretaceous* limestone and in the southwest of *Upper Cretaceous* limestone. The *Cretaceous* strata dip slightly towards southwest and are in a normal stratigraphic position, which is characteristic for the autochthonous basement. Because of that, the *Cretaceous* strata are considered to be a part of the autochthonous basement, broken off and displaced towards southwest. Due to the position and origin, it can be treated as a para-autochthonous nappe (Mlakar, 1969).

3) The Čekovnik Nappe consists of *Norian* dolomite and *Carnian* beds. The *Carnian* beds pass gradually into the *Norian* dolomite only once. In other places the contact between these rocks is a thrustplane (Mlakar, 1969).

4) The Idrija Nappe is composed by rocks ranging from the *Younger Paleozoic* to the *Norian* stage of *Triassic*. Because a part of the beds is repetitous, the third nappe is treated as consisting of two parts. The first part is considerably thinner than the second and its area is smaller as well. *Paleozoic* and *Lower Triassic* strata are in inverted stratigraphic position. The second part is found in a zone of 26 km in length between *Zgornja Kanomlja* and *Rovte*. The strata lies northwest of *Idrija* in an inverted position. In the East of *Idrija* the stratigraphic sequence is normal. The second part of the Idrija nappe appears on the surface only southeast of Urbanovec, extending towards *Rovte*. The Urbanovec-Zovčan fault strikes E-W and joins the Idrija fault near Sedej. This fault divides the Idrija nappe into two blocks. The northern one is built up of *Paleozoic* rocks only, whereas in the south *Triassic* rocks are found. In some places also *Upper Permian* rocks are preserved. The beds of the Idrija nappe are part of an overturned syncline, opened to the southwest (Mlakar, 1969).

5) The Žiri-Trnovo Nappe consists in the Idrija *Younger Paleozoic* to *Upper Triassic* strata. The beds are nearly everywhere in normal stratigraphic position. In a zone of about 7 km length between Urbanovec and Kurja vas the *Langobardian* conglomerate joins along a thrust plane the *Upper Paleozoic* clayey shale and in some places Gröden sandstone of the second part of the Idrija nappe. In the full length of the northern border of this zone the conglomerate lies on *Anisian* dolomite. The older stratigraphic units are northwards below the dolomite, dipping slightly in southern direction. South of *Bizjak* the Lom-Zavratec fault splits into two, the northern part called Logar fault. Both faults are probably of *Middle Triassic* age. The normal stratigraphic sequence, a great thickness and a large dimension of the bottom oblique sectional plane is characteristic for the Žiri-Trnovo nappe (Mlakar, 1969).

1.3.2. Geology at *Rovte* area

The whole region around *Rovte* is part of the Žiri-Trnovo nappe. It is placed on the transition from the Dinaric karst of inner Slovenia towards Prealps between the Hotenjsko Podolje karst plain on the west, the Logaško Polje on the south and the tectonic basin of Ljubljansko Barje (Ljubljana Moor) and Blegoš-Vrhnika range on the east (compare Appendix 2) (Otoničar & Mihevc, 2013).

The mountain *Vrh Trh* is topographically exposed and surrounded by four valleys. These valleys probably developed mainly along fault lines and at lithological boundaries. The mountain represents a relatively stable block where strata is disrupted by local strike-slip faults (Otoničar & Mihevc, 2013).

Otoničar & Mihevc (2013) described that a variety of non-carbonate and carbonate rocks of *Middle Permian* to *Upper Triassic* age intercalating through few hundred meters thick sequences occur (Fig. 4). An evaporate horizon up to 270 m thick has been found in core samples in the *Rovte* area. Čadež (1977) described that primarily anhydrite predominated over gypsum and later anhydrite partly altered to gypsum by hydration. The geological sketch of Vrh Trh (Fig. 5) shows a synclinal structure.

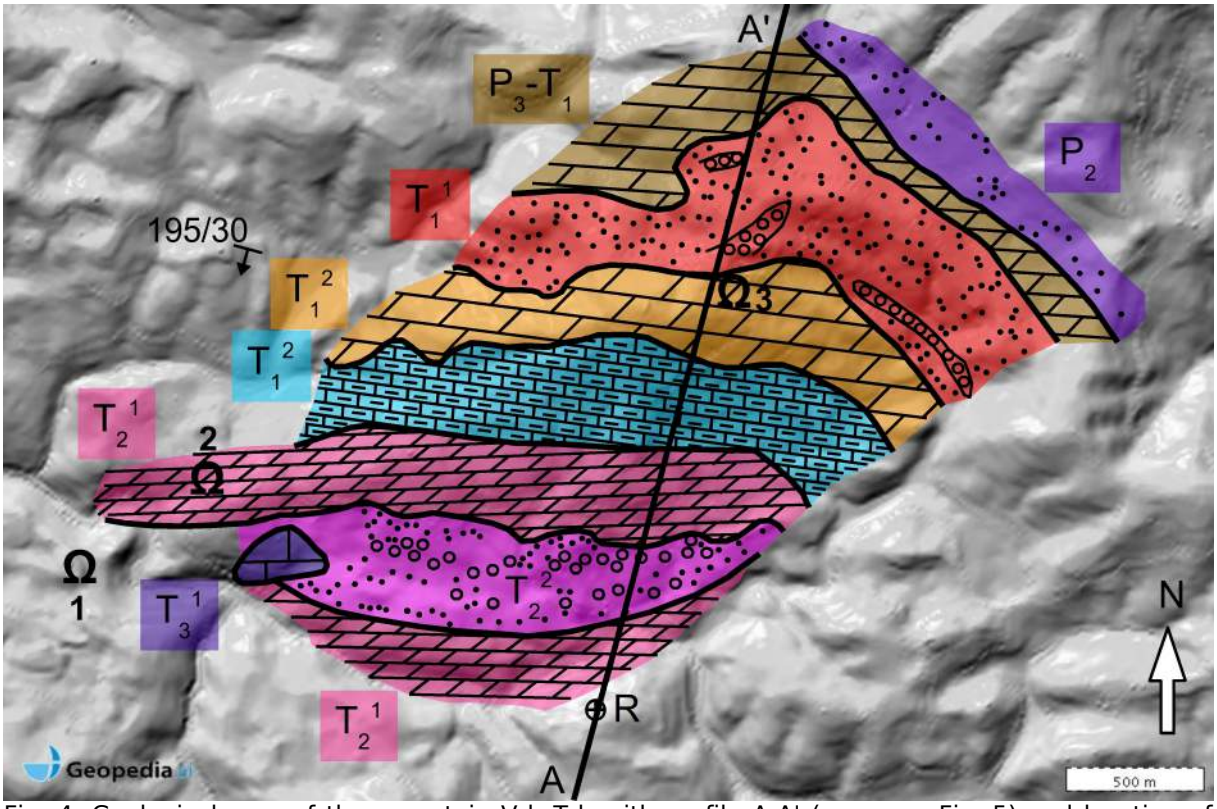

Fig. 4: Geological map of the mountain Vrh Trh with profile A-A' (compare Fig. 5) and location of caves, mean dip direction is 195/30, R: well Rodofov Mlin, 1: Matjaževe kamre, 2: Mravljetovo brezno v Gošarjevih rupah (in T_2^1), 3: Jama pri Sv. Treh kraljih (T_1^2), P_2: *Upper Permian* black and grey stratified dolomite, P_3-T_1: *Upper Permian* to *Lower Triassic*, T_1^1: *Lower Triassic* micaceous dolomite and granular dolomite, T_1^2: *Lower Triassic Upper Scythian Campil* grey granular dolomite and dark grey marly limestone, T_2^1: *Middle Triassic Anisian* light grey dolomite, T_3^1: *Upper Triassic* coarse-grained massive dolomite, personel communication with Otoničar, www.geopedia.si

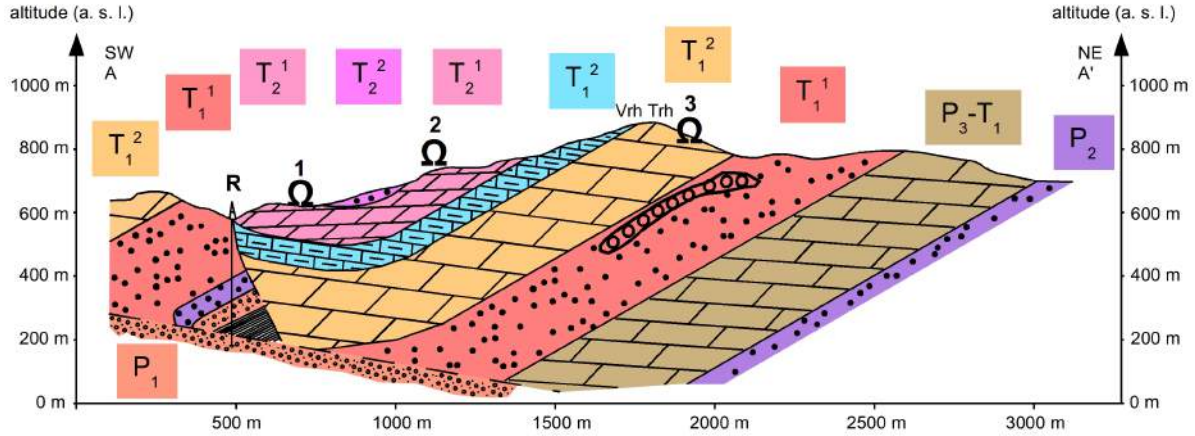

Fig. 5: Geological profile from A to A' considering a synclinal structure SW of Vrh Trh with different interpretation of the borehole profile of R (compare with Fig. 8), numbers show extrapolated position of caves, 1: Matjaževe kamre, 2: Mravljetovo brezno v Gošarjevih rupah (in T_2^1), 3: Jama pri Sv. Treh kraljih (T_1^2), P_1: *Lower Permian Gröden strata* grey and red quartz sandstone and conglomerate, P_2: *Upper Permian* black and grey stratified dolomite, P_3-T_1: *Upper Permian* to *Lower Triassic*, T_1^1: *Lower Triassic* micaceous dolomite and granular dolomite, T_1^2: *Lower Triassic Upper Scythian Campil* grey granular dolomite and dark grey marly limestone, T_2^1: *Middle Triassic Anisian* light grey dolomite (compare Fig. 4), personel communication with Otoničar.

The wells (Z: Zavčan, R: Rodofov Mlin and B: Bizjakov Mlin) in the *Rovte* area were drilled for the exploration of mercury from the mercury mine in Idrija in the 1960s and 70s. However, no exploitation of mercury was done, probably because mercury was not found or only in low concentrations.

Well Z (Zavčan)

Assuming that the well Z is more than 400 m deep and due to the constant outflow of around 213 l/min artesian in nature. All other wells near Z reach the nappe boundary and the underlying *Upper Triassic Norian stage* grey stratified dolomite (Fig. 5, Fig. 6, Fig. 8 and Fig. 9). Čadež (1977) mentioned, that gypsum appears to be more common in the *Upper Permian* and *Lower Scythian* dolomites compared to the *Middle Permian* sandstone, *Scythian* shale, and *Cordevolian* dolomite. From the profiles of Mlakar (1969) the following stratigraphic and lithological column in the underground at well Z can be expected (Table 1 and Fig. 6):

Depth [m]	Stratigraphy	Lithology
0 – 41	*Triassic - Langobardo strata*	grey dolomite and conglomerate
41 – 211	*Triassic - Anisian*	light grey dolomite
211 – 281	*Triassic – Scythian - Campil*	dark grey marly limestone
at 281	nappe boundary prolonged from the NE	
< 281	*Upper Triassic - Norian*	grey stratified dolomite

Table 1: Borehole profile from well Z (Zavčan), compare Fig. 6 (Mlakar, 1969).

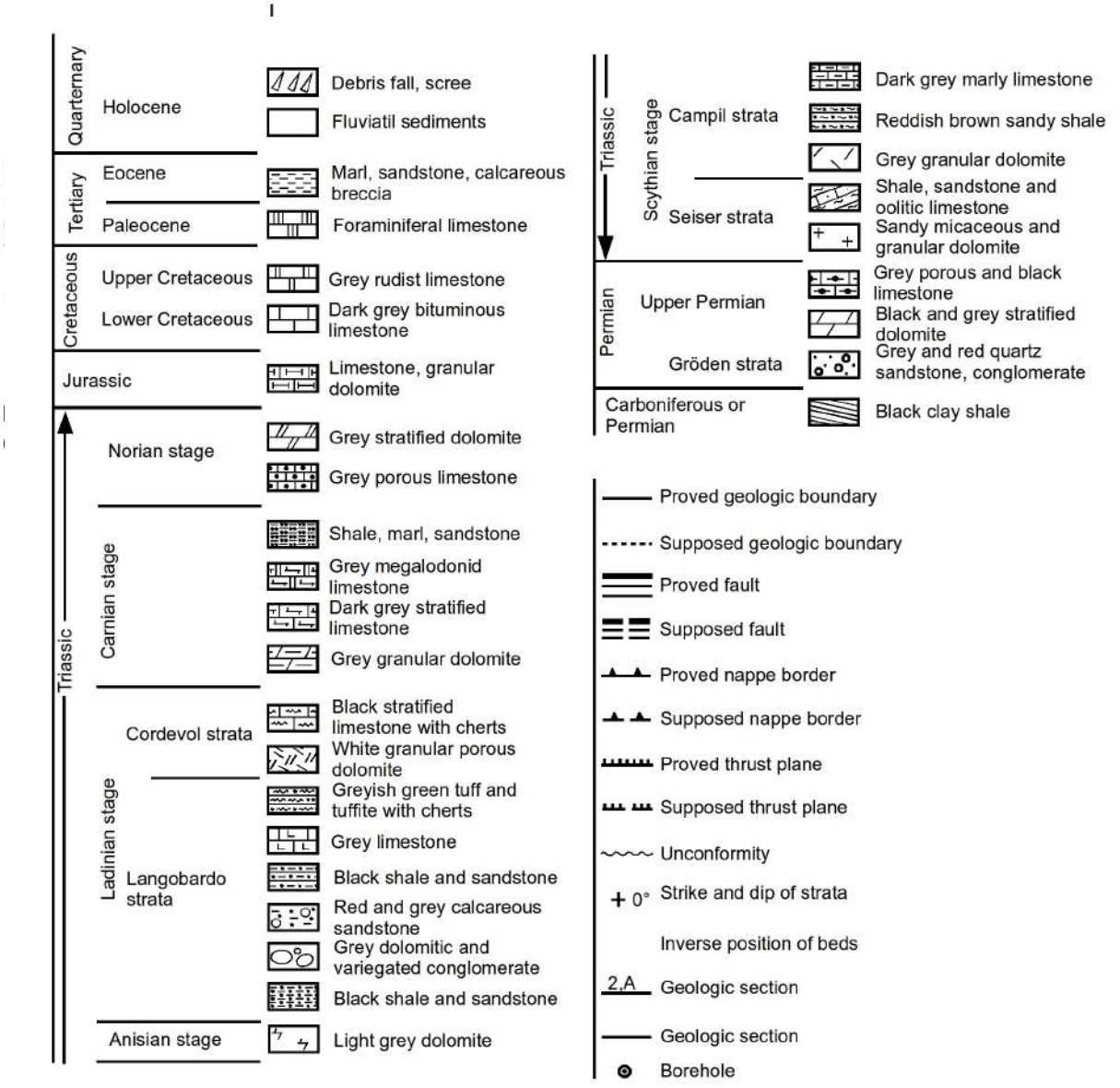

Fig. 7: Legend for the profiles Fig. 6, Fig. 8 and Fig. 9, revised Mlakar (1969)

Well R (Rodofov Mlin)

From the profiles of Mlakar (1969) one can assume that the well R is approximately 500 m deep. Mihevc (2005) mentions that the well R penetrates through the *Triassic* into *Permian* rocks through dolomite, limestone, shales and gypsum. From the profiles of Mlakar (1969) (Fig. 8) the following stratigraphic and lithological column in the underground at well R can be expected (Table 2):

Depth [m]	**Stratigraphy**	**Lithology**
0 – 61	*Triassic – Scythian - Seiser strata*	shale, sandstone and oolitic limestone
61 – 232	*Triassic - Scythian - Seiser*	sandy micaceous and granular dolomite
232 – 281	*Upper Permian*	black and grey stratified dolomite
at 281	proved fault, which dips with ≈ 65° in NE direction	
281 – 305	*Triassic – Scythian - Seiser*	sandy micaceous and granular dolomite
305 – 330	*Upper Permian*	black and grey stratified dolomite
330 – 415	*Permian Gröden strata*	grey and red quartz sandstone and conglomerate
415 – 451	*Carboniferous or Permian*	black clay shale
at 451	supposed fault, which dips with ≈ 10° in NE direction	
451 – 500	*Permian Gröden strata*	grey and red quartz sandstone and conglomerate
> 500	*Carboniferous or Permian*	black clay shale
> 500	nappe boundary with underlying *Upper Triassic - Norian*	grey stratified dolomite

Table 2: Borehole profile from well R (Rodofov Mlin), compare Fig. 8 (Mlakar, 1969).

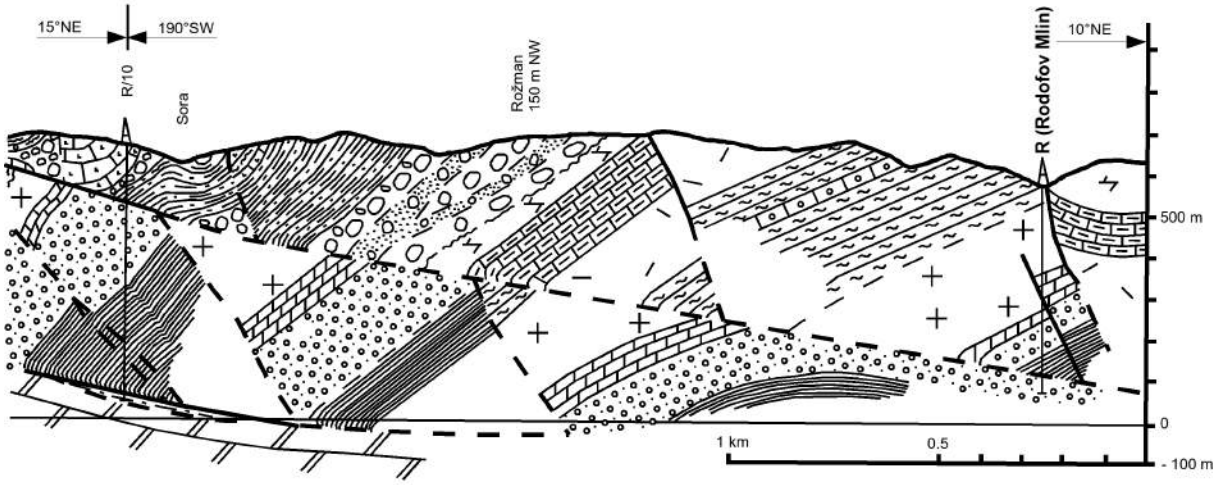

Fig. 8: Geological profile, SW of the well R (Rodofov Mlin), explanation see Fig. 7, revised Mlakar (1969).

Well B (Bizjakov Mlin)

From the profiles of Mlakar (1969) (Fig. 9) one can expect, that well B is approximately 645 m deep. Well B is not fully excavated, but constant outflow was visible and one can be expect that the well is confined (compare Appendix 10). From the profile of Mlakar (1969) the following stratigraphic and lithological column in the underground at well B can be expected:

Depth [m]	Stratigraphy	Lithology
0 – 70	*Triassic - Scythian - Campil*	dark grey marly limestone
70 – 145	*Triassic - Scythian - Campil*	grey granular dolomite
145 – 395	*Triassic - Scythian - Seiser*	shale, sandstone and oolithic limestone
395 – 645	*Triassic - Scythian - Seiser*	sandy micaceous and granular dolomite
at 645	supposed nappe boundary	
645 – 670	*Carboniferous or Permian*	black clay shale
> 670	*Upper Triassic - Norian*	grey stratified dolomite

Table 3: Borehole profile from well B (Bizjakov Mlin), compare Fig. 9 (Mlakar, 1969).

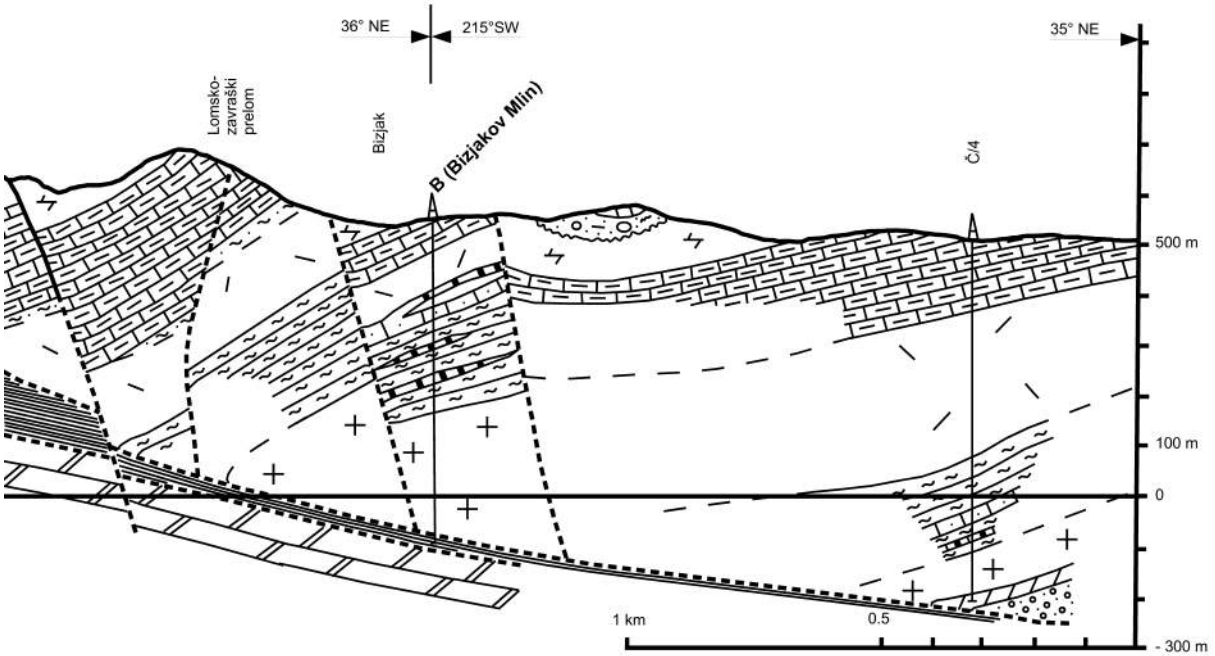

Fig. 9: Geological profile, SW and NE of the well B (Bizjakov Mlin), explanation see Fig. 7, revised Mlakar (1969).

From a hydrogeological point of view the main discharge of the wells Z, R and B comes from the *Upper Triassic Norian stage* grey stratified dolomite, outcropping NE and SW (compare Fig. 6, Fig. 8 and Fig. 9). Furthermore, the prolonged nappe boundary supports the deep flow pattern into the underground in NE and SW direction. This water is mixed with surface run-off, e. g. recharging at the Mt Vrh Trh. Mihevc (2005) suggests that the water from R is coming from a fractured karst aquifer, which supports the deep flow pattern. In the case of B and R the *Carboniferous or Permian* black clay shale, outcropping in the NE, acts as an aquiclude. Due to the low permeability of this aquiclude, the water is kept underneath and flows naturally (fault, boundary) or through the boreholes to the surface.

1.3.3. Three caves in the Rovte area

In the *Rovte* area near the mountain Vrh Trh (Three Kings) three caves occur: 1) Matjaževe Kamre, 2) Mravljetovo brezno v Gošarjevih rupah, 3) Jama pri Sv. Treh kraljih (Fig. 1 and Fig. 4). The caves developed in *Lower and Middle Triassic*

dolostone, intercalated between siliciclastic rocks. Otoničar & Mihevc (2013) show that all three caves exhibit clear ramiform and/or maze-like morphology indicating their possible hypogenic origin (Malabeh & Kempe, 2012). The orientation of the channels is similar to the direction of the faults and joints as Otoničar & Mihevc (2013) suggests.

The cave Jama pri Sv. Treh kraljih (see Appendix 3) had no known natural entrance and was discovered during an excavation of an artificial tunnel (Mihevc, 2005). The cave is 962 m long and 77 m deep (Mihevc, 1991). The tunnel and the cave are located just below the top of the mountain Vrh (884 m) at an elevation of 812 m. The first part of the tunnel reveals first *Triassic* dolomite and deeper inside *Lower Triassic* shales (Mihevc, 2005). Mihevc (2005) illustrate that the cave is a maze of passages developed in phreatic conditions along steep faults and fractures. The passages are slightly affected by vadose seepage waters. The cave is very similar to the cave Matjaževe Kamre and especially to Mravljetovo brezno v Gošarjevih rupah (Mihevc, 2005). In the cave Jama pri Sv. Treh kraljih, a „semi-natural model“ for hypogenic speleogenesis can be observed (Fig. 10). Here, sulfuric acid (H_2SO_4) is produced by the weathering of primary pyrite (FeS_2) rich shale. The pyrite oxidise due to percolating waters. The sulfuric acid dissolves the underlying marly dolostone or dolomitised limestone of the artificial tunnel. In this process goethite-ferrihydrite (rust) and gypsum is precipitated (Otoničar & Mihevc, 2013). The dissolution of pyrite can be one reason for the process of dedolomitisation. Obviously, this process is a recent phenomena in the cave Jama pri Sv. Treh kraljih (Fig. 10).

Fig. 10: Rusty rock: "semi-natural model" for hypogenic speleogenesis, (width: approx. 1.5 m), Photo: Otoničar.

The cave Mravljetovo brezno v Gošarjevih rupah (see Appendix 4) is 726 m long and 73 m deep. The altitude of the main entrance is 613 m a. s. l. and the cave is located at the eastern flank of the Sora valley 100 m above the river on the lower part of the mouuntain Vrh Trh (Otoničar et al., 2013). Čadež (1977) proposed that underground waters rich in hydrogen sulfide caused the decomposition of sulfates into elementar sulfur and calcite that occur associated with gypsum. The cave Mravljetovo brezno v Gošarjevih rupah developed in bedded fine to middle grained *Middle Triassic Anisian* dolostone. The channels exhibit ramiform and maze like orientation, which are oriented along faults and joints. The wall rock morphology shows features for dissolution with slowly flowing rising water (i. e. feeders, rising channels, cupolas, lack of scallops etc.). In turn, other features are characteristic for descending percolation waters (i. e. shafts, down cutting vadose meanders, fluvial sediments of sandy and gravel size particles etc.). Yellowish to reddish brown rocks can be found in the cave. These rocks seem to be an eroded, infilling deposit at first sight (Fig. 11), but turn out to be dedolomite. A gradual transition from this type of rock to the host rock (Fig. 12) can be observed. Furthermore, preserved echinoderm bioclasts can be found

both in the yellowish to reddish brown rock and in the host rock, which suggests similar origin (Otoničar et al., 2013).

Fig. 11: Transition from dolostone (dark grey) over partly dedolomitised dolostone (pale grey) to dedolomite (yellowish brown), revised Otoničar et al. (2013), Photo: Otoničar.

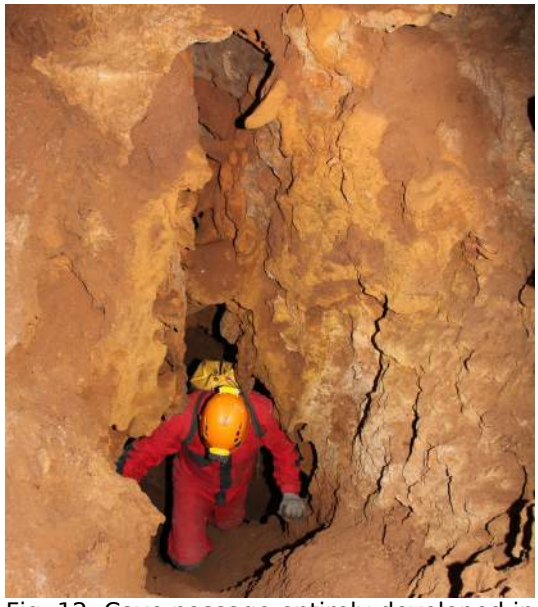

Fig. 12: Cave passage entirely developed in yellowish brown dedolomite, note the remnants of secondary brownish infilling clayey deposit, revised Otoničar et al. (2013), Photo: Otoničar.

Otoničar et al. (2013) described thin sections, which reveal the gradual transition between the host dolostone and dedolomite. At the transition dolomite crystals occur within calcite (Fig. 13). Otoničar et al. (2013) can distinguish several major textural groups of dedolomite crystals, coarse-grained xenotopic to locally hypidiotopic mosaic calcite, pseudospherulitic fibrous calcite, cone-like fibrous calcite, fibrous palisade calcite and brownish micritic calcite with or without meshy distributed needel fibre crystals or etched patches or individual crystals of coarser grained calcite mosaic (Fig. 14). In some places the needle-fibre crystals coalesce in xenotopic mosaic of fine-grained crystals and coarser-grained dedolomite crystals commonly include abundant inclusions or remnants of the host rock (Otoničar et al., 2013).

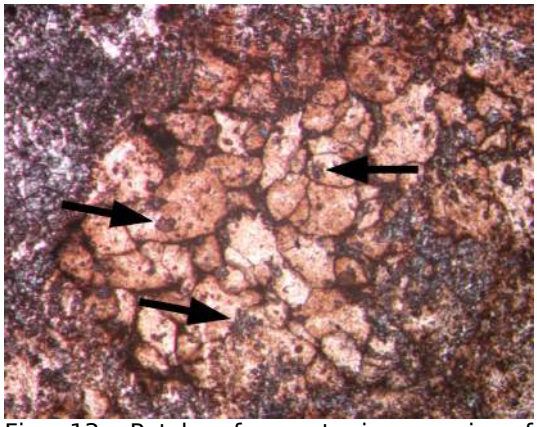

Fig. 13: Patch of xenotopic mosaic of calcite crystals locally showing pseudospherulitic texture (stained with alizarin red), note dolomite inclusions (grey, marked with black arrows), width: 2.2 mm, revised Otoničar et al. (2013), Photo: Otoničar.

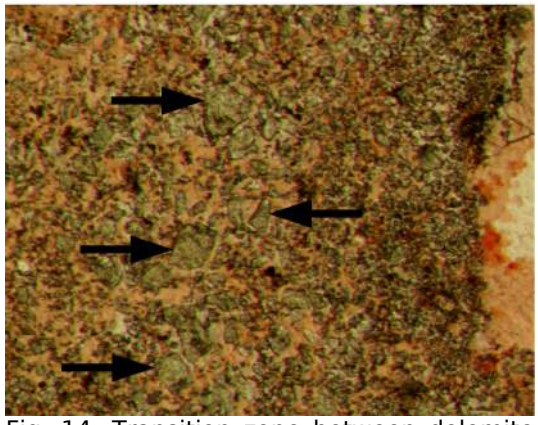

Fig. 14: Transition zone between dolomite (grey) and dedolomite (redish stained), note etched crystals of dolomite (marked with black arrows), width: 2 mm, revised Otoničar et al. (2013), Photo: Otoničar.

XRD analyses from Otoničar et al. (2012) and Otoničar et al. (2013) revealed that the unaltered greyish rock in the cave Mravljetovo brezno v Gošarjevih rupah is built mainly of dolomite. The yellowish brown altered rock is built of calcite with traces of dolomite in some samples. Otoničar et al. (2012) described pale dolostones with gradually higher content of calcite between the two end members dolomite and the altered rock. The yellowish to reddish brown colour of contains traces of Fe-hydroxides (i.e. goethite and ferrihydrite) (Otoničar et al., 2012). Furthermore, small amounts of kaolinite, illite, sericite and quartz have been detected in the walls (Otoničar et al., 2012). Otoničar et al. (2012) describes white, up to a few mm thick, crust at the cave wall. The crust is built of hydromagnesite. Other parts of the cave wall are covered with earthy light rusty-coloured silty material, which is built of gypsum with traces of goethite and ferrihydrite and sandy particles of calcite (Otoničar et al., 2012).

Otoničar et al. (2013) analysed thirteen samples of dolomite, yellowish brown calcite and transitional pale dolostone with gradually higher content of calcite for oxygen and carbon isotope composition (Table 4). Data from Otoničar et al. (2013) (Table 4) displays significant differences between dolostone host rock and yellowish brown calcite. Otoničar et al. (2013) proposed that the isotopic values of the yellowish brown calcite are characteristic for meteoric diagenesis and that

the $\delta^{13}C$ and $\delta^{18}O$ of the transition zone are in between the dolostone and yellowish brown calcite $\delta^{13}C$ and $\delta^{18}O$.

	$\delta^{13}C$ [‰]	**mean [‰]**	**std [‰]**	**$\delta^{18}O$ [‰]**	**mean [‰]**	**std [‰]**
A	-2.8 to -0.55	1.6	1.5	-0.51 to -2.84	-1.45	0.99
C	-2.7 to 5.45	-3.72	1.26	-3.92 to -5.23	-4.41	0.63
B	-6.5 to -8.42	-7.64	0.9	-5.12 to -6.27	-5.76	0.45

Table 4: Oxygen and Carbon isotope composition of A: dolostone (n = 4), B: yellowish brown calcite (n = 5), C: transition between dolomite and yellowish brown calcite (n = 4), data from Otoničar et al. (2013).

The third cave Matjaževe Kamre (see Appendix 5) is more than 300 m long and has its entrances near the Sora river (Mihevc, 2005). The cave is formed in *Middle Triassic* dolomite and dolomitic limestone (Mihevc, 1989). The entrance of the cave is 10 m above the river and the lowest part reaches the level of the river. The cave is developed in deep phreatic conditions along some faults and fractures. (Mihevc, 2005) distinguished an upper and a lower part of the cave. The upper part has wider passages and features for phreatic origin along faults. In some parts of the cave, gelifraction changed the walls and sediment on the floor. In the inner, lower part, phreatic features on the walls are still preserved. Some karstic springs occur in this part and on the lower side of the meander below the cave. (Mihevc, 2005) describes two types of karstic spring waters in the cave Matjaževe Kamre: 1) the deep karst waters, with stable temperature around 8°C and 2) the water with high variation of the temperature throughout the year.

1.3.4. Geology at the (thermal) springs and wells

Bled Hotel (BH)

BH is located northeast of the spring M and directly to the famous lake Bled (compare Appendix 1). The Bled Hotel Toplice utilise a 587.6 m deep geothermal well. The energy, extracted from the geothermal well, is used for the spa and heating and cooling of the Hotel. Before 1958 temperatures and discharge rates

of the thermal springs around the Bled Hotel Toplice were measured. In the year 1958 four shallow boreholes were drilled with pumping tests and thermologging. In the years 1967 and 1968 eight additional shallow boreholes and one deep well were drilled. The deep well struck inflows of thermal water in the depth between 546 and 568 m with a yield of 420 l/min and a water-temperature of 19°C (Nosan, 1973).

The surrounding rocks of Bled are of *Permian*, *Triassic*, *Tertiary* and *Quaternary* age (Nosan, 1973). Furthermore, the deep well revealed the following lithological column:

Depth	**Lithology**
0 to 60 m	*Quaternary* lacustrine and glacial sediments
60 to 106 m	*Oligocene* marine clay
106 to 546 m	grey dolomite
546 to 577.6 m	dark grey limestone (main aquifer)
577.6 to 587.6 m	dark grey dolomite

Table 5: Lithological column of BH, Nosan (1973).

Tectonically, there are many faults of NW-SE direction in the surroundings of Bled (compare Appendix 18). The well probably penetrated a fault with intensively fissured and broken dolomite and limestone. Along this fault thermal water find its way to the surface (Nosan, 1973) (Table 5).

Two aquifers discharge thermal water to the surroundings of the Hotel Toplice in Bled (Nosan, 1973). The shallow one is represented by the *Quaternary* lacustrine sediments with small quantities of thermal water in the gravel. Thermal water flows from the *Triassic* dolomite into this shallow aquifer. Thermal water flows probably along its contact with the *Oligocene* marine clay (Nosan, 1973).

Zmazek et al. (2002) proposed that hydrometerological parameters such as rainfall, air temperature, barometric pressure and room temperature did not affect the electrical conductivity and water temperature of BH. Zmazek et al.

(2002) proposed that electrical conductivity and water temperature at BH are promising for earthquake predictions, if they are measured frequently.

Cerkno (C or Ce-2/95) and T (Kopačnica)

The possibility of thermal water exploitation was investigated at *Cerkno* (compare Appendix 16) in the years 1994 to 1996. Three boreholes were drilled: one exploration borehole (Ce-1/94) of 134 m depth for temperature gradient determination, a hydrogeologic-exploration and exploitation borehole (Ce-2/95) of 2004 m depth that has tapped thermal water and the third exploitation borehole (Ce-3/96) that was unsuccessful due to technical reasons (Placer et al., 2000). The location of the borehole Ce-2/95 is in a narrow forealpine valley surrounded by the mountainous recharge region. Thus, the borehole is artesian. Placer et al. (2000) described the lithological column of the borehole Ce-2/95 as follows (Table 6, Table 7 and compare with Fig. 15):

Depth	Lithology
0 to 5 m	rampart
5 to 95 m	grayish to grayish-black slate with transitions to slaty siltstone of silky greasy luster (clastic rocks of *Carboniferous-Permian* age)
95 to 545 m	carbonates, clastic rocks, rhyolitic tuff and rhyolite (*Ladinian* rocks of the *Pseudozilian Formation*)
545 to 835 m	light gray partly nearly white dolomite with sparse remnants of stromatolites and loferites (*Norian & Rhaetian*, *Hauptdolomit*-Formation)
835 to 2004 m	medium gray limestone with sections of dolomitised limestone (*Jurassic, Malmian* age)

Table 6: Lithological column of the borehole Ce-2/95, Placer et al. (2000).

Date	Depth section	Outflow (l/s)	T (°C) at wellhead	Method
10.05.1995	0 – 544	1.5	21	point to point
02.06.1995	400 – 809	10	22	logging
12.06.1995	850 – 1100	50	27.5	point to point
22.06.1995	0 – 1200 (every 50 m); 1200 – 1500 (every 50 m)	60	30	point to point
07.07.1995	820 – 1940	60	30	logging
Remarks: Point to point measurements at every 10 m, somewhere more Temperature logging; values are read at every 10 m, somewhere 5 m				

Table 7: Temperature measurements in the Ce-2/95 boreholes at *Cerkno*, compare with Fig. 15 and Fig. 16, revised Placer et al. (2000).

Thermal conductivity from the borehole cores at a depth of 694 - 698 m is determined to 2.54 ± 0.16 W/mK (watt/meter*kelvin) and at a depth of 2003 - 2004 to 2.63 ± 0.02 W/mK (Placer et al., 2000). The highest temperature of 45.72°C was attained at the deepest measuring point at 1940 m (Placer et al., 2000). Deep waters from the *Cerkno* area have lower temperatures compared to the expected temperature under average geothermal gradients. The temperature gradient dT/dz from 0 to 850 m is 23.9 mK/m and from 850 to 1940 m 14.8 mK/m (Placer et al., 2000). Near to the *Cerkno* borehole Ce-2/95 (C), a second deep borehole was explored for thermal usage (small spa) near *Hotavlje* (T, Kopačnica, compare Appendix 17).

Placer et al. (2000) performed the first temperature measurements in the 134 m deep borehole in 1994. These temperature measurements revealed a geothermal gradient of 18 mK/m. This gradient is a result of deep circulation of cold meteoric water in the karstified and fractured aquifer.

Temperature was also measured sucessively 5 times during drilling and inflowing conditions by Placer et al. (2000) to deduce the inflow zones and temperature of the inflow water (Table 7). At a depth of 560 – 565 m the inflow from the formation is registered with 2 l/s, 23 bar and 24°C, due to the fractured zone under the thrust plane at 545 m depth. At almost all inflow zones a certainly smaller water quantity flows in from deeper fractures and leaves the boreholes at shallower depth. Therefore, the borehole can connect two or more fracture zones,

which are usually not connected. Greater quantities of water enter the borehole at the following depths [m]: 847 - 1150, 1178 - 1254, 1420 - 1453 and deeper than 1491 m. Therefore, the main inflows are connected to *Malmian* limestone and to a lesser degree to *Upper Triassic Hauptdolomit*. The main inflows correspond to hydrogeological characteristics of these rocks (Fig. 15 and Table 6).

The *Pseudozilian* beds of the fifth Blegoš nappe sheet and *Carboniferous-Permian* beds of the Trnovo nappe constitute a hydrological barrier (Fig. 16). The thrust plane between the fourth Blegoš nappe sheet and the central part of the Hrušica nappe probably represents a hydrological transition. According to Placer et al. (2000), thrust zones along carbonate rocks where the regions of medium and good permeability exist besides low permeable regions due to structural diversity of the thrust zone core are usual for this geological pattern (Placer et al., 2000).

Placer et al. (2000) suggests that the majority of the Blegoš-Vrhnika range (Appendix 2 and Fig. 16), especially their western and northern plane, can be included into the possible recharge hinterland of the borehole at *Cerkno*. *Triassic*, *Jurassic* and *Cretaceous* beds in the Trnovo nappe are, together with *Malmian* limestone in the Ce-2/95 borehole, divided by the thrust plane of the Trnovo nappe and partly by the fifth Blegoš nappe sheet. Therefore, indirect hydrological connection with them is possible (Placer et al., 2000).

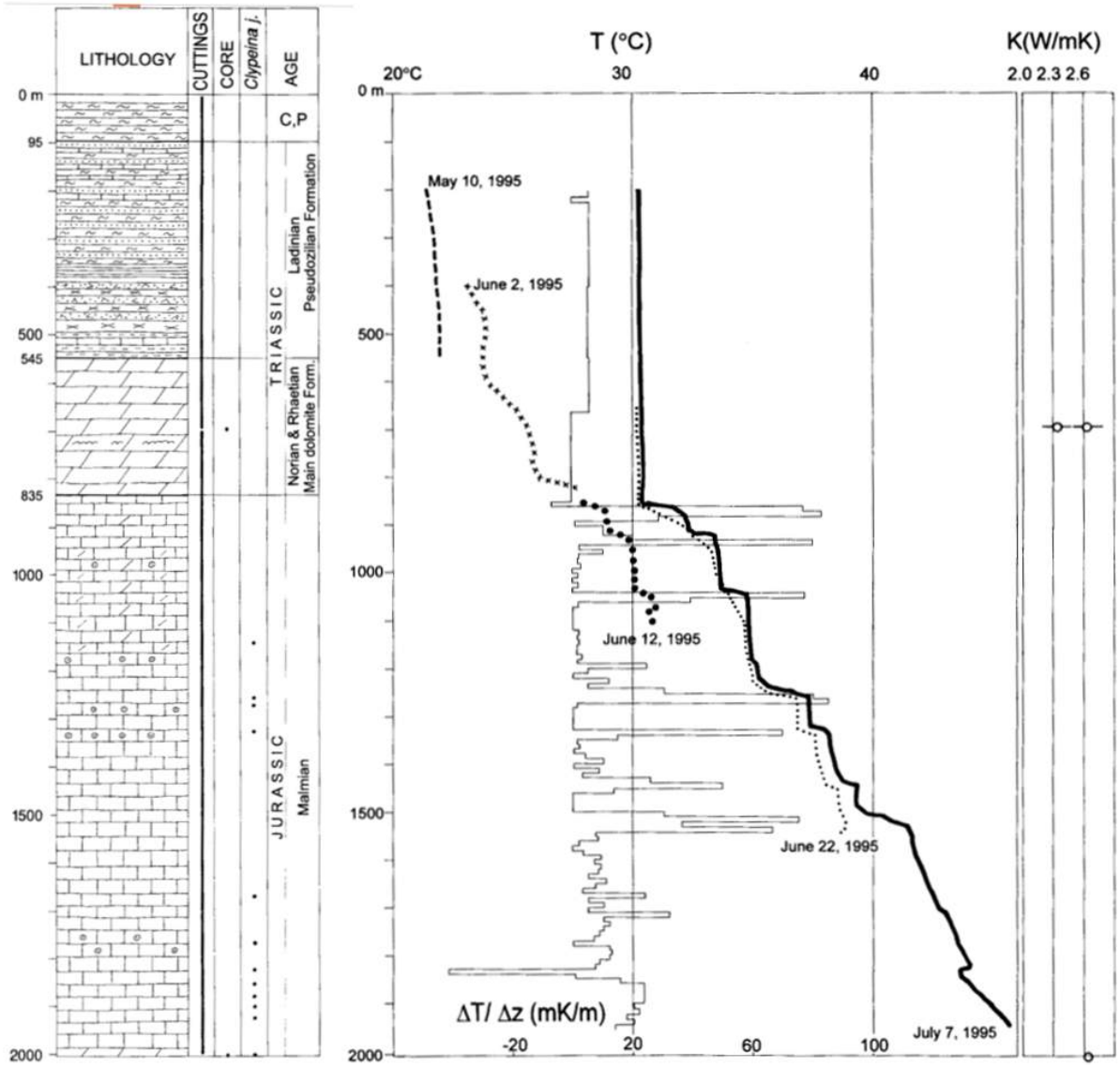

Fig. 15: Lithological column (left) and temperature logs of Ce-2/95 borehole at *Cerkno* (May to July 1995) with thermal conductivity values on core samples (694-698 m, 2003-2004 m, right). The gradient curve is pertinent to the 5th temperature log (July, 7.), dT/dz: temperature gradient (mK/m), T: temperature (°C), K: thermal conductivity (W/mK), revised Placer et al. (2000).

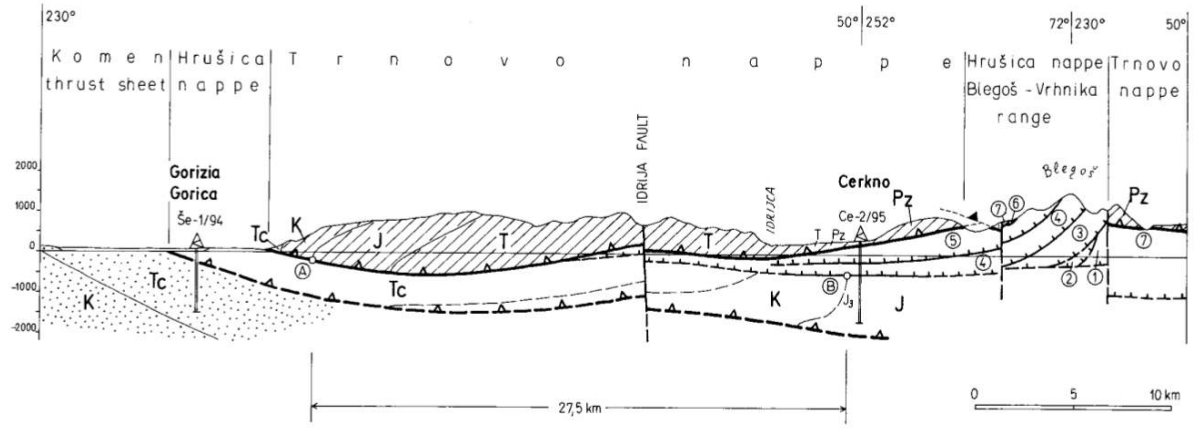

Fig. 16: Geological section from *Gorica* over *Cerkno* to Mt. Blegoš (compare Appendix 2), Pz: *Paleozoic*, T: *Triassic*, J: *Jurrasic*, K: *Cretaceous*, Tc: *Tertiary*, 1 – 7: Blegoš nappe sheets, Placer et al. (2000).

According to Nosan (1973), the common characteristics of the thermal springs/wells of BH, BA, BAA, ST, T and F are their appearence at the surface near shallow secondary faults. These secondary faults usually appear in distances of a few kilometres from the main faults. Thus, these secondary faults show a low temperature between 19 and 26°C. The geothermal gradient is the only source of heat for most of these low-temperature springs and wells. These low temperatures indicate a low geothermal gradient and low primary temperatures rather than an influence of cold groundwater (Nosan, 1973).

Zgornija Besnica (BA, BAA) and M (Mans Power) and L (Lipnica)

Sampling Points BA and BAA are located near to the settlement Zgornja Besnica and drains out at the bottom of the NW-SE striking slope (compare Appendix 27 and 28). The springs M and L are located northeast of the Jelovica plateau and drain the Jelovica plateau at very steep hill slopes (Fig. 17 and Appendix 25). On the Jelovica (karstic) plateau carbonate rocks with high permeability exist and mainly all rocks are in allochthonic or parautochthonic position.

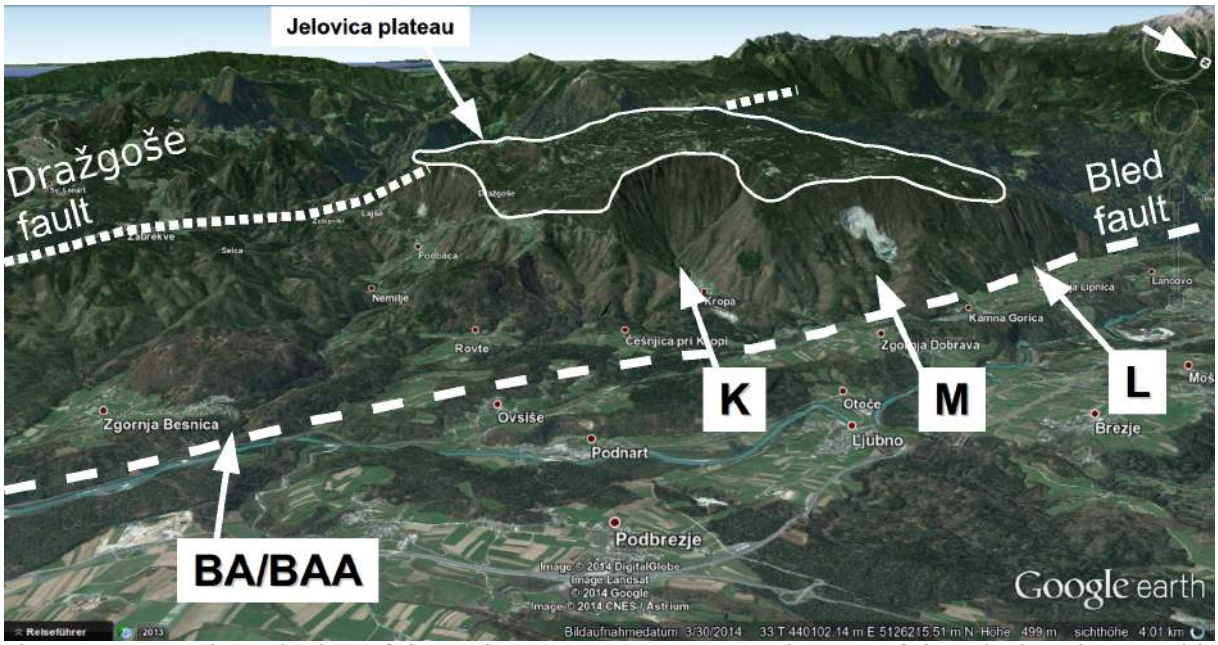

Fig. 17: 3D-GoogleEarth view of the springs BA, BAA, K, M, L and a part of the Jelovica plateau with Dražgoše fault southwest (fine dashed line) and Bled fault north (dashed line) of Jelovica plateau (approximately), direction of sight SW, GoogleEarth, requested 22.09.2014 11:49.

The thrusting and block tectonics are significant for the area around the springs K, M, L and BA/BAA. The main faults on the Jelovica plateau are of the Dinaric NW-SE direction, but faults perpendicular to this direction are also present. These faults are possible groundwater flow directions. The Jelovica plateau is clipped off by steep faults and is confined by the Bled fault in the northern and by the Dražgoše fault in the southern part (compare Fig. 17) (Brenčič, 2003).

Kroparica (K)

The Kroparica springs (K) are located at the northeastern part of the Jelovica plateau, approximately 1 km southwest of the town Kropa. The valley southwest of Kropa with the Kroparica springs ends in a semicircular shape (compare Fig. 17 and Appendix 26). The karstic springs and caverns are developed in the fine-grained sparitic dolomite intercalated with calcite and traces of quartz and pyrite. The dolomite consists of thin, up to 10 cm thick, bedded beds. The basic structure of the rock is not visible due to the late diagenetic dolomitisation (Brenčič, 2003).

In the uphill direction to the west an alternation of several rock types was found by Brenčič (2003):

altitude a. s. l. [m]	rock type
640 to 650	thick bedded to massive bituminised dolomite
650 to 660	talus material and soil, slope sediments and the bedrock is not visible, particles of pyroclastic rocks
from 660 on	thin bedded (layers up to 10 cm) dolomitised limestone
at 678	thick bedded dolomites with big 20 cm nodules of dark red coloured chert, below chert horizon dolomites with veins of quartz occur with same colour as the chert nodules in the upper part
up to 690	dolomite with some beds of dolomitic limestone
690 to 740	dark red and weathered keratophyre and pyroclastic rocks with fluidal structures
at 740	thin bedded dolomite, surface is karstified
above	magmatic and pyroclastic rocks, upper boundary is not clear due to hill slope gravel and rock falls, border between the *Upper Triassic* dolomites and limestone with lower magmatic rocks below is not clear

Table 8 Alternation of rocks in the uphill direction to the west from spring K, Brenčič (2003).

Claystone, marl and siltstone appear in the southeastern part of the Kroparica valley. Above these rocks thin-bedded limestone with very thin lenses of cherts are present. Around 900 m a. s. l. thin-bedded bituminous limestone and dolomite are present. The border between them is probably of tectonic nature. The waters from the Kroparica springs flow out from the Bača dolomite (Brenčič, 2003). Brenčič (2003) suggests that the reason for the spring appearance is the combination of lithostratigraphical and tectonic conditions. Furthermore, Brenčič (2003) suggests that the valley developed due to the significant convergence of tectonic lines.

S (Žveplenica), SR, ZE (above Žveplenica)

The spring S is located between the regionally important Idrija and Predjama faults. S is also situated 10 m south of the Dinaric oriented (NW-SE) Kobarid fault. Žveplenica spring is located in coarse-grained massive *Upper Triassic* dolomite with a thickness of 300 m (compare Fig. 18, Appendix 21 - 23). This tectonic

situation is typical for the External Dinarides (Mulec et al., 2010). ZE is located south of S and besides the main street.

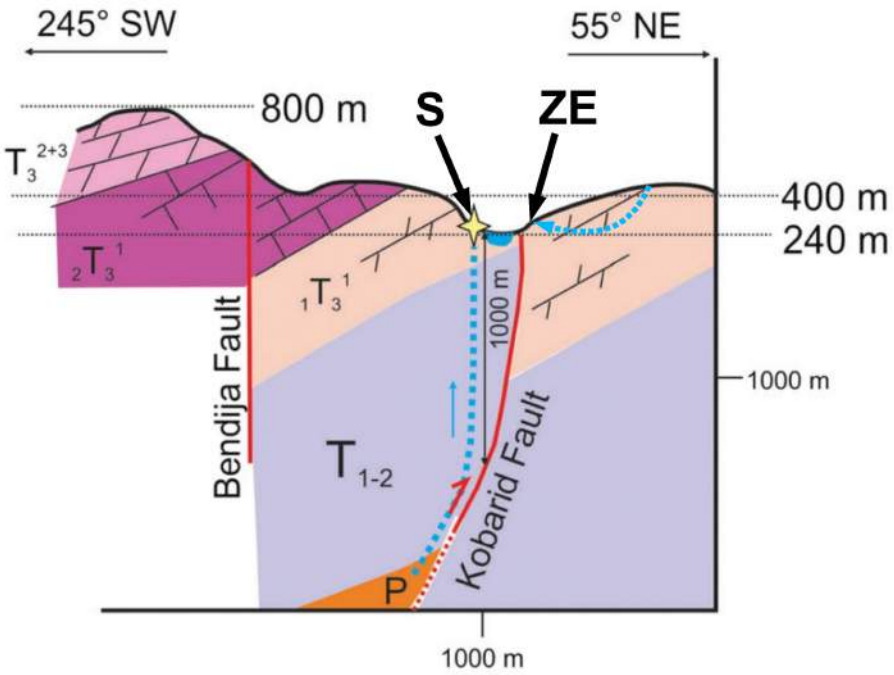

Fig. 18: Geological cross-section of Žveplenica spring with possible flow paths from the deeper underground (S) and surface spring (ZE) and extrapolated positions of spring S and ZE, P: *Upper Permian*, T_{1-2}: *Lower* to *Middle Triassic*, ${}_1T_3^1$: *Upper Triassic* coarse-grained massive dolomite, ${}_2T_3^1$: *Upper Triassic* massive and bedded dolomite, T_3^{2+3}: *Upper Triassic* dolomite, revised Mulec et al. (2014).

The Žveplenica spring (S) has sulfidic chemistry and discharges from *Late Triassic* dolomite with constant 2 l/min (Mulec et al., 2009). Mulec et al. (2014) suggests, due to the isotopic composition, that the waters of the Žveplenica and Studenec (ZE) originate from local precipitation. Furthermore, Mulec et al. (2014) suggests that the Žveplenica spring water is a mixture of local precipitation and sulfide-rich deep water.

1.4. Thermal heat flow and temperatures in Slovenia

Thermal springs have been known in *Slovenia* since Antiquity. The first evidence dates back to the late Iron (≈ 1300 to 700 a. BC (years before Christ))

and Roman Age (≈ 27 a. BC to 293 a. AD (years Anno Domini)). The development of the exploration and utilisation of thermal waters in the 18th and 19th century resulted in the emergence of health resorts. In this time the first investigations concerning the origin, chemistry and healing effects of thermal waters were done (Lapanje & Rman, 2009).

The heat flow rises from 30 mW/m² (milliwatt/meter²) in the western part to 65 mW/m² in the eastern part of *Slovenia* (Lapanje & Rman, 2009). Near *Koper* and in the middle part of *Slovenia* (near *Ljubljana*) a heat flow anomaly occurs with values of up to 80 mW/m², in between the areas in the north and in the south with low heat flow values (30 - 40 mW/m²). The expected temperature in 1000 m depth rises from west to east from 30°C to 66°C. A large temperature anomaly occurs in the east in Murska Sobota near Maribor and two smaller ones around Ljubljana and Koper (Fig. 19). These anomalies can be seen both in the temperatures in 1000 m depth and the heat flow pattern.

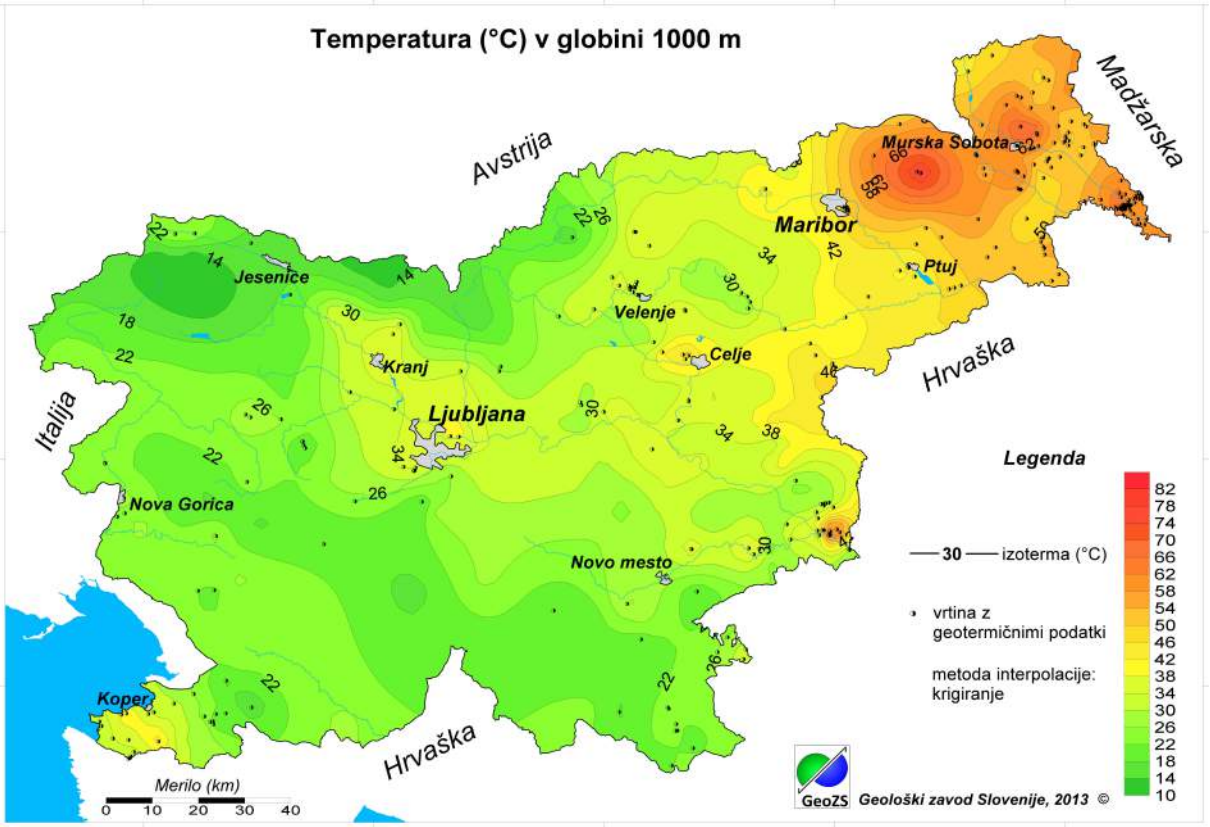

Fig. 19: Expected temperature [°C] in 1000 m depth in Slovenia, www.geo-zs.si, requested 06.11.2014 16:40.

Lapanje & Rman (2009) classify the geothermal systems in *Slovenia* in three different types. The **first type** represents low temperature geothermal systems with warm springs and fissure porosity. Thermal springs emerge at the intersection of two or more deep faults and drain the carbonate-aquifers. The characteristic temperature of these thermal waters at the surface is 20-50°C and the general water type of these geothermal systems is Ca^{2+}-Mg^{2+}-HCO_3^-. Locally SO_4^{2-}-ions occur due to gypsum or anhydrite dissolution. Representative locations among others are Kopačnica (T) and Vrhnika (F) (compare Appendix 17 and 20) (Lapanje & Rman, 2009).

Lapanje & Rman (2009) proposed that similiar fissure systems are common at the margins of the *Tertiary* sedimentary basins at the boundary between carbonate and clastic rocks. These systems have low permeability and low thermal conductivity. Representative locations among others are Bled (BH) and Spodnje Pirniče (ST) (compare Appendix 18 and 19) (Lapanje & Rman, 2009).

The **second type** represents low temperature geothermal systems with aquifers in sedimentary basins and of intergranular porosity. These systems occur in *Tertiary* clastic sediments and sedimentary rocks in NE-Slovenia. The predominant water type is Na^+-HCO_3^- (Lapanje & Rman, 2009). This type is of less interest for the presented study and no further description is made.

The **third type** represents low temperature geothermal systems with aquifers in the basement of sedimentary basins and with fissure porosity. They are found throughout Slovenia. In places where basement aquifers are formed in different *Mesozoic* and *Cenozoic* carbonate rocks lying beneath low permeable and heat insulating rocks, thermal water is mostly of the Ca^{2+}-Mg^{2+}-HCO_3^--type and has low mineralisation and almost no CO_2 (Lapanje & Rman, 2009). Thermal and thermomineral water in the basement of sedimentary basins is identified in *Cerkno* (C) and Zgornja Besnica (BA) (Lapanje & Rman, 2009).

1.5. Theoretical background

The theoretical background of the chemical and physical processes in karst and non-karst systems are of great importance for the understanding of these systems. The following theories and models describe the interactions between different hydrochemical parameters and ions.

1.5.1. Hydrochemistry

Electrical Balance

Two types of errors are described in chemical analyses: 1) precision or statistical errors which reflect random fluctuations in the analytical procedure, 2) accuracy or systematic errors displaying systematic deviations due to faulty procedures or interferences during analysis. Precision can be calculated by repeated analysis of the same sample. The accuracy of an hydrochemical analysis for major ions can be estimated from the electrical balance (E. B.) since the sum of positive and negative charges in the water be equal

$$electrical\,balance\,(E.B.,\%) = \left(\left(\frac{\sum cations}{\sum anions}\right) - 1\right) x\,100 \qquad (1)$$

where cation and anions are expressed as meq/l (equivalent concentration) and inserted with their charge sign (compare Appendix 6). The unit of the electrical balance is %. The sum of the equivalent concentrations of the cations is made out of Na^+, K^+, Mg^{2+}, Ca^{2+}. The sum of the equivalent concentrations of the anions is made of Cl^-, HCO_3^-, SO_4^{2-}, NO_3^-. Additionally, in reduced groundwater ferrous iron ($Fe^{2+/3+}$) or NH_4^+ and in acid water H^+ and Al^{3+} can be important and thus added to the electrical balance. Differences in electrical balances of up to 2 % are inevitable in almost all laboratories. In some cases a larger error must be accepted, but with deviations in excess of 5 % the sampling and analytical procedures should be examined (e. g. Appelo & Postma, 2005).

Carbonate system

Limestones and dolomites often form productive aquifers, called karst aquifers. The main minerals in these rocks are Mg^{2+}- and Ca^{2+}-carbonates, which dissolve easily in groundwater. Other karst aquifer rocks include either gypsum or salt. The groundwater flow is limited to more permeable fracture zones and karst channels forming the typical karst landscapes and features in caves.

The carbonate dissocation can be written as

$$H_2CO_3 \leftrightarrow CO_2 + H_2O \qquad \textbf{(2)}$$

$$H_2CO_3 \leftrightarrow H^+ + HCO_3^- \qquad \textbf{(3)}$$

$$HCO_3^{2-} \leftrightarrow H^+ + CO_3^{2-} \qquad \textbf{(4)}$$

The increase of CO_2 results in the increased dissolution of $CaCO_3$. The removal of CO_2 results in the precipitation of $CaCO_3$. Therefore, CO_2-partial pressure in water is essential to thrive and support karstification and thus speleogenesis or increase in permeability (e. g. Appelo & Postma, 2005). Plummer et al. (1978) showed that the calcite dissolution rate increases with increasing pCO_2 (Fig. 20).

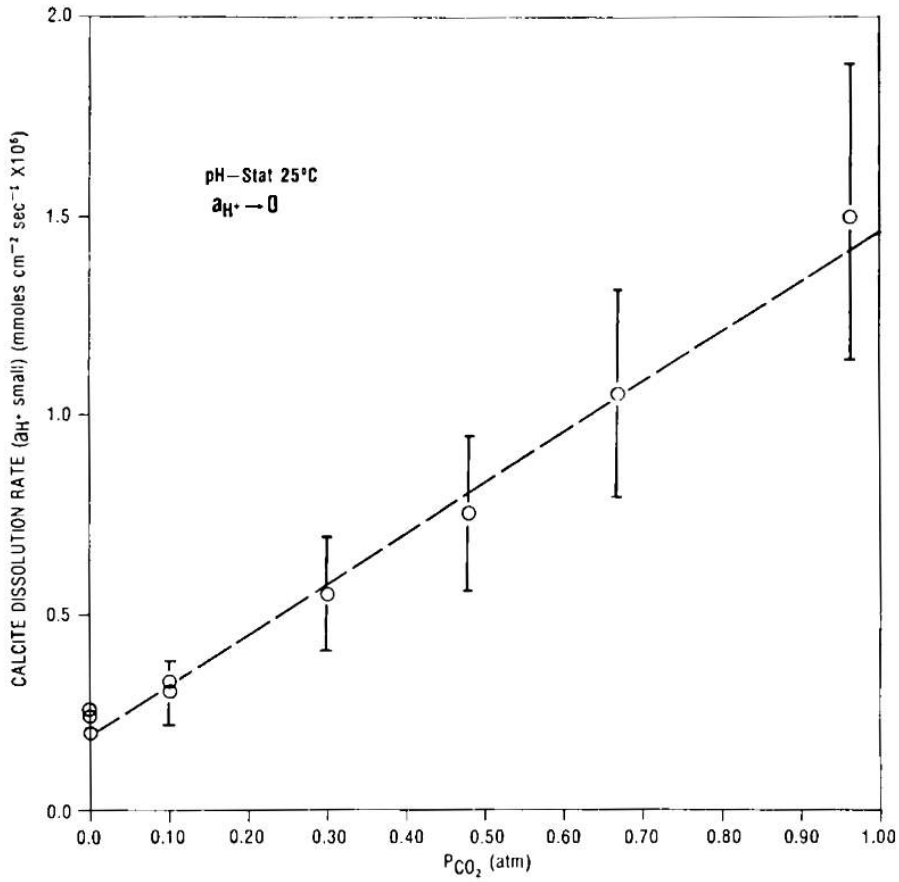

Fig. 20: Rate of calcite dissolution (with constant pH) as a function of bulk fluid pCO_2 in the absence of H^+ at 25°C, Plummer et al. (1978)

1.5.2. Dolomitisation and dedolomitisation

Dockal et al. (1988) describes dolomitisation as the process in which limestone is converted to dolomite rock. In this process, the original calcite minerals are replaced by dolomite minerals, usually because of Mg^{2+}-bearing waters. Dolomite rock can form by (1) replacement of another mineral such as calcite by dolomite, (2) growth of dolomite from the original rock or sediment and then the later removal of all or most of the other non-dolomite material, (3) growth of dolomite crystals between the solid components of a sediment and (4) possibly through primary deposition of dolomite (Dockal et al., 1988).

Theory of dedolomitisation

Karstification occurs both in dolomite and calcite aquifers. Dissolution of limestones ($CaCO_3$) can be described by

$$CaCO_3 + H_2O + CO_2 \leftrightarrow Ca^{2+} + 2HCO_3^-. \qquad \textbf{(5)}$$

Karstification of dolomite rocks occur due to the dissolution of dolomite, which can be written as

$$2CO_2\,(g) + 2H_2O + CaMg(CO_3)_2 \leftrightarrow Ca^{2+} + Mg^{2+} + 4HCO_3^-. \qquad \textbf{(6)}$$

In a monomineralic dolomite aquifer groundwater ideally contains equal amounts of Ca^{2+} and Mg^{2+} ($CaMg(CO_3)_2$ on the left side of equation 1) while the HCO_3^- concentration should be four times the Ca^{2+} and Mg^{2+} concentrations ($4HCO_3^-$) on the right side of equation 6). The point where groundwater is in equilibrium with both calcite and dolomite has special chemical properties, which can be written as

$$Ca^{2+} + CaMg(CO_3)_2 \leftrightarrow CaCO_3 + Mg^{2+}. \qquad \textbf{(7)}$$

According to Usdowski (1967), pore solutions with a molar-Ca^{2+}/Mg^{2+}-ratio of around 1.9 (30 to 40 Mol-% Mg^{2+}) and another predominant anion (SO_4^{2-} and CO_3^{2-}) are particularly common in nature. In Fig. 21 the frequency distributions

(rectangles at the x-axis) of Ca^{2+} and Mg^{2+} and the average values for the equilibrium of calcite and dolomite (a) and dolomite and magnesite (b) are displayed. The pore solutions contain much more Mg^{2+} compared to the equilibrium between calcite and dolomite (arrow towards higher Mg^{2+}-content). Therefore, in most cases, if a pore solution is in contact with limestone, a reaction under precipitation of dolomite occurs (Usdowski, 1967). This is exactly what happens in the process of dolomitisation.

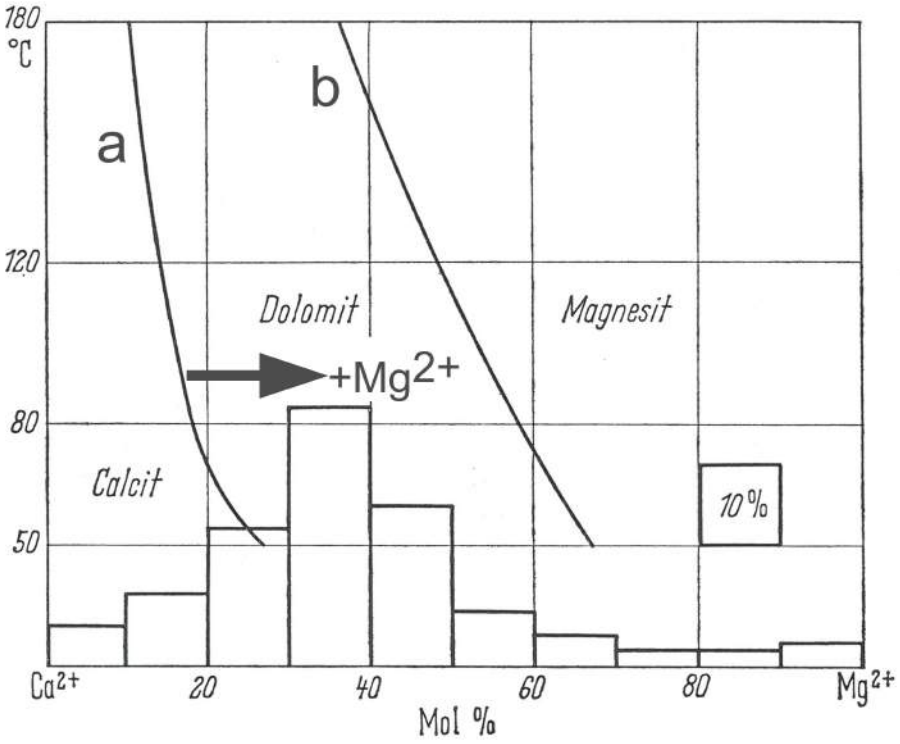

Fig. 21: Diagram of the equilibrium between calcite and dolomite (a) and the equilibrium between magnesite and dolomite (b) and the frequency distribution of Ca^{2+} and Mg^{2+} in pore solutions (rectangles at the x-axis), revised Usdowski (1967).

The chemical, stoichiometric formular of idealisied dolomite is $Ca_1Mg_1(CO_3)_2$. Chang et al. (1998) mentionend that mostly Ca-rich dolomite occur in nature. They list four dolomite analyses (beneath others from volcanic and metamorphic origin) from Eocene rocks of the Floridan Aquifer, from *Ordovician* Platteville Formation in Wisconsin, USA (Table 9 1-3) and from *Miocene* Monterey Formation in California, USA (Table 9 4). Table 9 shows that the chosen dolomites contain more Ca^{2+} (> 1.0) than Mg^{2+} (< 1.0). Therefore, Ca-rich dolomite has the chemical formular $Ca_{>1}Mg_{<1}(CO_3)_2$.

Ion/number	1	2	3	4
Ca^{2+}	1.124	1.006	1.087	1.105
Mg^{2+}	0.876	0.988	0.909	0.895
Fe^{2+}	-	0.006	0.004	-
$C^{2+/4+}$	2	2	2	2

Table 9: Number of ions of the basis of six oxygen (O), Chang et al. (1998).

Ogorelec & Rothe (1992) analysed samples from the Dachstein-limestone and the *Hauptdolomit*-Formation in southwest Slovenia. Their measurements show Ca^{2+} values from 21.3 to 22.1 % and Mg^{2+} values from 12.7 to 13.4 %, which equals to the Ca^{2+} and Mg^{2+} values for stoichiometric dolomite. All samples from Ogorelec & Rothe (1992) show a minimal excess of Ca^{2+} up to 3 %. In turn, the granular and well crystallised dolomite has an excess of Mg^{2+} up to 3 Mol% $MgCO_3$.

Fig. 22 shows the solubility diagram for the system calcite/Ca-rich dolomite at T = 10°C and $pPCO_2$ = 3.5 ($pPCO_2$ = partial pressure of CO_2). In this figure, path 0-a-b displays the dissolution of $CaMg(CO_3)_2$ and simultaneous precipitation of $CaCO_3$, which is one type of dedolomitisation. First (0), $CaCO_3$ is dissolving and being brought into the solution until equilibrium is reached. Then, $CaMg(CO_3)_2$ is dissolved and brought into the solution simultanously until the saturation curve of $CaCO_3$ has reached equilibrium (a). Furthermore, $CaMg(CO_3)_2$ is still dissolved and brought into the solution but now $CaCO_3$ is precipitated until the $CaMg(CO_3)_2$ saturation curve is reached (b) and both $CaMg(CO_3)_2$ and $CaCO_3$ are in eqilibrium. In this case the $[Mg^{2+}]/[Ca^{2+}]$-ratio becomes invariant (at constant temperature and pressure) (Wigley, 1973).

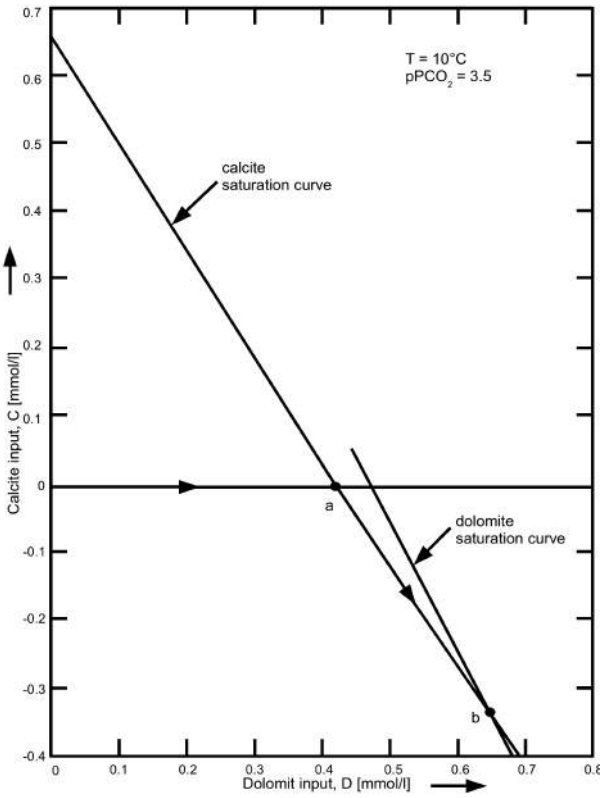

Fig. 22: Solubility diagram for the system calcite/Ca-rich dolomite at T = 10°C and $pPCO_2$ = 3.5, the path 0-a-b is the evolution path for the solution of Ca-rich dolomite toward saturation with respect to both dolomite and calcite at point b, revised Wigley (1973).

When simultaneous equilibrium with calcite and dolomite is combined with the dissolution of gypsum or anhydrite, the process of dedolomitisation takes place (Wigley, 1973). The dissolution of anhydrite or gypsum is described by

$$CaSO_4 \leftrightarrow Ca^{2+} + SO_4^{2-}. \quad \textbf{(8)}$$

The increasing Ca^{2+} concentration due to gypsum dissolution causes calcite to precipitate. The CO_3^{2-} concentration decreases as calcite precipitates and this provokes the dissolution of (ideal) dolomite ($CaMg(CO_3)_2$) and an increase of Mg^{2+} and Ca^{2+} concentration. The net result is that the dissolution of gypsum induces the transformation of dolomite to calcite in the rock and thus, produces waters with increased Mg^{2+}, Ca^{2+} and SO_4^{2-} concentrations. Dedolomitisation may occur in aquifers containing dolostones (dolomite-type carbonates) associated with gypsiferous layers (e. g. Appelo & Postma, 2005).

Fig. 23 shows solubility digrams of the system calcite-gypsum at T = 10°C and $pPCO_2$ = 3.5. In this figure, path 0 - 0.65 - a displays the dissolution of $CaSO_4$ and the simultaneous precipitation of $CaCO_3$, which is another type of dedolomitisation. First (0), $CaCO_3$ is dissolving and being brought into the solution until equilibrium is reached ($M_{Ca,\ calcite}$= 0.65). After that, $CaSO_4$ is dissolving and being brought into the solution simultanously until the saturation curve of $CaSO_4$ has reached equilibrium (a). In this step from $M_{Ca,\ calcite}$= 0.65 to a, the saturation curve of calcite (SATCAL = 0.0) decreases and thus, calcite is precipitated. Now, both $CaSO_4$ and $CaCO_3$ are in equilibrium.

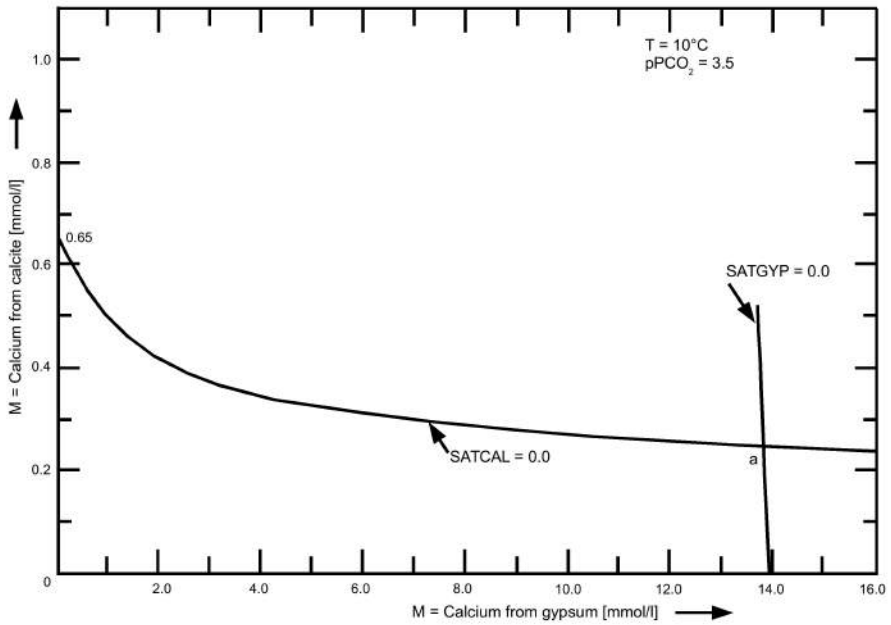

Fig. 23: Saturation index curves for calcite-gypsum solutions at T = 10°C and pPCO2 =3.52, the x- and y-axes show the relative contributions to the total calcium concentration from gypsum and calcite respectively, the solubility of each mineral is decreased by the presence of the other, revised Wigley (1973b).

Correlations of parameters for the process of dedolomitisation

According to Hanshaw & Back (1979) the process of dedolomitisation occurs in response to gypsum solution with calcite precipitation and corresponding effects on the CO_2 and pH. Dedolomitisation is the incongruent dissolution of dolomite to form calcite with a crystalline structure similar to dolomite (Hanshaw & Back,

1979), which was described by Wigley (1973) (compare Fig. 22 and Fig. 23). According to Back et al. (1983) SO_4^{2-} concentration shows a strong correlation with pH as a result of the combined effects of the dedolomitisation reaction (Fig. 24).

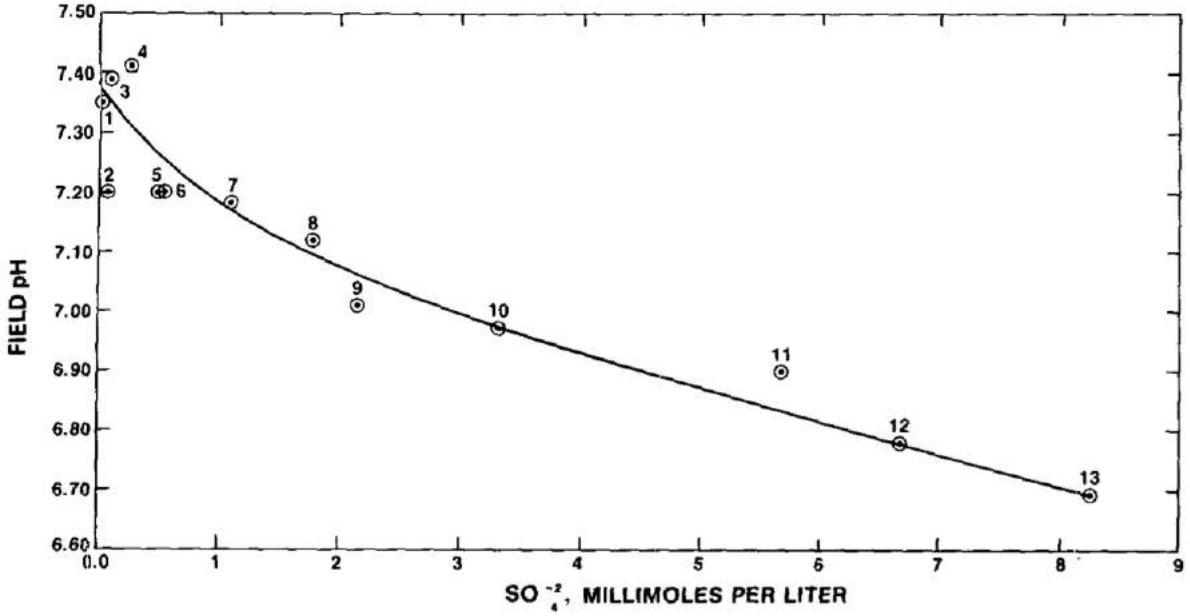

Fig. 24: Decrease in pH with increasing SO_4^{2-} concentration (Back et al., 1983).

Cardenal et al. (1993) distinguished two main hydrochemical processes in a *Triassic* gypsum-bearing carbonate aquifer in southern Spain: (1) incongruent dissolution of dolomite that determines the chemical composition of the less mineralised water, and (2) dedolomitisation which becomes predominant when the flow encounters interbedded gypsum. The first process was described in detail by Wigley (1973) (compare Fig. 22).

The general structure of the Alpujárride complex, studied in Cardenal et al. (1993) is characterised by superposition of a number of tectonic units or nappes. Additional sources for CO_2 are organic material (some samples smelt strongly of H_2S) and a deep source (where alkalinity is higher and fracture zones coincide). The studied aquifer is mostly confined where dedolomitisation was most clearly detected (Cardenal et al., 1993). That is in line with the hypothesis of Cardenal et al. (1993) in which the process of dedolomitisation is expected to take place in a

system closed to CO_2. Cardenal et al. (1994) discovered a correlation between Ca^{2+} and SO_4^{2-} concentration and Mg^{2+} and SO_4^{2-} concentration (Fig. 25).

Saunders & Toran (1994) pointed out three arguments for the evidence of dedolomitisation: (1) precipitation of authigenic calcite in gypsum dissolution cavities, (2) a decrease in groundwater-pH and (3) an increase in dissolved Ca^{2+}, Mg^{2+}, SO_4^{2-} concentration and TDS (Fig. 25).

Cardenal et al. (1993) distinguished that the dedolomitisation trend is marked by stabilisation or even a slight fall in the alkalinity value (Fig. 26). Furthermore, Cardenal et al. (1993) considered the additional dissolution of dolomite and/or calcite apart from dedolomitisation due to CO_2 enrichment from the presence of organic material.

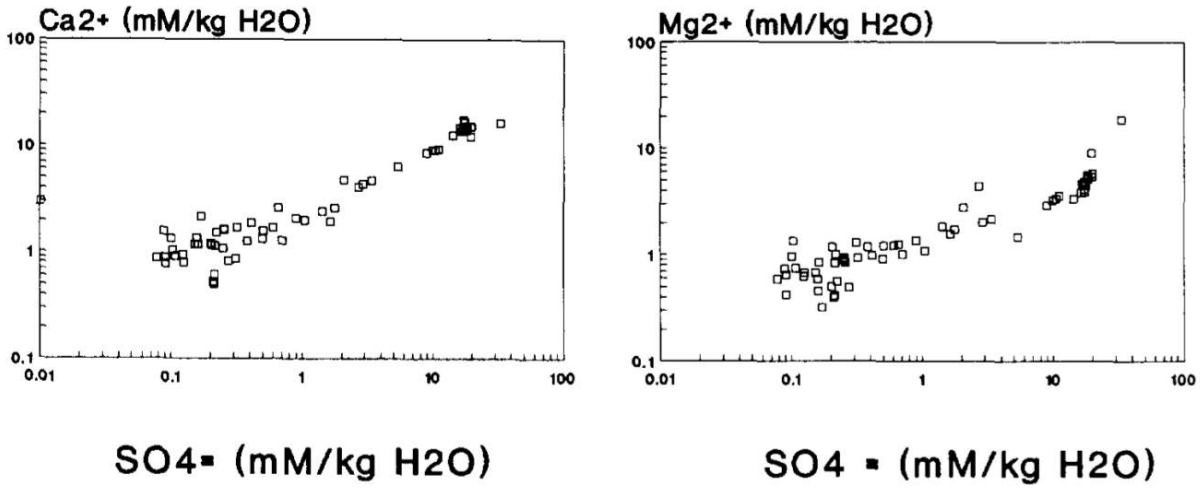

Fig. 25: Two diagrams of dissolved SO_4^{2-} concentration vs. Ca^{2+} (left) and dissolved SO_4^{2-} concentration vs. Mg^{2+} (right) from groundwaters in LasAlpujarras in southern Spain, Cardenal et al. (1994).

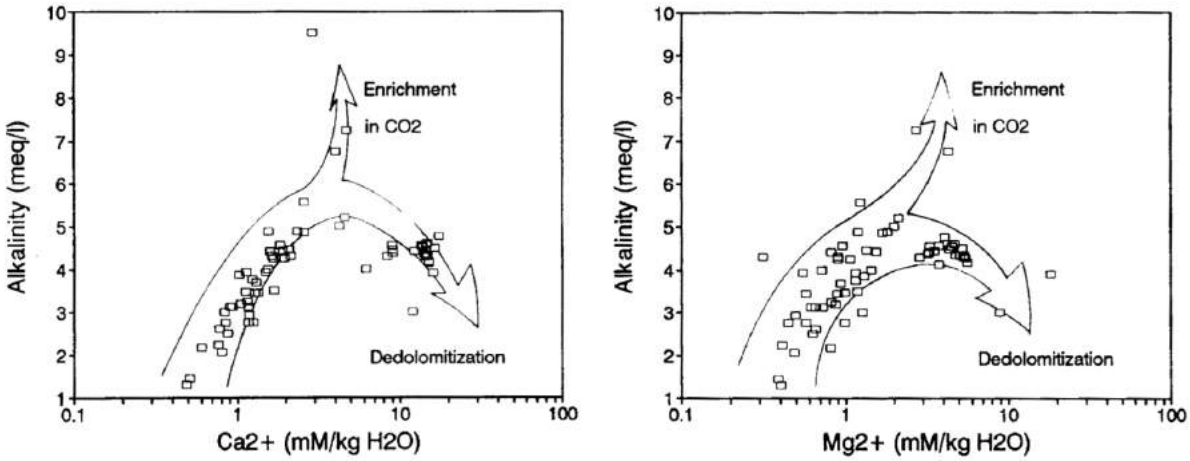

Fig. 26: Diagram of Ca^{2+} (left) and Mg^{2+} (right) contents vs. alkalinity (in meq/l of HCO_3^-) values, revised Cardenal et al. (1994).

Cardenal et al. (1994) distinguished two groups (Fig. 27). The first group indicates an inverse relation between HCO_3^- content and pH, corresponding to not very mineralised water in which incongruent dolomite dissolution is predominant and even the onset of dedolomitisation. The second group on the left in Fig. 27 represents more highly mineralised water, in which dedolomitisation has progressed significantly, with a stable HCO_3^- and a low pH (Cardenal et al., 1994).

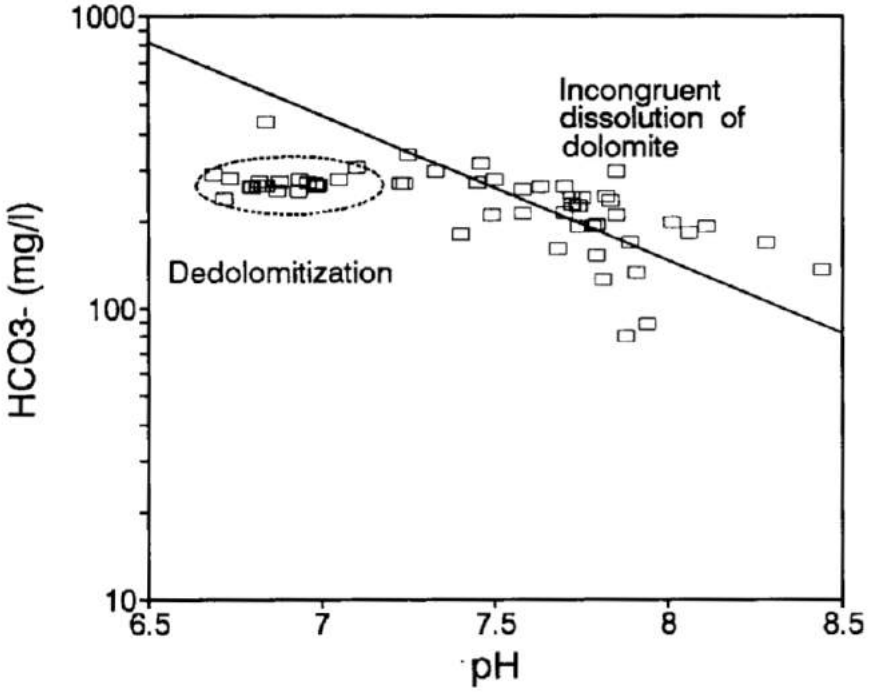

Fig. 27: Diagram of pH vs. alkalinity (in mg/l of HCO_3^-) values with the 15°C calcite-dolomite saturation line, revised Cardenal et al. (1994).

Bischoff et al. (1994) suggested, based on hydrochemical analyses, sulfur isotope composition, local stratigraphy and mass-balance modeling of Lake Banyoles in northeastern Spain, that the primary karst-forming process is dedolomitisation. A main statement in this publication is, that dedolomitisation causes karstification without exogenous acids. Bischoff et al. (1994) and Back et al. (1983) showed that the waters discharging from the suspected dedolomitisation area follow a specific trend in the Piper-Diagram (Fig. 28), in which the index numbers correspond to an increase of SO_4^{2-} concentration. The position of the index numbers on the diagram (Fig. 28) indicates the typical evolution of chemical character of water in carbonate aquifers that contain gypsum.

According to Back et al. (1983) a critical contribution of gypsum to the process of dedolomitisation is to provide an abundant supply of Ca^{2+} in order to maintain a low Mg^{2+}/Ca^{2+}-ratio. Thus, Back et al. (1983) verified with their field data the significance of the Mg^{2+}/Ca^{2+}-ratio regardless of the absolute concentration of Mg^{2+} or Ca^{2+} or their relative percentages. If the Mg^{2+}/Ca^{2+}-ratio is greater than 1, dolomite can form. If the Mg^{2+}/Ca^{2+}-ratio is lower than 1, dolomite will dissolve. According to Back et al. (1983) all samples from their field data have a Mg^{2+}/Ca^{2+}-ratio less than 1 (Fig. 28).

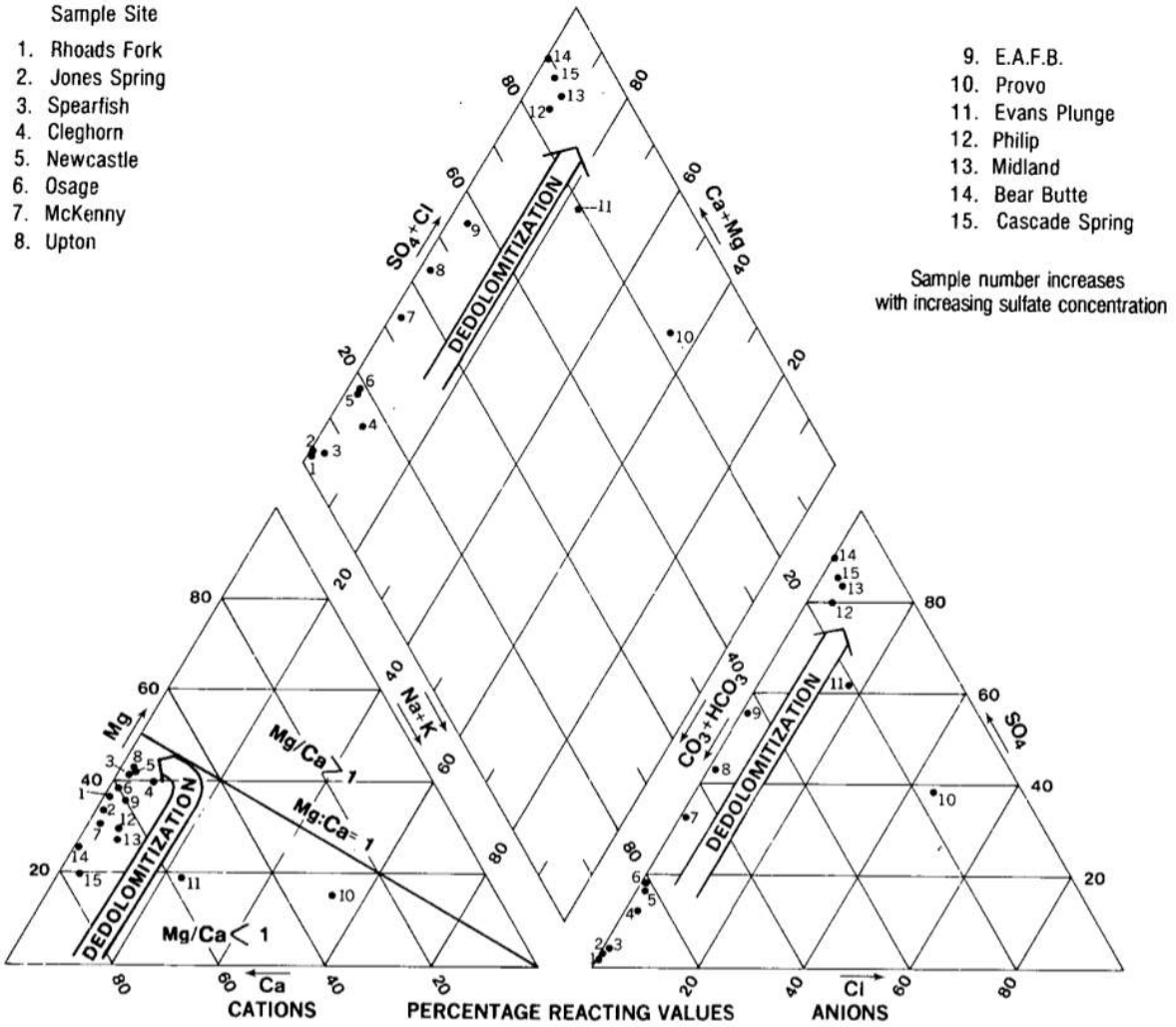

Fig. 28: Trilinear diagram (Piper-Diagram) showing chemical character of groundwater in the Pahasapa Limestone and the reactions controlling its chemical evolution (data in meq/l), the dedolomitisation reaction proceeds from lower to higher SO_4^{2-} concentration, from higher to lower total alkalinity and from molar-Mg^{2+}/Ca^{2+}-ratios < 1 to molar-Mg^{2+}/Ca^{2+}-ratios which are almost 1, Back et al. (1983).

Plummer et al. (1990) showed that two trends in total alkalinity as a function of dissolved SO_4^{2-} concentration exists for waters in the Madison Aquifer. According to Plummer et al. (1990) waters from the Madison Aquifer show a decrease in alkalinity with increasing SO_4^{2-} concentration (Fig. 29). Plummer et al. (1990) showed that the decrease in alkalinity is to be expected for the evolutionary paths following the dedolomitisation reaction.

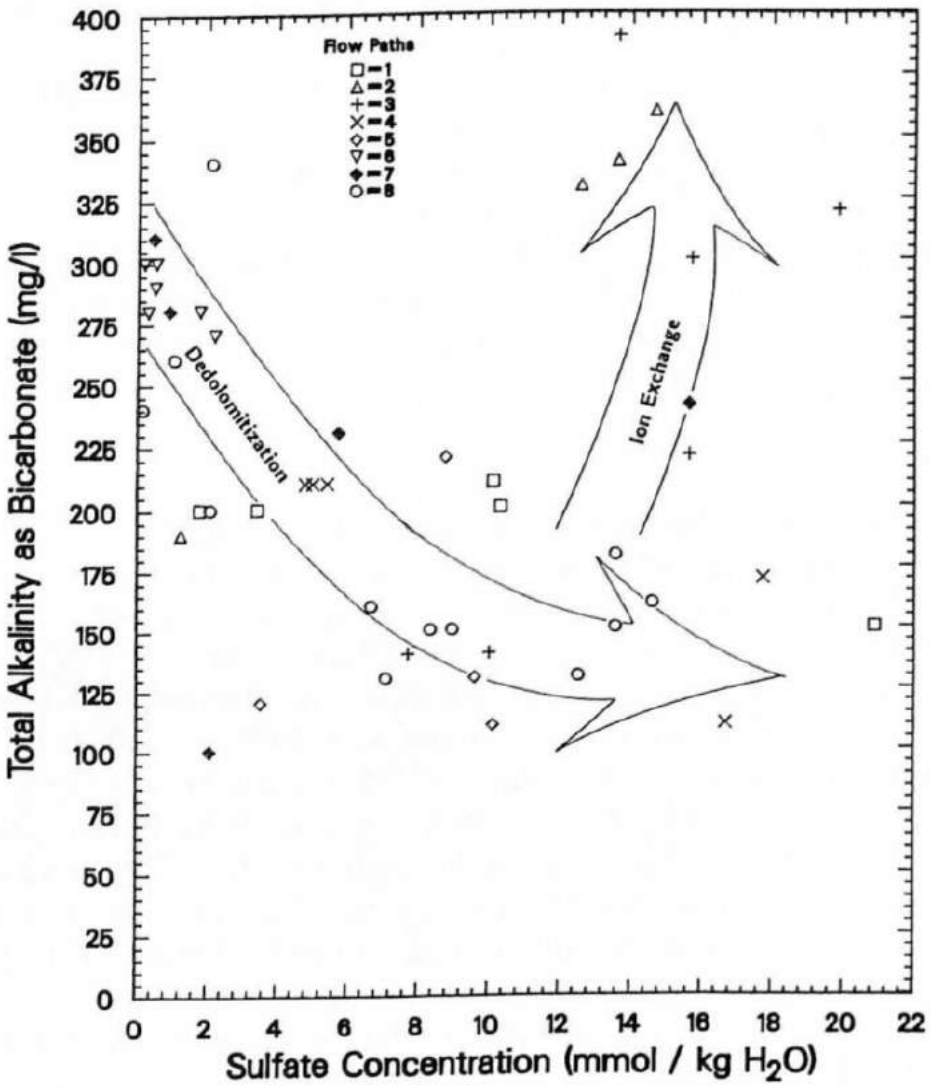

Fig. 29: Trends in total alkalinity as bicarbonate as a function of dissolved SO_4^{2-} concentration of waters from the Madison Aquifer, Plummer et al. (1990).

Plummer et al. (1990) also showed that the SI gypsum correlates with SO_4^{2-} concentration and that a slight oversaturation with respect to calcite is expected under conditions of dedolomitisation necessary to cause precipitation of calcite (Fig. 30).

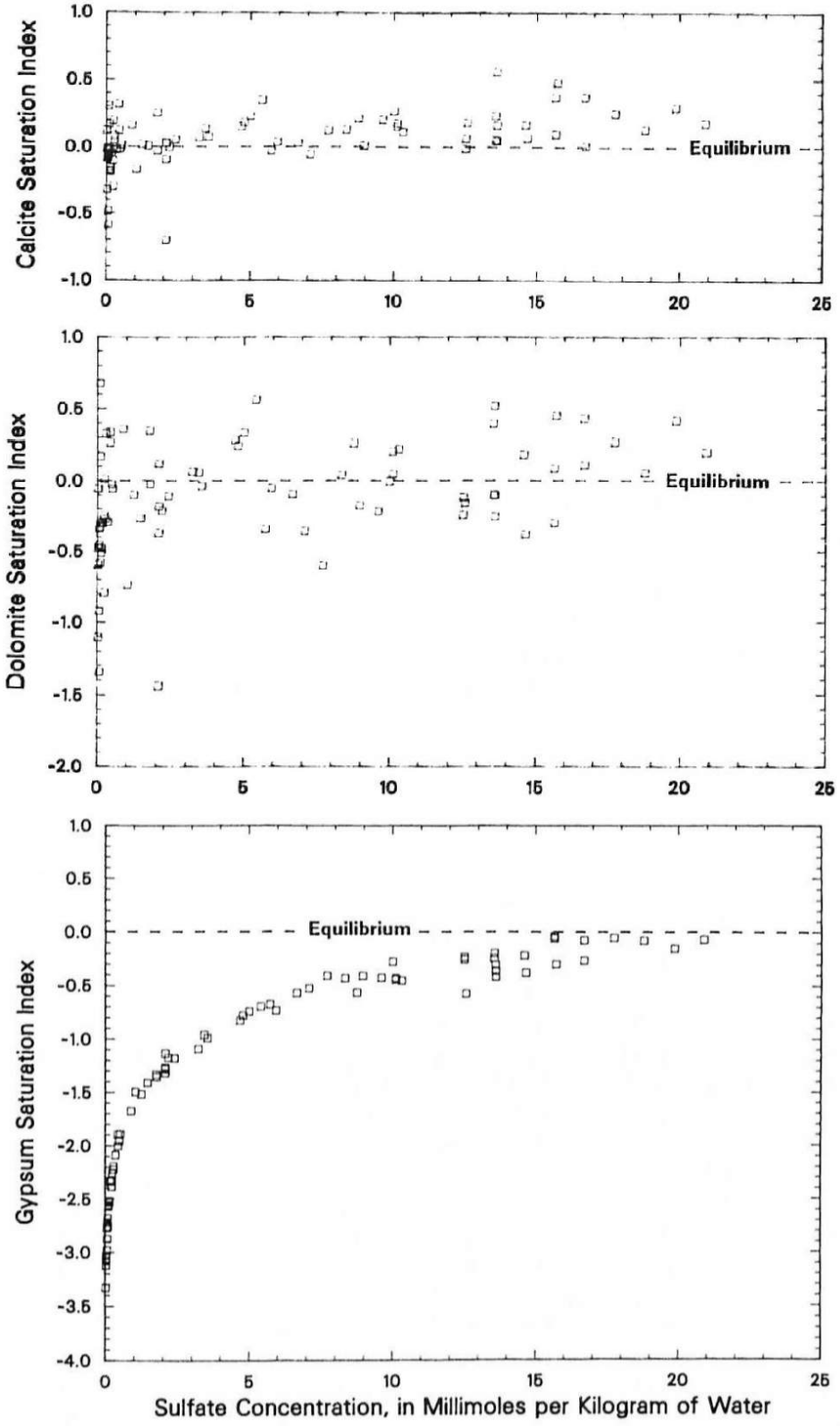

Fig. 30: Gypsum saturation indices as a function of total dissolved SO_4^{2-} concentration for wells and springs in the Madison aquifer, Plummer et al. (1990).

1.5.3. Speleogenesis and deep flow in karst aquifers

Speleogenesis

In the Encyclopedia of Caves, speleogenesis is described as a result of dissolution of soluble rocks by groundwater. Many factors and proccesses are involved, leading to the evolution of conduit networks in karst aquifers. The most important factors and proccesses are the local hydrology, lithology, structure, geochemical settings, and topography. Each factor imposes different parameters, which can change in time (e. g. Gabrovšek, 2012).

Three types of caves can be described: (1) those that develop in young, newly emerged rocks at the coast, (2) hypogene (deep) cavities that may be formed when rocks are buried and altered beneath later strata, and (3) epigene (unconfined) caves formed when the now diagenetically mature rocks are exposed to meteoric groundwater circulation (Ford et al., 2007).

Hypogenic karst is formed by bottom-up processes, which is initiated by up-welling deep waters. According to Klimchouk (2007) hypogenic speleogenesis is closely related to the concept of artesian or confined speleogenesis. In these aquifer conditions groundwater is under pressure in a bed or stratum by an impermeable rock or sediment above it. Permable geological features (e. g. faults) within the impermable rock, can initiate the hypogenic speleogenesis (Klimchouk, 2007). According to Kempe (2014) ascending „cave forming agents“ are either water or other compounds from the underground. Water rises either by thermal (compare Fig. 33) or by natural convection. Thermal convection is driven by the heat flow from the radioactive decay in the Earth's core. Natural convection is driven by the dissolution of a compound, which is easy to dissolve (Kempe, 2014).

The traditional karst (surface and subsurface) is formed by a top-down process with CO_2-containing meteoric water. The meteoric water flows into the epikarst and downward to the vadose and phreatic zones of the aquifer. Eventually, this water reappears at a karstic spring (Jones & White, 2012).

Dublyansky (2012) defines hydrothermal karst as the process of dissolution of cavities in the rocks under the action of hot waters. Thus, hydrothermal karst is a special case of hypogene karst. The lower limit of the hydrothermal environment

is 20°C. According to Dublyansky (2012) the evidence of the hydrothermal origin of a cave can be provided by (1) the presence of thermal waters in a cave, (2) the presence of hydrothermal minerals deposited on the cave walls and (3) the presence of isotopic alteration of the cave walls. It also includes characteristic morphological features, a lack of morphological features and a lack of association with the surface features of „conventional“ karst (Dublyansky, 2012).

Deep flow in Karst aquifers

White (2012) describes three types of permeabilities or porosities of a karst aquifer: (1) Matrix permeability is due to the pore spaces within the bedrock, (2) Fracture permeability is due to faults, fault systems and bedding planes and (3) Conduit permeability consists of solutionally generated caves.

The flow of water in conduits is similar to the flow in pipes and may be turbulent. The flow velocities are in the range of centimeters per second compared with meters per year in porous media aquifers. The properties of each component of the permeability are summarised in Fig. 31 and all aquifers can be categorised by the triple porosity model as illustrated in Fig. 32 (White, 2012).

Permeability	Aperture	Travel Time	Flow Mechanism	Guiding Equation	Distribution
Matrix	μm–mm	Long	Darcian flow field: laminar	$h_f = \frac{\eta v L}{\rho g (N d^2)}$	Continuous medium
Fracture	10 μm–10 mm	Intermediate	Cube law: mostly laminar, may be nonlinear components	$\frac{Q}{h} = \frac{C}{f} B^3$	Localized but statistically distributed
Conduit	10 mm–10 m	Short	Darcy–Weisbach: open channel and pipe flow turbulent	$h_f = \frac{f L v^2}{4 g r}$	Localized

Fig. 31: Characteristics of the three types of aquifer permeabilities, White (2012).

A special feature of karst aquifers is the presence of conduits, which act as networks of pipes carrying water rapidly through the aquifer. Many active conduits are located below the water table, in comparison to many caves, which lie above the active zone of groundwater circulation and are abandoned conduits. The degree of conduit development and the connection of the conduits to other types of permeability are highly variable. Water flows through conduits either as open channel flow (a stream with a free air surface) or as pipe flow (a completely water-filled tunnel) (White, 2012).

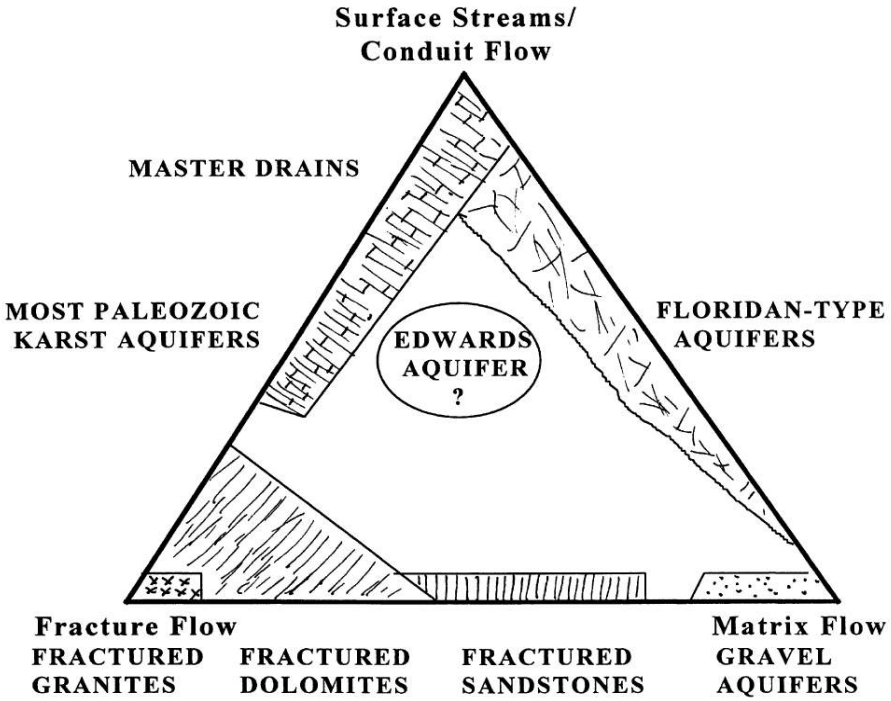

Fig. 32: Three types of aquifer permeability expressed as a tringular diagram. Normal aquifers would lie along the bottom of the triangle. Karst aquifers are those in which conduit permeability is an important component, White (2012).

The underground residence time of deep groundwaters is defined greater than 50 years (Goldbrunner, 1999). Chemical evidence of processes operating deep within an aquifer is masked by dilution or attenuation in shallower groundwaters, which tend to have shorter residence times and far higher flow rates than deep waters. Deep boreholes and tunnels can give insights into processes affecting deep groundwaters (Gunn et al., 2006).

Especially deep carbonate rock aquifers, most of which are to some degree karstified, are probably the most important thermal water resources outside of volcanic areas. Thermal water resources in continental carbonate rock aquifers are related to deep, regional flow systems. Fig. 33 shows a schematic illustration of groundwater flow and karstification processes in a deep and mostly hypogenic inland-carbonate system.

Because of the topographic gradients between the recharge area and the thermal springs, the flow system is primarily gravity-driven. Sedimentary compaction, tectonic compression and density differences act as additional driving forces. Recharge of the karst aquifer occurs at the epigenic karst and

water flows further to the underground causing deep epigenic karstification. In the upper part of the aquifer mixing corrosion can occur and water can discharge at a lukewarm spring. In the lower part of the aquifer mixing corrosion, as well as oxidation to H_2SO_4 can occur due to basinal fluids coming from the deeper sedimentary or crystalline rocks. Water is heated up due to terrestrial heat flux from the deep underground. In this part of the aquifer it is worth to build up a geothermal douplet, which can provide geothermal energy on the one hand and possible CO_2-sequestration on the other hand (see Fig. 33) (Goldscheider et al., 2010).

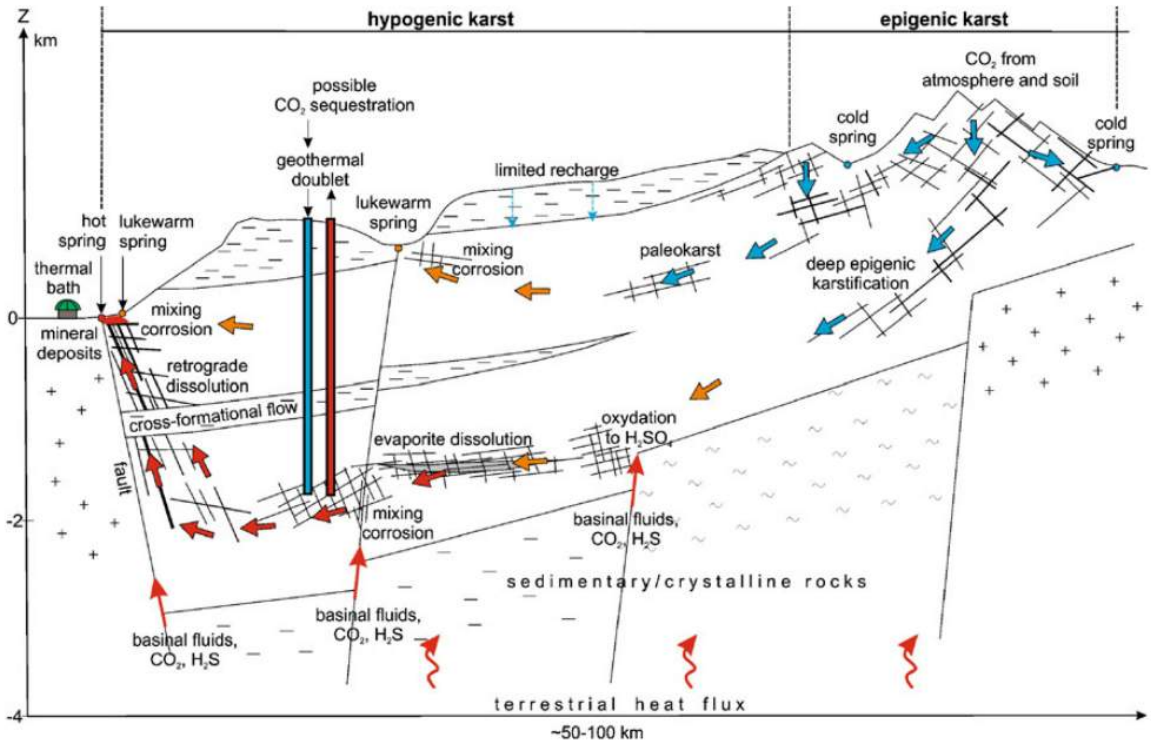

Fig. 33: Schematic illustration of groundwater flow and karstification processes in a deep and mostly hypogenic inland-carbonate rock system, arrows indicate the flow direction, blue to red arrows indicate cold to hot water temperatures, (Goldscheider et al., 2010).

1.5.4. Stable Isotopes ($\delta^{18}O$, oxygen and $\delta^{2}H$, hydrogen)

In the course of a chemical or physical reaction, isotope ratios vary and isotopic fractionation occurs. The specific formular to describe these fractionations is the δ notification. The formular for $\delta^{18}O$ and $\delta^{2}H$ is:

$$\delta 18O = \left(\frac{\frac{^{18}O}{^{16}O}sample - \frac{^{18}O}{^{16}O}standard}{\frac{^{18}O}{^{16}O}standard}\right) * 1000, \qquad \textbf{(9)}$$

$$\delta 2H = \left(\frac{\frac{^{2}H}{^{1}H}sample - \frac{^{2}H}{^{1}H}standard}{\frac{^{2}H}{^{1}H}standard}\right) * 1000, \qquad \textbf{(10)}$$

δ is expressed as the number of parts per mil (‰). The isotope ratios are expressed with the heavier isotope in the numerator (e. g. Allègre, 2008).

Water is built up of two hydrogen (H^{+}) and one oxygen (O^{2-}) ions. These ions have different isotopes: hydrogen (^{1}H, ^{2}H (D: deuterium), ^{3}H (T: tritium)), oxygen (^{18}O, ^{17}O, ^{16}O). Oxygen is the most abundant element on Earth and occurs in gaseous, liquid and solid compounds (e. g. Hoefs, 2009). H and O provide a dual system for tracking the origin of water and its subsequent movements (e. g. Criss et al., 2007). In the earths atmosphere, three isotopes of oxygen occur with the following abundances (e. g. Rosman & Taylor, 1998):

^{16}O	99.757 %
^{17}O	0.038 %
^{18}O	0.205 %
^{1}H	99.9885 %
^{2}H	0.0115 %

Table 10: Abundances of isotopes of oxygen and of hydrogen.

Two different δ-standards are in use: $\delta^{18}O$ VSMOW (Vienna Standard Mean Ocean Water) and $\delta^{18}O$ VPDB (Vienna Pee Dee Belemnite). This is due to two different categories of users. The VPDB scale is used in low-temperature studies in carbonates. PDB is a Cretaceous belemnite from the Pee Dee Formation. All other oxygen isotope analysis (waters, silicates, phosphates, sulfates, high-temperature carbonates) are given in relation to SMOW, which means Standard Mean Ocean Water (e. g. Hoefs, 2009).

The concentrations of ^{2}H and ^{18}O in meteoric waters at a given geographic location vary over time and reflect seasonal changes in temperature at single locations. In regions with large seasonal temperature changes variations are greater than in areas where such differences are small (e. g. Hoefs, 2009).

During individual storms at a given site large isotopic variations can occur. The source region and advection path of individual air masses also have a great influence on the isotopic composition (e. g. Criss et al., 2007). When vapor leaves the surface of the ocean, it cools as it rises. Rain is formed when the dew point is reached. During the removal of rain from a moist air mass, the residual vapor is continuously depleted in the heavy isotopes. This is because rain leaving the system is enrichd in ^{18}O and ^{2}H. Moving poleward and cooling down, additional rain is formed and contains less ^{18}O than the initial rain (Fig. 34, e. g. Hoefs, 2009).

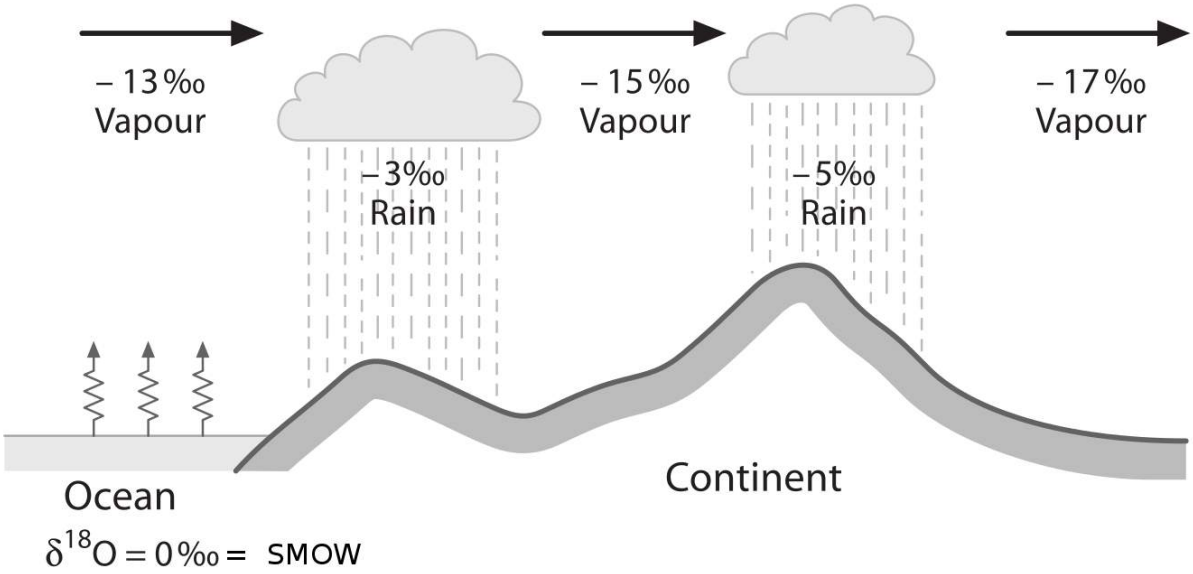

Fig. 34: Schematic O-isotope fractionation of water in the atmosphere (Hoefs, 2009).

Because of a corresponding difference in vapor pressure between $^{1}H_2O$ and $^{2}H_2O$ in one case and $H_2{}^{16}O$ and $H_2{}^{18}O$ in the other case, hydrogen isotopes are fractionated in proportion to oxygen isotopes in all processes concerning evaporation and condensation (e. g. Hoefs, 2009). Therefore, Craig (1961) defined this relationship by

$$\delta^{2}H = 8 * \delta^{18}O + 10, \quad \textbf{(11)}$$

which is generally known as the „Global Meteoric Water Line“ (GMWL). Besides the GMWL, the „Local Meteoric Water Line“ (LMWL) is used for more local and specific sites. Furthermore, Dansgaard (1964) defined the concept of „deuterium excess“ (DE):

$$DE = \delta^{2}H - 8 * \delta^{18}O, \quad \textbf{(12)}$$

where neither the numerical coefficient, 8, nor the deuterium excess, d, are really constant, because both depend on the local climatic processes. Varying influences of different sources of vapor with different isotope characteristics, different air mass trajectories, or evaporation and isotope exchange processes below the cloud base, may often lead to much more complex relationships between $\delta^{2}H$ and $\delta^{18}O$ at the local level (e. g. Hoefs, 2009).

Based on these equations, isotopic parameters can be used as natural tracers. They may provide valuable additional information on the altitude of the recharge area, the origin of the water, groundwater age and residence times (e. g. Goldscheider et al., 2007).

Vreča et al. (2006) defined Local Meteoric Water Lines (LMWL) for Slovenia and Croatia. They also observed distinct differences of meterological and isotopic data between continental and maritime stations (Table 11).

Station	Observation period	$\delta D/\delta^{18}O$ correlation equation	r	n
Ljubljana	2001-2003	$\delta D = (8.0 \pm 0.2)\ \delta^{18}O + (9.2 \pm 1.8)$	0.99	36
Ljubljana	1981-2003	$\delta D = (8.2 \pm 0.1)\ \delta^{18}O + (10.7 \pm 0.7)$	0.99	255
Portorož – Airport	2001-2003	$\delta D = (7.7 \pm 0.4)\ \delta^{18}O + (7.3 \pm 2.2)$	0.96	35
Kozina	2001-2003	$\delta D = (7.7 \pm 0.3)\ \delta^{18}O + (9.6 \pm 2.2)$	0.97	36
Zavižan (Croatia) – Mt. Velebit	2001-2003	$\delta D = (7.6 \pm 0.4)\ \delta^{18}O + (10.5 \pm 4.0)$	0.95	35

Table 11: Correlation equations for Local Meteoric Water Lines (LMWL) with r (correlation coefficient) and n (quantity) from Vreča et al. (2006).

2. Methods

2.1. Field Measurements (T, pH, EC, discharge)

Measurements in the field were carried out with a temperature-, pH- and electrical conductivity-meter. At each sampling point the well and spring waters were measured in-situ. Due to error reduction, measurements were carried out as near as possible to the outflow of the spring or well.

2.2. Discharge

The discharge (Q) is the volume of water per time unit, which flows out from wells or springs. The discharge can be very different (especially at karstic springs), due to bigger or smaller recharge areas (area where water infiltrates in the system). To determine the volume of the waters of the wells and springs, a bucket (r = 0.147 m, h = 0.157 m) was used. To determine time, a stopwatch (smartphone) was used. Errors occur due to wrong reading, loss of water and unprecise time measurements. Therefore, the calculated discharge is only an estimation.

$$V = 2 * \pi * r^2 * h \qquad \textbf{(13)}$$

$$Q = V / t \qquad \textbf{(14)}$$

2.3. Titration

Titration deals with the reaction of a given ion to a reagent of known concentration. The equivalence point is determined by means of a potentiometric measurement or a visual indicator (e. g. Hunkeler & Mudry, 2007).

Titration for Mg^{2+}, Mg^{2+} + Ca^{2+}, Cl^- and carbonates was carried out in 2013 in the laboratory in Postojna. Titration for carbonates was carried out in 2014 with a hand digital titrator (Fig. 35) directly in the field and in the lab in Darmstadt for comparison and checking.

Fig. 35: HACH digital hand titrator with equipment (Photo: Philipp).

Titration in the field was done with unfiltrated samples. Titration in the lab was done with filtrated samples. Filtration of water changes the pCO_2 and thus pH and alkalinity. Therefore, the titration in the lab cannot be reliable. Nevertheless, the lab titration shows almost similar HCO_3^- concentrations compared to earlier field titrations (Fig. 36). Therefore, the data from the titration in the lab is used for further calculations and discussions.

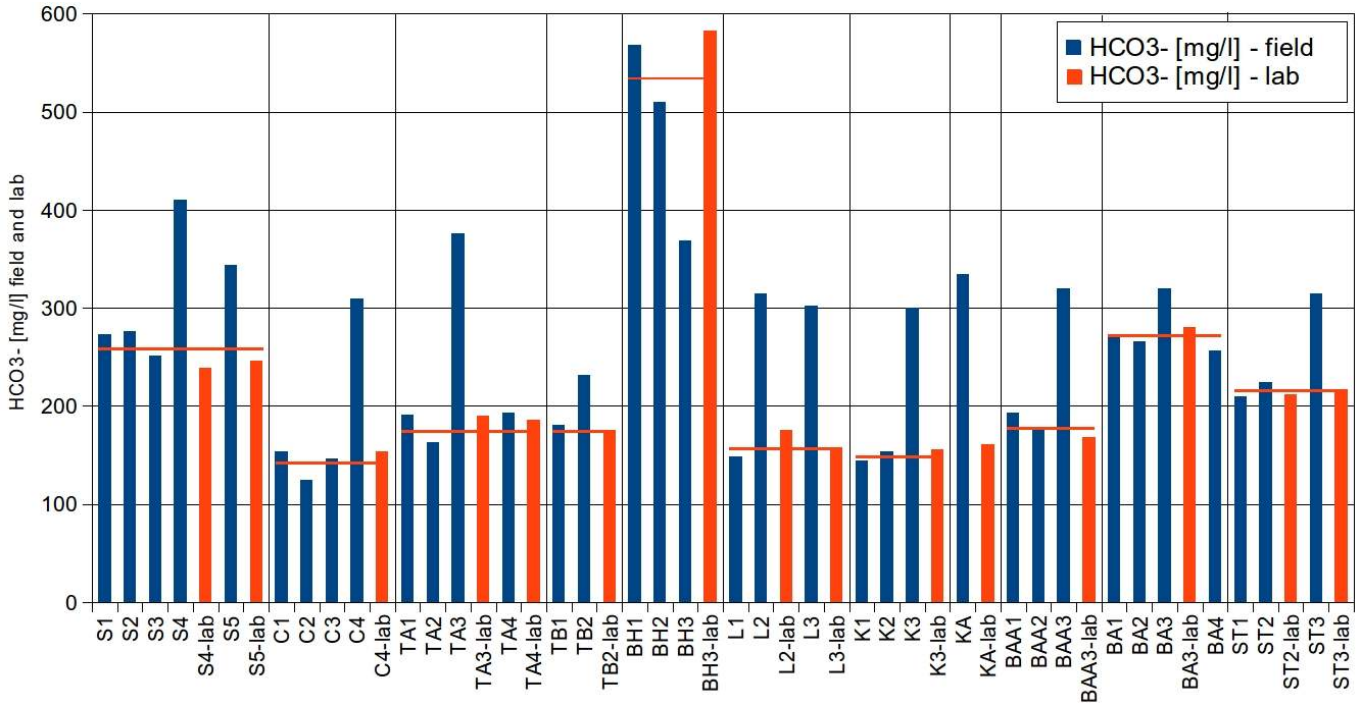

Fig. 36: HCO_3^- concentration from wells and springs, blue: HCO_3^- concentration from field data, and red: HCO_3^- concentration from lab data, red lines indicate approximate mean value with field and lab data.

2.4. Spectrophotometry

Spectrophotometry relies on the transformation of an ion of interest into a complex that adsorbs light at a specific wavelegth. With the Beer-Lambert equation the adsorption can be related to the concentration of the ion. This method is genereally very sensitive, but it has the disadvantage that for each ion a different reagent has to be used and that with some compounds interferences with other ions occur (e. g. Hunkeler & Mudry, 2007). This method was used to analyse Cl^-, NO_3^-, SO_4^{2-} and PO_4^{3-} in 2013 in the lab in Postojna.

2.5. Ion chromatography (IC)

Ion chromatography relies on the principle to elute a sample containing a mixture of ions within a column. This column specifically retards the different ions making it possible to separate them. At the end of the column a detector

provides a signal that is proportional to the content of the compound in the sample. Comparing the sample response with that of standards, it is possible to calculate the compound concentration (e. g. Hunkeler & Mudry, 2007). Ion chromatography was used to measure the major ions (anions: F^-, Cl^-, NO_2^-, Br^-, NO_3^-, PO_4^{3-}, SO_4^{2-}, cations: Li^+, Na^+, NH_4^+, K^+, Mg^{2+}, Ca^{2+}, Sr^{2+}) in 2013 and 2014 in the lab in Darmstadt (Fig. 37).

Fig. 37: Ion chromatography (IC) in the lab in Darmstadt (Photo: Philipp).

2.6. Atomic adsorption spectrometry (AAS)

Atomic adsorption spectrometry (AAS) relies on the possibility to promote atoms to a higher energy level by electromagnetic radiation. Before the measurement, the sample has to be volatilised. Because each element adsorbs at a different wavelength, only one element can be measured at a time (e. g. Hunkeler & Mudry, 2007). AAS was used for the two cations $Fe^{2+/3+}$ and Mn^{2+} in 2013 and 2014 in the lab in Darmstadt (Fig. 38).

Fig. 38: Atomic adsorption spectrometry (AAS) in the lab in Darmstadt (Photo: Philipp).

2.7. Picarro L2130-i Analyser (isotopes)

Both hydrogen isotope ratios (δ^2H) and oxygen isotope ratios ($\delta^{18}O$) were analysed using a fully automated Picarro L2130-i Cavity Rind Down Spectrometer (CRDS) isotope analyser connected to Picarro A0211 high precision vaporiser (Fig. 39). All values are expressed in the standard delta notation, as described in 1.5.4. Stable Isotopes ($\delta^{18}O$, oxygen and δ^2H, hydrogen).

Raw data were corrected for memory effects and machine drift during the run and normalised to the VSMOW/SLAP (Standard Light Antarctic Precipitation) scale. Normalisation was done following recommendations of Gonfiantini (1984) where values of 0 ‰ and -428 ‰ for δ^2H and 0‰ and -55.5 ‰ for $\delta^{18}O$ were assigned to VSMOW and SLAP, respectively. For this purpose, two laboratory standards, which were calibrated directly against VSMOW, were measured in each run.

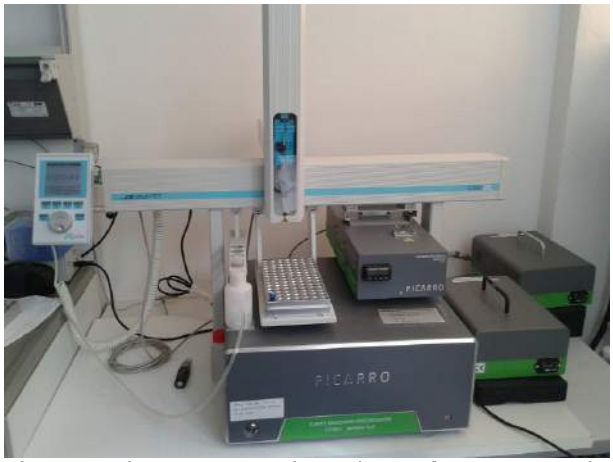

Fig. 39: Picarro L2130-i Analyser for Isotopes in the lab in Darmstadt (Photo: Philipp).

2.8. PHREEQC (Wateq4f.dat)

PHREEQC (pH-REdox-EQuilibrium) is a computer program for the simulation of chemical reactions and transport processes (geochemical model). The program is based on the equilibrium chemistry of aqueous solutions interacting with minerals, gases and solid solutions.

The geochemical model consists of several components, which are: 1) the input file describing the problem to be solved, 2) the geochemical database, 3) the parser reading the input file and deriving a series of equations from it, 4) the solver for a series of resulting nonlinear function (Newton-Rhapson), 5) the output file containing the results and optional 6) graphical or tabular presentations of results (e. g. Parkhurst & Appelo, 2012).

Fig. 40 shows the input file of M3 with all measured parameters (T, pH, ions). If one parameter is not given, the algorithm will set a default value for it, for example, if no pE value is given, pE is assumed to be 4 by default (e. g. Parkhurst & Appelo, 2012).

The output file (Fig. 41) consists of a standard output showing the equilibrium reactions and additional results like saturation indices. The structure of the output file is 1) Reading data base (the database including keywords), 2) Reading

input data (repetition of data and keywords from the input file), 3) Initial solution calculations (standard calculations) (e. g. Parkhurst & Appelo, 2012).

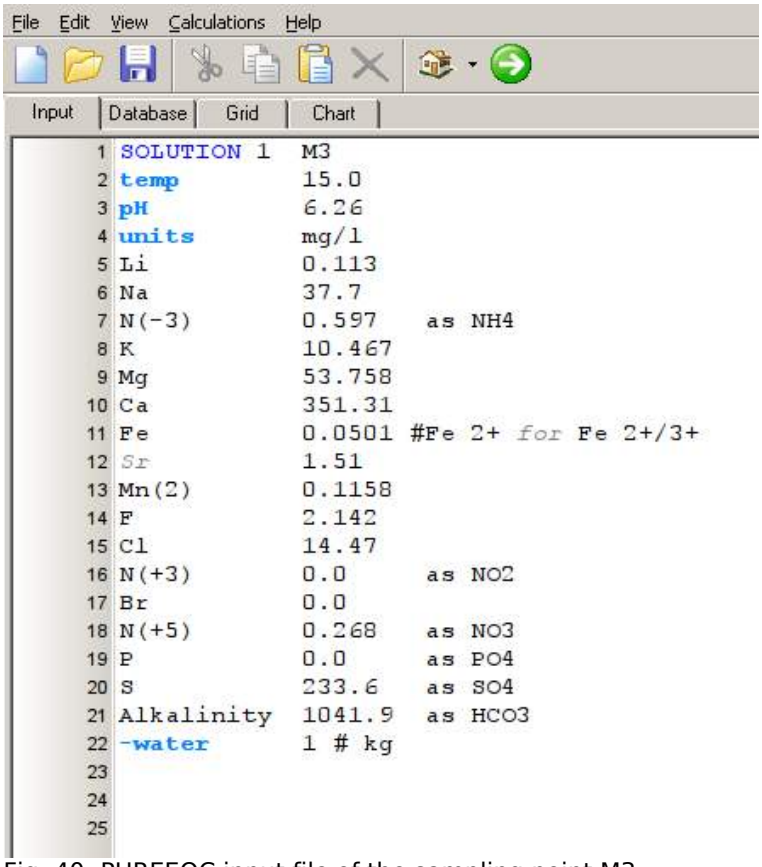

Fig. 40: PHREEQC input file of the sampling point M3.

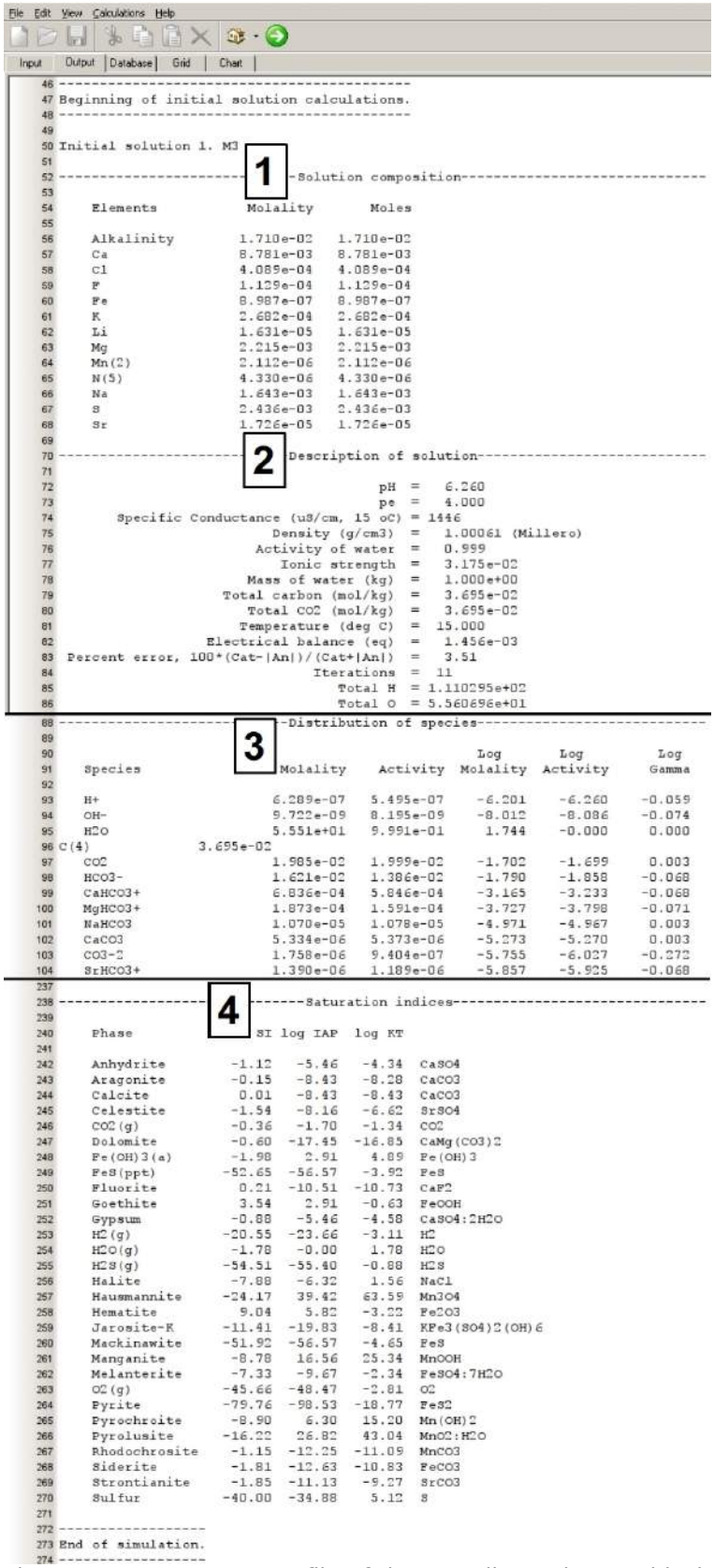

```
File  Edit  View  Calculations  Help
Input | Output | Database | Grid | Chart

Beginning of initial solution calculations.

Initial solution 1. M3

-----------------------1-Solution composition------------------------------

    Elements            Molality       Moles

    Alkalinity        1.710e-02   1.710e-02
    Ca                8.781e-03   8.781e-03
    Cl                4.089e-04   4.089e-04
    F                 1.129e-04   1.129e-04
    Fe                8.987e-07   8.987e-07
    K                 2.682e-04   2.682e-04
    Li                1.631e-05   1.631e-05
    Mg                2.215e-03   2.215e-03
    Mn(2)             2.112e-06   2.112e-06
    N(5)              4.330e-06   4.330e-06
    Na                1.643e-03   1.643e-03
    S                 2.436e-03   2.436e-03
    Sr                1.726e-05   1.726e-05

-----------------------2-Description of solution----------------------------

                                     pH  =   6.260
                                     pe  =   4.000
      Specific Conductance (uS/cm, 15 oC) = 1446
                          Density (g/cm3)  =   1.00061 (Millero)
                       Activity of water   =   0.999
                          Ionic strength   =   3.175e-02
                       Mass of water (kg)  =   1.000e+00
                   Total carbon (mol/kg)   =   3.695e-02
                      Total CO2 (mol/kg)   =   3.695e-02
                     Temperature (deg C)   =  15.000
                  Electrical balance (eq)  =   1.456e-03
Percent error, 100*(Cat-|An|)/(Cat+|An|)   =   3.51
                                Iterations  =  11
                                   Total H  = 1.110295e+02
                                   Total O  = 5.560898e+01

-----------------------3-Distribution of species----------------------------

                                                    Log         Log         Log
  Species                Molality    Activity    Molality    Activity    Gamma

  H+                   6.289e-07   5.495e-07    -6.201      -6.260      -0.059
  OH-                  9.722e-09   8.195e-09    -8.012      -8.086      -0.074
  H2O                  5.551e+01   9.991e-01     1.744      -0.000       0.000
C(4)          3.695e-02
  CO2                  1.985e-02   1.999e-02    -1.702      -1.699       0.003
  HCO3-                1.621e-02   1.386e-02    -1.790      -1.858      -0.068
  CaHCO3+              6.836e-04   5.846e-04    -3.165      -3.233      -0.068
  MgHCO3+              1.873e-04   1.591e-04    -3.727      -3.798      -0.071
  NaHCO3               1.070e-05   1.078e-05    -4.971      -4.967       0.003
  CaCO3                5.334e-06   5.373e-06    -5.273      -5.270       0.003
  CO3-2                1.758e-06   9.404e-07    -5.755      -6.027      -0.272
  SrHCO3+              1.390e-06   1.189e-06    -5.857      -5.925      -0.068

-----------------------4-------Saturation indices---------------------------

  Phase               SI log IAP  log KT

  Anhydrite         -1.12   -5.46   -4.34  CaSO4
  Aragonite         -0.15   -8.43   -8.28  CaCO3
  Calcite            0.01   -8.43   -8.43  CaCO3
  Celestite         -1.54   -8.16   -6.62  SrSO4
  CO2(g)            -0.36   -1.70   -1.34  CO2
  Dolomite          -0.60  -17.45  -16.85  CaMg(CO3)2
  Fe(OH)3(a)        -1.98    2.91    4.89  Fe(OH)3
  FeS(ppt)         -52.65  -56.57   -3.92  FeS
  Fluorite           0.21  -10.51  -10.73  CaF2
  Goethite           3.54    2.91   -0.63  FeOOH
  Gypsum            -0.88   -5.46   -4.58  CaSO4:2H2O
  H2(g)            -20.55  -23.66   -3.11  H2
  H2O(g)            -1.78   -0.00    1.78  H2O
  H2S(g)           -54.51  -55.40   -0.88  H2S
  Halite            -7.88   -6.32    1.56  NaCl
  Hausmannite      -24.17   39.42   63.59  Mn3O4
  Hematite           9.04    5.82   -3.22  Fe2O3
  Jarosite-K       -11.41  -19.83   -8.41  KFe3(SO4)2(OH)6
  Mackinawite      -51.92  -56.57   -4.65  FeS
  Manganite         -8.78   16.56   25.34  MnOOH
  Melanterite       -7.33   -9.67   -2.34  FeSO4:7H2O
  O2(g)            -45.66  -48.47   -2.81  O2
  Pyrite           -79.76  -98.53  -18.77  FeS2
  Pyrochroite       -8.90    6.30   15.20  Mn(OH)2
  Pyrolusite       -16.22   26.82   43.04  MnO2:H2O
  Rhodochrosite     -1.15  -12.25  -11.09  MnCO3
  Siderite          -1.81  -12.63  -10.83  FeCO3
  Strontianite      -1.85  -11.13   -9.27  SrCO3
  Sulfur           -40.00  -34.88    5.12  S

------------------
End of simulation.
------------------
```

Fig. 41: PHREEQC output file of the sampling point M3, black lines mark the border between pictures, 1 solution composition, 2 description of solution, 3 distribution of species (only a selection), 4 saturation indices.

2.9. Possible errors

The most important errors occur during direct sampling. No air should be left in the sampling vial and it should not be made out of material, which interacts with water. Therefore, it is recommended to use PE (Polyethylene)-bottles. Taking a sample with air head space will cause a change in pCO_2 and thus in pH and alkalinity. It is best to cool the samples directly or after the field work in a refrigerator. Additionally it is necessary to filter the samples to remove contamination of organic material and other solid particles directly in the field. If not filtered the sample will cause damage to the sensitive instruments in the analysis process afterwards.

To ensure high accuracies, the instruments should be calibrated before and after analysis. The quality of the entire analytical procedure can be assessed by calculating the electrical balance (compare 1.5.1 Hydrochemistry and Appendix 6).

68 % of the samples (63 ouf of 93) have an electrical balance error lower than 10 %. Thus, 30 samples have an electrical balance error higher than 10 %. 15 of these samples are cation errors (cation/anion > 1). 15 of these samples are anion errors (cation/anion < 1) (compare Fig. 42, Fig. 43 and Fig. 44).

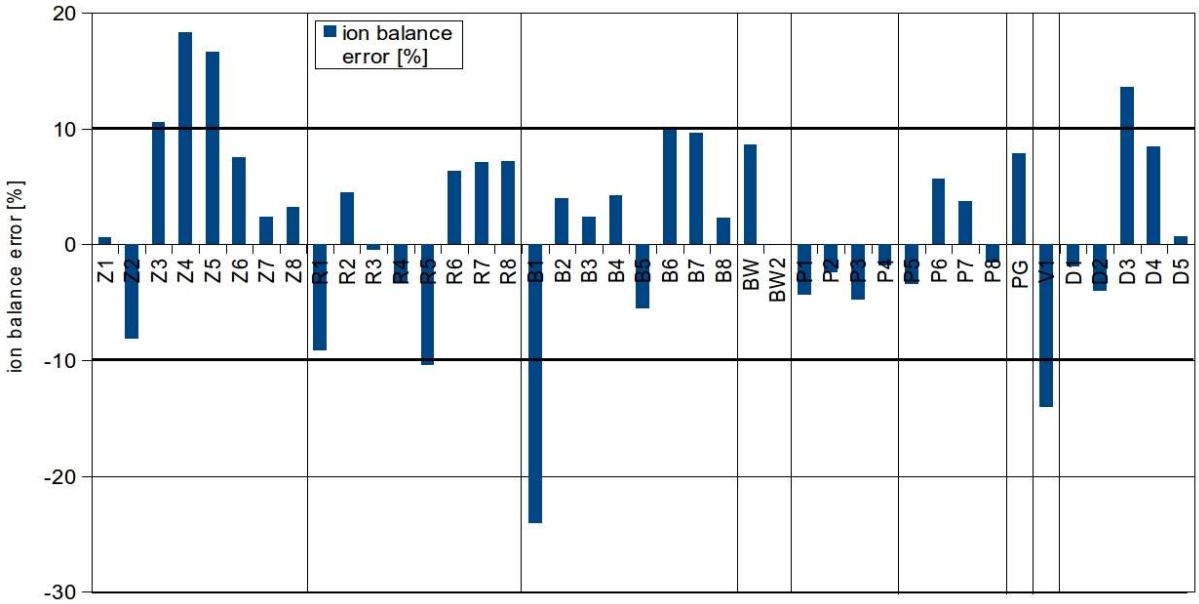

Fig. 42: Electrical ion balance error of wells and springs in *Rovte* area

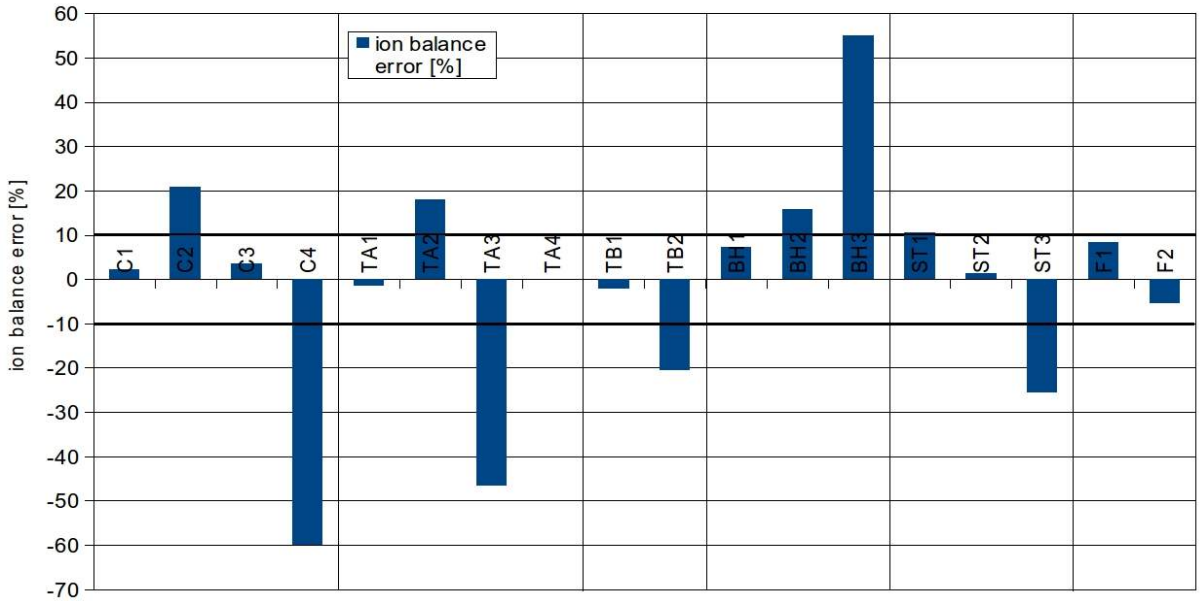

Fig. 43: Electrical ion balance error of thermal wells from *Cerkno/Kranj* area

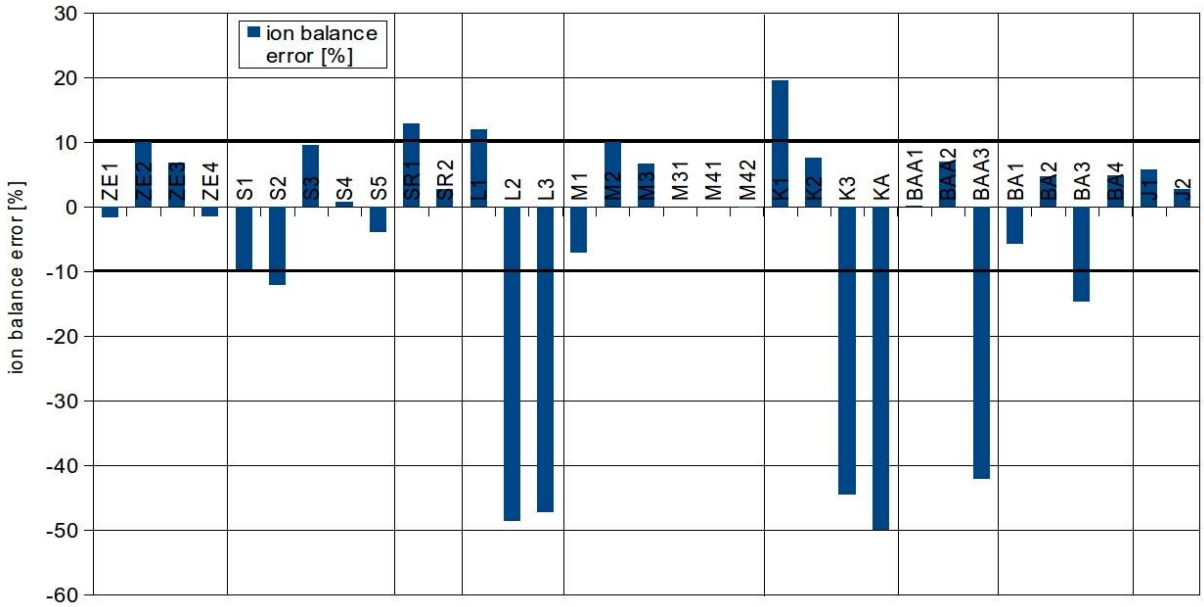

Fig. 44: Electrical ion balance error of subthermal and karstic springs from *Cerkno/Kranj* area

3. Results

3.1. Rovte

In the *Rovte* area waters from three deep wells (Z: Zavčan, R: Rodofov Mlin and B: Bizjakov Mlin), one karstic (P: Podklanec, PG: tube near Podklanec), two surface springs (V: Vrh, D: Dolenja) and one surface stream (BW: Bizjakov Mlin water) were sampled (compare Appendix 8 - 15).

Deep wells (Z, R and B)

The wells (Z, R and B) have mean temperatures of 10.1 ± 0.6 °C and a mean pH of 7.51 ±0.19. The mean electrical conductivity decreases from Z over R to B. This trend is visible in the Piper-Diagram, where the size of the symbols correspond to the total dissolved solids, which is in a close relation to the electrical conductivities (Fig. 47). Temperature, pH and the electrical conductivity remain almost constant at Z, R and B over the sampling period. Li^+, Na^+, NH_4^+, K^+, $Fe^{2+/3+}$, Sr^{2+} and Mn^{2+} concentrations of the wells range between 0.01 and 6.1 mg/l (B6, Na^+). The mean Mg^{2+} and Ca^{2+} concentrations increase and molar-Mg^{2+}/Ca^{2+}-ratios decrease from B over R to Z, which is also visible in the Piper-Diagram (Fig. 47). Sr^{2+} concentration increases from R over B to Z. The high standard deviations occur due to different Sr^{2+} concentrations at different sampling times (compare Appendix 6).

The wells show very low F^-, Br^-, NO_2^-, NO_3^- and PO_4^{3-} concentrations, which vary between 0.01 and 1.6 mg/l (Z6, Br^-). The mean Cl^- and SO_4^{2-} concentrations decrease from Z over R to B, which is also visible in the Piper-Diagram (Fig. 47) and in Fig. 45. The HCO_3^- concentrations decrease from B over Z to R. Isotope (δ^2H vs. $\delta^{18}O$) analysis shows, that the samples from Z and R are in the same range (Fig. 46, black and red circles), whereas samples from B (Fig. 46, orange

crosses) vary from the upper right corner near BW into the main clouds of Z and R. One outlier (R8) is located to lower $\delta^{18}O$ values to the left part of the diagram.

mean ± std	Z (Zavcan)	R (Rovte)	B (Bizjakov)
T [°C]	10.2 ± 0.5	9.5 ± 0.5	10.4 ± 0.4
pH	7.31 ± 0.31	7.63 ± 0.12	7.59 ± 0.11
EC [µS/cm]	1619 ± 49	782 ± 7	502 ± 25
Mg^{2+} [mg/l]	63.9 ± 6.4	40.2 ± 1.5	27.5 ± 3.8
Ca^{2+} [mg/l]	284.8 ± 11.0	101.6 ± 1.5	58.1 ± 6.1
molar-Mg^{2+}/Ca^{2+}-ratios	0.37 ± 0.03	0.65 ± 0.02	0.80 ± 0.18
Sr^{2+} [mg/l]	1.607 ± 1.375	0.592 ± 0.510	1.480 ± 2.523
Cl^- [mg/l]	1.912 ± 0.812	1.670 ± 0.257	1.139 ± 0.215
SO_4^{2-} [mg/l]	740.6 ± 65.2	273.3 ± 21.3	68.5 ± 28.4
HCO_3^- [mg/l]	180.8 ± 6.8	163.6 ± 7.7	235.2 ± 9.1

Table 12: Hydrochemical analyses (mean ± std) of deep wells in the *Rovte* area.

Springs (P, PG, V and D) and surface stream (BW)

BW has the highest temperature, followed by PG and V. P and D show the lowest mean temperatures. BW has the highest pH. P, PG, V and D have almost equal mean pH. PG shows the highest electrical conductivity. BW, P and V shows almost equal electrical conductivities. D shows the lowest mean electrical conductivity. Li^+, Na^+, NH_4^+, K^+, $Fe^{2+/3+}$, Sr^{2+}- and Mn^{2+} concentrations of the springs and surface stream range between 0.02 and 2.7 mg/l (D3, Na^+). BW, P and PG show the highest, V and D the lowest mean Mg^{2+} concentrations. V and D show the highest and BW, P and PG show the lowest mean Ca^{2+} concentrations. BW, P, and PG show the highest molar-Mg^{2+}/Ca^{2+}-ratios. V and D show the lowest mean molar-Mg^{2+}/Ca^{2+}-ratios (Fig. 48 and Table 13).

The springs and the surface stream show very low F^-, Br^-, NO_2^-, and PO_4^{3-} concentrations, which vary between 0.01 and 1.396 mg/l (PG, Br^-). The springs and the surface stream show very high Cl^- and NO_3^- concentrations compared to the wells (Fig. 45). Vice versa, the springs and surface stream show very low SO_4^{2-} concentrations (Fig. 45 and Fig. 47). BW, P and PG show almost equal mean

HCO_3^- concentrations. V shows the highest and D the lowest mean HCO_3^- concentrations (Table 13).

mean ± std	P	PG	V	D	BW
T [°C]	9.0 ± 0.5	12.4	10.3	8.8 ± 0.1	15.3
pH	7.87 ± 0.12	7.67	7.86	7.39 ± 0.19	8.48
EC [µS/cm]	370 ± 42	407	496	356 ± 6	390
Mg^{2+} [mg/l]	19.2 ± 4.2	23.8	8.9	10.2 ± 0.8	24
Ca^{2+} [mg/l]	47.6 ± 3.9	50.5	69.7	56.0 ± 0.9	48.6
molar-Mg^{2+}/Ca^{2+}-ratios	0.66 ± 0.1	0.78	0.21	0.30 ± 0.02	0.81
HCO_3^- [mg/l]	233.8 ± 27.9	241.6	270.2	199.2 ± 11.2	236.7

Table 13: Hydrochemical analyses (mean ± std) of karstic springs and subsurface waters in the *Rovte* area.

Hydrochemical and isotopic considerations

From a hydrochemical point of view the waters of well Z should discharge from a geological layer with intercalated gypsum or anhydrite, due to the fact that the waters from well Z are sulfate type Ca^{2+}-waters. B has higher HCO_3^- concentrations than Z and R. Therefore, waters from B discharge from a geological layer with less gypsum or anhydrite and more dolomite or limestone. The waters from well R are bicarbonate type Ca^{2+}-waters. The waters from R have less SO_4^{2-} and Ca^{2+} concentrations compared to Z. Therefore, waters from R discharge from both gypsum and anhydrite and dolomite or limestone layers (Fig. 6, Fig. 47 and Table 12). Waters from Z, R and B have low Cl^-, NO_3^- and PO_4^{3-} concentrations, showing that the waters are not contaminated with fertilisers or road salt (Fig. 45).

According to Mihevc (2005) origin of sulphur from well R is probably in layers of *Lower Triassic* gypsum that were intersected by the borehole, supporting the expectation of underlying gypsum in the underground of *Rovte*. Additionally, the saturation indices show that Z and R are undersaturated with respect to anhydrite, gypsum and dolomite and oversaturated with respect to calcite. This

indicates the possible dedolomitisation reaction in the underground at Z and R (compare 3.2.3. Precipitation of calcite and dissolution of dolomite).

One recharge area of the waters from R is the area around the mountain Vrh Trh northeast of the borehole R. The water flows into the underground and upward along the fault or the borehole (compare Fig. 5). Another hydrogeological origin of waters from Z and R is the *Norian stage* grey stratified dolomite aquifer below the *Carboniferous* or *Permian* black clay shale aquiclude and the nappe boundary (compare Fig. 6 and Fig. 8). The waters from Z and R discharge from both Mt. Vrh Trh and the *Norian stage* dolomite aquifer. This can be concluded from the isotope data (Fig. 46), because waters from Z and R have no large variation.

B shows a bigger variation of the isotope data compared to Z and R. Because of that, waters from B are mixed with meteoric waters from the subsurface. Therefore, B had a short residence time in the underground. All measured isotopes are above the GMWL and correlate to the LMWL of Mt. Velebit in Croatia.

Furthermore, P and D are temporarily in the same range as the wells (Z, R and B), but vary in a wide range from higher δ^2H and $\delta^{18}O$ to lower δ^2H and $\delta^{18}O$. BW and BW2 are located in the upper right corner and V in the lower left corner of the diagram. δ^2H and $\delta^{18}O$ of the wells Z and R are in the same range, except B and the other surface springs, which have large variations.

The waters from P, PG and D are bicarbonate type Ca-waters (Fig. 47). Waters from P originate from the karstic plateau in the SW, which is mostly build up of dolomite and dolomitic and variegated conglomerate (compare Appendix 12). Isotope data from P (Fig. 46) support the origin from the plateau in the SW, because P shows a large hydrochemical and isotopic variation compared to Z or R. PG shows similar values compared to P, due to the fact that PG is used for water supply for households from the spring P. Only the temperature from PG is higher, because the water is heated up in a tube on the way to the household.

The waters from V and D show high Cl^-, NO_3^- and PO_4^{3-} concentrations (Fig. 45). Additionally, D shows isotope variations compared to Z and R (Fig. 46). Because of that, one can expect that the waters from V and D are surface run-off waters, that are contaminated with fertilisers and/or road salt from the last winter.

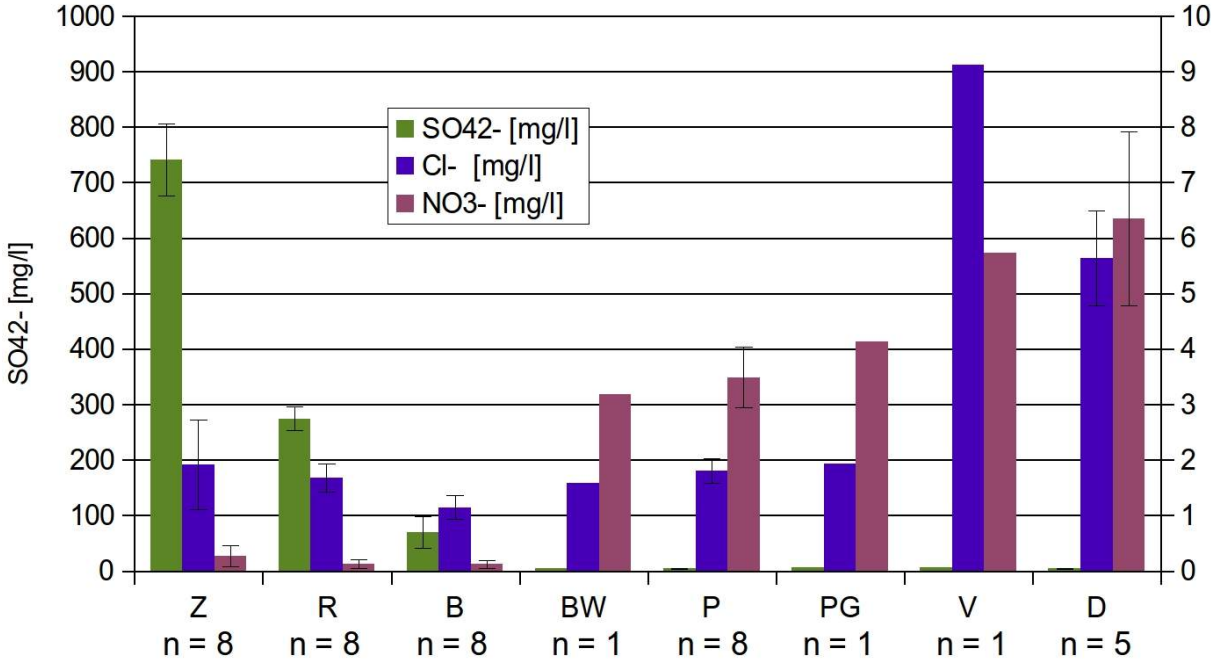

Fig. 45: Mean and standard deviation of SO_4^{2-}, Cl^- and NO_3^- concentrations from wells and springs in the *Rovte* area.

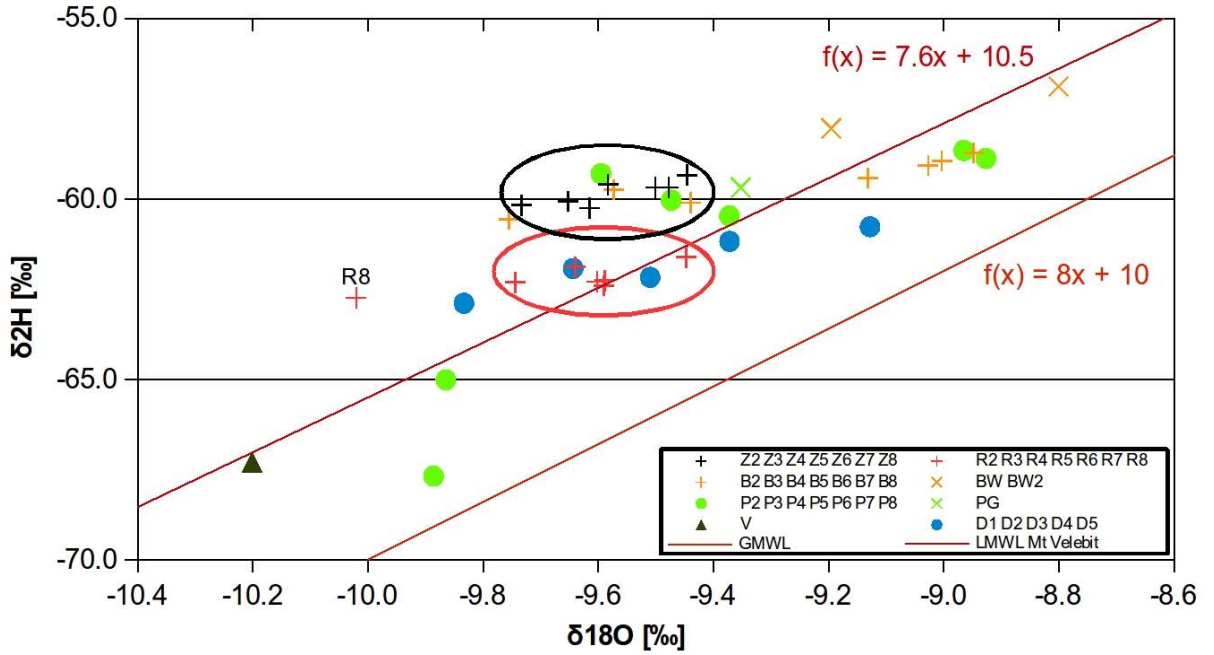

Fig. 46: Isotopes (δ^2H vs. $\delta^{18}O$) of deep wells and springs in the *Rovte* area.

3.2. Dedolomitisation in the Rovte area

One purpose of this work is to find arguments for an ongoing process of dedolomitisation in the underground of the *Rovte* area. For this purpose, former publications dealing with the process of dedolomitisation (compare 1.5.2. Dolomitisation and dedolomitisation) were investigated. In these publications, hydrochemical dependencies for dedolomitisation were found. In the following chapters possible dependencies based on the measured data from the *Rovte* area are presented.

3.2.1. Trend in the Piper-Diagram

Hanshaw & Back (1979), Back et al. (1983) and Bischoff et al. (1994) showed a specific trend in the Piper-Diagram (Fig. 28) for the dedolomitisation reaction. A similiar evolution of waters (Fig. 28) can be observed in the Piper-Diagram of the *Rovte* area (Fig. 47). Therefore, one can expect that Z and R recharge from the same aquifer, which intercalate with gypsum.

From the data displayed in the Piper-Diagram (Fig. 47) three trends can be deduced: 1. from lower to higher SO_4^{2-} concentration, 2. from higher to lower total alkalinity and 3. from molar-Mg^{2+}/Ca^{2+}-ratios lower than 1 to molar-Mg^{2+}/Ca^{2+}-ratios of almost 1. The last trend is also the third argument for dedolomitisation, which is a preferential removing of Mg^{2+} as indicated by a molar-Mg^{2+}/Ca^{2+}-ratio less than 1.

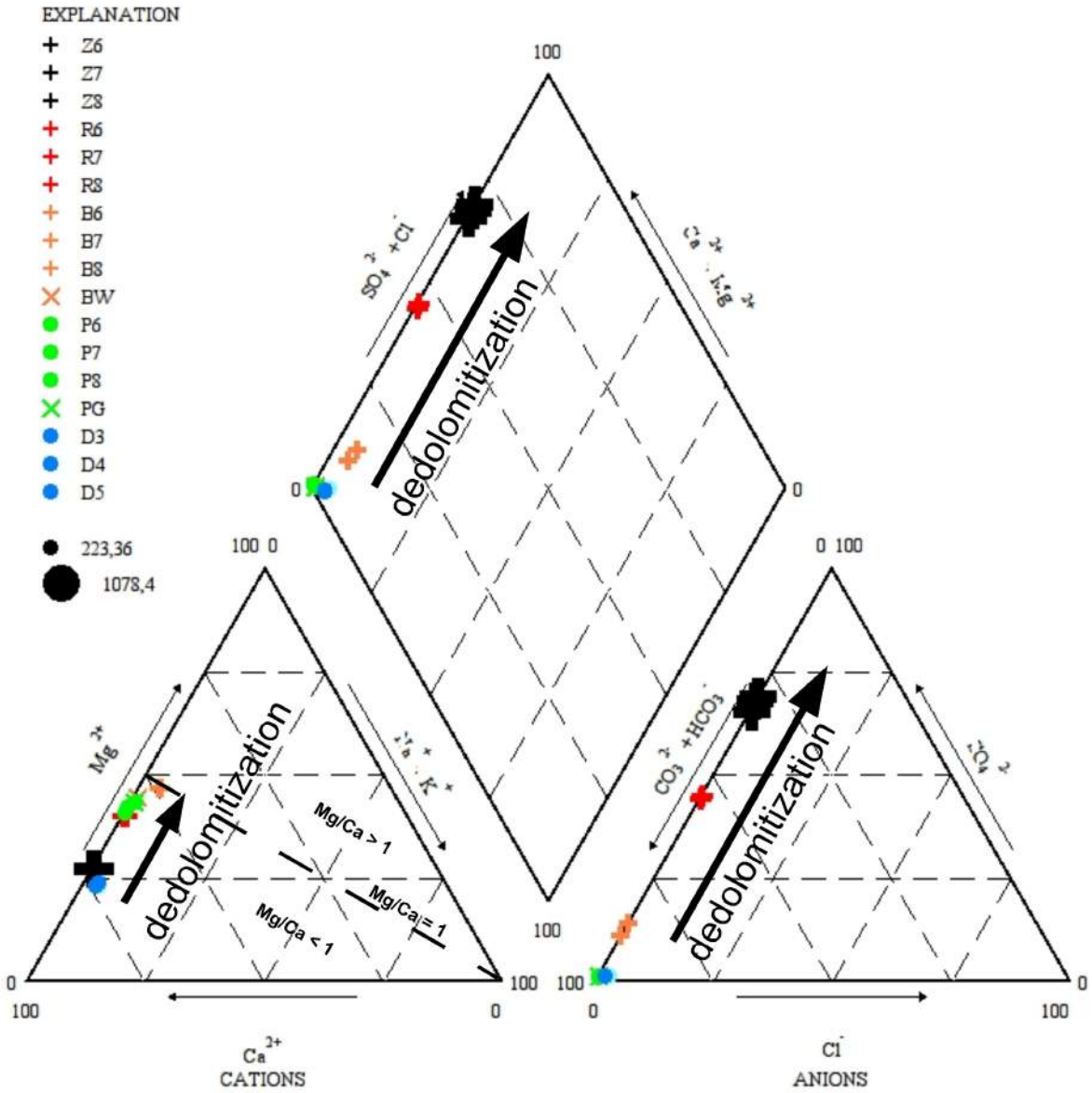

Fig. 47: Hydrochemistry (Piper diagram) of deep wells (Z, R and B) and springs (P, PG and D) in *Rovte* area, size of symbols correspond to total dissolved solids.

3.2.2. Mg^{2+}/Ca^{2+}-ratio

Another argument for the process of dedolomitisation is the Mg^{2+}/Ca^{2+}-ratio. Back et al. (1983) (compare 1.5.2. Dolomitisation and dedolomitisation) showed the significance of the Mg^{2+}/Ca^{2+}-ratio for the dedolomitisation reaction. Fig. 48 shows that the mean molar-Mg^{2+}/Ca^{2+}-ratio is less than 1 in every sample. Z, V

and D show the lowest mean molar-Mg^{2+}/Ca^{2+}-ratio. B, BW and PG show slightly higher mean molar-Mg^{2+}/Ca^{2+}-ratios compared to R and P. Z, R and D show no significant variation, whereas B and P have a large variation compared to the other sampling points. The mean molar-Mg^{2+}/Ca^{2+}-ratio increases from Z to R to B. This trend is also visible in the Piper-Diagram (Fig. 47). Therefore, the intercalated gypsum in the underground of *Rovte* (compare 1.3.2. Geology at Rovte area) provides an abundant supply of Ca^{2+} to the system and thus maintains a molar-Mg^{2+}/Ca^{2+}-ratio less than 1.

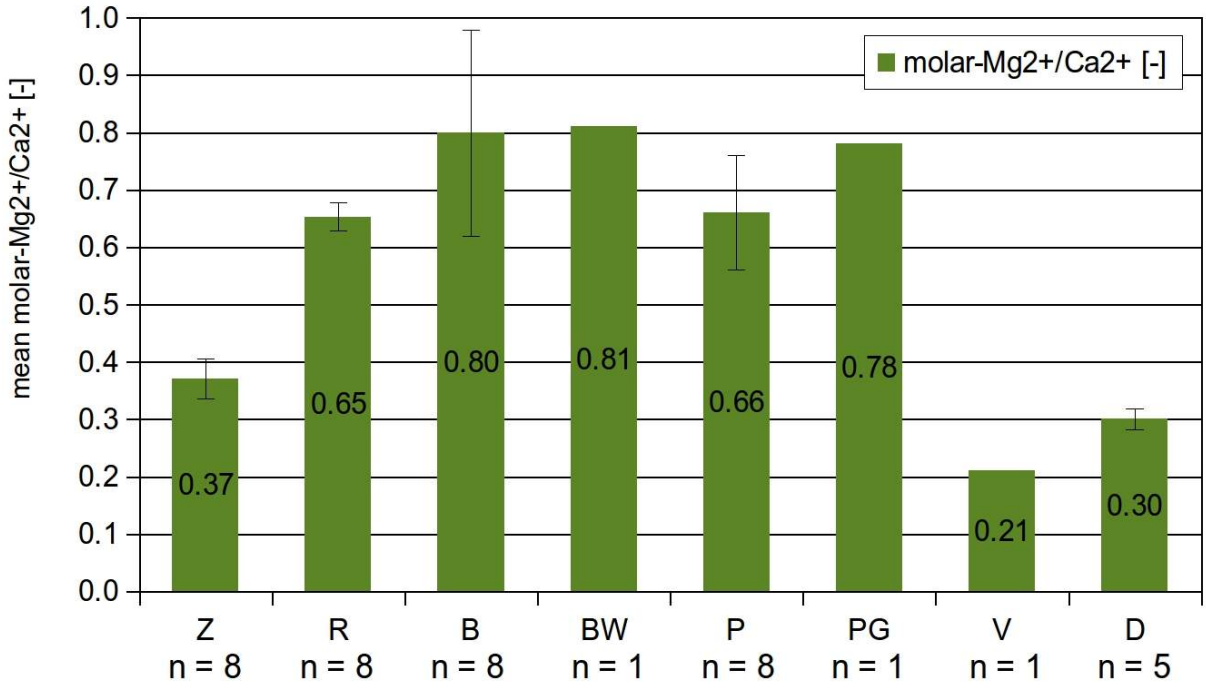

Fig. 48: Mean molar-Mg^{2+}/Ca^{2+}-ratios from wells and springs in the *Rovte* area.

3.2.3. Precipitation of calcite and dissolution of dolomite

Calculated saturation indices show an undersaturation with respect to gypsum and anhydrite (decreasing from Z to R to B, Fig. 49). BW, P, PG, V and D have the lowest SI gypsum and SI anhydrite.

If an uncertainty range of ± 0.5 is considered for the saturation indices for dolomite and calcite (Fig. 50), then the waters from the sampling points Z, R and B are in equilibrium with dolomite and calcite.

If the uncertainty range of ± 0.5 is neglected for the saturation indices, the waters from Z, R and B are undersaturated with respect to dolomite. SI dolomite is increasing from Z to R to B. At the same time the samples are oversaturated with respect to calcite, decreasing from Z to R to B (Fig. 49 and Fig. 50). Therefore, calcite could precipitate and dolomite could dissolve. This case Back et al. (1983) described for the process of dedolomitisation.

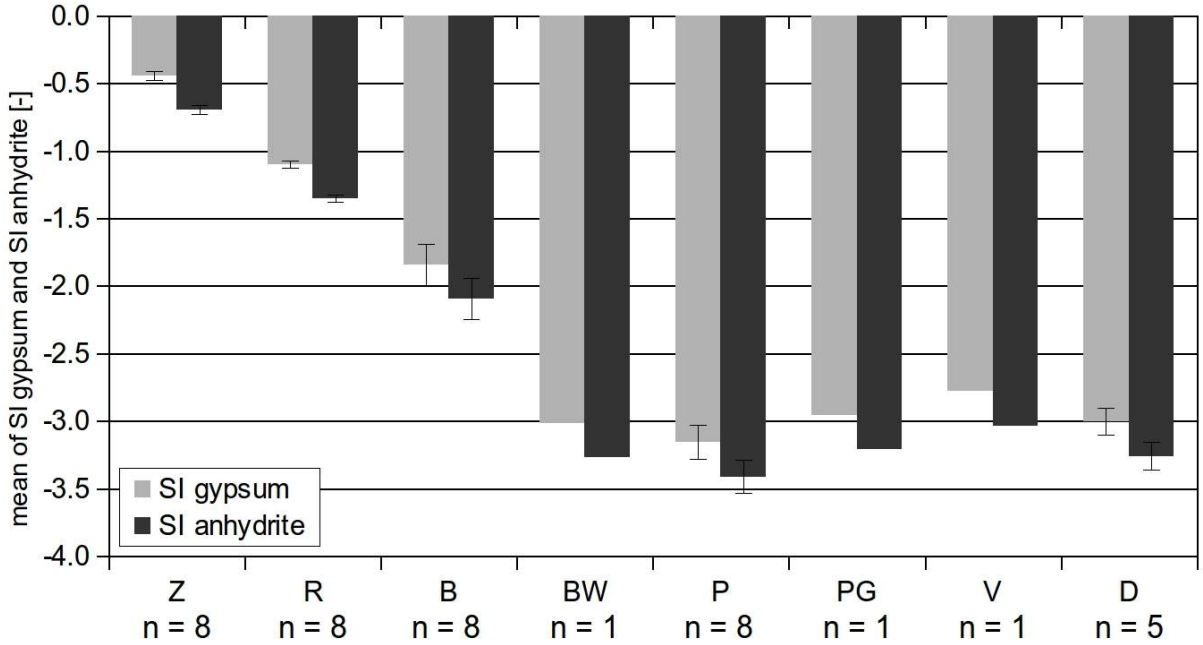

Fig. 49: Mean with standard deviation of the SI gypsum and SI anhydrite from wells and springs in the *Rovte* area.

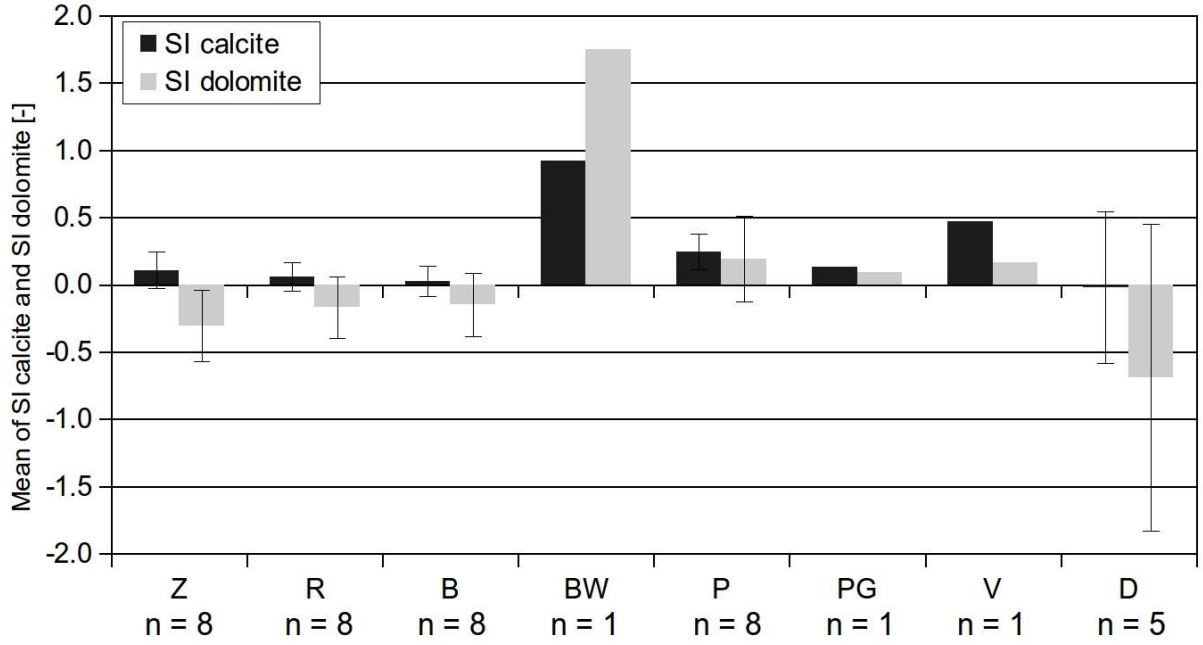

Fig. 50: Mean with standard deviation of the SI calcite and SI dolomite from wells and springs in the *Rovte* area, note the high saturation indices of calcite and dolomite from BW (due to the outgassing of CO_2).

3.2.4. Correlation between pH and SO_4^{2-} concentration

Back et al. (1983) showed from field measurements that pH decreases with increasing SO_4^{2-} concentration (Fig. 24), indicating dedolomitisation. The coefficient of determination for pH and SO_4^{2-} concentration is 0.53 including all three sampling points and much lower for each sampling points (almost 0.00 for B, 0.20 for Z and 0.24 for R) (Fig. 51). The t-Test for the correlation between pH and SO_4^{2-} concentration shows a positive relation, because the calculated test value 4.0 is higher than the comparitive value 2.5 (f =22, P = 98%). Thus, a relation between pH and SO_4^{2-} concentration exists.

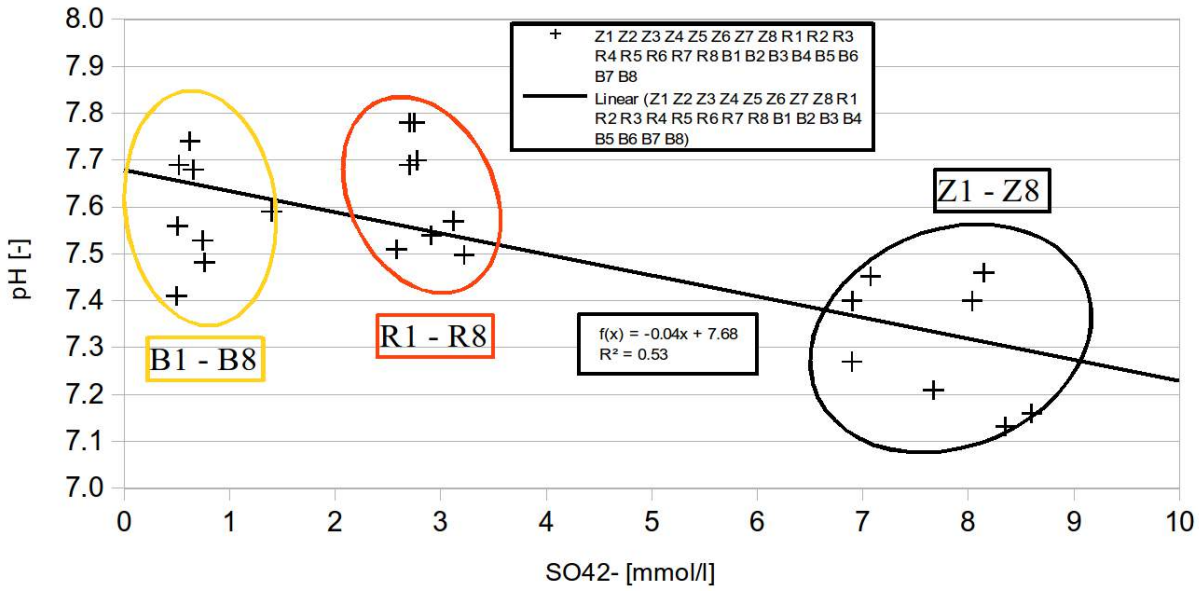

Fig. 51: pH vs. SO_4^{2-} concentration with linear regression line and coefficient of correlation (R^2), data from *Rovte* area (Z, R and B).

3.2.5. Correlation between SI gypsum and SO_4^{2-} concentration

The diagram for SI gypsum vs. SO_4^{2-} concentration (Fig. 52) shows a coefficient of determination of 0.99 for all three sampling points Z, R and B. In Fig. 53 and Fig. 52 the SI gypsum, SI anhydrite and SI calcite increase with increasing SO_4^{2-} concentration (from B to R to Z) and SI dolomite decreases with increasing SO_4^{2-} concentration (from B to R to Z). Therefore, all three sampling points are slightly oversaturated with respect to calcite, which is expected under conditions of

dedolomitisation necessary to cause precipitation of calcite (Plummer et al., 1990).

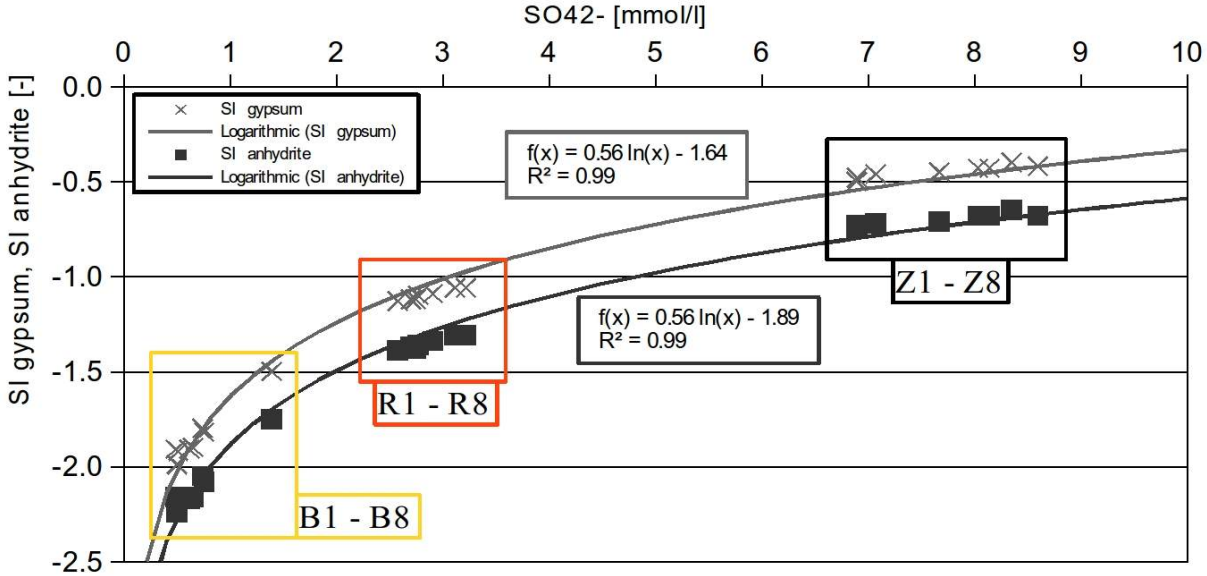

Fig. 52: SI gypsum vs. SO_4^{2-} and SI anhydrite vs. SO_4^{2-} with logarithmic regression line, data from *Rovte* area (Z, R and B).

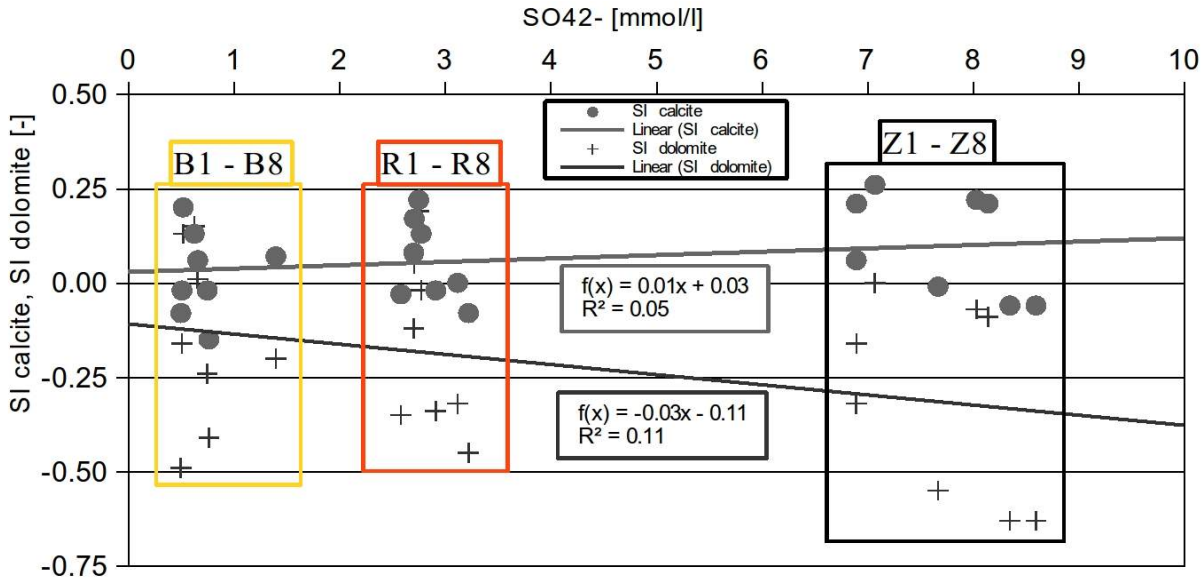

Fig. 53: SI calcite vs. SO_4^{2-} and SI dolomite vs. SO_4^{2-} with logarithmic regression line (Datenreihe), data from *Rovte* area (Z, R and B).

3.2.6. Trend in total alkalinity and SO_4^{2-} concentration

Plummer et al. (1990) also showed that two trends in total alkalinity as a function of dissolved SO_4^{2-} concentration exists (compare Fig. 29). If the measured data (Fig. 54) are plotted similar to the diagram described above (Fig. 29), one can detect the same trend of the dedolomitisation reaction from higher to lower CO_3^{2-} concentration with increasing SO_4^{2-} concentration.

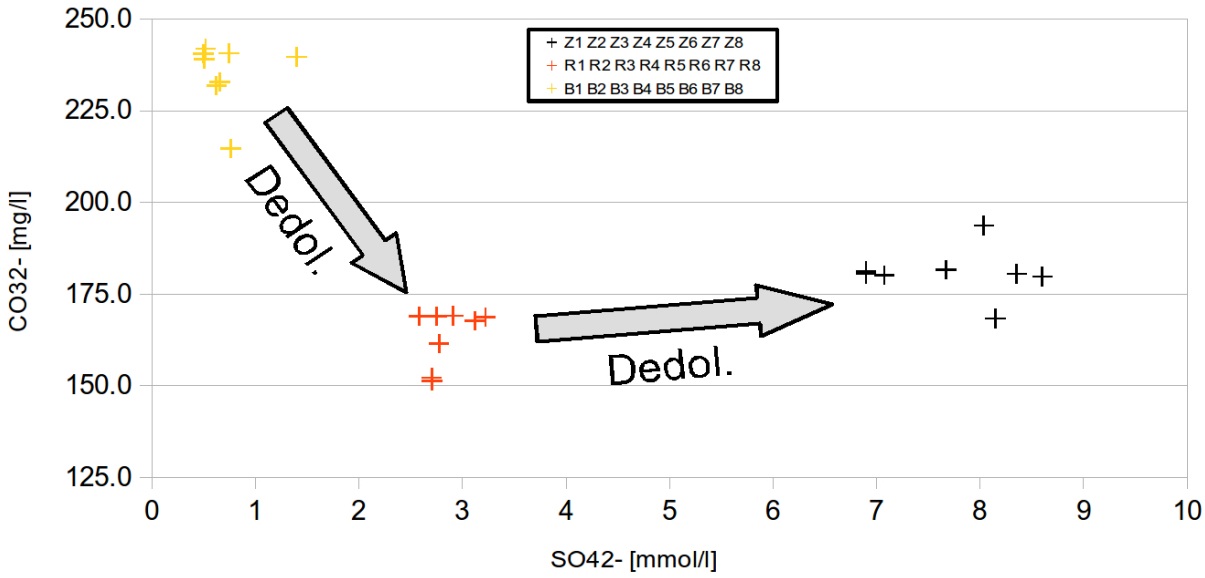

Fig. 54: Diagram of CO_3^{2-} vs. SO_4^{2-} concentration with sampling points Z, R and B.

3.2.7. Correlation between Ca^{2+}, Mg^{2+} and SO_4^{2-} concentration

Cardenal et al. (1994) observed a correlation between Ca^{2+} and SO_4^{2-} concentration and Mg^{2+} and SO_4^{2-} concentration in the case of the chemical evolution of groundwater in Triassic gypsum-bearing carbonate aquifers in southern Spain (Fig. 25). The measured data also show a correlation (R^2=0.90) between Mg^{2+} and SO_4^{2-} concentration (Fig. 55) and a correlation (R^2=0.97) between Ca^{2+} and SO_4^{2-} concentration (Fig. 56).

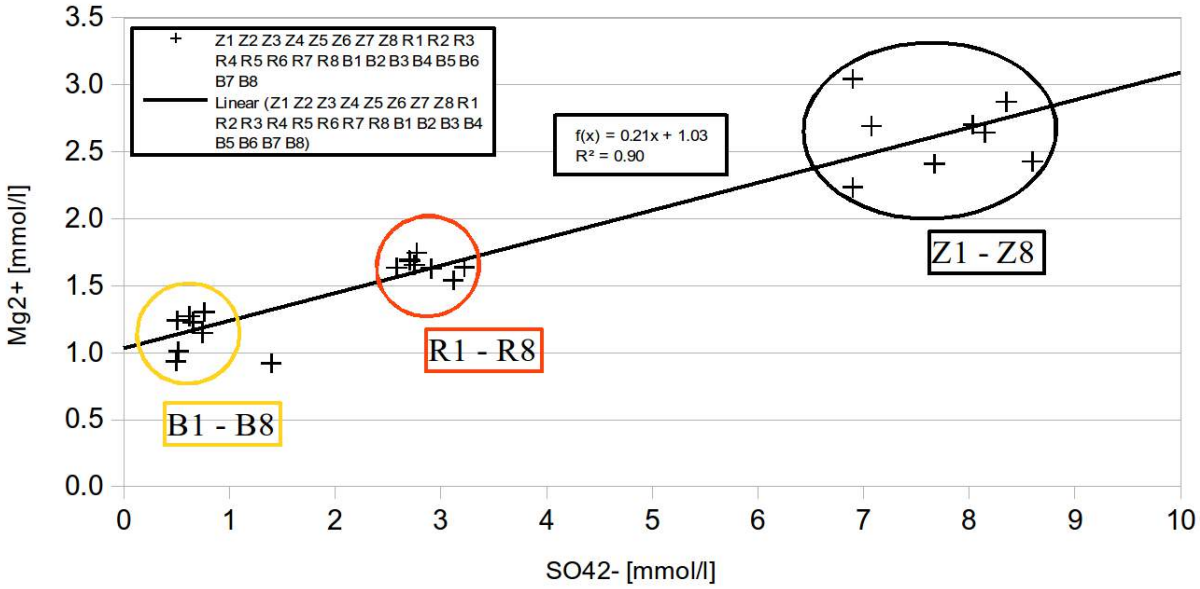

Fig. 55: Diagram of the Mg^{2+} vs. SO_4^{2-} concentration from measured data in the *Rovte* area (B, R and Z).

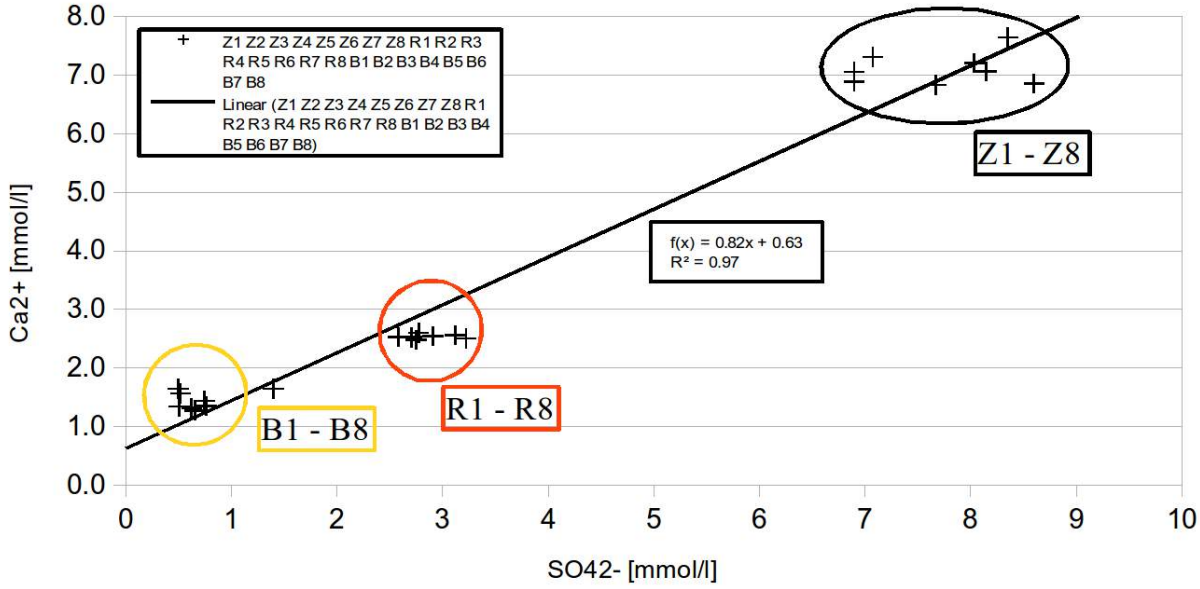

Fig. 56: Diagram of the Ca^{2+} vs. SO_4^{2-} concentration from measured data in the *Rovte* area (B, R and Z).

3.2.8. Stabilisation or slight fall of alkalinity

Cardenal et al. (1994) observed that the dedolomitisation trend is marked by stabilisation or even slight fall in the alkalinity (Fig. 26). Z and R show lower

alkalinity compared to B and P. Furthermore, Ca^{2+} concentration is higher than the Mg^{2+} concentration only at the wells Z and R. Therefore, the specific trend of stabilised or even fall of alkalinity occurs at the wells Z and R (Fig. 57).

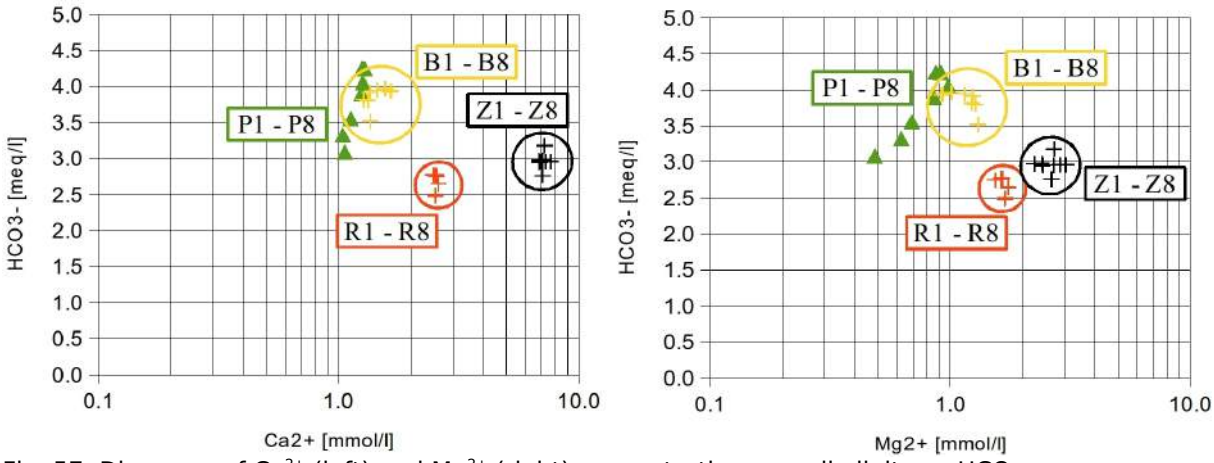

Fig. 57: Diagrams of Ca^{2+} (left) and Mg^{2+} (right) concentrations vs. alkalinity as HCO_3^-

Furthermore, Cardenal et al. (1994) distinguished two groups (Fig. 27) in their sampling campaign. One group, showing an inverse relation of HCO_3^- and pH and another group, showing a significantly progressed dedolomitisation. The comparison of the data from *Rovte* area with the data from Cardenal et al. (1994) reveals that our data shows no specific groups. Thus, it is an argument against dedolomitisation.

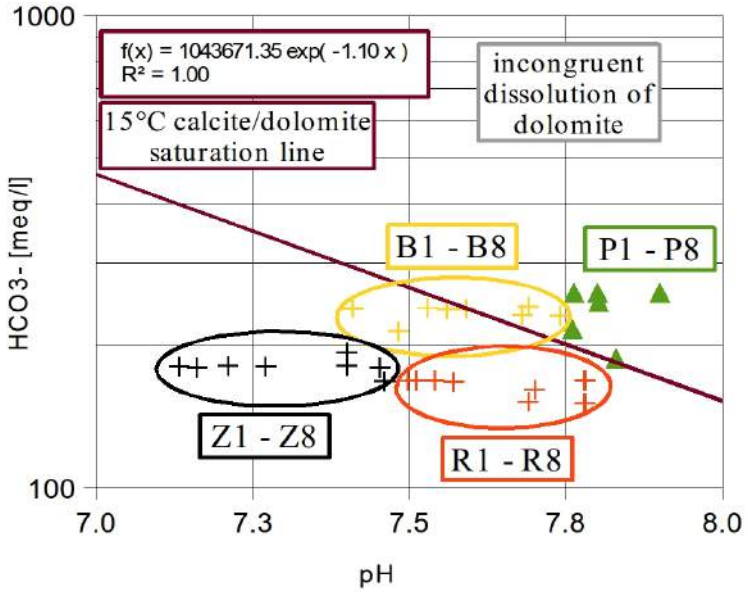

Fig. 58: Diagram of HCO_3^- concentration vs. pH with the 15°C calcite/dolomite saturation line

3.3. Cerkno/Kranj

In the *Cerkno/Kranj* area, waters from five deep and thermal wells (C: *Cerkno* Hotel, T: Kopačnica (Hotavlje), BH: Bled Hotel, ST: Spodnje Pirniče, F: Furnalove), eight (partly thermal) springs (ZE: above Žveplenica, S: Žveplenica, L: Lipnica, M: Mans power, K: Kroparica, BAA: Zgornja Besnica A, BA: Zgornja Besnica, J: Divje Jezero), and one surface stream (SR: Žveplenica river) were sampled (compare Appendix 16 - 29).

The wells were drilled for geothermal exploration and heating/cooling utilisation. The springs are partly karstic. Almost all waters in the *Kranj/Cerkno* area are Ca^{2+}-Mg^{2+}-HCO_3^--type waters (Fig. 59 and Fig. 62). Only BA and C show two outliers with higher Cl^- concentrations. This is also visible in the Piper-Diagram (Fig. 59) and in the Cl^- concentration diagrams (Fig. 60 and Fig. 64).

3.3.1. Deep and thermal wells

The thermal wells C, TB, BH and F have almost equal mean outflow temperatures, followed by TA and ST. C has the highest mean pH, followed by TA, TB, ST and F with almost equal mean pH. BH has the lowest mean pH. BH has the highest mean electrical conductivity, followed by F. TA, TB and ST have almost equal mean electrical conductivities. C has the lowest mean electrical conductivity. Li^+, NH_4^+, K^+, $Fe^{2+/3+}$, Sr^{2+} and Mn^{2+} concentrations of the thermal wells range between 0.0 and 1.372 mg/l (TB, K^+). BH and ST have the highest, C, TB and F moderate and TA the lowest mean Na^+ concentrations. All thermal wells have constant Na^+ concentrations (e. g. Fig. 63). BH and F have the highest mean Mg^{2+} concentrations. TA, TB and ST have moderate and almost equal mean Mg^{2+} concentrations. C has the lowest mean Mg^{2+} concentrations. BH has the highest mean Ca^{2+} concentrations. ST and F have moderate and almost equal mean Ca^{2+} concentrations. TA and TB have slightly lower mean Ca^{2+} concentrations than ST and F. C has the lowest mean Ca^{2+} concentrations. TA, TB and F have the highest mean molar-Mg^{2+}/Ca^{2+}-ratios, followed by ST. C and BH have the lowest mean molar-Mg^{2+}/Ca^{2+}-ratios.

The thermal wells have very low F^-, Br^-, NO_2^-, NO_3^- and PO_4^{3-} concentrations, which vary between 0.01 and 1.804 ± 0.046 mg/l (TA, NO_3^-), except C with a mean F^- concentration of 3.367± 0.012 mg/l and ST with a mean NO_3^- concentration of 4.435 ± 0.178 mg/l. Almost all thermal wells have low Cl^- concentrations, only C shows one high Cl^- concentration at the sampling date 24.06.2014 (C4, Fig. 60). This is also visible in the Piper-Diagram (Fig. 59): one of the brown crosses of C is an outlier in direction of higher SO_4^{2-} and Cl^- concentrations. BH and F have the highest mean SO_4^{2-} concentrations, followed by TB. C and TA have slightly lower mean SO_4^{2-} concentrations than TB. ST has the lowest mean SO_4^{2-} concentrations. BH has the highest, F, ST, TA and TB moderate, and C has the lowest mean HCO_3^- concentrations (Table 14).

Isotope (δ^2H vs. $\delta^{18}O$) analysis (Fig. 61) shows, that the samples of T, ST, F and two samples of C are in the same range. The samples from BH have lower δ^2H and $\delta^{18}O$ values. Almost all samples are near to the LMWL, except four outliers (BH1, ST1, C1 and C2).

mean ± std	**C**	**TA**	**TB**	**BH**	**ST**	**F**
T [°C]	24.3 ± 3.5	20.4 ± 0.0	23 ± 0.1	23.1 ±1.0	20.3 ± 0.1	23.9 ± 0.1
pH	8.03 ± 0.08	7.61 ± 0.16	7.63 ± 0.23	6.86 ± 0.07	7.50 ± 0.18	7.76 ± 0.11
EC [µS/cm]	284 ± 3	325 ± 6	323 ± 9	915 ± 41	336 ± 50	442 ± 12
Na^+ [mg/l]	1.882 ± 0.034	0.858 ± 0.106	1.337	5.657 ± 0.482	2.466 ± 0.508	1.135 ± 0.198
Mg^{2+} [mg/l]	16.5 ± 0.2	19.7 ± 0.7	18.8 ± 0.5	38.7 ± 1.3	20.4 ± 0.4	27.1 ± 0.1
Ca^{2+} [mg/l]	30.6 ± 0.5	36.1 ± 0.9	35.3 ± 1.7	142.1 ± 3.6	44.2 ± 0.3	50.4 ± 0.1
molar-Mg^{2+}/Ca^{2+}-ratios	0.54 ± 0.1	0.90 ± 0.05	0.89 ± 0.06	0.45 ± 0.0	0.76 ± 0.02	0.89 ± 0.1
Cl^- [mg/l]	17.522 ± 33.016	0.956 ± 0.276	0.844 ± 0.419	1.657 ± 0.164	1.868 ± 0.235	1.064 ± 0.006
SO_4^{2-} [mg/l]	13.3 ± 0.8	11.5 ± 0.6	19.9± 0.7	29.5± 4.1	4.5 ± 0.5	25.6± 6.2
HCO_3^- [mg/l]	144.5 ± 13.8	182.7 ± 13.1	176.8 ± 5.1	553.9 ± 38.7	212.3 ± 2.5	254.4 ± 19.9

Table 14: Hydrochemical analyses (mean ± std) of thermal wells in the *Kranj/Cerkno* area.

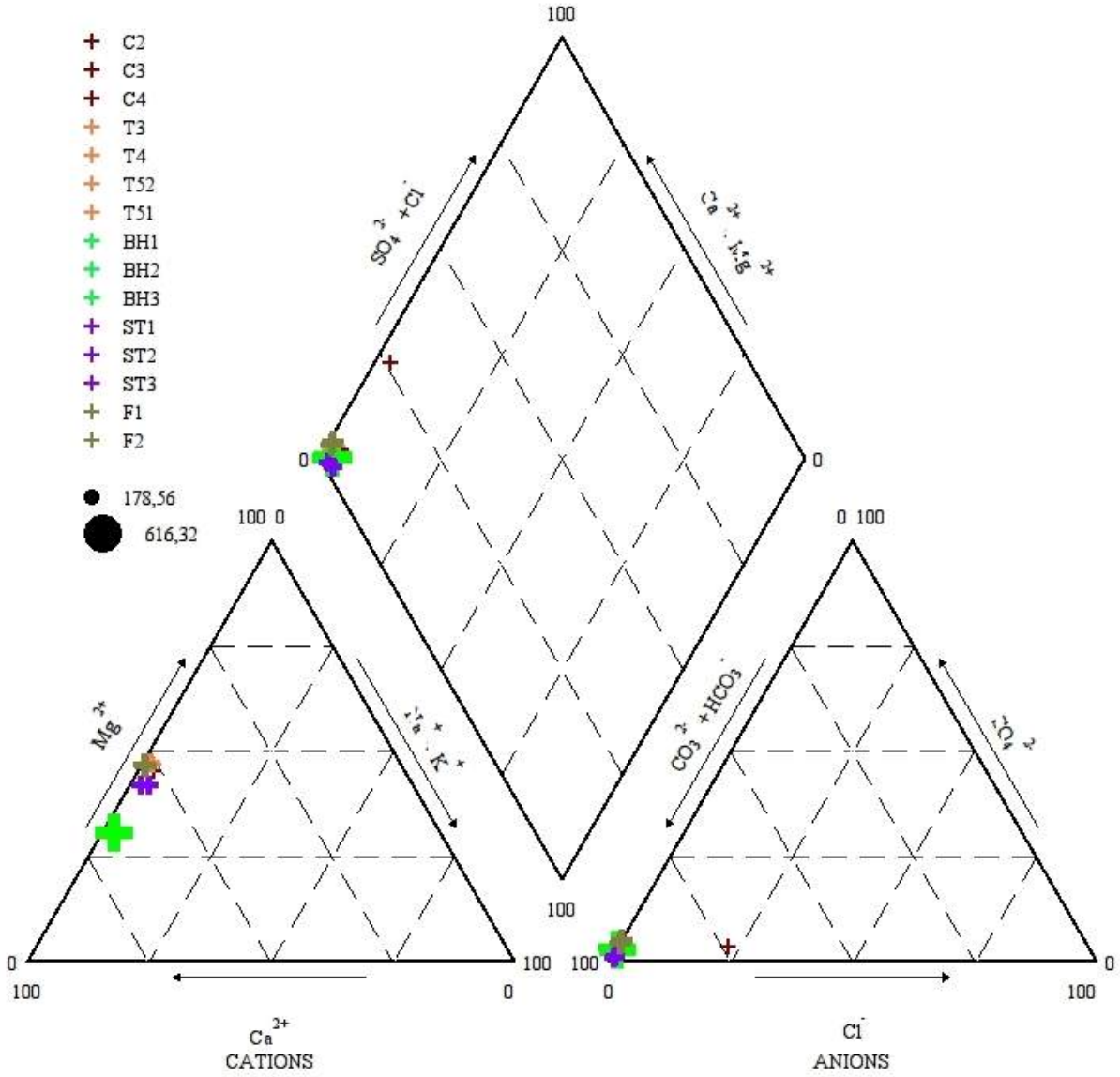

Fig. 59: Hydrochemistry (Piper diagram) of deep, thermal wells (C, T, BH, ST and F) in *Kranj/Cerkno* area.

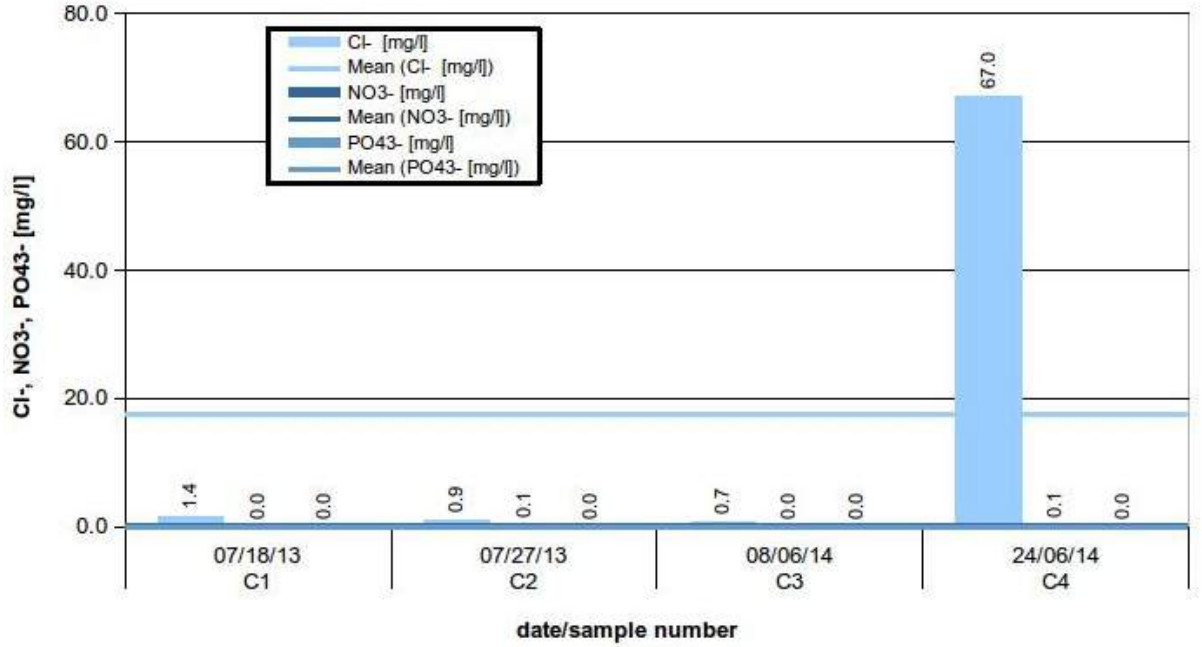

Fig. 60: Cl^-, NO_3^- and PO_4^{3-} concentrations of thermal deep well C.

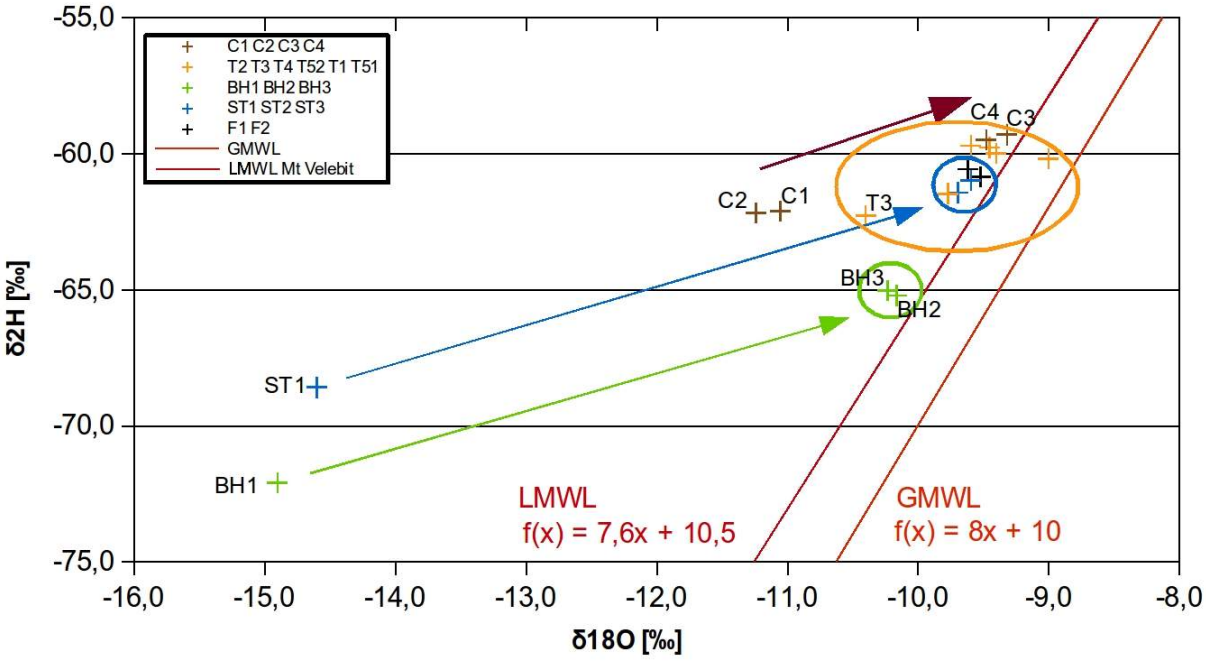

Fig. 61: Isotopes (δ^2H vs. $\delta^{18}O$) of deep and thermal wells (C, T, BH, ST and F) in *Kranj/Cerkno* area, outliers are BH1, ST1, C1 and C2.

Waters from **C and T** (TA and TB) show nearly the same values and concentrations (Appendix 6). Therefore, C and T (probably) discharge from the same aquifer, namely the *Malmian* limestone and to a lesser degree to *Upper*

Triassic Hauptdolomit (compare Fig. 15, Fig. 16 and Appendix 2). Only the temperature and pH is higher and electrical conductivity, Mg^{2+}, Ca^{2+} and HCO_3^- concentration are lower at C compared to T. The NO_3^- concentration is higher at TA compared to TB. The higher NO_3^- concentration at TA occurs because the water is filtered by the Kopačnica spa for balneologic usage. That is why two points were sampled, namely TA and TB (see Appendix 17).

Due to a heavy precipitation event in the time from 24. to 26.06.2014 in NW-Slovenia (Fig. 67) and the concurrent high Cl^- and Na^+ concentrations at C and BA, a hydraulic connection between C and BA could be possible. Due to the high Cl^- and Na^+ concentrations during the heavy precipitation event (Fig. 67), one can expect that stagnant high-ionised water was moved from the karstic basins to fast flowing areas and finally to the borehole C and the spring BA. Another explanation for the higher Na^+ and Cl^- concentrations are intercalated salt layers in the underground of the borehole C or a small footprint of anthropogenic road salt from the mount Blegoš range (Fig. 16).

Waters from **BH** discharge from the same aquifer as L does and is mixed with subsurface water, because $\delta^{18}O$ and $\delta^{2}H$ data (and especially the outliers) from BH and L are almost in the same range (compare Fig. 61 and Fig. 65).

In 1972 three reconnaissance boreholes were drilled at BH, revealing that the thermal water rises from the depth along the contact of *Triassic* dolomite and impervious *Tertiary* marl in a fault of NW-SE direction (Nosan (1973) (compare Appendix 18). Nosan (1973) showed, that the temperature is for 2.6°C lower than the temperature of the spring during the extremely arid summer of 1971. Because of that it can be assumed that the thermal water is mixed with cold groundwater in the shallow zone before rising to the surface (Nosan, 1973).

F is a borehole near the city of Vrhnika (Appendix 20). The exploitation for the leather industry (industrial process heating) from the company Siliko has been interrupted since 2009 in Vrhnika (Rajver et al., 2013). According to Lapanje & Rman (2009) waters from F are bicarbonate type Ca^{2+}-Mg^{2+}-waters and have a temperature of 24°C.

3.3.2. Karstic and (partly) subthermal springs

The subthermal springs M and BA have the highest mean temperatures in the group of springs. The karstic springs J, BAA, ZE and S have moderate mean temperatures, and L and K have the lowest mean temperatures. The temperature of the surface stream SR is higher than the temperature of the subthermal springs M and BA. SR has the highest mean pH. L and K have almost equal mean pH. ZE, S, BAA and BA have also almost equal mean pH, but slightly lower than L and K. M has the lowest mean pH. M has the highest electrical conductivity, ZE, S and BA moderate, SR, L, K, BAA and J the lowest mean electrical conductivities (Fig. 62). Li^+, NH_4^+, K^+, $Fe^{2+/3+}$, Sr^{2+} and Mn^{2+} concentrations of the karstic and subthermal springs range between 0.01 and 1.510 ± 0.930 mg/l (M, Sr^{2+}). Only M shows very high K^+ concentrations and Na^+ concentrations compared to the other springs and wells. The subthermal spring BA shows a very high Na^+ concentration at the sampling date 25.06.2015 (BA4, Fig. 63). Also, S, BAA and J have high mean Na^+ concentrations compared to the other springs. ZE, L and K have low mean Na^+ concentrations. SR has moderate mean Na^+ concentrations compared to the other springs. M has the highest, ZE, S, SR, BA and J have moderate, L, K, BAA have the lowest mean Mg^{2+} concentrations. M has the highest, BA moderate, BAA, ZE, S, SR, L, K and J the lowest mean Ca^{2+} concentrations. ZE, S and SR have high, BA and J moderate, K and BAA low, L and M very low mean molar-Mg^{2+}/Ca^{2+}-ratios (compare lower left triangle of Fig. 62).

The subthermal and karstic springs have low F^-, Br^-, NO_2^- and PO_4^{3-} concentrations, which vary between 0.01 and 0.507 ± 0.878 mg/l (BA, Br^-). Only spring M has very high F^- (2.338 ± 0.312 mg/l) and Br^- concentrations (2.853 mg/l). M has the highest, BAA, J and S moderate, SR, L and K low mean Cl^- concentrations. BA4 (22.5 mg/l) has very high Cl^- concentrations, compared to BA1, BA2 and BA3 (Fig. 64). This is also visible in the Piper-Diagram (Fig. 62), as the dark pink circle of BA moves slightly to higher Na^+ and Cl^- concentrations. M has the highest, S, BAA and BA have moderate, SR, L, K and J have low mean SO_4^{2-} concentrations. M has the highest, ZE, S and BA have moderate, SR, BAA, J, L and K have low mean HCO_3^- concentrations (Table 15 and Table 16).

Isotope (δ^2H vs. $\delta^{18}O$) analysis (Fig. 65) shows, that the samples of ZE and S are in the same range. The samples of ZE, S, K and M have no or small variations

and therefore build up a cloudlike shape, as indicated by the circles in Fig. 65. There are two outliers (M2 and K3), which are moved to lower δ^2H and $\delta^{18}O$ values. Thus, ZE, S, K and M have a larger recharge area and are mixed up with many waters due to the low variations (Fig. 65). The other sampling points (C, T, BH, ST, L, BAA and BA) show large variations. Because of that, waters are not mixed up and have an direct meteoric origin. The outliers approximately fall on the LMWL and above the GMWL, whereas the isotopes of L, BAA and BA vary over a large range from lower δ^2H and $\delta^{18}O$ to higher δ^2H and $\delta^{18}O$. The isotopes of SR and J are in the upper right corner near to the two clouds of ZE and S.

mean ± std	**ZE**	**S**	**SR**	**L**	**M**
T [°C]	10.8 ± 0.1	10.7 ± 0.0	16.5 ± 2.9	6.8 ± 0.1	15.1 ± 0.1
pH	7.44 ± 0.18	7.56 ± 0.14	8.33 ± 0.20	8.02 ± 0.19	6.15 ± 0.09
EC [µS/cm]	392 ± 9	424 ± 7	302 ± 20	247 ± 18	1955 ± 55
Na^+ [mg/l]	0.443 ± 0.192	5.431 ± 2.356	1.161 ± 0.135	0.435 ± 0.253	37.358 ± 1.140
K^+ [mg/l]	0.150 ± 0.158	0.697 ± 0.324	0.286 ± 0.045	0.086 ± 0.089	10.942 ± 0.902
Mg^{2+} [mg/l]	25.2 ± 0.4	23.9 ± 1.0	17.8 ± 1.9	6.3 ± 0.8	56.0 ± 4.5
Ca^{2+} [mg/l]	46.0 ± 0.8	45.8 ± 0.9	36.4 ± 0.9	43.9 ± 0.8	356.5 ± 19.4
molar-Mg^{2+}/Ca^{2+}-ratios	0.90 ± 0.01	0.86 ± 0.02	0.81 ± 0.6	0.24 ± 0.03	0.26 ± 0.10
Cl^- [mg/l]	1.209 ± 0.403	2.473 ± 1.297	0.779 ± 0.105	0.470 ± 0.063	13.657 ± 2.539
SO_4^{2-} [mg/l]	1.9 ± 1.3	12.7 ± 8.2	3.2 ± 0.3	1.9 ± 0.5	258.3 ± 33.7
HCO_3^- [mg/l]	251.9 ± 13.5	257.1 ± 16.5	180 ± 2.6	160.2 ± 13.9	1064.5 ± 24.6

Table 15: Hydrochemical analyses (mean ± std) of karstic and subthermal springs in the *Cerkno/Kranj* area.

mean ± std	K	KA	BAA	BA	J
T [°C]	7.0 ± 0.2	8.0	11.7 ± 0.1	15.7 ± 0.6	12.9 ± 5.9
pH [-]	8.02 ± 0.14	7.0	7.57 ± 0.2	7.34 ± 0.17	8.35 ± 0.43
EC [µS/cm]	256 ± 18	256	314 ± 16	464 ± 28	282 ± 42
Na^+ [mg/l]	0.521 ± 0.364	0.360	4.455 ± 0.143	11.298 ± 8.715	2.179 ± 0.088
K^+ [mg/l]	0.094 ± 0.162	0.053	0.694 ± 0.104	1.096 ± 0.310	0.266 ± 0.034
Mg^{2+} [mg/l]	9.6 ± 1.1	8.1	9.4 ± 1.1	17.1 ± 1.6	12.4 ± 1.0
Ca^{2+} [mg/l]	41.0 ± 0.2	42.1	47.9 ± 1.7	64.1 ± 0.8	38.9 ± 7.3
molar-Mg^{2+}/Ca^{2+}-ratios	0.39 ± 0.05	0.32	0.32 ± 0.03	0.44 ± 0.04	0.53 ± 0.06
Cl^- [mg/l]	0.565 ± 0.109	0.469	3.586 ± 0.159	8.137 ± 9.608	3.177 ± 0.339
SO_4^{2-} [mg/l]	2.5 ± 0.4	2.1	8.3 ± 1.7	16.3 ± 3.0	2.6 ± 0.1
HCO_3^- [mg/l]	151.3 ± 6.4	161.0	179.8 ± 12.3	268.6 ± 10.2	166.5 ± 20.0

Table 16: Hydrochemical analyses (mean ± std) of karstic and subthermal springs in the *Cerkno/Kranj* area, continuation of Table 15.

ZE (compare Appendix 21) is a surface run-off water, because ZE shows high NO_3^- and PO_4^{3-} concentrations compared to **S** or the wells, due to possible occuring fertilisers from the above located meadow.

Divje Jezero (J) is called „wild lake“ in Slovenian. This name comes from the different outflow of the spring over the year. The spring is drained by a huge karst plateau in the southwest of the lake (compare Appendix 29). The measurements of the waters from J reveal a bicarboante type Ca^{2+}-water (Fig. 62), which is characteristic for karstic waters in this area.

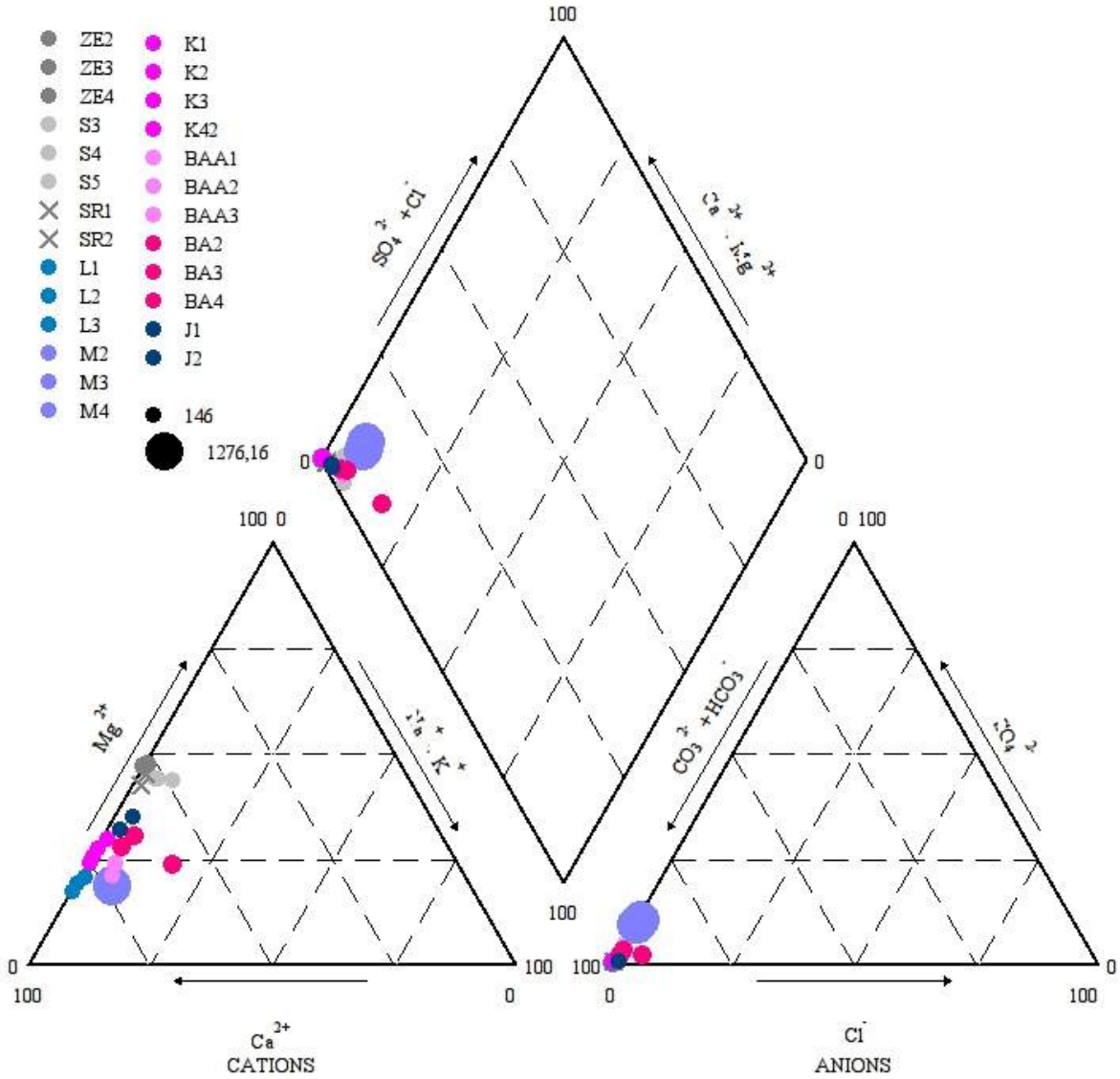

Fig. 62: Hydrochemistry (Piper diagram) of karstic springs (ZE, S, L, M, K, BAA, BA and J) and surface streams (SR) in *Kranj/Cerkno* area.

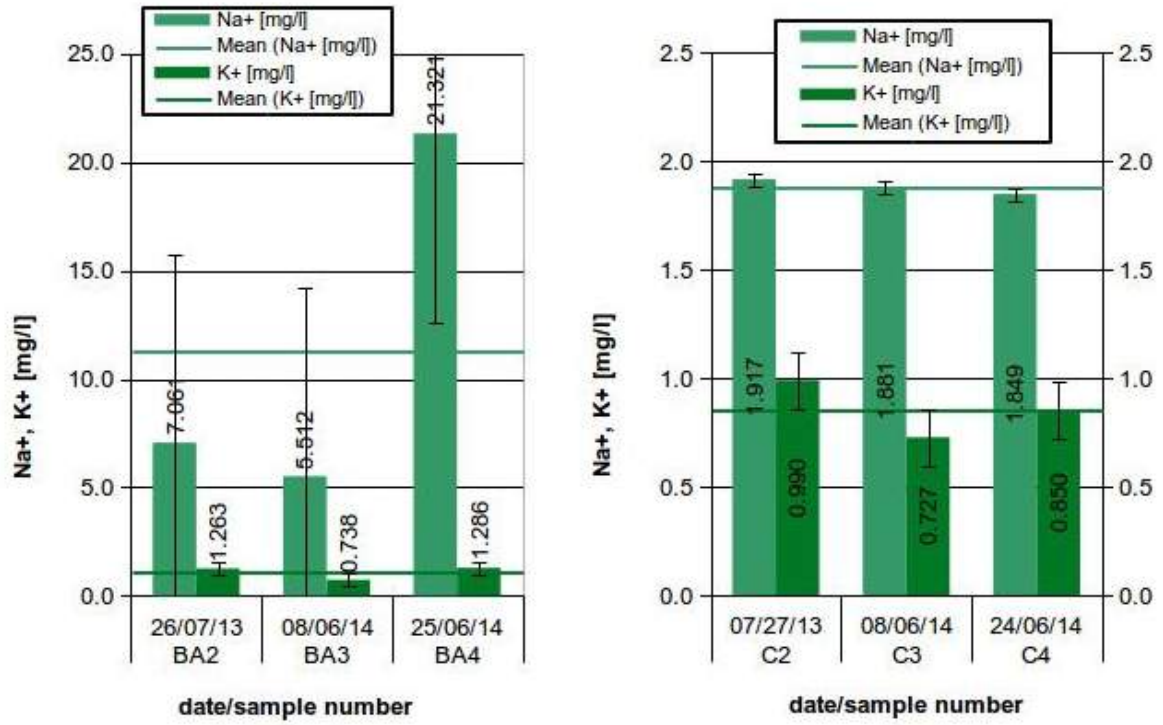

Fig. 63: Na^+, K^+ concentrations of thermal spring BA and deep well C.

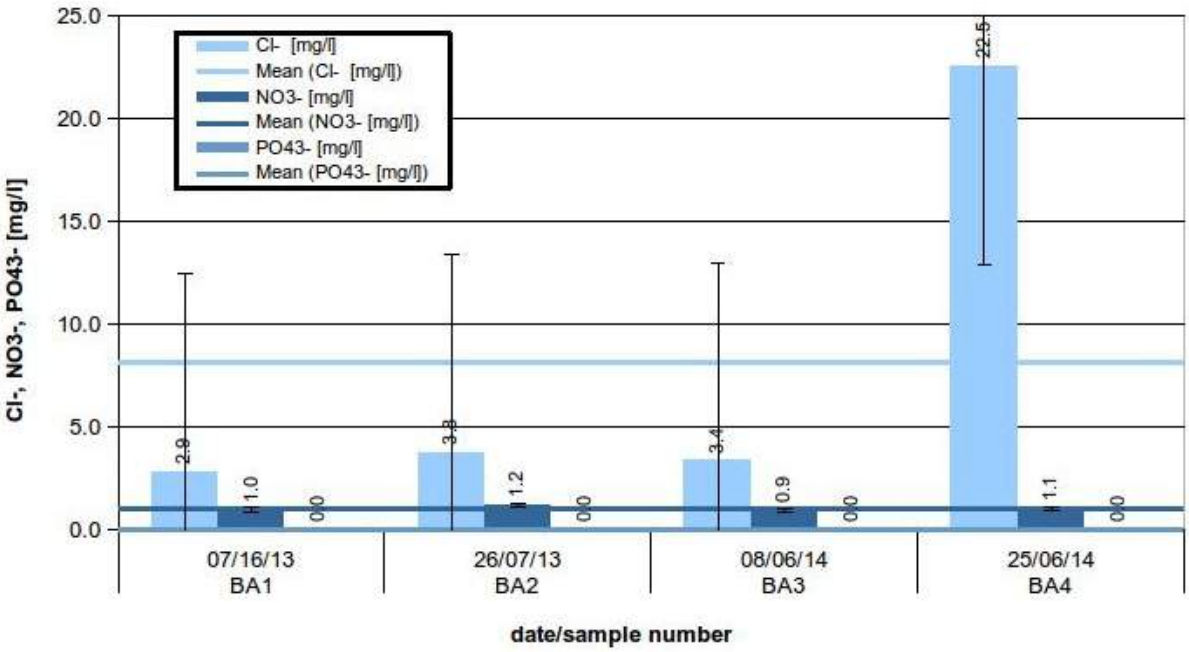

Fig. 64: Cl^-, NO_3^- and PO_4^{3-} concentrations concentrations of subthermal spring BA.

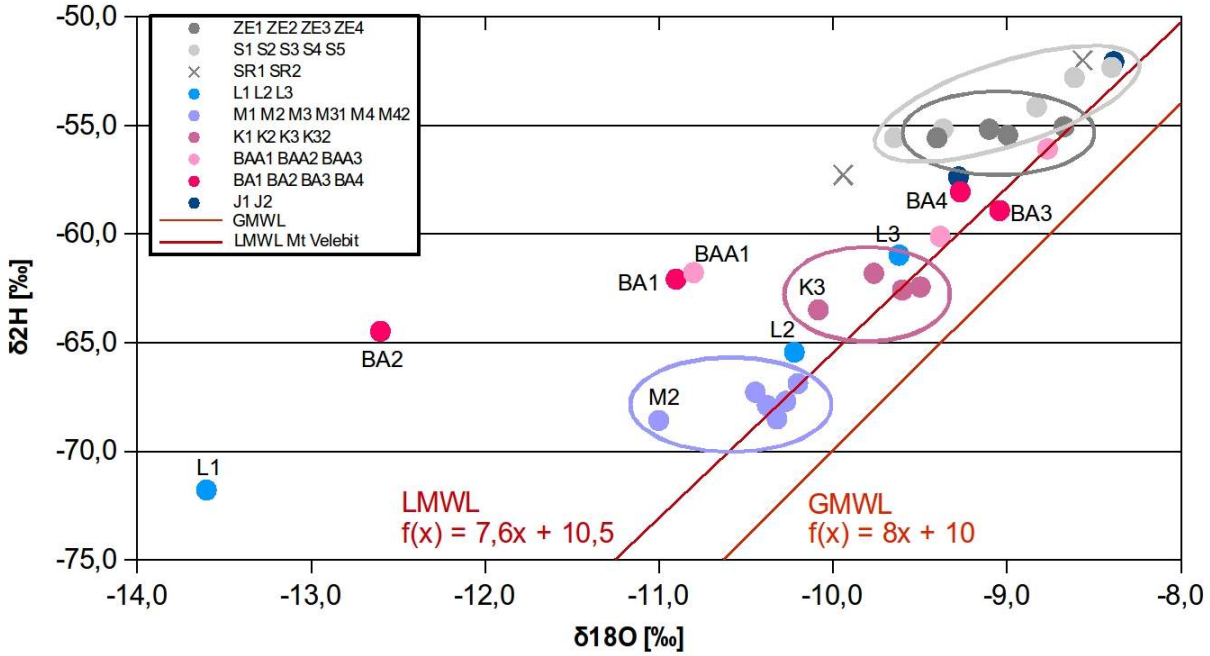

Fig. 65: Isotopes (δ^2H vs. $\delta^{18}O$) of (partly thermal) springs (M, ZE, S, L, K, BAA, BA and J) and surface stream (SR) in *Kranj/Cerkno* area.

The spring M is known as „Kisli studentic“ in Slovenian, which means sour spring. The spring M is located north of the spring K and southeast of L. A quarry (Kamnolom Kamna Gorica) is located near to the spring M. Several faults and fractures can be seen at the quarry, where one of these faults is very distinct (Fig. 66 A). This fault dips approximately 50 to 60° in SE direction. So the trend of this fault is SW to NE, which fits approximately as a prolongation to the spring M (compare Appendix 25).

Furthermore, red precipitation (probably iron oxides), several concrete-like rocks (Fig. 66 B) and remnants of Travertine dams (Fig. 66 C) can be found near the ouflow of M. These phenomenas occur due to the high dissolved solids in the waters from M and thus, the oversaturation of minerals, which precipitate (oxidation) in contact to oxygen in the air.

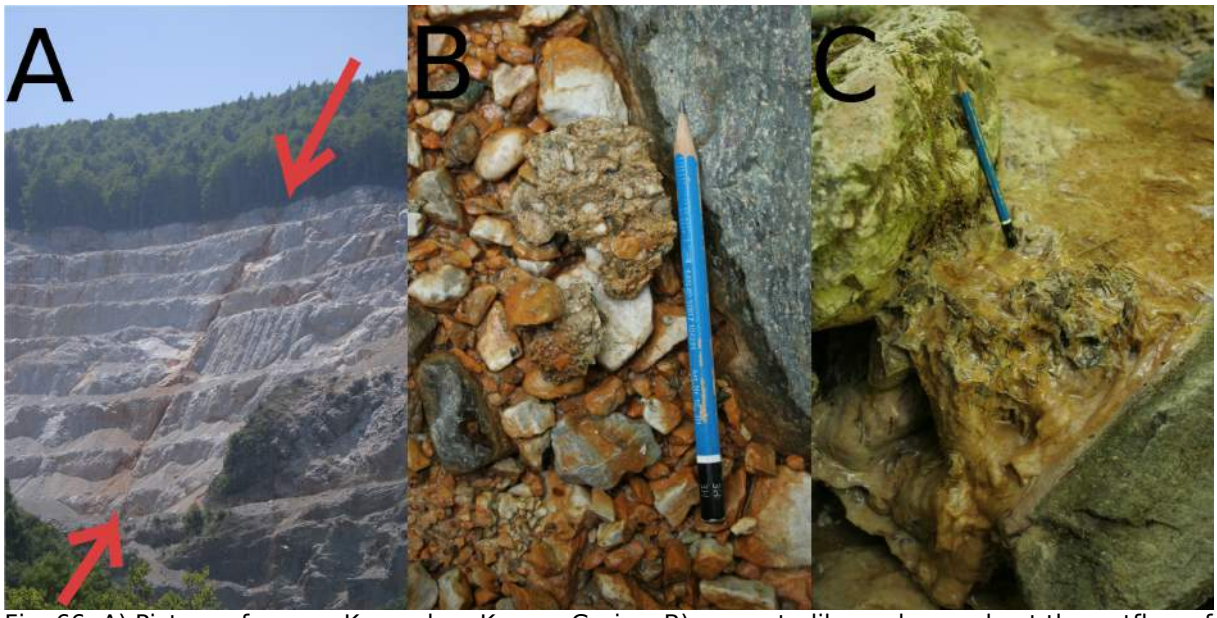

Fig. 66: A) Picture of quarry Kamnolom Kamna Gorica, B) concrete-like rock sample at the outflow of M above red precipitated gravel, C) remnant of a Travertine dam at the outflow of M, Photos: Philipp.

At K (Kroparica) (compare Appendix 26), several outflows are present (e.g. Fig. 20 A). Their discharges vary due to the amount of rainfall (precipitation). Only two springs wer measured due to low outflows at Kroparica. Due to a high precipitation event from 24.06.2014 to 26.06.2014 in NW-Slovenia (Fig. 67), discharge of all springs at Kroparica was very high (e. g. Fig. 20 B). Considering a dilution of stagnant water with new juvenile meteoric water in the underground, one can expect that the temperatue, electrical conductivity and most of the ion concentrations decrease.

Analysis of the water samples from K and L (high flood event waters and low flood event waters) show, that temperatures, electrical conductivities and Na^+ and K^+ concentrations are lower at the sampling date 25.06.2014 (high flood event) compared to earlier sampling dates (compare Appendix 6). The hydraulic component of karstic areas is an important factor, controlling the discharge and hydrochemistry of the waters.

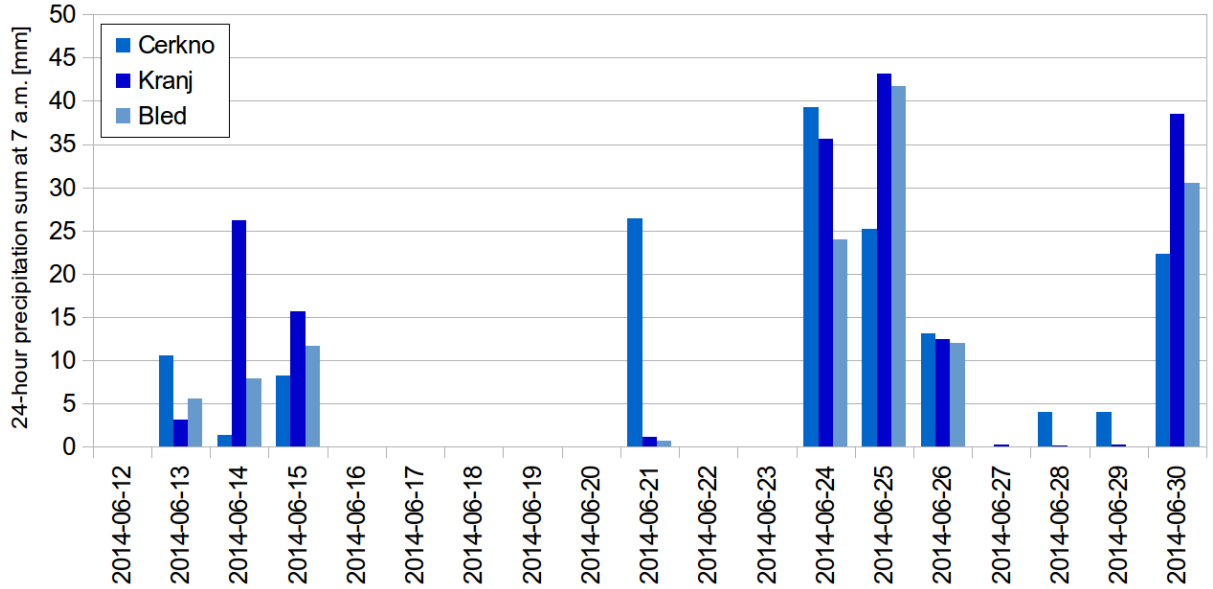

Fig. 67: 24-hour precipitation sum at 7 a.m. in mm at station *Cerkno* (marin blue), *Kranj* (dark blue) and Bled (light blue), www.meteo.si, requested 15.01.2014 10:34.

Fig. 68: Pictures of one outflow at K, A: no discharge (width: 3 m), B: high discharge due to the precipitation event from 24. to 26.06.2014 (width; 2 m), Photos: Philipp.

4. Discussion

4.1. Comparison to data from other studies

4.1.1. Z, R, B and BW

R is a confined aquifer with a constant outflow of 672 l/min. This value differs from the one of Eleršek & Mulec (2014), which is 900 l/m. Due to measurement errors and seasonal fluctuations one can assume that the true discharge is in between these values. R shows the same values compared to Eleršek & Mulec (2014). Only the SO_4^{2-} concentrations from Eleršek & Mulec (2014) are approximately twice of the measured values from R (compare Appendix 6 and 7) and the HCO_3^- concentration from Eleršek & Mulec (2014) is approximately 0.8 times lower than the measured values from R (Table 17).

Deep Well R	**Philipp (2013 and 2014)**	**Eleršek & Mulec (2014)**
	mean ± std	mean ± std
T [°C]	9.5 ± 0.5	9.2 ± 0.0
pH	7.63 ± 0.12	7.70 ± 0.11
EC [µS/cm]	782 ± 7	777 ± 8
NH_4^+ [mg/l]	0.009 ± 0.016	< 0.1
Cl^- [mg/l]	1.67 ± 0.26	3.5
NO_3^- [mg/l]	0.117 ± 0.084	0.2
PO_4^{3-} [mg/l]	0.003 ± 0.006	< 0.1
SO_4^{2-} [mg/l]	273.3 ± 21.3	471.4
HCO_3^- [mg/l]	163.6 ± 7.7	135.1
Q [l/min]	672	900

Table 17: Comparison of measured data and data from Eleršek & Mulec (2014) from the well R, Dis.: discharge.

Furthermore, Eleršek & Mulec (2014) demonstrated that some eukaryotic algae, and especially diatoms, can thrive well and compose abundant biofilms in an environment with sulphide at the borehole R. Eleršek & Mulec (2014) detected, despite the strong characteristic smell of hydrogen sulphide, a relatively low concentration of dissolved sulphide in the water during their sampling campaigns. The low concentration might have been linked to the quick degassing of the sulphide due to the strong water pressure of the well water.

BW is a surface run-off water, because the temperature, pH and NO_3^- concentration (compare Fig. 45, Fig. 47 and Appendix 6) is much higher and the δ^2H values varies over a much larger range compared to Z, R and B. Furthermore, both BW isotope samples plot in a different range than Z, R and B (Fig. 46).

No hydrochemical data from the literature exists for the springs and surface waters P, PG, V, D and J. Thus, no discussion and comparison is made.

4.1.2. S (Žveplenica), SR, ZE (above Žveplenica)

S and ZE show nearly the same temperature, pH and HCO_3^- concentrations. The electrical conductivitiy, pH, Li^+, Na^+, K^+, PO_4^{3-}, SO_4^{2-} and Cl^- concentrations are higher at S. NO_3^- concentration is higher at ZE (Table 18 and Table 19). SR was taken for comparison from the river near to S and due to that shows a different temperature and pH.

Isotope analysis ($\delta^{18}O$ and δ^2H, Fig. 65) from Mulec et al. (2010) and Mulec et al. (2014) are nearly the same compared to the measured isotope analysis (Table 18). This indicates a long residence time of water in the underground (> 5 months) (Mulec et al., 2010).

Karstic spring S	Philipp (2013 and 2014)	Mulec et al. (2009)	Mulec et al. (2010)	Mulec et al. (2011)	Mulec et al. (2014)
	mean ± std	mean ± std	mean ± std	mean ± std	mean ± std
T [°C]	10.7 ± 0.0	10.4 ± 0.2	10.5 ± 0.2	10.5 ± 0.2	10.6 ± 0.2
pH	7.6 ± 0.1	7.6 ± 0.2	7.56 ± 0.12	7.58 ± 0.12	7.58 ± 0.1
EC [µS/cm]	424 ± 7	415 ± 9	419 ± 9	420 ± 9	418 ± 7
NH_4^+ [mg/l]	0.0 ± 0.0	-	0	b. d.	< 0.1
Cl^- [mg/l]	2.5 ± 1.3	-	-	-	11.5
NO_3^- [mg/l]	0.6 ± 0.6	-	0	b. d.	< 0.1
PO_4^{3-} [mg/l]	0.1 ± 0.0	-	-	-	< 0.1
SO_4^{2-} [mg/l]	12.7 ± 8.2	-	9.9	9.9	9
HCO_3^- [mg/l]	257.1 ± 16.4	-	-	-	223.2
$\delta^{18}O$ [‰]	-9.0 ± 0.5	-	const.	-	-8
δ^2H [‰]	-54 ± 1.4	-	-	-	-53.3
Q [l/min]	0.84	2	1.8	1.8	1.5 -2.0

Table 18: Comparison of measured data and data from Mulec et al. (2009), Mulec et al. (2010), Mulec et al. (2011) and Mulec et al. (2014) from the karstic spring S, b. d.: below detection, const.: constant, Dis.: discharge.

Surface spring ZE	Philipp (2013 and 2014)	Eleršek & Mulec (2014)	Mulec et al. (2014)
	mean ± std	mean ± std	mean ± std
T [°C]	10.8 ± 0.1	10.6 ± 0.2	10.6 ± 0.2
pH	7.33 ± 0.18	7.6 ± 0.1	7.6 ± 0.1
EC [µS/cm]	393 ± 9	392 ± 6	392 ± 6
Cl^- [mg/l]	1.2 ± 0.4	10.2	10.2
NO_3^- [mg/l]	2.5 ± 0.3	1.9	1.9
PO_4^{3-} [mg/l]	0.005 ± 0.01	< 0.1	< 0.1
SO_4^{2-} [mg/l]	1.9 ± 1.3	2.2	2.2
HCO_3^- [mg/l]	251.9 ± 13.5	139.7	139.7
Q [l/min]	122 ± 65.1	13-60	13-60

Table 19: Comparison of measured data and data from Eleršek & Mulec (2014) and Mulec et al. (2014) from the surface spring ZE, Dis.: discharge.

4.1.3. C (Cerkno Borehole), T (Kopačnica, Hotavlje), BA/A (Zg. Bes. A)

The discharge from Nosan (1973) and Kralj (2004) for BA is given with 90 to 120 l/m and 60 to 120 l/m. Nosan (1973) measured a temperature of 21°C and Kralj (2004) of 18°C at BA, which are both higher compared to the measured temperatures (15.7 ± 0.6°C).

The results from C and T are nearly the same compared to Lapanje (2006) and Kralj (2004) (Table 20 and Table 21). According to Placer et al. (2000) outflow and temperature at C is 600 l/min and 30°C, which is 5 °C lower compared to the measured temperatures. This differences could come from different sampling points or the cooling of the water on the way to the spa. Another reason due to the single geothermal use (no doublet system) could be that the reservoir which is used for the geothermal exploration is already cooling down, because only an injection well is installed and a reinjection well is missing. The outlet temperature (27.6 °C) from Rajver et al. (2010) is nearly the same compared to the measured temperature. Thus, measured temperatures are the outlet and not the inlet temperature. According to Lapanje & Rman (2009) C has a temperature of 28°C and Kopačnica (T) of 24°C.

Thermal well T	Philipp (2013 and 2014)	Lapanje (2006)	Kralj (2004)
	mean ± std	-	mean
T [°C]	21.2 ± 1.4	24	20 – 22, 20.2
pH	7.6 ± 0.2	7.91	7.72
EC [µS/cm]	324 ± 6	-	-
TDS [mg/l]	-	215	-
Li^+ [mg/l]	0.0 ± 0.0	-	0.002
Na^+ [mg/l]	1.0 ± 0.3	1.3	1.6
NH_4^+ [mg/l]	0.0 ± 0.0	< 0.006	< 0.01
K^+ [mg/l]	1.0 ± 0.3	1.6	1.1
Mg^{2+} [mg/l]	19.4 ± 0.7	22.4	22
Ca^{2+} [mg/l]	35.8 ± 1.1	35.8	39
$Fe^{2+/3+}$ [mg/l]	0.0 ± 0.0	-	0.011
Sr^{2+} [mg/l]	0.2 ± 0.2	-	0.113
F^- [mg/l]	0.5 ± 0.0	-	0.24
Cl^- [mg/l]	0.9 ± 0.3	0.6	1
Br^- [mg/l]	0.3 ± 0.5	-	0.09
NO_2^- [mg/l]	0.0 ± 0.0	-	< 0.01
NO_3^- [mg/l]	1.3 ± 0.7	-	2.2
PO_4^{3-} [mg/l]	0.0 ± 0.0	-	0.01
SO_4^{2-} [mg/l]	14.3 ± 4.4	23.8	17
HCO_3^- [mg/l]	180.7 ± 10.8	181	195

Table 20: Comparison of measured data and data from Lapanje (2006) and Kralj (2004) from the thermal well T.

Thermal well C	Philipp (2013 and 2014)	Lapanje (2006)
	mean ± std	-
T [°C]	24.3 ± 3.5	30
pH	8.0 ± 0.1	8
EC [µS/cm]	284 ± 3	-
TDS [mg/l]	-	215
Na^+ [mg/l]	1.9 ± 0.0	2.2
NH_4^+ [mg/l]	0.1 ± 0.0	0
K^+ [mg/l]	0.9 ± 0.1	1.1
Mg^{2+} [mg/l]	16.5 ± 0.2	17.7
Ca^{2+} [mg/l]	30.6 ± 0.5	30.9
Cl^- [mg/l]	17.5 ± 33.0	1.1
SO_4^{2-} [mg/l]	13.3 ± 0.8	17
HCO_3^- [mg/l]	144.5 ± 13.8	145

Table 21: Comparison of measured data and data from Lapanje (2006) from the thermal well C.

4.1.4. BH (Bled Hotel Toplice)

Compared to the data from Zmazek et al. (2002) with average values of 840 ± 60 µS/cm and 22.0 ± 0.1 °C, the measured data (Table 22 and Appendix 6) shows slightly higher electrical conductivity and temperatures. Measured temperatures are slightly higher compared to Kralj (2004) and Nosan (1973) with 19-22 °C and Lapanje & Rman (2009) with 22°C (compare Table 22). The discharge given from Kralj (2004) is 300 l/m, whereas Nosan (1973) gives a discharge of 720 to 840 l/m. Therefore, discharge for the thermal well BH is in between these values. The data from Lapanje (2006) shows higher pH, K^+, Cl^- and SO_4^{2-} concentration and lower temperature, Mg^{2+}, Ca^{2+} and HCO_3^- concentrations compared to the measured data (compare Table 22). The differences in these parameters could come from different in-situ equipment (compare 2.1 Field Measurements (T, pH, EC, discharge)) and/or different sampling points within the hotel building. Compared to Lapanje (2006) Na^+ concentrations (28 mg/l) is nearly 5 times higher than the measured data. One reason for this high Na^+ concentration from Lapanje (2006) could be that a high-flood event occured

during their sampling time, which would be the same phenomena at the thermal well C and subthermal spring BA (compare Fig. 63 and Fig. 64).

Thermal well BH	Philipp (2013 and 2014)	Lapanje (2006)
	mean ± std	-
T [°C]	23.1 ± 1.0	21.7
pH	6.9 ± 0.1	8.2
EC [µS/cm]	915 ± 41	-
TDS [mg/l]	-	691
Na^+ [mg/l]	5.7 ± 0.5	28
NH_4^+ [mg/l]	0.0 ± 0.0	<0.1
K^+ [mg/l]	1.0 ± 0.4	2.5
Mg^{2+} [mg/l]	38.7 ± 1.3	23
Ca^{2+} [mg/l]	142.1 ± 3.6	113
Cl^- [mg/l]	1.7 ± 0.2	2.5
SO_4^{2-} [mg/l]	29.5 ± 4.1	38.1
HCO_3^- [mg/l]	553.9 ± 38.7	482

Table 22: Comparison of measured data and data from Lapanje (2006) from the thermal well BH.

4.1.5. M (Man's Power), K (Kroparica), L (Lipnica)

Only for Lipnica (L) hydrochemical data from literature is available. Mezga (2014) measured almost all main cation- and anion-concentrations and standard parameters (Table 23). The hydrochemical data from Mezga (2014) is almost the same compared to the measured data. Only temperature, electrical conductivity, Ca^{2+}, HCO_3^- concentration, $\delta^{18}O$ and δ^2H are higher compared to Mezga (2014).

Differences in the concentrations and parameters could come from different sampling times and points and different discharges due to precipitation, which leads to a different hydrochemistry of the waters, changing in short periods of days or weeks.

Karstic spring L	Philipp (2013 and 2014)	Mezga (2014)
	mean ± std	mean ± std
T [°C]	6.8 ± 0.1	7.2 ± 0.1
pH	8.0 ± 0.2	7.98 ± 0.1
EC [µS/cm]	247 ± 18	276 ± 3
Na^+ [mg/l]	0.4 ± 0.3	0.5 ± 0.1
NH_4^+ [mg/l]	0.0 ± 0.0	0.01 ± 0
K^+ [mg/l]	0.1 ± 0.0	0.12 ± 0.01
Mg^{2+} [mg/l]	6.3 ± 0.8	6.4 ± 0.2
Ca^{2+} [mg/l]	43.9 ± 0.8	47 ± 1
$Fe^{2+/3+}$ [mg/l]	0.0 ± 0.0	0.0125 ± 0.01061
Mn^{2+} [mg/l]	0.0 ± 0.0	0.00043 ± 0.00028
Cl^- [mg/l]	0.5 ± 0.1	0.41 ± 0.05
Br^- [mg/l]	0.3 ± 0.5	0.006 ± 0.0
NO_3^- [mg/l]	1.9 ± 0.4	2.37 ± 0.16
SO_4^{2-} [mg/l]	1.9 ± 0.5	2.69 ± 0.52
HCO_3^- [mg/l]	160.2 ± 13.9	196 ± 37
$\delta^{18}O$ [‰]	-11.1 ± 2.1	-8.85 ± 0.15
δ^2H [‰]	-66.1 ± 5.4	-57.8 ± 0.8

Table 23: Comparison of measured data and data from Mezga (2014) from the spring L.

4.1.6. ST (Spodnje Pirniče), F (Furnalove Toplice)

Until the year 1972 the temperature and discharge rates of the spring ST (Appendix 19) was measured periodically from Nosan (1973). According to Nosan (1973) discharge varys from 360 to 480 l/min and temperatures from 18 to 23°C, which fits to the measured temperatures and others from Kralj (2004), Lapanje (2006) and Lapanje & Rman (2009) (20.0°C). The comparison of other data (concentrations and parameters) from Kralj (2004) and Lapanje (2006) show no significant differences (compare Table 24).

Thermal well ST	Philipp (2013 and 2014)	Lapanje (2006)	Kralj (2004)
	mean ± std	-	-
T [°C]	20.3 ± 0.1	20.1	18 – 23.2, 20.4
pH	7.5 ± 0.2	7.81	7.85
EC [µS/cm]	336 ± 50	-	-
TDS [mg/l]	-	305	-
Li^+ [mg/l]	0.0 ± 0.0	-	0.002
Na^+ [mg/l]	2.5 ± 0.5	2.7	3.5
NH_4^+ [mg/l]	0.0 ± 0.0	< 0.02	< 0.01
K^+ [mg/l]	0.7 ± 0.6	0.65	1.1
Mg^{2+} [mg/l]	20.4 ± 0.4	23	20
Ca^{2+} [mg/l]	44.2 ± 0.3	42.8	46
$Fe^{2+/3+}$ [mg/l]	0.0 ± 0.0	-	0.02
Sr^{2+} [mg/l]	0.0 ± 0.0	-	0.0587
Mn^{2+} [mg/l]	0.0 ± 0.0	-	0.0001
F^- [mg/l]	0.1 ± 0.0	-	0.02
Cl^- [mg/l]	1.9 ± 0.2	1.8	2.5
Br^- [mg/l]	0.4 ± 0.7	-	0.11
NO_2^- [mg/l]	0.0 ± 0.0	-	< 0.01
NO_3^- [mg/l]	4.4 ± 0.2	-	< 2
PO_4^{3-} [mg/l]	0.0 ± 0.0	-	< 0.02
SO_4^{2-} [mg/l]	4.5 ± 0.5	5.34	6
HCO_3^- [mg/l]	212.3 ± 2.5	225	230
Q [l/min]	-	-	60 - 300

Table 24: Comparison of measured data and data from Lapanje (2006) and Kralj (2004) from the thermal well ST.

As well as for ST, data from F (Table 25) is almost the same compared to Kralj (2004), Lapanje (2006) and the data from the leather company Siliko. Only Na^+ concentration is lower and Mg^{2+}, Ca^{2+}, and SO_4^{2-} concentrations are slightly higher compared to the data from Lapanje (2006). The higher concentrations may come from a higher dissolution of the impervious marl in the underground (Nosan, 1973).

Thermal well F	Philipp (2013 and 2014)	Lapanje, A. (2006)
	mean ± std	-
T [°C]	23.9 ± 0.1	23.8
pH	7.8 ± 0.1	7.6
EC [µS/cm]	443 ± 12	-
TDS [mg/l]	-	352
Na^+ [mg/l]	1.1 ± 0.2	2.6
NH_4^+ [mg/l]	0.0 ± 0.0	< 0.05
K^+ [mg/l]	0.2 ± 0.1	0.9
Mg^{2+} [mg/l]	27.1 ± 0.1	25.8
Ca^{2+} [mg/l]	50.4 ± 0.1	48.4
Cl^- [mg/l]	1.1 ± 0.0	2
SO_4^{2-} [mg/l]	25.6 ± 6.1	17
HCO_3^- [mg/l]	254.4 ± 19.9	253

Table 25: Comparison of measured data and data from Lapanje (2006) from the thermal well F.

5. Conclusion

Ongoing dedolomitisation

One purpose of this work is to find arguments for the process of dedolomitisation in the underground of the *Rovte* area (Fig. 4). Former publications about the *Rovte* area (compare 1.3.2 Geology at Rovte area) showed that dedolomite occurs in caves which are located on top of and around the mountain Vrh Trh in the *Rovte* area. All three caves reveal rock features and mineralogical evidence for past dedolomitisation.

Čadež (1977) found intercalated gypsum in the stratigraphic horizons, where the dedolomite caves occur. The dissolution of gypsum can be one reason for dedolomitisation (compare 1.5.2 Dolomitisation and dedolomitisation). Therefore, one can argue that the geology at the *Rovte* area is one argument for the dedolomitisation in the underground.

From hydrochemical data (Appendix 6) we can detect three trends in the Piper-Diagram (Fig. 47): 1. from lower to higher SO_4^{2-} concentration, 2. from higher to lower total alkalinity and 3. from molar-Mg^{2+}/Ca^{2+}-ratios smaller than 1 to almost 1. The last trend is also the third argument for dedolomitisation which is a preferential removing of Mg^{2+} due to a molar-Mg^{2+}/Ca^{2+}-ratio smaller than 1.

Back et al. (1983) showed from field measurements that pH decreases with increasing SO_4^{2-} concentration (Fig. 24), indicating dedolomitisation. Due to the calculated t-Test (compare 3.2.4. Correlation between pH and SO42-concentration), a relation between pH and SO_4^{2-} concentration exists.

From the saturation indices of calcite, dolomite and gypsum we can see that the waters from the wells in the *Rovte* area are slightly oversaturated with respect to calcite and undersaturated with respect to dolomite and gypsum. Furthermore, the SI calcite increases and SI dolomite decreases with increasing SO_4^{2-} concentration (Fig. 53). These are the conditions for dedolomitisation (Plummer et al., 1990).

The argument of the correlation between SI gypsum and SO_4^{2-} concentration for dedolomitisation must be denied, because the calculation from PHREEQC contains the SO_4^{2-} concentration in the input file. Nevertheless, the coefficient of determination is 0.99.

Plummer et al. (1990) showed that SO_4^{2-} concentrations increase with decreasing HCO_3^- concentrations, which can be seen in the measured data from Z, R and B (Fig. 29 and Fig. 54). The correlation between Ca^{2+} and SO_4^{2-} and Mg^{2+} and SO_4^{2-} concentrations (Cardenal et al., 1994) can be seen from the sampling points Z, R and B (Fig. 55 and Fig. 56).

Cardenal et al. (1994) distinguished that the dedolomitisation trend is marked by stabilisation or even a slight fall in the alkalinity (Fig. 26). One can observe that this specific trend occurs at the wells Z and R (Fig. 57). Furthermore, Cardenal et al. (1994) distinguished two groups in their field data. One group indicating the predominant incongruent dissolution of dolomite and another group with significantly progressed dedolomitisation. In the data from the *Rovte* area no such groups can be found (Fig. 58). Thus, it is an argument against dedolomitisation.

These arguments (Pro) imply that dedolomitisation is still an ongoing process in the underground. Other hydrochemical processes, however, play a role in these systems due to the argument against dedolomitisation (Contra).

	Argument	Literature	Pro or Contra
1	Geology at *Rovte* area with intercalated gypsum	Čadež (1977), Mlakar (1969)	Pro
2	Trend in the Piper-Diagram	e. g. Back et al. (1983)	Pro
3	Molar-Mg^{2+}/Ca^{2+}-ratio	e. g. Back et al. (1983)	Pro
4	Precipitation of calcite and dissolution of dolomite	e. g. Plummer et al. (1990)	Pro
5	Correlation between pH and SO_4^{2-} concentration	e. g. Back et al. (1983)	Pro
6	Correlation between SI gypsum and SO_4^{2-} concentration	e. g. Plummer et al. (1990)	Pro
7	Trend in total alkalinity and SO_4^{2-} concentration	e. g. Plummer et al. (1990)	Pro
8	Correlation between Ca^{2+}, Mg^{2+} and SO_4^{2-} concentration	e. g. Cardenal et al. (1994)	Pro
9	Stabilisation or slight fall of alkalinity	e. g. Cardenal et al. (1994)	Pro
10	Two groups in the diagram HCO_3^- vs. pH	e. g. Cardenal et al. (1994)	Contra

Table 26: Arguments for (Pro) and against (Contra) for dedolomitisation.

Hydrochemical Characterisation of thermal wells and springs

The second purpose of this work was to characterise the hydrochemical composition of the thermal wells and springs in NW-Slovenia. Almost all waters from the thermal wells and springs are Ca^{2+}-Mg^{2+}-HCO_3^--type waters (Fig. 59 and Fig. 62). Furthermore, it is suggested due to the high Na^+ and Cl^- concentration at C4 (Fig. 60) and BA (Fig. 63 and Fig. 64) that a hydraulic connection between the well C and BA exists.

In accordance with the results and investigations of this work one can say that a deep flow pattern in NW-Slovenia exists, where recharge of the deep aquifer system (namely the *Upper Triassic Norian stage* grey stratified dolomite) occurs. The deep aquifer system is drained by the boreholes and subthermal springs (compare Fig. 6, Fig. 7, Fig. 8 and Fig. 9).

Outlook

In order to improve the stability of the hydrochemical data for the *Rovte* and *Cerkno/Kranj* area, it would be necessary to sample a much longer time, much more frequently, more parameters (e. g. pO_2, pCO_2 and Tritium) and on specific times, especially while precipitation events occur. The analysis of waters from additional sampling points (e. g. Tolminska korita, a subthermal spring NW of Cerkno) would help to achieve a better understanding of the deep karstic system in NW-Slovenia. These improvements would help to achieve better and more robust results. In order to avoid possible errors in future work, it is necessary to measure two samples of each point to guarantee an accurate analysis procedure and to have reliability of in-situ measurements (e. g. alkalinity titration).

Further research in the *Rovte* area could determine the source of dedolomitisation. The source of dedolomitisation could be either the gypsum in the underground or the pyrite oxidation in the cave (compare Fig. 10). This includes analyses of sulfate isotopes ($\delta^{34}S$) in the waters of the wells Z, R and B, of the pyrite in the cave and of the gypsum in the geological strata.

A detailed basic geological mapping of the *Rovte* area and the areas around the thermal wells and springs would improve the hydrogeological understanding on a regional scale.

Furthermore, borehole geophysics (video- and data-log) could determine the inflow zones and characteristics of the boreholes and wells. Hydraulic measurements could be pumping or tracer-tests which determine the flow paths in the system and possible maximum discharges for (geothermal) utilisation.

A 3D-modelling with the input of outcrop analogue studies, thermoscanner data (thermal conductivities), hydrochemical data and tracer-test data would improve the understanding of the deep flow of waters in NW-Slovenia.

6. Note of Thanks

First, I thank Tadej Slabe for the acceptance of the application for an internship at the Karst Research Institute in Postojna (Slovenia) in 2013. With his decision it was possible to learn a lot about Karst, directly in the homeland of Karst research: Slovenia.

I thank Prof. Kempe from the Institute of Applied Geosciences (TUD) for the helpful remarks, scientific support and critisism. I thank PhD Bojan Otoničar for his kind welcome in Slovenia during my internship and for the assistance in questions concerning basic geological and speleological knowledge of NW-Slovenia (namely *Rovte* and *Cerkno*/*Kranj* area).

I thank all members of the Karst Research Institute in Postojna (Slovenia) for the acceptance and welcome during my internship. Special thanks goes to PhD Franci Gabrovšek for the assistance with PHREEQC-problems, BSc. Petra Gostiničar for Arc-GIS questions and Mateja Zadel for the help in the lab in Postonja.

I thank the laboratory staff of the Institute of Applies Geosciences (TUD) for the help with analysis procedures, namely Rainer Brannolte, Zahra Neumann and Gabi Schubert.

I thank my brother Dr. Sebastian T. Philipp for English corrections and psychological support. I thank Hanna Lucks for the last English corrections shortly before submission. I thank my love Julia Zießmer for the acceptance of my absence during the last weeks of this work. Last but not least, I thank my parents Bernd and Sabine Philipp for their support in terms of financial aspects and wonderful sailing trips in the summer during my studies.

7. List of References

7.1. Literature

Allègre, C. (2008): Isotope Geology, Cambridge University Press, Cambridge, 512 pp.

Appelo, C. A. J., Postma, D. (2005): Geochemistry, groundwater and pollution, A. A. Balkema Publishers, Leiden, 649 pp.

Back, W., Hanshaw, B. B., Plummer, L. N., Rahn, P. H., Rightmire, C. T., Rubin, M. (1983): Process and rate of dedolomitization: Mass transfer and 14C dating in a regional carbonate aquifer, In: Geological Society of America Bulletin, 94:1415-1429

Bischoff, J. L., Juliá, R., Shanks, W. C., Rosenbauer, R. J. (1994): Karstification without carbonic acid: Bedrock dissolution by gypsum-driven dedolomitization, In: Geology, 22:995-998

Brenčič, M. (2003): Hydrogeological conditions of the Kroparica recharge area, Jelovica, Slovenia, In: Geologija, 46/2:281-306

Čadež, F. (1977): Sadra in anhidrit na Idrijskem, gypsum and anhydrite occurrences in Idria region, In: Geologija, 20/289-301

Cardenal, J., Benavente, J., Cruz-Sanjulián, J. J. (1994): Chemical evolution of groundwater in Triassic gypsum-bearing carbonate aquifers (Las Alpujarras, southern Spain), In: Journal of Hydrology, Elsevier Science, 161:3-30

Cohen, K. M., Finney, S. C., Gibbard, P. L., Fan, J.-X. (2014): The ICS International Chronostratigraphic Chart, Episodes 36:199-204

Craig, H. (1961): Isotopic variations in meteoric waters, In: Science, 133:1702-1703

Criss, R., Davisson, L., Surbeck, H., Winston, W. (2007): Isotopic methods, In: Goldscheider, N., Drew, D. (eds): Methods in Karst Hydrogeology, International Contributions to Hydrogeology, IAH, Taylor & Francis, Leiden, 26:264

Dockal, J. A. (1988): Thermodynamic and kinetic description of dolomitization of calcite and calcitization of dolomite (dedolomitization), In: Carbonates and Evaporites, 3:125-141

Dublyansky, Y. (2012): Hydrothermal caves, In: White, W. B., Culver, D. C. (eds.): Encyclopedia of caves, Elsevier, Amsterdam, 962 pp.

Eleršek, T., Mulec, J. (2014): The algal community at an ecoline of a cold sulphidic spring (Sovra artesian borehole, Slovenia), In: Environmental Earth Sciences, 71:5255-5261

Ford, D., Williams, P. (2007): Karst Hydrogeology and Geomorphology, John Wiley & Sons, England, 678 pp.

Gabrovšek, F. (2012): Speleogenesis, Telogenetic, In: White, W. B., Culver, D. C. (eds.): Encyclopedia of caves, Elsevier, Amsterdam, 962 pp.

Goldbrunner, J. E. (1999): Hydrogeology of Deep Groundwaters in Austria, In: Mitt. Österr. Geol. Ges., Wien, 92:281-294

Goldscheider, N., Mádl-Szőnyi, J., Erőss, A, Schill, E. (2010): Review: Thermal water resources in carbonate rock aquifers, In: Hydrogeology Journal, 18:1303-1318

Goldscheider, N., Drew, D., Worthington, S. (2007): Introduction, In: Goldscheider, N., Drew, D. (eds): Methods in Karst Hydrogeology, International Contributions to Hydrogeology, IAH, Taylor & Francis, Leiden, 26:264

Gonfiantini, R. (1984): Advisory group meeting on stable isotope reference samples for geochemical and hydrological investigations, Vienna, 19 – 21 September 1983, report to the Director General: Vienna, International Atomic Energy Agency, 77 pp.

Gunn, J., Bottrell, S. H., Lowe, D. J., Worthington, S. R. H. (2006): Deep groundwater flow and geochemical processes in limestone aquifers: evidence from thermal waters in Derbyshire, England, UK, In: Hydrogeology Journal, 14:868-881

Hanshaw, B. B., Back, W. (1979): Major geochemical processes in the evolution of carboante-aquifer systems, In: Journal of Hydrology, ElSevier, 43:287-312

Hoefs, J. (2009): Stable Isotope Geochemistry, Springer Verlag, Berlin, 6th edition, 285 pp.

Hunkeler, D. Mudry, J. (2007): Hydrochemical methods, In: Goldscheider, N., Drew, D. (eds): Methods in Karst Hydrogeology, International Contributions to Hydrogeology, IAH, Taylor & Francis, Leiden, 26:264

Jones, K. J., White, W. B. (2012): Karst, In: White, W. B., Culver, D. C. (eds.): Encyclopedia of caves, Elsevier, Amsterdam, 962 pp.

Kempe, S. (2014): Hypogene limestone caves in Germany: geochemical background and regionality, In: Klimchouk, A., Sasowsky, I., Mylroie, J., Engel, S. A., Engel, A. S. (eds): Hypogene Cave Morphologies, selected papers and abstracts of the symposium held February 2 – 7, 2014, San Salvador Island, Bahamas, Karst Waters Institute Special Publication 18, 111 pp.

Klimchouk, A. (2007): Hypogene Speleogenesis: Hydrogeological and Morphogenetic Perspective, Special Paper No. 1, National Cave and Karst Research Institute, Carlsbad, New Mexico, 118 pp.

Kralj, P. (2004): Chemical composition of low temperature (< 20-40 °C) thermal waters in Slovenia, In: Environmental Geology, 46:635-642

Lapanje, A. (2006): Origin and chemical composition of thermal and thermomineral waters in Slovenia, In: Geologija, 49/2:347-370

Lapanje, A., Rman, N. (2009): Thermal and thermomineral water, In: Pleničar, M., Ogorelec, B., Novak, M. (eds): Geologija Slovenije – The Geology of Slovenia, 612 pp.

Malabeh, A. A., Kempe, S. (2012): Hypogene point karstification along Wadi Sirhan Graben (Jordan): A sign of oilfield degassing?, In: Acta Carsologica, Postojna, 41/1:35-45

Mezga, K. (2014): Natural hydrochemical background and dynamics of groundwater in Slovenia, Dissertation at the University of Nova Gorica Graduate School, 492 pp.

Mihevc, A. (1989): Matjaževe Kamre, In: Naše jame, Ljubljana, 31:66-72

Mihevc, A. (1991): Jama pri Sv. Treh kraljih, In: Naše jame, Ljubljana, 33:28-37

Mihevc, A. (2005): Excursion to dolomite karst of Logaške Rovte, 13th International Karstological School „Classical karst“: Karst in various rocks, GuideBook, Postojna, Slovenia, 27th – 30th June 2005, 42 pp.

Mlakar, I. (1969): Krovna Zgradba Idrijsko Žirovskega Ozemlja, In: Geologija, Geological Transactions and Reports, Ljubljana, Vol. 12, 72 pp.

Mulec, J., Oarga, A., Schiller, E. K., Perşoiu, A., Holko, L., Šebela, S (2014): Assessment of the physical environment of epigean invertebrates in a unique habitat: the case of a karst sulfidic spring, Slovenia, In: Ecohydrology, Wiley Online Library, 9 pp.

Nosan, A. (1973): Termalni in mineralni vrelci v Sloveniji, In: Geologija, Geological transactions and reports, 16:5-81

Ogorelec, B., Rothe, P. (1992): Mikrofazies, Diagenese und Geochemie des Dachsteinkalkes und Hauptdolomits in Süd-West-Slowenien, In: Geologija, 35:81-181

Otoničar, B., Mihevc, A. (2013): Geology and Speleogenesis of Vrh Sv. Treh Kraljev, 21st International Karstological School „Classical Karst“: Hypogene Speleogenesis (between theory and reality...), GuideBook, Postojna, Slovenia, 10th – 14th June 2013, 98 pp.

Otoničar, B., Tyc, A., Osborne, R. A. L., Bzowska, G. (2012): Mravljetovo Brezno Gošarjevih rupah cave: dissolution of dedolomite, 20th International Karstological School „Classical Karst“: Karst forms and processes, GuideBook, Postojna, Slovenia, 18th – 21st 2012, 80 pp.

Otoničar, B., Tyc, A., Sznober, N. (2013): Mravljetovo Brezno Gošarjevih rupah cave: dissolution of dedolomite, 21st International Karstological School „Classical Karst“: Hypogene Speleogenesis (between theory and reality...), GuideBook, Postojna, Slovenia, 10th – 14th June 2013, 98 pp.

Parkhurst, D. L., Appelo, C. A. J. (1999): User's guide to PHREEQC (Version 2) – a computer program for Speciation, Batch-Reaction, One-Dimensional

Transport, and Inverse Geochemical Calculations, Water-Resources Investigations Report 99-4259, Denver, Colorado, 326 pp.

Placer, L., Rajver, D., Trajanova, M., Ogorelec, B., Skaberne, D. & Mlakar, I. (2000): Borehole Ce-2/95 at Cerkno at the boundary between the Southern Alps and the External Dinarides (Slovenia), In: Geologija, Ljubljana, 43/2:251-266

Plummer, L. N., Busby, J. F., Lee, R. W., Hanshaw, B. B. (1990): Geochemical Modeling of the Madison Aquifer in Parts of Montana, Wyoming and South Dakota, In: Water Resources Research, 26/9:1981-2014

Plummer, L. N., Wigley, T. M. L., Parkhurst, D. L. (1978): The kinetics of calcite dissolution in CO_2-water systems at 5°C to 60°C and 0.0 to 1.0 atm CO_2, In: American Journal of Science, 278:179-216

Rajver, D., Lapanje, A., Rman, N. (2010): Geothermal Development in Slovenia: Country Update Report 2005-2009, Proceedings World Geothermal Congress 2010, Bali, Indonesia, 25th – 29th April 2010, 10 pp.

Rajver, D., Prestor, J., Lapanje, A., Rman, N. (2013): Geothermal Energy Use: Country Update for Slovenia, European Geothermal Congress 2013, Pisa, Italy, 3rd - 7th June 2013, 16 pp.

Rosman, J. R., Taylor, P. D. (1998): Isotopic compositions of the elements (technical report): commission on atomic weights and isotopic abundances, In: Pure Applied Chemistry, 70:217-235

Saunders, J. A., Toran, L. E. (1994): Evidence of dedolomitization and mixing in Paleozoic carbonates near Oak Ridge, Tennesee, In: Ground Water, 32:207-214

Schmid, S. M., Bernoulli, D., Fuegenschuh, B., Matenco, L., Schefer, S., Schuster, R., Tischler, M., Ustaszewski, K. (2008): The Alpine-Carpathian-Dinaridic orogenic system: correlation and evolution of tectonic units, In: Swiss Journal of Geosciences, 101:139-183

Sznober, N. (2012): Ground plan of Mravljetovo Brezno Gošarjevih Rupah, Czestochowa caving club, Poland

Usdowski, H.-E. (1967): Die Genese von Dolomit in Sedimenten, In: Engelhardt, W. v., Zeamann, J. (Edt.): Mineralogie und Petrographie in Einzeldarstellungen, Springer-Verlag, 4:95

Vrabec, M., Šmuc, A., Pleničar, M., Buser, S. (2009): Geological evolution of Slovenia – an overview, In: Pleničar, M., Ogorelec, B., Novak, M. (eds): Geologija Slovenije – The Geology of Slovenia, 612 pp.

Vreča, P., Bronić, I. K., Horvatinčić, N., Barešić, J. (2006): Isotopic characteristics of precipitation in Slovenia and Croatia: Comparison of continental and maritime stations, In: Journal of Hydrology, 330:457-469

White, B. W. (2012): Hydrogeology of Karst Aquifers, In: White, W. B., Culver, D. C. (eds.): Encyclopedia of caves, Elsevier, Amsterdam, 962 pp.

Wigley, T. M. L. (1973): The incongruent solution of dolomite, In: Geochimica et Cosmochimica Acta, Pergamon Press, 37:1397-1402

Wigley, T. M. L. (1973b): Chemical evolution of the system calcite-gypsum-water, In: Can. J. Earth Sci., 10:306-315

Zmazek, B., Italiano, F., Živčić, M., Vaupotič, J., Kobal, I., Martinelli, G. (2002): Geochemical monitoring of thermal waters in Slovenia: relationships to seismic activity, In: Applied Radiation and Isotopes, Pergamon, 57:919-930

7.2. Internet

http://www.geo-zs.si/UserFiles/677/Image/Geotermalne_karte/T1000k_v2013dec.jpg, requested 06.11.2014 16:40

http://meteo.arso.gov.si/met/en/app/webmet/, requested 15.01.2014, 10:34

7.3. List of figures

7.4. List of tables

7.5. List of abbreviations

a. s. l.	above sea level
BAA	Zgornija Besnica A
BA	Zgornija Besnica
BH	Bled Hotel
BW	Bizjakov Mlin water
B	Bizjakov Mlin
C	Cerkno
CRDS	Cavity Rind Down Spectrometer
D	Dolenja
E. B.	electrical balance
EC	electrical conductivity
eds	editors
Fig.	Figure
F	Furnalove Toplice
PHREEQC	pH-REdox-EQuilibrium
J	Divje Jezero
K	Izvir Kroparice
L	Lipnica
M	Mans power
ma ago	million years ago
std	standard deviation
IC	ion chromatography
Q	discharge
PG	tube from Podklanec
P	Podklanec
R	Rodofov Mlin
S	Zeplinica
SI	saturation indices
SLAP	Standard Light Antarctic Precipitation
SR	Zeplinica river
ST	Straza spodnje Pirniče
TDS	total dissolved solids
T	Toplice Hotavlje, Kopačnica
VSMOW	Vienna Standard Mean Ocean Water
V	Vrh
ZE	above Zeplinica
Z	Zavč an

Appendix

1) **Relief map with sampling points**
2) **Tectonic maps of the Rovte and Cerkno area**
3) **Map of Jama pri Sv. Treh kraljih**
4) **Map of cave Mravljetovo brezno v Gošarjevih rupah**
5) **Map of cave Matjaževe Kamre**
6) **Hydrochemistry and Isotopes of sampling points**
7) **Statistical data of each parameter and sampling point**
8) **Z (Zavčan)**
9) **R (Rodofov mlin)**
10) **B (Bizjakov mlin)**
11) **BW (Bizjakov mlin water)**
12) **P (Podklanec)**
13) **PG (Podklanec G)**
14) **V (Vrh)**
15) **D (Dolini)**
16) **C (Cerkno Hotel)**
17) **T (Toplice Hotavlje, Kopačnica)**
18) **BH (Bled Hotel)**
19) **ST (Straza spodnje Pirniče)**
20) **F (Furnalove Toplice)**
21) **ZE (above Zeplinica)**
22) **S (Zeplinica)**
23) **SR (Zeplinica river)**
24) **L (Lipnica)**
25) **M (Mans power)**
26) **K (Izvir Kroparice)**
27) **BAA (Zgornja Besnica A)**
28) **BA (Zgornja Besnica)**
29) **J (Divje Jezero)**

1) Relief map with sampling points

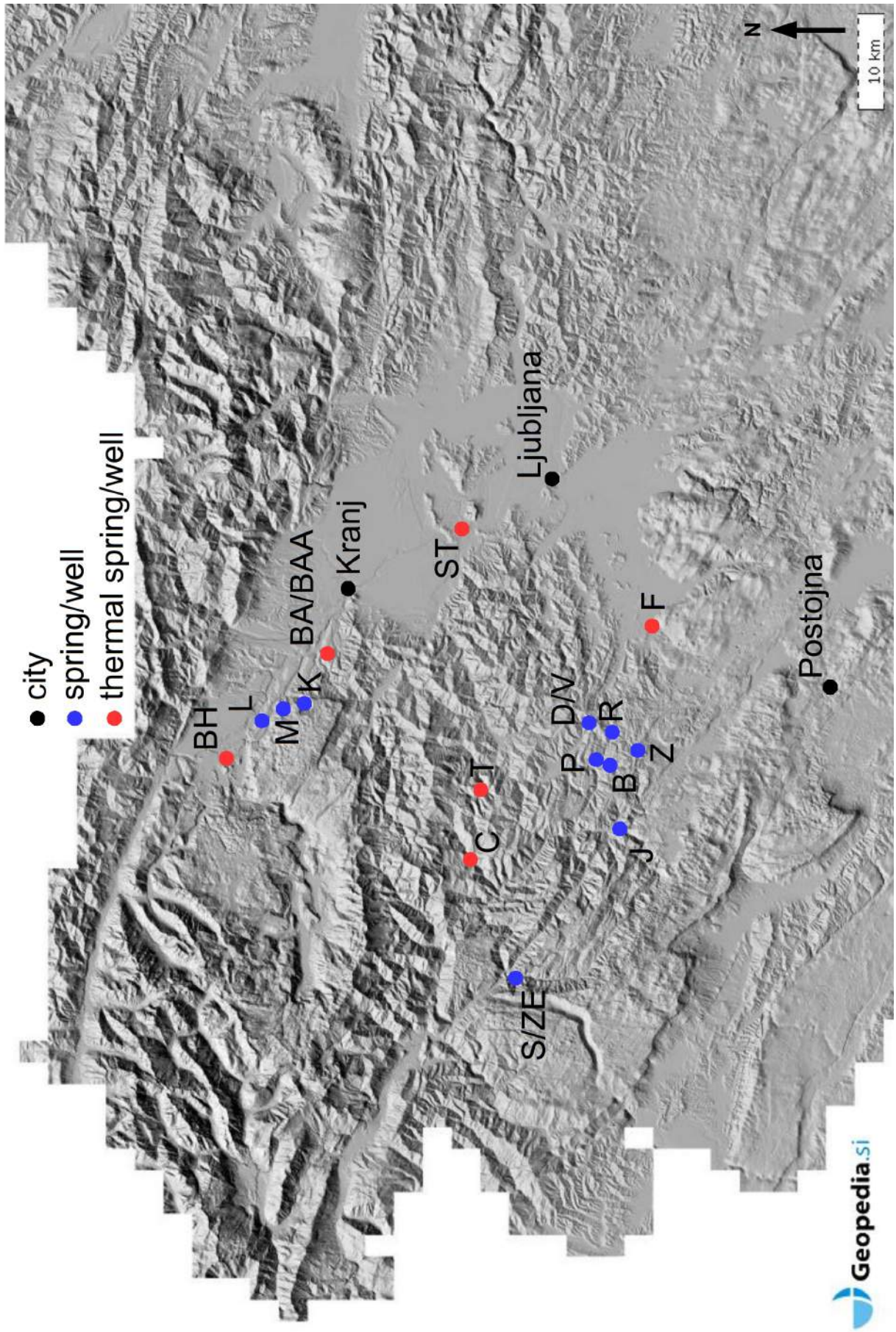

2) Tectonic maps of the Rovte and Cerkno area

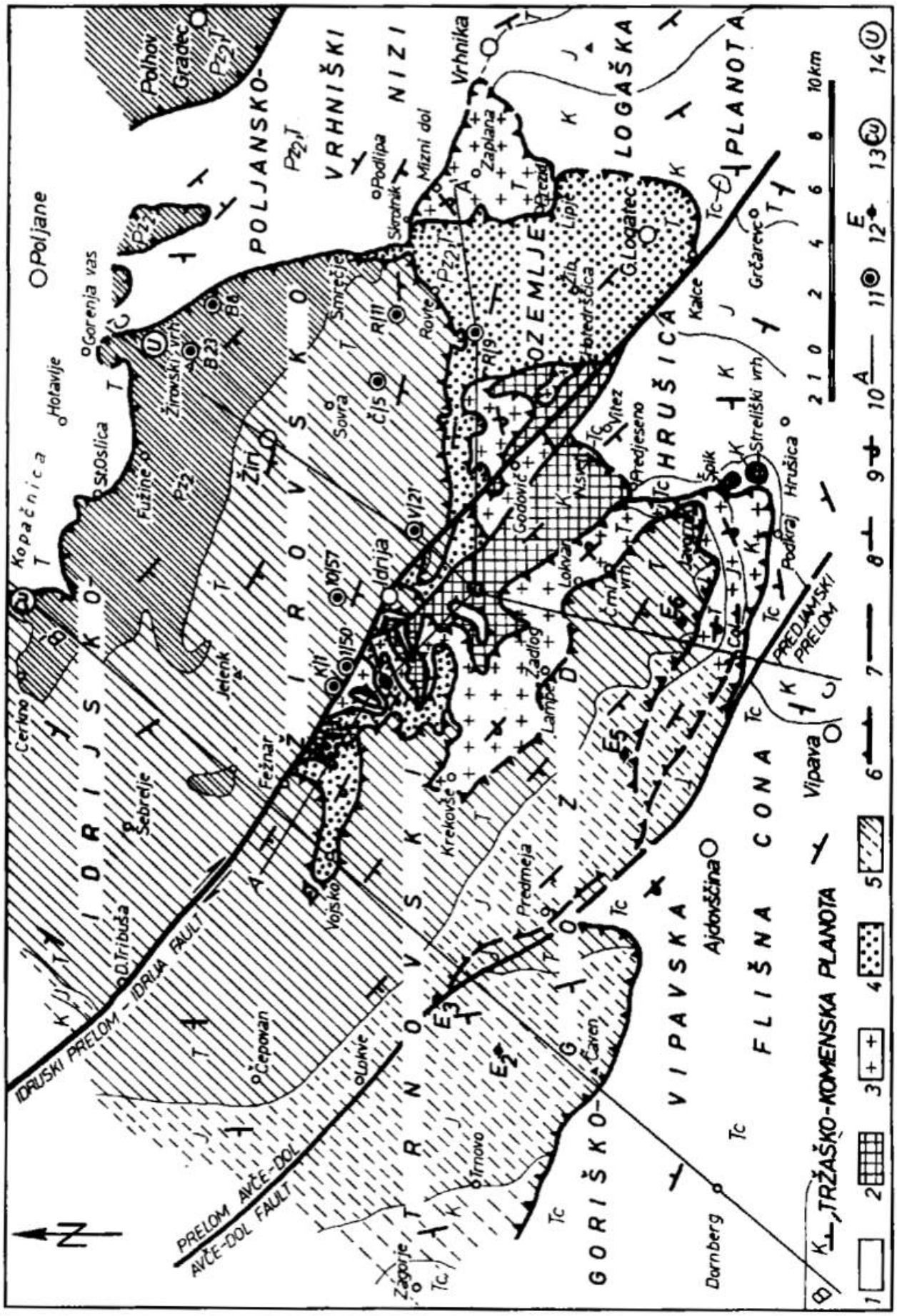

Description: Tectonic map of the Idrija region, 1 Autochthonous basement, 2 Koševnik nappe, 3 Čekovnik nappe, 4 Idrija nappe, 5 Žiri-Trnovo nappe, 6 nappe border, 7 fault, 8 Normal sequence, 9 Inverted sequence, 10 Section, 11 Borehole, 12 Geoelectrical sounding, 13 Copper ore deposit Škofje, 14 Uranium ore deposit Gorenja Vas, P_{z2} Upper Paleozoic beds, T Triassic beds, J Jurrasic beds, K Cretaceous beds, Tc Tertiary beds (Mlakar, 1969)

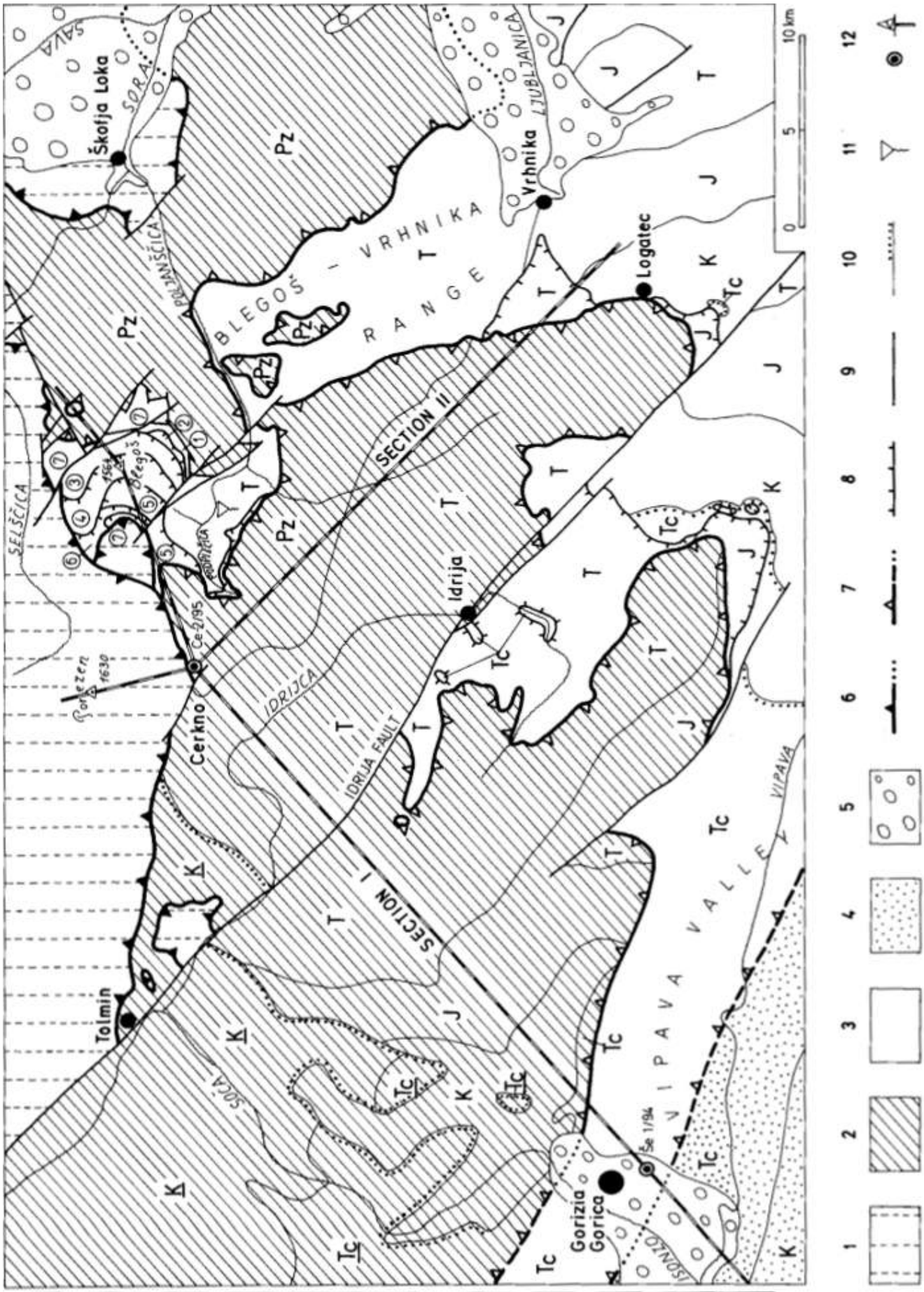

Description: Tectonic sketch of the northwestern part of the External Dinarides, 1 Southern Alps, 2 Trnovo nappe, 3 Hrušica nappe, 4 Komen thrust sheet, 5 Alluvium, 6 Southalpine thrust front, 7 Nappe Boundary in the External Dinarides, 8 Boundary of the intermediate nappe horse, 9 Fault, 10 Geologic Boundary - normal, unconformity, 11 Thermal spring in the Kopačnica (T), 12 Borehole - in the tectonic sketch, in the section, Pz, T, J, K, Tc - Rocks of the central part of the External Dinarides, K, Tc - Rocks of the margin of the External Dinarides, (1) to (7) The Mt. Blegoš nappe sheets (Placer et al., 2000)

3) Map of Jama pri Sv. Treh kraljih

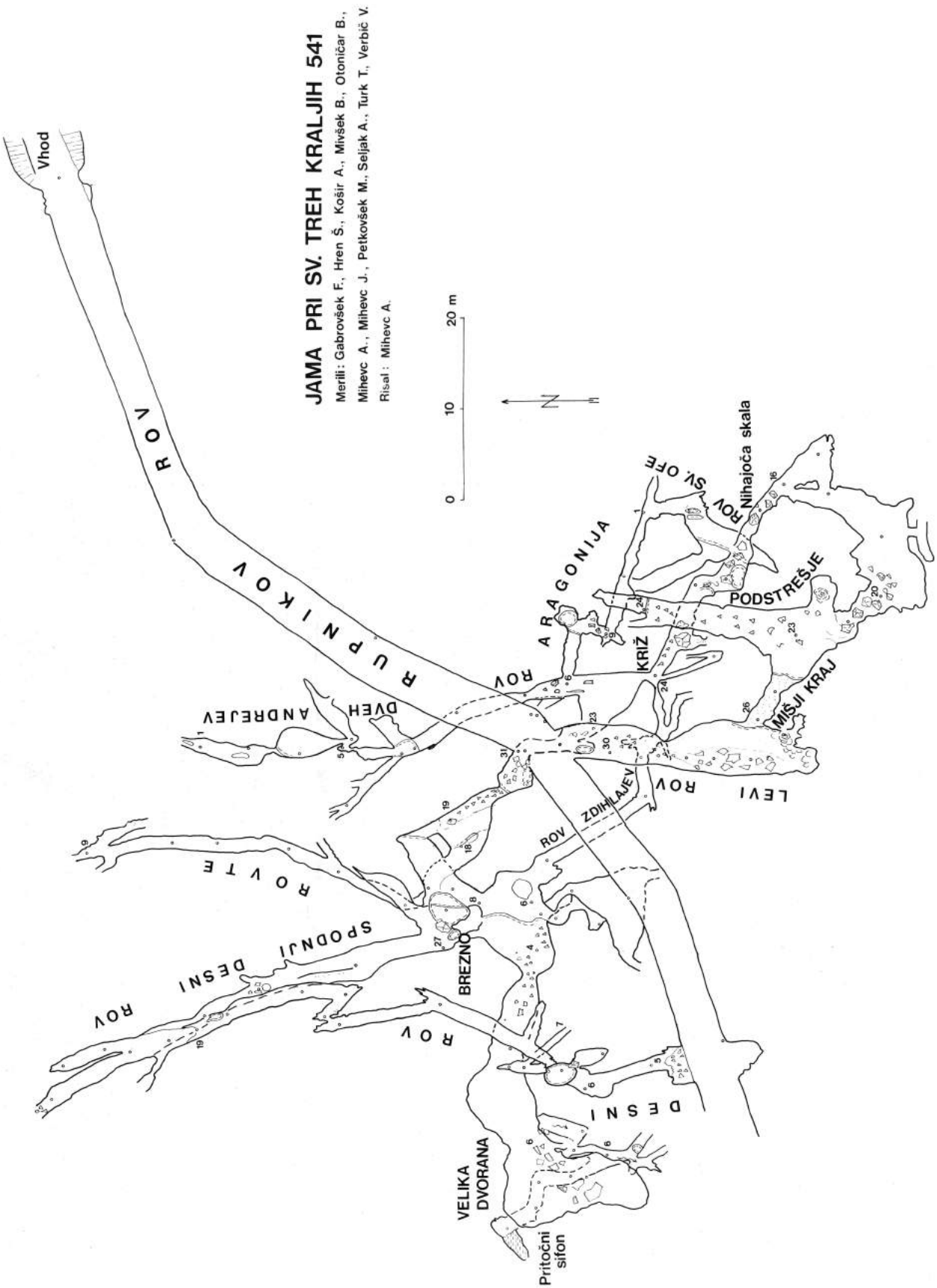

4) Map of cave Mravljetovo brezno v Gošarjevih rupah

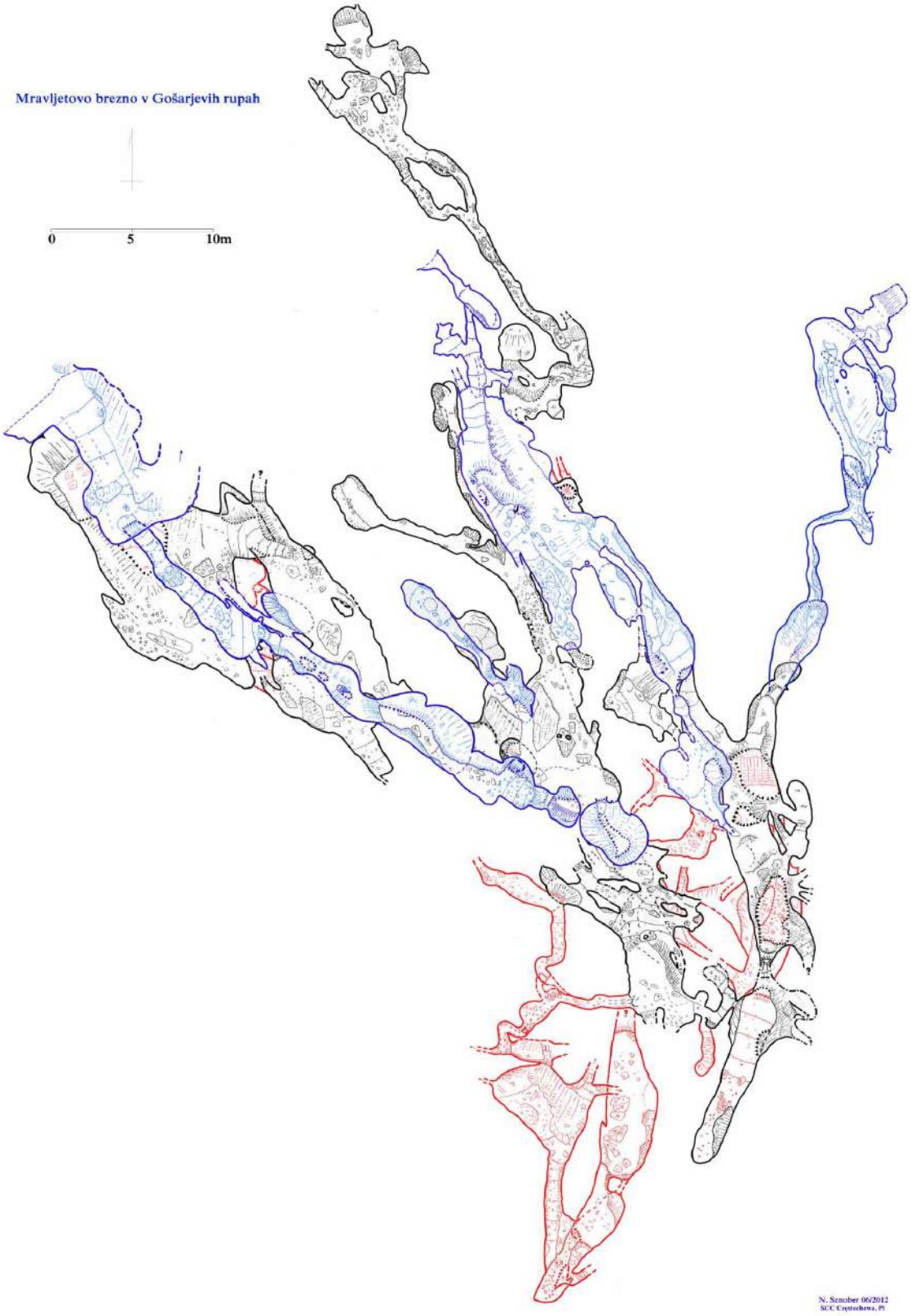

5) Map of cave Matjaževe Kamre

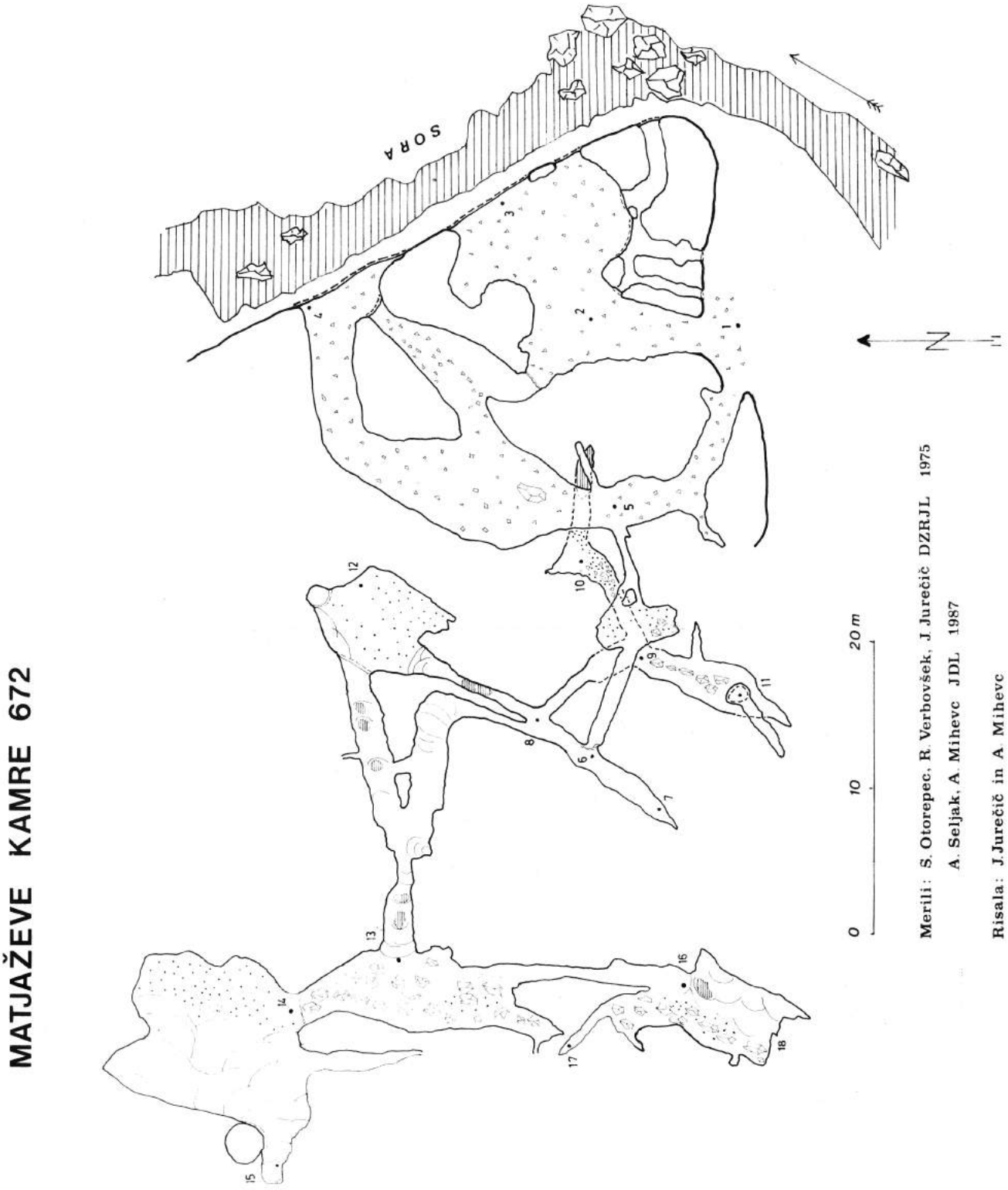

6) Hydrochemistry and Isotopes of sampling points

Ident	Coordinates (zone 33T)		altitude	Field measurements				Analysis Lab Post/Darm			
	easting	northing	[m]	date	T [°C]	pH	EC [µS/cm]	date	T [°C]	pH	EC [µS/cm]
Z1	436480.44	5091629.63	612	04/17/13	10.2	7.21	1564	04/18/13	22.8	7.2	
Z2	436480.44	5091629.63	612	04/25/13	11.4	7.16	1548	04/26/13	24.4	7.2	
Z3	436480.44	5091629.63	612	05/08/13	10.4	7.40	1597	05/09/13	21.4	7.5	
Z4	436480.44	5091629.63	612	07/02/13	10.0	7.27	1636	07/03/13	20.1	7.3	1615
Z5	436480.44	5091629.63	612	07/18/13	10.0	7.45	1673	07/19/13			
Z6	436480.44	5091629.63	612	07/27/13	10.0	7.13	1685	07/29/13	17.3		1580
Z7	436480.44	5091629.63	612	06/06/14	10.0	7.46	1608	07/08/14			
Z8	436480.44	5091629.63	612	06/23/14	10.0	7.40	1640	07/08/14			
R1	435351.31	5094276.77	597	04/17/13	9.4	7.57	780	04/18/13	22.4	7.6	
R2	435351.31	5094276.77	597	04/25/13	10.1	7.51	779	04/26/13	24.3	7.6	
R3	435351.31	5094276.77	597	05/08/13	10.5	7.78	783	05/09/13	21.1	7.8	
R4	435351.31	5094276.77	597	07/02/13	9.3	7.54	782	07/03/13	19.6	7.6	778
R5	435351.31	5094276.77	597	07/17/13	9.3	7.50	789	07/19/13			
R6	435351.31	5094276.77	597	07/27/13	9.4	7.70	793	07/29/13	18.7		762
R7	435351.31	5094276.77	597	06/06/14	9.2	7.78	774	07/08/14			
R8	435351.31	5094276.77	597	06/23/14	9.2	7.69	775	07/08/14			
B1	431558.15	5094547.05	564	04/17/13	10.4	7.59	509	04/18/13	22.7	7.7	
B2	431558.15	5094547.05	564	04/25/13	10.2	7.41	509	04/26/13	24.5	7.5	
B3	431558.15	5094547.05	564	05/08/13	11.4	7.69	515	05/09/13	21.1	7.8	
B4	431558.15	5094547.05	564	07/02/13	10.3	7.56	508	07/03/13	19.3	7.6	508
B5	431558.15	5094547.05	564	07/18/13	10.3	7.53	516	07/19/13			
B6	431558.15	5094547.05	564	07/27/13	10.3	7.48	516	07/29/13	19.2		502
B7	431558.15	5094547.05	564	06/06/14	10.2	7.74	498	07/08/14			
B8	431558.15	5094547.05	564	06/23/14	10.2	7.68	441	07/08/14			
BW	431538.00	5094533.00	564	07/27/13	15.3	8.48	390	07/29/13	20.0		380
BW2	431538.00	5094533.00	564								
P1	432398.05	5095111.16	528	04/17/13	8.3	7.83	299	04/18/13	22.5	7.9	
P2	432398.05	5095111.16	528	04/25/13	8.4	7.76	343	04/26/13	24.5	7.8	
P3	432398.05	5095111.16	528	05/08/13	9.9	8.02	323	05/09/13	21.1	8.1	
P4	432398.05	5095111.16	528	07/02/13	8.9	7.80	405	07/03/13	19.2	7.8	406
P5	432398.05	5095111.16	528	07/18/13	9.1	7.76	409	07/19/13			
P6	432398.05	5095111.16	528	07/27/13	9.3	7.80	407	07/29/13	18.3		392
P7	432398.05	5095111.16	528	06/06/14	8.8	8.09	376	07/08/14			
P8	432398.05	5095111.16	528	06/23/14	9.0	7.90	389	07/08/14			
PG	432497.30	5095249.43	502	07/27/13	12.4	7.67	407	07/29/13	20.1		399
V1	434907.72	5095222.98	724	05/08/13	10.3	7.86	496	05/09/13	21.8	7.9	
D1	435291.85	5095754.87	739	07/02/13	8.9	7.50	355	07/03/13	19.7	7.5	356
D2	435291.85	5095754.87	739	07/17/13	8.8	7.17	363	07/19/13			
D3	435291.85	5095754.87	739	27/07/13	8.9	7.20	362	07/29/13	20.7		369
D4	435291.85	5095754.87	739	06/06/14	8.6	7.53	349	07/09/14			
D5	435291.85	5095754.87	739	06/23/14	8.7	7.54	353	07/09/14			
C1	421836.24	5108725.83	320	18/07/13	20.1	7.91	288	07/19/13			
C2	421836.24	5108725.83	320	27/07/13	22.8	8.07	284	07/29/13	20.2		276
C3	421836.24	5108725.83	320	08/06/14	27.5	8.10	281	07/08/14			
C4	421836.24	5108725.83	320	24/06/14	27.0	8.04	282	07/08/14			
TA1	429483.70	5107717.93	469	18/07/13	20.4	7.44	330	07/19/13			
TA2	429483.70	5107717.93	469	27/07/13	20.4	7.50	330	07/29/13	20.2		320
TA3	429483.70	5107717.93	469	07/06/14	20.3	7.78	320	07/08/14			
TA4	429483.70	5107717.93	469	24/06/14	20.4	7.72	320	07/08/14			
TB1	429483.70	5107717.93	469	18/07/13	23.1	7.47	329	07/19/13			
TB2	429483.70	5107717.93	469	24/06/14	23.0	7.79	317	07/08/14			
BH1	431335.06	5135067.15	482	26/07/13	23.8	6.79	963	07/29/13	19.9		902
BH2	431335.06	5135067.15	482	08/06/14	23.5	6.86	891	07/09/14			
BH3	431335.06	5135067.15	482	25/06/14	22.0	6.93	892	07/09/14			

Ident	Coordinates (zone 33T)		altitude	Field measurements				Analysis Lab Post/Darm			
	easting	northing	[m]	date	T [°C]	pH	EC [µS/cm]	date	T [°C]	pH	EC [µS/cm]
ST1	456074.77	5108989.34	310	26/07/13	20.4	7.32	372	07/29/13	19.7		358
ST2	456074.77	5108989.34	310	08/06/14	20.3	7.68	279	07/09/14			
ST3	456074.77	5108989.34	310	25/06/14	20.2	7.51	358	07/09/14			
F1	445541.92	5089672.36	322	06/06/14	23.9	7.84	434	07/08/14			
F2	445541.92	5089672.36	322	06/23/14	23.8	7.68	451	07/08/14			
ZE1	409419.72	5101988.16	259	18/07/13	10.8	7.20	401	07/19/13			
ZE2	409419.72	5101988.16	259	27/07/13	10.9	7.48	400	07/29/13	19.7		391
ZE3	409419.72	5101988.16	259	07/06/14	10.6	7.62	385	07/08/14			
ZE4	409419.72	5101988.16	259	24/06/14	10.8	7.46	384	07/08/14			
S1	409292.20	5102119.24	251	07/02/13	10.7	7.54	423	07/03/13	22.2	7.8	425
S2	409292.20	5102119.24	251	18/07/13	10.7	7.41	431	07/19/13			
S3	409292.20	5102119.24	251	27/07/13	10.8	7.44	432	07/29/13	20.3		421
S4	409292.20	5102119.24	251	07/06/14	10.7	7.72	417	07/09/14			
S5	409292.20	5102119.24	251	24/06/14	10.8	7.68	419	07/09/14			
SR1	409307.00	5102111.00	250	27/07/13	18.5	8.19	316	07/29/13	19.9		309
SR2	409307.00	5102111.00	250	24/06/14	14.5	8.47	288	07/09/14			
L1	435252.73	5129983.41	510	26/07/13	7.0	7.86	264	07/29/13	19.8		259
L2	435252.73	5129983.41	510	08/06/14	6.8	8.23	247	07/09/14			
L3	435252.73	5129983.41	510	25/06/14	6.7	7.98	229	07/09/14			
M1	437400.49	5128564.02	572	16/07/13	15.2	6.05	1995	07/17/13	19.8	6.1	1987
M2	437400.49	5128564.02	572	26/07/13	15.3	6.11	1994	07/29/13	20.2		1925
M3	437400.49	5128564.02	572	08/06/14	15.0	6.26	1951	07/08/14			
M31	437400.49	5128564.02	572	25/06/14							
M41	437400.49	5128564.02	572	25/06/14							
M42	437400.49	5128564.02	572	25/06/14	15.0	6.17	1878	07/08/14			
K1	437947.54	5126062.27	630	26/07/13	7.3	7.90	273	07/29/13	19.6		267
K2	437947.54	5126062.27	630	08/06/14	7.0	8.17	259	07/09/14			
K3	437947.54	5126062.27	630	25/06/14	6.9	7.98	237	07/09/14			
KA	437947.54	5126062.27	630	25/06/14	7.0	8.00	256	07/09/14			
BAA1	443017.38	5124442.20	435	26/07/13	11.8	7.34	328	07/29/13	19.9		321
BAA2	443017.38	5124442.20	435	08/06/14	11.6	7.69	318	07/09/14			
BAA3	443017.38	5124442.20	435	25/06/14	11.9	7.69	297	07/09/14			
BA1	443141.85	5124441.62	437	16/07/13	16.2	7.08	469	07/17/13	20.1	7.1	467
BA2	443141.85	5124441.62	437	26/07/13	16.3	7.44	465	07/29/13	19.8		457
BA3	443141.85	5124441.62	437	08/06/14	15.3	7.44	427	07/09/14			
BA4	443141.85	5124441.62	437	25/06/14	15.1	7.38	495	07/09/14			
J1	424704.34	5092496.53	614	07/06/14	8.7	8.04	312	07/09/14			
J2	424704.34	5092496.53	614	24/06/14	8.7	8.65	252	07/09/14			

b. d.: below detection limit

Ident	Li^+			Na^+			NH_4^+			K^+		
	mg/l	mmol/l	meq/l	mg/l	mmol/l	meq/l	mg/l	mmol/l	meq/l	mg/l	mmol/l	meq/l
Z1												
Z2												
Z3												
Z4												
Z5												
Z6	b. d.	b. d.	b. d.	4.765	0.207	0.207	0.019	0.001	0.001	0.801	0.020	0.020
Z7	b. d.	b. d.	b. d.	1.926	0.084	0.084	b. d.	b. d.	b. d.	b. d.	b. d.	b. d.
Z8	b. d.	b. d.	b. d.	3.288	0.143	0.143	b. d.	b. d.	b. d.	0.294	0.008	0.008
R1												
R2												
R3												
R4												
R5												
R6	b. d.	b. d.	b. d.	1.905	0.083	0.083	0.027	0.001	0.001	0.560	0.014	0.014
R7	b. d.	b. d.	b. d.	1.360	0.059	0.059	b. d.	b. d.	b. d.	0.126	0.003	0.003
R8	b. d.	b. d.	b. d.	1.549	0.067	0.067	b. d.	b. d.	b. d.	0.162	0.004	0.004
B1												
B2												
B3												
B4												
B5												
B6	0.008	0.001	0.001	6.116	0.266	0.266	0.072	0.004	0.004	1.137	0.029	0.029
B7	0.016	0.002	0.002	5.646	0.246	0.246	0.151	0.008	0.008	0.788	0.020	0.020
B8	b. d.	b. d.	b. d.	5.773	0.251	0.251	0.084	0.005	0.005	0.812	0.021	0.021
BW	b. d.	b. d.	b. d.	0.858	0.037	0.037	0.039	0.002	0.002	0.338	0.009	0.009
BW2												
P1												
P2												
P3												
P4												
P5												
P6	b. d.	b. d.	b. d.	1.214	0.053	0.053	0.064	0.004	0.004	0.508	0.013	0.013
P7	b. d.	b. d.	b. d.	0.620	0.027	0.027	b. d.	b. d.	b. d.	b. d.	b. d.	b. d.
P8	b. d.	b. d.	b. d.	0.453	0.020	0.020	b. d.	b. d.	b. d.	b. d.	b. d.	b. d.
PG	b. d.	b. d.	b. d.	1.088	0.047	0.047	0.080	0.004	0.004	0.443	0.011	0.011
V1												
D1												
D2												
D3	b. d.	b. d.	b. d.	2.717	0.118	0.118	0.063	0.003	0.003	1.550	0.040	0.040
D4	b. d.	b. d.	b. d.	2.619	0.114	0.114	0.028	0.002	0.002	0.591	0.015	0.015
D5	b. d.	b. d.	b. d.	2.724	0.118	0.118	b. d.	b. d.	b. d.	0.747	0.019	0.019
C1												
C2	0.003	0.000	0.000	1.917	0.083	0.083	0.096	0.005	0.005	0.990	0.025	0.025
C3	0.005	0.001	0.001	1.881	0.082	0.082	0.033	0.002	0.002	0.727	0.019	0.019
C4	0.003	0.000	0.000	1.849	0.080	0.080	0.033	0.002	0.002	0.850	0.022	0.022
TA1												
TA2	b. d.	b. d.	b. d.	0.807	0.035	0.035	0.067	0.004	0.004	1.191	0.030	0.030
TA3	b. d.	b. d.	b. d.	0.980	0.043	0.043	0.033	0.002	0.002	0.738	0.019	0.019
TA4	b. d.	b. d.	b. d.	0.786	0.034	0.034	0.021	0.001	0.001	0.735	0.019	0.019
TB1												
TB2	0.004	0.001	0.001	1.337	0.058	0.058	0.032	0.002	0.002	1.372	0.035	0.035
BH1	0.011	0.002	0.002	6.210	0.270	0.270	0.040	0.002	0.002	1.504	0.038	0.038
BH2	b. d.	b. d.	b. d.	5.428	0.236	0.236	b. d.	b. d.	b. d.	0.756	0.019	0.019
BH3	b. d.	b. d.	b. d.	5.332	0.232	0.232	b. d.	b. d.	b. d.	0.764	0.020	0.020

Ident	Li^+			Na^+			NH_4^+			K^+		
	mg/l	mmol/l	meq/l	mg/l	mmol/l	meq/l	mg/l	mmol/l	meq/l	mg/l	mmol/l	meq/l
ST1	b. d.	b. d.	b. d.	3.043	0.132	0.132	0.080	0.004	0.004	1.385	0.035	0.035
ST2	b. d.	b. d.	b. d.	2.089	0.091	0.091	b. d.	b. d.	b. d.	0.302	0.008	0.008
ST3	b. d.	b. d.	b. d.	2.265	0.099	0.099	b. d.	b. d.	b. d.	0.307	0.008	0.008
F1	b. d.	b. d.	b. d.	0.995	0.043	0.043	b. d.	b. d.	b. d.	0.135	0.003	0.003
F2	b. d.	b. d.	b. d.	1.275	0.055	0.055	b. d.	b. d.	b. d.	0.232	0.006	0.006
ZE1												
ZE2	b. d.	b. d.	b. d.	0.583	0.025	0.025	0.035	0.002	0.002	0.315	0.008	0.008
ZE3	b. d.	b. d.	b. d.	0.521	0.023	0.023	b. d.	b. d.	b. d.	0.134	0.003	0.003
ZE4	b. d.	b. d.	b. d.	0.224	0.010	0.010	b. d.	b. d.	b. d.	b. d.	b. d.	b. d.
S1												
S2												
S3	0.008	0.001	0.001	8.130	0.354	0.354	0.056	0.003	0.003	1.070	0.027	0.027
S4	b. d.	b. d.	b. d.	3.782	0.165	0.165	b. d.	b. d.	b. d.	0.486	0.012	0.012
S5	b. d.	b. d.	b. d.	4.382	0.191	0.191	0.043	0.002	0.002	0.536	0.014	0.014
SR1	b. d.	b. d.	b. d.	1.065	0.046	0.046	0.146	0.008	0.008	0.318	0.008	0.008
SR2	b. d.	b. d.	b. d.	1.256	0.055	0.055	0.012	0.001	0.001	0.254	0.006	0.006
L1	b. d.	b. d.	b. d.	0.717	0.031	0.031	0.052	0.003	0.003	0.189	0.005	0.005
L2	b. d.	b. d.	b. d.	0.361	0.016	0.016	b. d.	b. d.	b. d.	0.045	0.001	0.001
L3	b. d.	b. d.	b. d.	0.228	0.010	0.010	b. d.	b. d.	b. d.	0.025	0.001	0.001
M1												
M2	0.136	0.020	0.020	38.288	1.665	1.665	0.219	0.012	0.012	11.982	0.306	0.306
M3	0.113	0.016	0.016	37.700	1.640	1.640	0.597	0.033	0.033	10.467	0.268	0.268
M31												
M41												
M42	0.108	0.016	0.016	36.087	1.570	1.570	0.456	0.025	0.025	10.377	0.265	0.265
K1	b. d.	b. d.	b. d.	0.941	0.041	0.041	0.056	0.003	0.003	0.281	0.007	0.007
K2	b. d.	b. d.	b. d.	0.297	0.013	0.013	b. d.	b. d.	b. d.	b. d.	b. d.	b. d.
K3	b. d.	b. d.	b. d.	0.324	0.014	0.014	b. d.	b. d.	b. d.	b. d.	b. d.	b. d.
KA	b. d.	b. d.	b. d.	0.360	0.016	0.016	b. d.	b. d.	b. d.	0.053	0.001	0.001
BAA1	b. d.	b. d.	b. d.	4.514	0.196	0.196	0.048	0.003	0.003	0.787	0.020	0.020
BAA2	0.003	0.000	0.000	4.292	0.187	0.187	0.017	0.001	0.001	0.582	0.015	0.015
BAA3	b. d.	b. d.	b. d.	4.558	0.198	0.198	0.024	0.001	0.001	0.712	0.018	0.018
BA1												
BA2	b. d.	b. d.	b. d.	7.061	0.307	0.307	0.059	0.003	0.003	1.263	0.032	0.032
BA3	0.007	0.001	0.001	5.512	0.240	0.240	0.043	0.002	0.002	0.738	0.019	0.019
BA4	b. d.	b. d.	b. d.	21.321	0.927	0.927	0.091	0.005	0.005	1.286	0.033	0.033
J1	b. d.	b. d.	b. d.	2.116	0.092	0.092	0.020	0.001	0.001	0.242	0.006	0.006
J2	b. d.	b. d.	b. d.	2.241	0.097	0.097	0.018	0.001	0.001	0.290	0.007	0.007

Ident	Mg^{2+}			Ca^{2+}			$Mg^{2+} + Ca^{2+}$	Mg^{2+}/Ca^{2+}	Mg^{2+}/Ca^{2+}
	mg/l	mmol/l	meq/l	mg/l	mmol/l	meq/l	mg/l	-	-
Z1	58.600	2.411	4.8	273.800	6.832	13.7	332.4	0.21	0.35
Z2	59.000	2.427	4.9	274.600	6.852	13.7	333.6	0.21	0.35
Z3	54.300	2.234	4.5	282.800	7.056	14.1	337.1	0.19	0.32
Z4	74.000	3.045	6.1	276.200	6.892	13.8	350.2	0.27	0.44
Z5	65.400	2.691	5.4	293.000	7.311	14.6	358.4	0.22	0.37
Z6	69.804	2.872	5.7	306.256	7.641	15.3	376.1	0.23	0.38
Z7	64.276	2.645	5.3	283.155	7.065	14.1	347.4	0.23	0.37
Z8	65.674	2.702	5.4	288.731	7.204	14.4	354.4	0.23	0.38
R1	37.400	1.539	3.1	102.800	2.565	5.1	140.2	0.36	0.60
R2	39.700	1.633	3.3	101.400	2.530	5.1	141.1	0.39	0.65
R3	40.200	1.654	3.3	99.400	2.480	5.0	139.6	0.40	0.67
R4	39.600	1.629	3.3	102.100	2.548	5.1	141.7	0.39	0.64
R5	39.800	1.638	3.3	100.500	2.508	5.0	140.3	0.40	0.65
R6	42.400	1.744	3.5	104.308	2.603	5.2	146.7	0.41	0.67
R7	41.027	1.688	3.4	101.241	2.526	5.1	142.3	0.41	0.67
R8	41.127	1.692	3.4	101.029	2.521	5.0	142.2	0.41	0.67
B1	22.400	0.922	1.8	65.900	1.644	3.3	88.3	0.34	0.56
B2	22.700	0.934	1.9	66.100	1.649	3.3	88.8	0.34	0.57
B3	24.600	1.012	2.0	62.700	1.564	3.1	87.3	0.39	0.65
B4	30.200	1.243	2.5	53.900	1.345	2.7	84.1	0.56	0.92
B5	27.900	1.148	2.3	57.800	1.442	2.9	85.7	0.48	0.80
B6	31.691	1.304	2.6	54.203	1.352	2.7	85.9	0.58	0.96
B7	30.909	1.272	2.5	52.956	1.321	2.6	83.9	0.58	0.96
B8	29.880	1.229	2.5	50.897	1.270	2.5	80.8	0.59	0.97
BW	23.973	0.986	2.0	48.638	1.214	2.4	72.6	0.49	0.81
BW2									
P1	11.800	0.485	1.0	42.500	1.060	2.1	54.3	0.28	0.46
P2	16.800	0.691	1.4	45.000	1.123	2.2	61.8	0.37	0.62
P3	15.200	0.625	1.3	41.600	1.038	2.1	56.8	0.37	0.60
P4	22.000	0.905	1.8	50.300	1.255	2.5	72.3	0.44	0.72
P5	21.100	0.868	1.7	51.300	1.280	2.6	72.4	0.41	0.68
P6	23.881	0.983	2.0	50.489	1.260	2.5	74.4	0.47	0.78
P7	20.787	0.855	1.7	49.692	1.240	2.5	70.5	0.42	0.69
P8	22.250	0.915	1.8	50.013	1.248	2.5	72.3	0.44	0.73
PG	23.817	0.980	2.0	50.497	1.260	2.5	74.3	0.47	0.78
V1	8.900	0.366	0.7	69.700	1.739	3.5	78.6	0.13	0.21
D1	9.200	0.379	0.8	55.100	1.375	2.7	64.3	0.17	0.28
D2	9.500	0.391	0.8	55.600	1.387	2.8	65.1	0.17	0.28
D3	10.832	0.446	0.9	57.233	1.428	2.9	68.1	0.19	0.31
D4	10.930	0.450	0.9	55.476	1.384	2.8	66.4	0.20	0.32
D5	10.650	0.438	0.9	56.771	1.417	2.8	67.4	0.19	0.31
C1	16.600	0.683	1.4	30.300	0.756	1.5	46.9	0.55	0.90
C2	16.727	0.688	1.4	31.315	0.781	1.6	48.0	0.53	0.88
C3	16.322	0.672	1.3	30.527	0.762	1.5	46.8	0.53	0.88
C4	16.205	0.667	1.3	30.251	0.755	1.5	46.5	0.54	0.88
TA1	18.700	0.769	1.5	37.100	0.926	1.9	55.8	0.50	0.83
TA2	20.395	0.839	1.7	36.548	0.912	1.8	56.9	0.56	0.92
TA3	19.869	0.817	1.6	35.337	0.882	1.8	55.2	0.56	0.93
TA4	19.894	0.819	1.6	35.345	0.882	1.8	55.2	0.56	0.93
TB1	18.500	0.761	1.5	36.500	0.911	1.8	55.0	0.51	0.84
TB2	19.161	0.788	1.6	34.096	0.851	1.7	53.3	0.56	0.93
BH1	40.172	1.653	3.3	146.272	3.650	7.3	186.4	0.27	0.45
BH2	38.099	1.568	3.1	140.657	3.510	7.0	178.8	0.27	0.45
BH3	37.731	1.552	3.1	139.475	3.480	7.0	177.2	0.27	0.45

Ident	Mg^{2+}			Ca^{2+}			$Mg^{2+} + Ca^{2+}$	Mg^{2+}/Ca^{2+}	Mg^{2+}/Ca^{2+}
	mg/l	mmol/l	meq/l	mg/l	mmol/l	meq/l	mg/l	-	-
ST1	20.817	0.856	1.7	44.200	1.103	2.2	65.0	0.47	0.78
ST2	20.073	0.826	1.7	43.898	1.095	2.2	64.0	0.46	0.75
ST3	20.331	0.836	1.7	44.452	1.109	2.2	64.8	0.46	0.75
F1	27.195	1.119	2.2	50.390	1.257	2.5	77.6	0.54	0.89
F2	27.001	1.111	2.2	50.312	1.255	2.5	77.3	0.54	0.88
ZE1	24.900	1.024	2.0	44.900	1.120	2.2	69.8	0.55	0.91
ZE2	25.714	1.058	2.1	46.596	1.163	2.3	72.3	0.55	0.91
ZE3	25.006	1.029	2.1	46.213	1.153	2.3	71.2	0.54	0.89
ZE4	25.173	1.036	2.1	46.446	1.159	2.3	71.6	0.54	0.89
S1	23.800	0.979	2.0	45.800	1.143	2.3	69.6	0.52	0.86
S2	23.700	0.975	2.0	45.800	1.143	2.3	69.5	0.52	0.85
S3	25.462	1.048	2.1	46.968	1.172	2.3	72.4	0.54	0.89
S4	22.741	0.936	1.9	44.497	1.110	2.2	67.2	0.51	0.84
S5	23.956	0.986	2.0	46.176	1.152	2.3	70.1	0.52	0.86
SR1	19.106	0.786	1.6	37.046	0.924	1.8	56.2	0.52	0.85
SR2	16.471	0.678	1.4	35.773	0.893	1.8	52.2	0.46	0.76
L1	7.169	0.295	0.6	44.683	1.115	2.2	51.9	0.16	0.26
L2	6.282	0.258	0.5	43.133	1.076	2.2	49.4	0.15	0.24
L3	5.550	0.228	0.5	43.779	1.092	2.2	49.3	0.13	0.21
M1	60.100	2.473	4.9	359.100	8.960	17.9	419.2	0.17	0.28
M2	59.487	2.448	4.9	381.222	9.512	19.0	440.7	0.16	0.26
M3	53.758	2.212	4.4	351.310	8.766	17.5	405.1	0.15	0.25
M31									
M41									
M42	50.743	2.088	4.2	334.495	8.346	16.7	385.2	0.15	0.25
K1	10.842	0.446	0.9	40.988	1.023	2.0	51.8	0.26	0.44
K2	9.427	0.388	0.8	40.818	1.018	2.0	50.2	0.23	0.38
K3	8.628	0.355	0.7	41.136	1.026	2.1	49.8	0.21	0.35
KA	8.122	0.334	0.7	42.081	1.050	2.1	50.2	0.19	0.32
BAA1	10.142	0.417	0.8	49.292	1.230	2.5	59.4	0.21	0.34
BAA2	10.016	0.412	0.8	48.435	1.209	2.4	58.5	0.21	0.34
BAA3	8.117	0.334	0.7	46.032	1.149	2.3	54.1	0.18	0.29
BA1	17.600	0.724	1.4	63.800	1.592	3.2	81.4	0.28	0.45
BA2	19.154	0.788	1.6	65.045	1.623	3.2	84.2	0.29	0.49
BA3	16.318	0.671	1.3	64.253	1.603	3.2	80.6	0.25	0.42
BA4	15.405	0.634	1.3	63.214	1.577	3.2	78.6	0.24	0.40
J1	13.126	0.540	1.1	44.018	1.098	2.2	57.1	0.30	0.49
J2	11.745	0.483	1.0	33.727	0.842	1.7	45.5	0.35	0.57

Ident	$Fe^{2+/3+}$			Sr^{2+}			Mn^{2+}			F^{-}		
	mg/l	mmol/l	meq/l	mg/l	mmol/l	meq/l	mg/l	mmol/l	meq/l	mg/l	mmol/l	meq/l
Z1												
Z2												
Z3												
Z4												
Z5												
Z6	0.447	0.008	0.016	0.020	0.000	0.000	0.006	0.000	0.000	0.325	0.017	0.017
Z7	0.047	0.001	0.002	2.445	0.028	0.056	0.008	0.000	0.000	0.090	0.005	0.005
Z8	0.069	0.001	0.002	2.356	0.027	0.054	0.011	0.000	0.000	0.686	0.036	0.036
R1												
R2												
R3												
R4												
R5												
R6	0.071	0.001	0.003	0.006	0.000	0.000	0.011	0.000	0.000	0.114	0.006	0.006
R7	0.045	0.001	0.002	0.830	0.009	0.019	0.008	0.000	0.000	0.074	0.004	0.004
R8	0.597	0.011	0.021	0.939	0.011	0.021	0.015	0.000	0.001	0.048	0.003	0.003
B1												
B2												
B3												
B4												
B5												
B6	0.146	0.003	0.005	0.046	0.001	0.001	0.007	0.000	0.000	0.191	0.010	0.010
B7	0.057	0.001	0.002	4.393	0.050	0.100	0.009	0.000	0.000	0.080	0.004	0.004
B8	0.031	0.001	0.001	b. d.	b. d.	b. d.	0.016	0.000	0.001	0.117	0.006	0.006
BW	0.040	0.001	0.001	0.002	0.000	0.000	0.005	0.000	0.000	0.070	0.004	0.004
BW2												
P1												
P2												
P3												
P4												
P5												
P6	0.036	0.001	0.001	0.002	0.000	0.000	0.003	0.000	0.000	0.072	0.004	0.004
P7	0.037	0.001	0.001	b. d.	b. d.	b. d.	0.004	0.000	0.000	0.035	0.002	0.002
P8	0.044	0.001	0.002	0.233	0.003	0.005	0.007	0.000	0.000	0.037	0.002	0.002
PG	0.028	0.000	0.001	0.002	0.000	0.000	0.005	0.000	0.000	0.114	0.006	0.006
V1												
D1												
D2												
D3	0.064	0.001	0.002	0.001	0.000	0.000	0.018	0.000	0.001	0.074	0.004	0.004
D4	b. d.	b. d.	b. d.	0.352	0.004	0.008	0.001	0.000	0.000	0.034	0.002	0.002
D5	b. d.	b. d.	b. d.	0.471	0.005	0.011	0.003	0.000	0.000	0.032	0.002	0.002
C1												
C2	0.697	0.012	0.025	0.002	0.000	0.000	0.037	0.001	0.001	3.353	0.176	0.176
C3	0.021	0.000	0.001	0.294	0.003	0.007	0.005	0.000	0.000	3.375	0.178	0.178
C4	0.344	0.006	0.012	0.338	0.004	0.008	0.009	0.000	0.000	3.374	0.178	0.178
TA1												
TA2	0.052	0.001	0.002	0.001	0.000	0.000	0.006	0.000	0.000	0.519	0.027	0.027
TA3	b. d.	b. d.	b. d.	0.115	0.001	0.003	b. d.	b. d.	b. d.	0.528	0.028	0.028
TA4	b. d.	b. d.	b. d.	0.121	0.001	0.003	b. d.	b. d.	b. d.	0.483	0.025	0.025
TB1												
TB2	b. d.	b. d.	b. d.	0.387	0.004	0.009	b. d.	b. d.	b. d.	0.598	0.031	0.031
BH1	0.061	0.001	0.002	0.002	0.000	0.000	0.011	0.000	0.000	0.410	0.022	0.022
BH2	0.022	0.000	0.001	0.526	0.006	0.012	0.008	0.000	0.000	0.312	0.016	0.016
BH3	0.009	0.000	0.000	0.580	0.007	0.013	0.004	0.000	0.000	0.310	0.016	0.016

Ident	$Fe^{2+/3+}$			Sr^{2+}			Mn^{2+}			F^{-}		
	mg/l	mmol/l	meq/l	mg/l	mmol/l	meq/l	mg/l	mmol/l	meq/l	mg/l	mmol/l	meq/l
ST1	0.036	0.001	0.001	b. d.	b. d.	b. d.	0.032	0.001	0.001	0.125	0.007	0.007
ST2	0.013	0.000	0.000	b. d.	b. d.	b. d.	0.002	0.000	0.000	0.057	0.003	0.003
ST3	0.003	0.000	0.000	b. d.	b. d.	b. d.	0.002	0.000	0.000	0.055	0.003	0.003
F1	b. d.	b. d.	b. d.	0.388	0.004	0.009	b. d.	b. d.	b. d.	0.137	0.007	0.007
F2	b. d.	b. d.	b. d.	0.455	0.005	0.010	b. d.	b. d.	b. d.	0.161	0.008	0.008
ZE1												
ZE2	0.034	0.001	0.001	b. d.	b. d.	b. d.	0.004	0.000	0.000	0.075	0.004	0.004
ZE3	b. d.	b. d.	b. d.	b. d.	b. d.	b. d.	b. d.	b. d.	b. d.	0.330	0.017	0.017
ZE4	b. d.	b. d.	b. d.	b. d.	b. d.	b. d.	b. d.	b. d.	b. d.	0.031	0.002	0.002
S1												
S2												
S3	0.031	0.001	0.001	b. d.	b. d.	b. d.	0.006	0.000	0.000	0.220	0.012	0.012
S4	0.026	0.000	0.001	b. d.	b. d.	b. d.	0.003	0.000	0.000	0.071	0.004	0.004
S5	0.012	0.000	0.000	b. d.	b. d.	b. d.	0.014	0.000	0.001	0.310	0.016	0.016
SR1	0.070	0.001	0.002	0.001	0.000	0.000	0.005	0.000	0.000	0.065	0.003	0.003
SR2	0.016	0.000	0.001	0.076	0.001	0.002	0.014	0.000	0.000	0.036	0.002	0.002
L1	0.050	0.001	0.002	b. d.	b. d.	b. d.	0.007	0.000	0.000	0.048	0.003	0.003
L2	0.019	0.000	0.001	b. d.	b. d.	b. d.	0.002	0.000	0.000	0.022	0.001	0.001
L3	0.042	0.001	0.002	b. d.	b. d.	b. d.	0.002	0.000	0.000	0.019	0.001	0.001
M1												
M2	0.013	0.000	0.000	0.006	0.000	0.000	0.116	0.002	0.004	2.697	0.142	0.142
M3	0.050	0.001	0.002	1.510	0.017	0.034	0.116	0.002	0.004	2.142	0.113	0.113
M31												
M41												
M42	b. d.	b. d.	b. d.	1.706	0.019	0.039	0.112	0.002	0.004	2.174	0.114	0.114
K1	0.019	0.000	0.001	b. d.	b. d.	b. d.	0.008	0.000	0.000	0.058	0.003	0.003
K2	0.011	0.000	0.000	b. d.	b. d.	b. d.	0.001	0.000	0.000	0.024	0.001	0.001
K3	0.018	0.000	0.001	b. d.	b. d.	b. d.	0.001	0.000	0.000	0.023	0.001	0.001
KA	0.004	0.000	0.000	b. d.	b. d.	b. d.	b. d.	b. d.	b. d.	0.014	0.001	0.001
BAA1	0.055	0.001	0.002	0.001	0.000	0.000	0.011	0.000	0.000	0.103	0.005	0.005
BAA2	0.021	0.000	0.001	0.103	0.001	0.002	0.001	0.000	0.000	0.088	0.005	0.005
BAA3	0.070	0.001	0.003	0.111	0.001	0.003	0.012	0.000	0.000	0.065	0.003	0.003
BA1												
BA2	0.045	0.001	0.002	0.002	0.000	0.000	0.012	0.000	0.000	0.209	0.011	0.011
BA3	0.013	0.000	0.000	0.117	0.001	0.003	0.001	0.000	0.000	0.129	0.007	0.007
BA4	0.018	0.000	0.001	0.238	0.003	0.005	0.007	0.000	0.000	0.121	0.006	0.006
J1	0.015	0.000	0.001	b. d.	b. d.	b. d.	0.001	0.000	0.000	0.036	0.002	0.002
J2	0.029	0.001	0.001	b. d.	b. d.	b. d.	0.003	0.000	0.000	0.028	0.001	0.001

Ident	Cl^-			NO_2^-			Br^-			NO_3^-		
	mg/l	mmol/l	meq/l	mg/l	mmol/l	meq/l	mg/l	mmol/l	meq/l	mg/l	mmol/l	meq/l
Z1	1.430	0.040	0.040							0.188	0.003	0.003
Z2	1.710	0.048	0.048							0.267	0.004	0.004
Z3	1.430	0.040	0.040							0.007	0.000	0.000
Z4	1.430	0.040	0.040							0.150	0.002	0.002
Z5	1.430	0.040	0.040							0.124	0.002	0.002
Z6	2.389	0.067	0.067	b. d.	b. d.	b. d.	1.638	0.020	0.020	0.322	0.005	0.005
Z7	1.725	0.049	0.049	b. d.	b. d.	b. d.	b. d.	b. d.	b. d.	0.353	0.006	0.006
Z8	3.752	0.106	0.106	b. d.	b. d.	b. d.	b. d.	b. d.	b. d.	0.635	0.010	0.010
R1	1.710	0.048	0.048							0.062	0.001	0.001
R2	1.430	0.040	0.040							0.070	0.001	0.001
R3	1.430	0.040	0.040							0.020	0.000	0.000
R4	1.430	0.040	0.040							0.165	0.003	0.003
R5	1.710	0.048	0.048							0.079	0.001	0.001
R6	1.890	0.053	0.053	b. d.	b. d.	b. d.	1.192	0.015	0.015	0.288	0.005	0.005
R7	1.607	0.045	0.045	b. d.	b. d.	b. d.	b. d.	b. d.	b. d.	0.150	0.002	0.002
R8	2.154	0.061	0.061	b. d.	b. d.	b. d.	b. d.	b. d.	b. d.	0.102	0.002	0.002
B1	1.430	0.040	0.040							0.040	0.001	0.001
B2	1.140	0.032	0.032							0.214	0.003	0.003
B3	1.140	0.032	0.032							0.026	0.000	0.000
B4	1.140	0.032	0.032							0.056	0.001	0.001
B5	1.430	0.040	0.040							0.183	0.003	0.003
B6	1.102	0.031	0.031	0.003	0.000	0.000	1.368	0.017	0.017	0.188	0.003	0.003
B7	0.834	0.024	0.024	b. d.	b. d.	b. d.	b. d.	b. d.	b. d.	0.131	0.002	0.002
B8	0.896	0.025	0.025	b. d.	b. d.	b. d.	b. d.	b. d.	b. d.	0.061	0.001	0.001
BW	1.569	0.044	0.044	b. d.	b. d.	b. d.	1.306	0.016	0.016	3.177	0.051	0.051
BW2												
P1	1.710	0.048	0.048							3.365	0.054	0.054
P2	1.710	0.048	0.048							3.675	0.059	0.059
P3	2.000	0.056	0.056							3.215	0.052	0.052
P4	1.710	0.048	0.048							3.107	0.050	0.050
P5	2.000	0.056	0.056							4.488	0.072	0.072
P6	2.134	0.060	0.060	0.004	0.000	0.000	1.296	0.016	0.016	4.018	0.065	0.065
P7	1.574	0.044	0.044	b. d.	b. d.	b. d.	b. d.	b. d.	b. d.	2.874	0.046	0.046
P8	1.516	0.043	0.043	b. d.	b. d.	b. d.	b. d.	b. d.	b. d.	3.125	0.050	0.050
PG	1.927	0.054	0.054	b. d.	b. d.	b. d.	1.396	0.017	0.017	4.127	0.067	0.067
V1	9.120	0.257	0.257							5.729	0.092	0.092
D1	4.560	0.129	0.129							4.293	0.069	0.069
D2	5.420	0.153	0.153							7.835	0.126	0.126
D3	6.936	0.196	0.196	b. d.	b. d.	b. d.	1.116	0.014	0.014	7.945	0.128	0.128
D4	5.574	0.157	0.157	b. d.	b. d.	b. d.	b. d.	b. d.	b. d.	5.439	0.088	0.088
D5	5.655	0.160	0.160	b. d.	b. d.	b. d.	b. d.	b. d.	b. d.	6.233	0.101	0.101
C1	1.430	0.040	0.040							0.034	0.001	0.001
C2	0.902	0.025	0.025	0.006	0.000	0.000	0.850	0.011	0.011	0.146	0.002	0.002
C3	0.712	0.020	0.020	b. d.	b. d.	b. d.	b. d.	b. d.	b. d.	0.030	0.000	0.000
C4	67.044	1.891	1.891	b. d.	b. d.	b. d.	b. d.	b. d.	b. d.	0.059	0.001	0.001
TA1	1.140	0.032	0.032							1.805	0.029	0.029
TA2	0.812	0.023	0.023	b. d.	b. d.	b. d.	1.007	0.013	0.013	1.823	0.029	0.029
TA3	1.229	0.035	0.035	b. d.	b. d.	b. d.	b. d.	b. d.	b. d.	1.802	0.029	0.029
TA4	0.642	0.018	0.018	b. d.	b. d.	b. d.	b. d.	b. d.	b. d.	1.719	0.028	0.028
TB1	1.140	0.032	0.032							0.477	0.008	0.008
TB2	0.548	0.015	0.015	b. d.	b. d.	b. d.	b. d.	b. d.	b. d.	0.411	0.007	0.007
BH1	1.811	0.051	0.051	b. d.	b. d.	b. d.	3.723	0.047	0.047	1.328	0.021	0.021
BH2	1.676	0.047	0.047	b. d.	b. d.	b. d.	b. d.	b. d.	b. d.	0.375	0.006	0.006
BH3	1.485	0.042	0.042	b. d.	b. d.	b. d.	b. d.	b. d.	b. d.	0.723	0.012	0.012

Ident	Cl^-			NO_2^-			Br^-			NO_3^-		
	mg/l	mmol/l	meq/l	mg/l	mmol/l	meq/l	mg/l	mmol/l	meq/l	mg/l	mmol/l	meq/l
ST1	2.140	0.060	0.060	b. d.	b. d.	b. d.	1.253	0.016	0.016	4.643	0.075	0.075
ST2	1.735	0.049	0.049	b. d.	b. d.	b. d.	b. d.	b. d.	b. d.	4.326	0.070	0.070
ST3	1.730	0.049	0.049	b. d.	b. d.	b. d.	b. d.	b. d.	b. d.	4.345	0.070	0.070
F1	1.068	0.030	0.030	b. d.	b. d.	b. d.	b. d.	b. d.	b. d.	1.138	0.018	0.018
F2	1.060	0.030	0.030	b. d.	b. d.	b. d.	b. d.	b. d.	b. d.	1.088	0.018	0.018
ZE1	1.430	0.040	0.040							2.857	0.046	0.046
ZE2	0.980	0.028	0.028	0.012	0.000	0.000	1.334	0.017	0.017	2.450	0.040	0.040
ZE3	1.652	0.047	0.047	b. d.	b. d.	b. d.	b. d.	b. d.	b. d.	2.290	0.037	0.037
ZE4	0.773	0.022	0.022	b. d.	b. d.	b. d.	b. d.	b. d.	b. d.	2.213	0.036	0.036
S1	4.280	0.121	0.121							0.211	0.003	0.003
S2	3.420	0.096	0.096							0.118	0.002	0.002
S3	1.717	0.048	0.048	b. d.	b. d.	b. d.	1.430	0.018	0.018	0.355	0.006	0.006
S4	1.462	0.041	0.041	b. d.	b. d.	b. d.	b. d.	b. d.	b. d.	1.506	0.024	0.024
S5	1.485	0.042	0.042	b. d.	b. d.	b. d.	b. d.	b. d.	b. d.	0.723	0.012	0.012
SR1	0.853	0.024	0.024	0.133	0.003	0.003	0.980	0.012	0.012	3.356	0.054	0.054
SR2	0.704	0.020	0.020	0.025	0.001	0.001	b. d.	b. d.	b. d.	3.364	0.054	0.054
L1	0.496	0.014	0.014	b. d.	b. d.	b. d.	0.833	0.010	0.010	2.340	0.038	0.038
L2	0.516	0.015	0.015	0.016	0.000	0.000	b. d.	b. d.	b. d.	1.693	0.027	0.027
L3	0.399	0.011	0.011	0.103	0.002	0.002	b. d.	b. d.	b. d.	1.780	0.029	0.029
M1	10.260	0.289	0.289							0.084	0.001	0.001
M2	16.327	0.461	0.461	b. d.	b. d.	b. d.	8.559	0.107	0.107	1.564	0.025	0.025
M3	14.470	0.408	0.408	b. d.	b. d.	b. d.	b. d.	b. d.	b. d.	0.268	0.004	0.004
M31												
M41												
M42	13.570	0.383	0.383	b. d.	b. d.	b. d.	b. d.	b. d.	b. d.	0.277	0.004	0.004
K1	0.604	0.017	0.017	0.001	0.000	0.000	0.862	0.011	0.011	2.848	0.046	0.046
K2	0.649	0.018	0.018	b. d.	b. d.	b. d.	b. d.	b. d.	b. d.	2.405	0.039	0.039
K3	0.442	0.012	0.012	b. d.	b. d.	b. d.	b. d.	b. d.	b. d.	2.364	0.038	0.038
KA	0.469	0.013	0.013	0.012	0.000	0.000	b. d.	b. d.	b. d.	2.172	0.035	0.035
BAA1	3.512	0.099	0.099	b. d.	b. d.	b. d.	0.989	0.012	0.012	1.697	0.027	0.027
BAA2	3.489	0.098	0.098	b. d.	b. d.	b. d.	b. d.	b. d.	b. d.	1.358	0.022	0.022
BAA3	3.757	0.106	0.106	0.010	0.000	0.000	b. d.	b. d.	b. d.	1.297	0.021	0.021
BA1	2.850	0.080	0.080							1.004	0.016	0.016
BA2	3.788	0.107	0.107	b. d.	b. d.	b. d.	1.521	0.019	0.019	1.221	0.020	0.020
BA3	3.373	0.095	0.095	0.027	0.001	0.001	b. d.	b. d.	b. d.	0.948	0.015	0.015
BA4	22.537	0.636	0.636	b. d.	b. d.	b. d.	b. d.	b. d.	b. d.	1.065	0.017	0.017
J1	3.416	0.096	0.096	b. d.	b. d.	b. d.	b. d.	b. d.	b. d.	4.993	0.081	0.081
J2	2.937	0.083	0.083	0.033	0.001	0.001	b. d.	b. d.	b. d.	2.811	0.045	0.045

Ident	PO_4^{3-}			SO_4^{2-}			HCO_3^- (Field)			HCO_3^- (Lab)		
	mg/l	mmol/l	meq/l	mg/l	mmol/l	meq/l	mg/l	mmol/l	meq/l	mg/l	mmol/l	meq/l
Z1	0.004	0.000	0.000	736.960	7.672	15.343	181.7	3.0	3.0			
Z2	b. d.	b. d.	b. d.	826.120	8.600	17.200	179.8	2.9	2.9			
Z3	0.002	0.000	0.000	662.720	6.899	13.798	181.3	3.0	3.0			
Z4	0.008	0.000	0.000	662.480	6.896	13.793	180.6	3.0	3.0			
Z5	0.010	0.000	0.000	679.520	7.074	14.147	180.2	3.0	3.0			
Z6	b. d.	b. d.	b. d.	802.360	8.352	16.705	180.6	3.0	3.0			
Z7	b. d.	b. d.	b. d.	782.511	8.146	16.292	168.4	2.8	2.8			
Z8	b. d.	b. d.	b. d.	771.890	8.035	16.071	193.7	3.2	3.2			
R1	b. d.	b. d.	b. d.	299.580	3.119	6.237	167.7	2.7	2.7			
R2	b. d.	b. d.	b. d.	247.870	2.580	5.161	169.0	2.8	2.8			
R3	0.004	0.000	0.000	264.080	2.749	5.498	169.0	2.8	2.8			
R4	0.017	0.000	0.001	279.600	2.911	5.821	169.1	2.8	2.8			
R5	0.002	0.000	0.000	309.440	3.221	6.442	168.7	2.8	2.8			
R6	b. d.	b. d.	b. d.	266.403	2.773	5.546	161.5	2.6	2.6			
R7	b. d.	b. d.	b. d.	260.073	2.707	5.415	151.3	2.5	2.5			
R8	b. d.	b. d.	b. d.	259.591	2.702	5.405	152.3	2.5	2.5			
B1	0.011	0.000	0.000	134.110	1.396	2.792	239.7	3.9	3.9			
B2	b. d.	b. d.	b. d.	47.590	0.495	0.991	240.6	3.9	3.9			
B3	0.005	0.000	0.000	49.720	0.518	1.035	241.9	4.0	4.0			
B4	0.009	0.000	0.000	48.620	0.506	1.012	239.0	3.9	3.9			
B5	0.031	0.000	0.001	71.670	0.746	1.492	240.7	3.9	3.9			
B6	b. d.	b. d.	b. d.	73.099	0.761	1.522	214.7	3.5	3.5			
B7	b. d.	b. d.	b. d.	59.841	0.623	1.246	231.8	3.8	3.8			
B8	b. d.	b. d.	b. d.	62.980	0.656	1.311	232.8	3.8	3.8			
BW	b. d.	b. d.	b. d.	4.783	0.050	0.100	236.7	3.9	3.9			
BW2												
P1	0.024	0.000	0.001	2.330	0.024	0.049	188.0	3.1	3.1			
P2	b. d.	b. d.	b. d.	2.570	0.027	0.054	217.0	3.6	3.6			
P3	0.027	0.000	0.001	2.730	0.028	0.057	203.0	3.3	3.3			
P4	0.033	0.000	0.001	2.910	0.030	0.061	258.7	4.2	4.2			
P5	b. d.	b. d.	b. d.	3.450	0.036	0.072	259.1	4.2	4.2			
P6	b. d.	b. d.	b. d.	5.303	0.055	0.110	247.4	4.1	4.1			
P7	b. d.	b. d.	b. d.	3.572	0.037	0.074	237.9	3.9	3.9			
P8	b. d.	b. d.	b. d.	3.909	0.041	0.081	259.1	4.2	4.2			
PG	0.008	0.000	0.000	5.159	0.054	0.107	241.6	4.0	4.0			
V1	0.127	0.001	0.004	5.480	0.057	0.114	270.2	4.4	4.4			
D1	0.084	0.001	0.003	2.690	0.028	0.056	202.5	3.3	3.3			
D2	0.122	0.001	0.004	3.470	0.036	0.072	204.4	3.3	3.3			
D3	b. d.	b. d.	b. d.	4.902	0.051	0.102	183.0	3.0	3.0			
D4	b. d.	b. d.	b. d.	3.970	0.041	0.083	194.0	3.2	3.2			
D5	b. d.	b. d.	b. d.	4.311	0.045	0.090	212.3	3.5	3.5			
C1	b. d.	b. d.	b. d.	12.270	0.128	0.255	153.5	2.5	2.5			
C2	b. d.	b. d.	b. d.	14.257	0.148	0.297	124.4	2.0	2.0			
C3	b. d.	b. d.	b. d.	13.382	0.139	0.279	146.4	2.4	2.4			
C4	b. d.	b. d.	b. d.	13.390	0.139	0.279	309.9	5.1	5.1	153.7	2.5	2.5
TA1	0.037	0.000	0.001	11.520	0.120	0.240	191.5	3.1	3.1			
TA2	b. d.	b. d.	b. d.	12.412	0.129	0.258	163.5	2.7	2.7			
TA3	b. d.	b. d.	b. d.	11.171	0.116	0.233	375.8	6.2	6.2	190.3	3.1	3.1
TA4	b. d.	b. d.	b. d.	10.930	0.114	0.228	192.8	3.2	3.2	185.4	3.0	3.0
TB1	b. d.	b. d.	b. d.	20.360	0.212	0.424	180.4	3.0	3.0			
TB2	b. d.	b. d.	b. d.	19.417	0.202	0.404	231.8	3.8	3.8	173.2	2.8	3.1
BH1	b. d.	b. d.	b. d.	34.182	0.356	0.712	568.5	9.3	9.3			
BH2	b. d.	b. d.	b. d.	27.412	0.285	0.571	510.0	8.4	8.4			
BH3	b. d.	b. d.	b. d.	26.851	0.280	0.559	368.4	6.0	6.0	583.2	9.6	9.6

Ident	PO_4^{3-}			SO_4^{2-}			HCO_3^- (Field)			HCO_3^- (Lab)		
	mg/l	mmol/l	meq/l	mg/l	mmol/l	meq/l	mg/l	mmol/l	meq/l	mg/l	mmol/l	meq/l
ST1	b. d.	b. d.	b. d.	5.091	0.053	0.106	209.8	3.4	3.4			
ST2	b. d.	b. d.	b. d.	4.267	0.044	0.089	224.5	3.7	3.7	212.3	3.5	3.5
ST3	b. d.	b. d.	b. d.	4.259	0.044	0.089	314.8	5.2	5.2	214.7	3.5	3.5
F1	b. d.	b. d.	b. d.	21.277	0.221	0.443	240.3	3.9	3.9			
F2	b. d.	b. d.	b. d.	29.852	0.311	0.622	268.4	4.4	4.4			
ZE1	0.019	0.000	0.001	0.000	0.000	0.000	260.7	4.3	4.3			
ZE2	b. d.	b. d.	b. d.	2.788	0.029	0.058	239.1	3.9	3.9			
ZE3	b. d.	b. d.	b. d.	2.400	0.025	0.050	241.6	4.0	4.0			
ZE4	b. d.	b. d.	b. d.	2.252	0.023	0.047	266.0	4.4	4.4			
S1	0.112	0.001	0.004	6.210	0.065	0.129	272.7	4.5	4.5			
S2	0.148	0.002	0.005	9.000	0.094	0.187	276.1	4.5	4.5			
S3	b. d.	b. d.	b. d.	9.678	0.101	0.201	251.3	4.1	4.1			
S4	b. d.	b. d.	b. d.	11.921	0.124	0.248	409.9	3.9	3.9	239.1	6.7	6.7
S5	b. d.	b. d.	b. d.	26.851	0.280	0.559	344.0	4.0	4.0	246.4	5.6	5.6
SR1	b. d.	b. d.	b. d.	3.368	0.035	0.070	178.1	2.9	2.9			
SR2	b. d.	b. d.	b. d.	2.967	0.031	0.062	181.8	3.0	3.0			
L1	b. d.	b. d.	b. d.	2.479	0.026	0.052	148.8	2.4	2.4			
L2	b. d.	b. d.	b. d.	1.813	0.019	0.038	314.8	5.2	5.2	175.7	2.9	2.9
L3	b. d.	b. d.	b. d.	1.396	0.015	0.029	302.6	5.0	5.0	156.2	2.6	2.6
M1	0.209	0.002	0.007	303.530	3.160	6.319	1098.3	18.0	18.0			
M2	b. d.	b. d.	b. d.	264.336	2.752	5.503	1051.6	17.2	17.2			
M3	b. d.	b. d.	b. d.	233.607	2.432	4.864	1041.9	17.1	17.1			
M31												
M41												
M42	b. d.	b. d.	b. d.	231.665	2.412	4.823	1066.3	17.5	17.5			
K1	b. d.	b. d.	b. d.	3.029	0.032	0.063	144.0	2.4	2.4			
K2	b. d.	b. d.	b. d.	2.369	0.025	0.049	153.7	2.5	2.5			
K3	b. d.	b. d.	b. d.	2.223	0.023	0.046	300.1	4.9	4.9	156.2	2.6	2.6
KA	b. d.	b. d.	b. d.	2.088	0.022	0.043	334.3	5.5	5.5	161.0	2.6	2.6
BAA1	b. d.	b. d.	b. d.	9.817	0.102	0.204	192.8	3.2	3.2			
BAA2	b. d.	b. d.	b. d.	8.599	0.090	0.179	178.1	2.9	2.9			
BAA3	b. d.	b. d.	b. d.	6.534	0.068	0.136	319.6	5.2	5.2	168.4	2.8	2.8
BA1	0.016	0.000	0.001	17.600	0.183	0.366	271.6	4.5	4.5			
BA2	0.010	0.000	0.000	19.879	0.207	0.414	266.0	4.4	4.4			
BA3	b. d.	b. d.	b. d.	13.861	0.144	0.289	319.6	5.2	5.2	280.6	4.6	4.6
BA4	b. d.	b. d.	b. d.	13.701	0.143	0.285	256.2	4.2	4.2			
J1	b. d.	b. d.	b. d.	2.540	0.026	0.053	180.6	3.0	3.0			
J2	b. d.	b. d.	b. d.	2.612	0.027	0.054	152.3	2.5	2.5			

Ident	sum cations	sum anions	sum ions	cations/ anions	ion balance error [%]	SI				Isotopes	
	meq/l	meq/l	meq/l			Gyp	Anh	Calc	Dol	$\delta^{18}O$ (‰)	$\delta^{2}H$ (‰)
Z1	18.49	18.36	36.85	1.01	0.66	-0.45	-0.71	-0.01	-0.55		
Z2	18.56	20.20	38.76	0.92	-8.12	-0.42	-0.68	-0.06	-0.63	-9.73	-60.19
Z3	18.58	16.81	35.39	1.11	10.54	-0.48	-0.73	0.21	-0.16	-9.48	-59.70
Z4	19.87	16.80	36.67	1.18	18.32	-0.50	-0.75	0.06	-0.32	-9.61	-60.27
Z5	20.00	17.14	37.15	1.17	16.68	-0.46	-0.72	0.26	0.00	-9.65	-60.08
Z6	21.27	19.77	41.05	1.08	7.57	-0.40	-0.65	-0.06	-0.63	-9.46	-59.74
Z7	19.56	19.11	38.67	1.02	2.36	-0.43	-0.68	0.21	-0.09	-9.45	-59.36
Z8	20.02	19.40	39.42	1.03	3.21	-0.43	-0.68	0.22	-0.07	-9.58	-59.62
R1	8.21	9.04	17.24	0.91	-9.16	-1.06	-1.31	0.00	-0.32		
R2	8.33	7.97	16.30	1.04	4.47	-1.13	-1.39	-0.03	-0.35	-9.64	-61.91
R3	8.27	8.31	16.58	1.00	-0.48	-1.12	-1.38	0.22	0.19	-9.45	-61.63
R4	8.35	8.64	16.99	0.97	-3.27	-1.09	-1.34	-0.02	-0.34	-9.59	-62.28
R5	8.29	9.26	17.55	0.90	-10.44	-1.06	-1.31	-0.08	-0.45	-9.60	-62.31
R6	8.80	8.27	17.07	1.06	6.33	-1.10	-1.36	0.13	-0.02	-9.59	-62.42
R7	8.51	7.95	16.46	1.07	7.12	-1.12	-1.37	0.17	0.05	-9.74	-62.33
R8	8.54	7.97	16.51	1.07	7.22	-1.12	-1.37	0.08	-0.12	-10.02	-62.76
B1	5.13	6.76	11.89	0.76	-24.11	-1.50	-1.75	0.07	-0.20		
B2	5.17	4.97	10.14	1.04	3.96	-1.91	-2.16	-0.08	-0.49	-9.03	-59.09
B3	5.15	5.03	10.19	1.02	2.40	-1.92	-2.17	0.20	0.13	-8.95	-58.74
B4	5.17	4.96	10.14	1.04	4.28	-1.99	-2.24	-0.02	-0.16	-9.13	-59.43
B5	5.18	5.48	10.66	0.95	-5.49	-1.80	-2.05	-0.02	-0.24	-9.44	-60.12
B6	5.62	5.10	10.72	1.10	10.14	-1.82	-2.08	-0.15	-0.41	-9.00	-58.96
B7	5.57	5.07	10.64	1.10	9.66	-1.91	-2.17	0.13	0.15	-9.75	-60.58
B8	5.28	5.16	10.44	1.02	2.28	-1.90	-2.16	0.06	0.01	-9.57	-59.76
BW	4.45	4.09	8.54	1.09	8.68	-3.02	-3.27	0.92	1.75	-8.76	-56.92
BW2					-	-	-	-	-	-9.19	-58.06
P1	3.09	3.23	6.32	0.96	-4.36	-3.31	-3.56	0.07	-0.33		
P2	3.63	3.72	7.35	0.98	-2.40	-3.26	-3.52	0.07	-0.19	-9.86	-65.03
P3	3.33	3.49	6.82	0.95	-4.76	-3.27	-3.52	0.29	0.27	-9.89	-67.70
P4	4.32	4.40	8.72	0.98	-1.80	-3.19	-3.45	0.23	0.20	-9.37	-60.49
P5	4.30	4.45	8.74	0.97	-3.39	-3.11	-3.37	0.20	0.12	-8.93	-58.90
P6	4.56	4.31	8.87	1.06	5.69	-2.94	-3.19	0.22	0.21	-8.96	-58.68
P7	4.22	4.07	8.28	1.04	3.76	-3.10	-3.36	0.47	0.67	-9.47	-60.05
P8	4.35	4.42	8.78	0.98	-1.57	-3.07	-3.33	0.33	0.40	-9.59	-59.32
PG	4.54	4.21	8.76	1.08	7.89	-2.96	-3.21	0.13	0.1	-9.35	-59.70
V1	4.21	4.90	9.11	0.86	-14.00	-2.78	-3.04	0.47	0.16	-10.23	-67.29
D1	3.51	3.58	7.08	0.98	-1.92	-3.15	-3.41	-0.11	-0.91	-9.51	-62.19
D2	3.56	3.71	7.26	0.96	-4.02	-3.04	-3.30	-0.44	-1.55	-9.37	-61.19
D3	3.91	3.44	7.35	1.14	13.62	-2.88	-3.14	-0.44	-1.51	-9.13	-60.79
D4	3.81	3.51	7.32	1.08	8.48	-2.99	-3.24	-0.11	-0.83	-9.83	-62.91
D5	3.86	3.83	7.69	1.01	0.71	-2.95	-3.20	-0.05	-0.73	-9.64	-61.94
C1	2.88	2.81	5.69	1.02	2.35	-2.75	-2.99	0.09	0.20	-11.05	-62.12
C2	3.08	2.55	5.63	1.21	20.75	-2.68	-2.91	0.20	0.45	-11.24	-62.20
C3	2.98	2.88	5.85	1.04	3.51	-2.73	-2.94	0.36	0.81	-9.32	-59.32
C4	2.97	7.43	10.40	0.40	-60.04	-2.75	-2.96	0.29	0.69	-9.48	-59.51
TA1	3.39	3.44	6.83	0.99	-1.47	-2.72	-2.96	-0.20	-0.41	-9.42	-59.96
TA2	3.57	3.03	6.60	1.18	17.93	-2.69	-2.93	-0.21	-0.39	-10.43	-62.29
TA3	3.46	6.48	9.95	0.53	-46.56	-2.76	-2.99	0.11	0.26	-9.45	-59.79
TA4	3.46	3.46	6.92	1.00	-0.02	-2.76	-3.00	0.04	0.13	-9.59	-59.72
TB1	3.34	3.42	6.76	0.98	-2.24	-2.49	-2.71	-0.17	-0.30	-9.04	-60.21
TB2	3.38	4.26	7.64	0.79	-20.54	-2.53	-2.76	0.10	0.28	-9.77	-61.49
BH1	10.92	10.17	21.09	1.07	7.38	-1.90	-2.12	0.14	0.06	-14.85	-72.08
BH2	10.42	9.00	19.42	1.16	15.82	-2.00	-2.22	0.16	0.08	-10.16	-65.22
BH3	10.33	6.67	17.00	1.55	54.95	-2.01	-2.24	0.25	0.25	-10.23	-65.05

Ident	sum cations	sum anions	sum ions	cations/ anions	ion balance error [%]	SI				Isotopes	
	meq/l	meq/l	meq/l			Gyp	Anh	Calc	Dol	$\delta^{18}O$ (‰)	$\delta^{2}H$ (‰)
ST1	4.09	3.70	7.80	1.11	10.57	-3.02	-3.26	-0.21	-0.46	-14.59	-68.60
ST2	3.94	3.89	7.83	1.01	1.33	-3.10	-3.33	0.15	0.24	-9.59	-61.00
ST3	4.00	5.37	9.37	0.74	-25.55	-3.09	-3.33	-0.01	-0.08	-9.69	-61.44
F1	4.81	4.44	9.24	1.08	8.36	-2.39	-2.61	0.44	0.95	-9.62	-60.59
F2	4.80	5.08	9.88	0.95	-5.36	-2.25	-2.48	0.32	0.71	-9.52	-60.87
ZE1	4.29	4.36	8.65	0.98	-1.61	-	-	-0.38	-0.88	-9.13	-55.20
ZE2	4.48	4.06	8.54	1.10	10.17	-3.25	-3.51	-0.12	-0.37	-9.44	-55.64
ZE3	4.39	4.11	8.50	1.07	6.80	-3.32	-3.57	0.01	-0.11	-8.67	-55.08
ZE4	4.40	4.47	8.86	0.99	-1.49	-3.35	-3.60	-0.10	-0.33	-8.99	-55.47
S1	4.24	4.73	8.97	0.90	-10.20	-2.91	-3.17	-0.02	-0.19	-9.65	-55.59
S2	4.24	4.82	9.05	0.88	-12.04	-2.75	-3.01	-0.14	-0.44	-9.36	-55.19
S3	4.83	4.40	9.23	1.10	9.58	-2.72	-2.97	-0.14	-0.42	-8.83	-54.17
S4	4.27	4.24	8.51	1.01	0.80	-2.64	-2.89	0.09	0.03	-8.61	-52.82
S5	4.48	4.67	9.15	0.96	-3.94	-2.28	-2.54	0.07	-0.01	-8.40	-52.35
SR1	3.49	3.09	6.57	1.13	12.98	-3.25	-3.49	0.48	0.94	-9.94	-57.31
SR2	3.21	3.12	6.32	1.03	2.80	-3.30	-3.55	0.69	1.24	-8.56	-52.03
L1	2.86	2.55	5.42	1.12	11.97	-3.24	-3.49	0.01	-0.72	-13.62	-71.84
L2	2.69	5.24	7.93	0.51	-48.73	-3.39	-3.64	0.42	0.06	-10.22	-65.46
L3	2.65	5.03	7.69	0.53	-47.26	-3.49	-3.74	0.14	-0.57	-9.62	-60.99
M1	22.87	24.62	47.48	0.93	-7.11	-0.77	-1.02	-0.18	-0.93	-10.17	-66.88
M2	25.93	23.47	49.40	1.10	10.46	-0.81	-1.06	-0.11	-0.82	-11.01	-68.58
M3	23.95	22.46	46.42	1.07	6.62	-0.88	-1.12	0.00	-0.60	-10.27	-67.72
M31					-	-	-	-	-	-10.32	-68.53
M41					-	-	-	-	-	-10.38	-67.92
M42	22.79	22.80	45.59	1.00	-0.06	-0.89	-1.14	-0.09	-0.80	-10.44	-67.30
K1	2.99	2.50	5.49	1.20	19.60	-3.19	-3.45	0.00	-0.52	-9.62	-62.57
K2	2.83	2.63	5.45	1.08	7.59	-3.30	-3.55	0.28	0.00	-9.50	-62.46
K3	2.78	5.02	7.79	0.55	-44.63	-3.32	-3.57	0.11	-0.40	-10.08	-63.51
KA	2.79	5.57	8.36	0.50	-50.01	-3.34	-3.59	0.15	-0.35	-9.76	-61.83
BAA1	3.52	3.51	7.02	1.00	0.21	-2.64	-2.90	-0.30	-1.13	-10.77	-61.80
BAA2	3.45	3.22	6.67	1.07	6.96	-2.70	-2.96	0.01	-0.52	-9.38	-60.13
BAA3	3.19	5.50	8.69	0.58	-42.08	-2.83	-3.09	-0.03	-0.65	-8.76	-56.11
BA1	4.63	4.91	9.55	0.94	-5.75	-2.35	-2.60	-0.26	-0.86	-10.95	-62.06
BA2	5.17	4.93	10.10	1.05	4.80	-2.30	-2.54	0.09	-0.12	-12.63	-64.50
BA3	4.81	5.64	10.46	0.85	-14.70	-2.45	-2.70	0.10	-0.18	-9.04	-58.95
BA4	5.39	5.14	10.54	1.05	4.87	-2.46	-2.71	-0.01	-0.43	-9.27	-58.08
J1	3.38	3.19	6.57	1.06	5.80	-3.26	-3.52	0.27	0.12	-9.28	-57.40
J2	2.76	2.68	5.44	1.03	2.83	-3.34	-3.60	0.68	1.00	-8.38	-52.10
					-5 to 5	-0.05 to 0.05					
					-5 to -10 and 5 to 10	-0.05 to -0.1 and 0.05 to 0.1					
					< -10 and > 10	< -0.1 and > 0.1					

7) Statistical data of each parameter and sampling point

	T [°C]																						
Sample	Z	R	B	BW	P	PG	V	D	C	TA	TB	BH	ST	F	ZE	S	SR	L	M	K	KA	BAA	BA	J
Mean	10.2	9.5	10.4	15.3	9.0	12.4	10.3	8.8	24.3	20.4	23.0	23.1	20.3	23.9	10.8	10.7	16.5	6.8	15.1	7.0	8.0	11.7	15.7	12.9
Median	10.0	9.3	10.3	15.3	9.0	12.4	10.3	8.8	24.9	20.4	23.0	23.5	20.3	23.9	10.8	10.7	16.5	6.8	15.1	7.0	8.0	11.8	15.8	12.9
Std	0.5	0.5	0.4	-	0.5	-	-	0.1	3.5	0.0	0.1	1.0	0.1	0.1	0.1	0.0	2.9	0.1	0.1	0.2	-	0.1	0.6	5.9
Min	10.0	9.2	10.2	15.3	8.3	12.4	10.3	8.6	20.1	20.3	23.0	22.0	20.2	23.8	10.6	10.7	14.5	6.7	15.0	6.9	8.0	11.6	15.1	8.7
Max	11.4	10.5	11.4	15.3	9.9	12.4	10.3	8.9	27.5	20.4	23.1	23.8	20.4	23.9	10.9	10.8	18.5	7.0	15.3	7.3	8.0	11.9	16.3	17.1
Q0.25	10.0	9.3	10.2	15.3	8.7	12.4	10.3	8.7	22.1	20.3	23.0	22.7	20.3	23.8	10.8	10.7	15.5	6.8	15.0	6.9	8.0	11.7	15.3	10.8
Q0.75	10.3	9.6	10.3	15.3	9.2	12.4	10.3	8.9	27.1	20.4	23.1	23.6	20.3	23.9	10.8	10.8	17.5	6.9	15.2	7.1	8.0	11.8	16.2	15.0

	pH [-]																						
Sample	Z	R	B	BW	P	PG	V	D	C	TA	TB	BH	ST	F	ZE	S	SR	L	M	K	KA	BAA	BA	J
Mean	7.31	7.63	7.59	8.48	7.87	7.67	7.86	7.39	8.03	7.61	7.63	6.86	7.50	7.76	7.44	7.56	8.33	8.02	6.15	8.02	7.00	7.57	7.34	8.35
Median	7.34	7.63	7.58	8.48	7.82	7.67	7.86	7.50	8.05	7.61	7.63	6.86	7.51	7.76	7.47	7.54	8.33	7.98	6.14	7.98	7.00	7.69	7.41	8.35
Std	0.13	0.12	0.11	-	0.12	-	-	0.19	0.08	0.16	0.23	0.07	0.18	0.11	0.18	0.14	0.20	0.19	0.09	0.14	-	0.20	0.17	0.43
Min	7.13	7.50	7.41	8.48	7.76	7.67	7.86	7.17	7.91	7.44	7.47	6.79	7.32	7.68	7.20	7.41	8.19	7.86	6.05	7.90	7.00	7.34	7.08	8.04
Max	7.46	7.78	7.74	8.48	8.09	7.67	7.86	7.54	8.10	7.78	7.79	6.93	7.68	7.84	7.62	7.72	8.47	8.23	6.26	8.17	7.00	7.69	7.44	8.65
Q0.25	7.20	7.53	7.52	8.48	7.79	7.67	7.86	7.20	8.01	7.49	7.55	6.83	7.42	7.72	7.39	7.44	8.26	7.92	6.09	7.94	7.00	7.52	7.31	8.19
Q0.75	7.41	7.72	7.68	8.48	7.93	7.67	7.86	7.53	8.08	7.74	7.71	6.90	7.60	7.80	7.51	7.68	8.40	8.11	6.19	8.08	7.00	7.69	7.44	8.50

	EC [µS/cm]																						
Sample	Z	R	B	BW	P	PG	V	D	C	TA	TB	BH	ST	F	ZE	S	SR	L	M	K	KA	BAA	BA	J
Mean	1618.9	781.9	501.5	390.0	368.9	407.0	496.0	356.4	283.8	325.0	323.0	915.3	336.3	442.5	392.5	424.4	302.0	246.7	1954.5	256.3	256.0	314.3	464.0	282.0
Median	1622.0	781.0	509.0	390.0	382.5	407.0	496.0	355.0	283.0	325.0	323.0	892.0	358.0	442.5	392.5	423.0	302.0	247.0	1972.5	259.0	256.0	318.0	467.0	282.0
Std	48.8	6.5	25.2	-	42.2	-	-	6.0	3.1	5.8	8.5	41.3	50.1	12.0	9.3	6.8	19.8	17.5	55.0	18.1	-	15.8	28.0	42.4
Min	1548.0	774.0	441.0	390.0	299.0	407.0	496.0	349.0	281.0	320.0	317.0	891.0	279.0	434.0	384.0	417.0	288.0	229.0	1878.0	237.0	256.0	297.0	427.0	252.0
Max	1685.0	793.0	516.0	390.0	409.0	407.0	496.0	363.0	288.0	330.0	329.0	963.0	372.0	451.0	401.0	432.0	316.0	264.0	1995.0	273.0	256.0	328.0	495.0	312.0
Q0.25	1588.8	778.0	505.5	390.0	338.0	407.0	496.0	353.0	281.8	320.0	320.0	891.5	318.5	438.3	384.8	419.0	295.0	238.0	1932.8	248.0	256.0	307.5	455.5	267.0
Q0.75	1648.3	784.5	515.3	390.0	405.5	407.0	496.0	362.0	285.0	330.0	326.0	927.5	365.0	446.8	400.3	431.0	309.0	255.5	1994.3	266.0	256.0	323.0	475.5	297.0

	Li^+ [mg/l]																						
Sample	Z	R	B	BW	P	PG	V	D	C	TA	TB	BH	ST	F	ZE	S	SR	L	M	K	KA	BAA	BA	J
Mean	b. d.	b. d.	0.008	b. d.	b. d.	b. d.	-	b. d.	0.004	b. d.	0.004	0.004	b. d.	b. d.	b. d.	0.003	b. d.	b. d.	0.119	b. d.	b. d.	0.001	0.002	b. d.
Median	b. d.	b. d.	0.008	b. d.	b. d.	b. d.	-	b. d.	0.003	b. d.	0.004	0.000	b. d.	b. d.	b. d.	0.000	b. d.	b. d.	0.113	b. d.	b. d.	0.000	0.000	b. d.
Std	b. d.	b. d.	0.008	b. d.	b. d.	b. d.	-	b. d.	0.001	b. d.	-	0.006	b. d.	b. d.	b. d.	0.005	b. d.	b. d.	0.015	b. d.	b. d.	0.002	0.004	b. d.
Min	b. d.	b. d.	0.000	b. d.	b. d.	b. d.	-	b. d.	0.003	b. d.	0.004	0.000	b. d.	b. d.	b. d.	0.000	b. d.	b. d.	0.108	b. d.	b. d.	0.000	0.000	b. d.
Max	b. d.	b. d.	0.016	b. d.	b. d.	b. d.	-	b. d.	0.005	b. d.	0.004	0.011	b. d.	b. d.	b. d.	0.008	b. d.	b. d.	0.136	b. d.	b. d.	0.003	0.007	b. d.
Q0.25	b. d.	b. d.	0.004	b. d.	b. d.	b. d.	-	b. d.	0.003	b. d.	0.004	0.000	b. d.	b. d.	b. d.	0.000	b. d.	b. d.	0.111	b. d.	b. d.	0.000	0.000	b. d.
Q0.75	b. d.	b. d.	0.012	b. d.	b. d.	b. d.	-	b. d.	0.004	b. d.	0.004	0.006	b. d.	b. d.	b. d.	0.004	b. d.	b. d.	0.125	b. d.	b. d.	0.002	0.004	b. d.

	Na^+ [mg/l]																						
Sample	Z	R	B	BW	P	PG	V	D	C	TA	TB	BH	ST	F	ZE	S	SR	L	M	K	KA	BAA	BA	J
Mean	3.326	1.605	5.845	0.858	0.762	1.088	-	2.687	1.882	0.858	1.337	5.657	2.466	1.135	0.443	5.431	1.161	0.435	37.358	0.521	0.360	4.455	11.298	2.179
Median	3.288	1.549	5.773	0.858	0.620	1.088	-	2.717	1.881	0.807	1.337	5.428	2.265	1.135	0.521	4.382	1.161	0.361	37.700	0.324	0.360	4.514	7.061	2.179
Std	1.420	0.277	0.243	-	0.400	-	-	0.059	0.034	0.106	-	0.482	0.508	0.198	0.192	2.356	0.135	0.253	1.140	0.364	-	0.143	8.715	0.088
Min	1.926	1.360	5.646	0.858	0.453	1.088	-	2.619	1.849	0.786	1.337	5.332	2.089	0.995	0.224	3.782	1.065	0.228	36.087	0.297	0.360	4.292	5.512	2.116
Max	4.765	1.905	6.116	0.858	1.214	1.088	-	2.724	1.917	0.980	1.337	6.210	3.043	1.275	0.583	8.130	1.256	0.717	38.288	0.941	0.360	4.558	21.321	2.241
Q0.25	2.607	1.455	5.710	0.858	0.537	1.088	-	2.668	1.865	0.797	1.337	5.380	2.177	1.065	0.373	4.082	1.113	0.295	36.894	0.311	0.360	4.403	6.287	2.147
Q0.75	4.027	1.727	5.945	0.858	0.917	1.088	-	2.721	1.899	0.894	1.337	5.819	2.654	1.205	0.552	6.256	1.208	0.539	37.994	0.633	0.360	4.536	14.191	2.210

	NH_4^+ [mg/l]																							
Sample	Z	R	B	BW	P	PG	V	D	C	TA	TB	BH	ST	F	ZE	S	SR	L	M	K	KA	BAA	BA	J
Mean	0.006	0.009	0.102	0.039	0.021	0.080	-	0.030	0.054	0.040	0.032	0.013	0.027	b. d.	0.012	0.033	0.079	0.017	0.424	0.019	b. d.	0.030	0.064	0.019
Median	0.000	0.000	0.084	0.039	0.000	0.080	-	0.028	0.033	0.033	0.032	0.000	0.000	b. d.	0.000	0.043	0.079	0.000	0.456	0.000	b. d.	0.024	0.059	0.019
Std	0.011	0.016	0.043	-	0.037	-	-	0.032	0.036	0.024	-	0.023	0.046	b. d.	0.020	0.029	0.095	0.030	0.191	0.032	b. d.	0.016	0.024	0.001
Min	0.000	0.000	0.072	0.039	0.000	0.080	-	0.000	0.033	0.021	0.032	0.000	0.000	b. d.	0.000	0.000	0.012	0.000	0.219	0.000	b. d.	0.017	0.043	0.018
Max	0.019	0.027	0.151	0.039	0.064	0.080	-	0.063	0.096	0.067	0.032	0.040	0.080	b. d.	0.035	0.056	0.146	0.052	0.597	0.056	b. d.	0.048	0.091	0.020
Q0.25	0.000	0.000	0.078	0.039	0.000	0.080	-	0.014	0.033	0.027	0.032	0.000	0.000	b. d.	0.000	0.022	0.046	0.000	0.338	0.000	b. d.	0.021	0.051	0.019
Q0.75	0.010	0.014	0.118	0.039	0.032	0.080	-	0.046	0.065	0.050	0.032	0.020	0.040	b. d.	0.018	0.050	0.113	0.026	0.527	0.028	b. d.	0.036	0.075	0.020

	K^+ [mg/l]																							
Sample	Z	R	B	BW	P	PG	V	D	C	TA	TB	BH	ST	F	ZE	S	SR	L	M	K	KA	BAA	BA	J
Mean	0.365	0.283	0.912	0.338	0.169	0.443	-	0.963	0.856	0.888	1.372	1.008	0.665	0.184	0.150	0.697	0.286	0.086	10.942	0.094	0.053	0.694	1.096	0.266
Median	0.294	0.162	0.812	0.338	0.000	0.443	-	0.747	0.850	0.738	1.372	0.764	0.307	0.184	0.134	0.536	0.286	0.045	10.467	0.000	0.053	0.712	1.263	0.266
Std	0.405	0.241	0.195	-	0.293	-	-	0.515	0.132	0.262	-	0.430	0.624	0.069	0.158	0.324	0.045	0.089	0.902	0.162	-	0.104	0.310	0.034
Min	0.000	0.126	0.788	0.338	0.000	0.443	-	0.591	0.727	0.735	1.372	0.756	0.302	0.135	0.000	0.486	0.254	0.025	10.377	0.000	0.053	0.582	0.738	0.242
Max	0.801	0.560	1.137	0.338	0.508	0.443	-	1.550	0.990	1.191	1.372	1.504	1.385	0.232	0.315	1.070	0.318	0.189	11.982	0.281	0.053	0.787	1.286	0.290
Q0.25	0.147	0.144	0.800	0.338	0.000	0.443	-	0.669	0.789	0.737	1.372	0.760	0.305	0.159	0.067	0.511	0.270	0.035	10.422	0.000	0.053	0.647	1.001	0.254
Q0.75	0.548	0.361	0.975	0.338	0.254	0.443	-	1.149	0.920	0.965	1.372	1.134	0.846	0.208	0.225	0.803	0.302	0.117	11.225	0.141	0.053	0.750	1.275	0.278

	Mg^{2+} [mg/l]																							
Sample	Z	R	B	BW	P	PG	V	D	C	TA	TB	BH	ST	F	ZE	S	SR	L	M	K	KA	BAA	BA	J
Mean	63.9	40.2	27.5	24.0	19.2	23.8	8.9	10.2	16.5	19.7	18.8	38.7	20.4	27.1	25.2	23.9	17.8	6.3	56.0	9.6	8.1	9.4	17.1	12.4
Median	64.8	40.0	28.9	24.0	20.9	23.8	8.9	10.7	16.5	19.9	18.8	38.1	20.3	27.1	25.1	23.8	17.8	6.3	56.6	9.4	8.1	10.0	17.0	12.4
Std	6.4	1.5	3.8	-	4.2	-	-	0.8	0.2	0.7	0.5	1.3	0.4	0.1	0.4	1.0	1.9	0.8	4.5	1.1	-	1.1	1.6	1.0
Min	54.3	37.4	22.4	24.0	11.8	23.8	8.9	9.2	16.2	18.7	18.5	37.7	20.1	27.0	24.9	22.7	16.5	5.6	50.7	8.6	8.1	8.1	15.4	11.7
Max	74.0	42.4	31.7	24.0	23.9	23.8	8.9	10.9	16.7	20.4	19.2	40.2	20.8	27.2	25.7	25.5	19.1	7.2	60.1	10.8	8.1	10.1	19.2	13.1
Q0.25	58.9	39.7	24.1	24.0	16.4	23.8	8.9	9.5	16.3	19.6	18.7	37.9	20.2	27.0	25.0	23.7	17.1	5.9	53.0	9.0	8.1	9.1	16.1	12.1
Q0.75	66.7	41.1	30.4	24.0	22.1	23.8	8.9	10.8	16.6	20.0	19.0	39.1	20.6	27.1	25.3	24.0	18.4	6.7	59.6	10.1	8.1	10.1	18.0	12.8

	Ca^{2+} [mg/l]																							
Sample	Z	R	B	BW	P	PG	V	D	C	TA	TB	BH	ST	F	ZE	S	SR	L	M	K	KA	BAA	BA	J
Mean	284.8	101.6	58.1	48.6	47.6	50.5	69.7	56.0	30.6	36.1	35.3	142.1	44.2	50.4	46.0	45.8	36.4	43.9	356.5	41.0	42.1	47.9	64.1	38.9
Median	283.0	101.3	56.0	48.6	49.9	50.5	69.7	55.6	30.4	35.9	35.3	140.7	44.2	50.4	46.3	45.8	36.4	43.8	355.2	41.0	42.1	48.4	64.0	38.9
Std	11.0	1.5	6.1	-	3.9	-	-	0.9	0.5	0.9	1.7	3.6	0.3	0.1	0.8	0.9	0.9	0.8	19.4	0.2	-	1.7	0.8	7.3
Min	273.8	99.4	50.9	48.6	41.6	50.5	69.7	55.1	30.3	35.3	34.1	139.5	43.9	50.3	44.9	44.5	35.8	43.1	334.5	40.8	42.1	46.0	63.2	33.7
Max	306.3	104.3	66.1	48.6	51.3	50.5	69.7	57.2	31.3	37.1	36.5	146.3	44.5	50.4	46.6	47.0	37.0	44.7	381.2	41.1	42.1	49.3	65.0	44.0
Q0.25	275.8	100.9	53.7	48.6	44.4	50.5	69.7	55.5	30.3	35.3	34.7	140.1	44.0	50.3	45.9	45.8	36.1	43.5	347.1	40.9	42.1	47.2	63.7	36.3
Q0.75	289.8	102.3	63.5	48.6	50.3	50.5	69.7	56.8	30.7	36.7	35.9	143.5	44.3	50.4	46.5	46.2	36.7	44.2	364.6	41.1	42.1	48.9	64.5	41.4

	Mg^{2+} + Ca^{2+} [mg/l]																							
Sample	Z	R	B	BW	P	PG	V	D	C	TA	TB	BH	ST	F	ZE	S	SR	L	M	K	KA	BAA	BA	J
Mean	348.7	141.8	85.6	72.6	66.8	74.3	78.6	66.3	47.1	55.8	54.1	180.8	64.6	77.4	71.2	69.8	54.2	50.2	412.6	50.6	50.2	57.3	81.2	51.3
Median	348.8	141.4	85.8	72.6	71.4	74.3	78.6	66.4	46.9	55.5	54.1	178.8	64.8	77.4	71.4	69.6	54.2	49.4	412.1	50.2	50.2	58.5	81.0	51.3
Std	14.7	2.2	2.6	-	8.0	-	-	1.6	0.7	0.8	1.2	4.9	0.5	0.2	1.1	1.9	2.8	1.4	23.4	1.1	-	2.8	2.3	8.3
Min	332.4	139.6	80.8	72.6	54.3	74.3	78.6	64.3	46.5	55.2	53.3	177.2	64.0	77.3	69.8	67.2	52.2	49.3	385.2	49.8	50.2	54.1	78.6	45.5
Max	376.1	146.7	88.8	72.6	74.4	74.3	78.6	68.1	48.0	56.9	55.0	186.4	65.0	77.6	72.3	72.4	56.2	51.9	440.7	51.8	50.2	59.4	84.2	57.1
Q0.25	336.2	140.3	84.1	72.6	60.6	74.3	78.6	65.1	46.8	55.2	53.7	178.0	64.4	77.4	70.9	69.5	53.2	49.4	400.1	50.0	50.2	56.3	80.1	48.4
Q0.75	355.4	142.2	87.6	72.6	72.3	74.3	78.6	67.4	47.2	56.1	54.6	182.6	64.9	77.5	71.8	70.1	55.2	50.6	424.6	51.0	50.2	58.9	82.1	54.2

	molar-Mg^{2+}/Ca^{2+}																							
Sample	Z	R	B	BW	P	PG	V	D	C	TA	TB	BH	ST	F	ZE	S	SR	L	M	K	KA	BAA	BA	J
Mean	0.37	0.65	0.80	0.81	0.66	0.78	0.21	0.30	0.54	0.90	0.89	0.45	0.76	0.89	0.90	0.86	0.81	0.24	0.26	0.39	0.32	0.32	0.44	0.53
Median	0.37	0.66	0.86	0.81	0.69	0.78	0.21	0.31	0.55	0.93	0.89	0.45	0.75	0.89	0.90	0.86	0.81	0.24	0.26	0.38	0.32	0.34	0.44	0.53
Std	0.03	0.02	0.18	-	0.10	-	-	0.02	0.01	0.05	0.06	0.00	0.02	0.01	0.01	0.02	0.06	0.03	0.01	0.05	-	0.03	0.04	0.06
Min	0.32	0.60	0.56	0.81	0.46	0.78	0.21	0.28	0.53	0.83	0.84	0.45	0.75	0.88	0.89	0.84	0.76	0.21	0.25	0.35	0.32	0.29	0.40	0.49
Max	0.44	0.67	0.97	0.81	0.78	0.78	0.21	0.32	0.55	0.93	0.93	0.45	0.78	0.89	0.91	0.89	0.85	0.26	0.28	0.44	0.32	0.34	0.49	0.57
Q0.25	0.35	0.65	0.63	0.81	0.62	0.78	0.21	0.28	0.54	0.90	0.86	0.45	0.75	0.88	0.89	0.85	0.78	0.23	0.25	0.37	0.32	0.32	0.42	0.51
Q0.75	0.38	0.67	0.96	0.81	0.72	0.78	0.21	0.31	0.55	0.93	0.91	0.45	0.77	0.89	0.91	0.86	0.83	0.25	0.27	0.41	0.32	0.34	0.46	0.55

	$Fe^{2+/3+}$ [mg/l]																							
Sample	Z	R	B	BW	P	PG	V	D	C	TA	TB	BH	ST	F	ZE	S	SR	L	M	K	KA	BAA	BA	J
Mean	0.188	0.238	0.078	0.040	0.039	0.028	-	0.021	0.354	0.017	0.000	0.031	0.017	0.000	0.011	0.023	0.043	0.037	0.021	0.016	0.004	0.049	0.026	0.022
Median	0.069	0.071	0.057	0.040	0.037	0.028	-	0.000	0.344	0.000	0.000	0.022	0.013	0.000	0.000	0.026	0.043	0.042	0.013	0.018	0.004	0.055	0.018	0.022
Std	0.225	0.311	0.061	-	0.005	-	-	0.037	0.338	0.030	-	0.027	0.017	0.000	0.020	0.010	0.038	0.016	0.026	0.005	-	0.025	0.017	0.009
Min	0.047	0.045	0.031	0.040	0.036	0.028	-	0.000	0.021	0.000	0.000	0.009	0.003	0.000	0.000	0.012	0.016	0.019	0.000	0.011	0.004	0.021	0.013	0.015
Max	0.447	0.597	0.146	0.040	0.044	0.028	-	0.064	0.697	0.052	0.000	0.061	0.036	0.000	0.034	0.031	0.070	0.050	0.050	0.019	0.004	0.070	0.045	0.029
Q0.25	0.058	0.058	0.044	0.040	0.036	0.028	-	0.000	0.183	0.000	0.000	0.016	0.008	0.000	0.000	0.019	0.029	0.031	0.006	0.014	0.004	0.038	0.016	0.019
Q0.75	0.258	0.334	0.102	0.040	0.040	0.028	-	0.032	0.521	0.026	0.000	0.042	0.024	0.000	0.017	0.028	0.056	0.046	0.032	0.019	0.004	0.063	0.032	0.025

	Sr^{2+} [mg/l]																							
Sample	Z	R	B	BW	P	PG	V	D	C	TA	TB	BH	ST	F	ZE	S	SR	L	M	K	KA	BAA	BA	J
Mean	1.607	0.592	1.480	0.002	0.078	0.002	-	0.275	0.211	0.079	0.387	0.369	0.000	0.422	0.000	0.000	0.038	0.000	1.074	0.000	0.000	0.072	0.119	0.000
Median	2.356	0.830	0.046	0.002	0.002	0.002	-	0.352	0.294	0.115	0.387	0.526	0.000	0.422	0.000	0.000	0.038	0.000	1.510	0.000	0.000	0.103	0.117	0.000
Std	1.375	0.510	2.523	-	0.134	-	-	0.244	0.182	0.068	-	0.319	0.000	0.047	0.000	0.000	0.053	0.000	0.930	0.000	-	0.061	0.118	0.000
Min	0.020	0.006	0.000	0.002	0.000	0.002	-	0.001	0.002	0.001	0.387	0.002	0.000	0.388	0.000	0.000	0.001	0.000	0.006	0.000	0.000	0.001	0.002	0.000
Max	2.445	0.939	4.393	0.002	0.233	0.002	-	0.471	0.338	0.121	0.387	0.580	0.000	0.455	0.000	0.000	0.076	0.000	1.706	0.000	0.000	0.111	0.238	0.000
Q0.25	1.188	0.418	0.023	0.002	0.001	0.002	-	0.177	0.148	0.058	0.387	0.264	0.000	0.405	0.000	0.000	0.020	0.000	0.758	0.000	0.000	0.052	0.059	0.000
Q0.75	2.401	0.885	2.220	0.002	0.117	0.002	-	0.412	0.316	0.118	0.387	0.553	0.000	0.438	0.000	0.000	0.057	0.000	1.608	0.000	0.000	0.107	0.178	0.000

	Mn^{2+} [mg/l]																							
Sample	Z	R	B	BW	P	PG	V	D	C	TA	TB	BH	ST	F	ZE	S	SR	L	M	K	KA	BAA	BA	J
Mean	0.008	0.011	0.010	0.005	0.005	0.005	-	0.008	0.017	0.002	0.000	0.007	0.012	0.000	0.001	0.008	0.009	0.004	0.114	0.003	0.000	0.008	0.007	0.002
Median	0.008	0.011	0.009	0.005	0.004	0.005	-	0.003	0.009	0.000	0.000	0.008	0.002	0.000	0.000	0.006	0.009	0.002	0.116	0.001	0.000	0.011	0.007	0.002
Std	0.002	0.004	0.005	-	0.002	-	-	0.009	0.017	0.004	-	0.003	0.017	0.000	0.002	0.006	0.006	0.003	0.002	0.004	-	0.006	0.005	0.002
Min	0.006	0.008	0.007	0.005	0.003	0.005	-	0.001	0.005	0.000	0.000	0.004	0.002	0.000	0.000	0.003	0.005	0.002	0.112	0.001	0.000	0.001	0.001	0.001
Max	0.011	0.015	0.016	0.005	0.007	0.005	-	0.018	0.037	0.006	0.000	0.011	0.032	0.000	0.004	0.014	0.014	0.007	0.116	0.008	0.000	0.012	0.012	0.003
Q0.25	0.007	0.009	0.008	0.005	0.003	0.005	-	0.002	0.007	0.000	0.000	0.006	0.002	0.000	0.000	0.004	0.007	0.002	0.114	0.001	0.000	0.006	0.004	0.001
Q0.75	0.009	0.013	0.012	0.005	0.005	0.005	-	0.011	0.023	0.003	0.000	0.009	0.017	0.000	0.002	0.010	0.012	0.005	0.116	0.005	0.000	0.012	0.009	0.002

	F^- [mg/l]																							
Sample	Z	R	B	BW	P	PG	V	D	C	TA	TB	BH	ST	F	ZE	S	SR	L	M	K	KA	BAA	BA	J
Mean	0.367	0.079	0.129	0.070	0.048	0.114	-	0.047	3.367	0.510	0.598	0.344	0.079	0.149	0.145	0.200	0.051	0.030	2.338	0.035	0.014	0.085	0.153	0.032
Median	0.325	0.074	0.117	0.070	0.037	0.114	-	0.034	3.374	0.519	0.598	0.312	0.057	0.149	0.075	0.220	0.051	0.022	2.174	0.024	0.014	0.088	0.129	0.032
Std	0.300	0.033	0.057	-	0.021	-	-	0.024	0.012	0.024	-	0.057	0.040	0.017	0.161	0.121	0.021	0.016	0.312	0.020	-	0.019	0.049	0.006
Min	0.090	0.048	0.080	0.070	0.035	0.114	-	0.032	3.353	0.483	0.598	0.310	0.055	0.137	0.031	0.071	0.036	0.019	2.142	0.023	0.014	0.065	0.121	0.028
Max	0.686	0.114	0.191	0.070	0.072	0.114	-	0.074	3.375	0.528	0.598	0.410	0.125	0.161	0.330	0.310	0.065	0.048	2.697	0.058	0.014	0.103	0.209	0.036
Q0.25	0.208	0.061	0.099	0.070	0.036	0.114	-	0.033	3.364	0.501	0.598	0.311	0.056	0.143	0.053	0.146	0.043	0.021	2.158	0.024	0.014	0.077	0.125	0.030
Q0.75	0.506	0.094	0.154	0.070	0.055	0.114	-	0.054	3.375	0.524	0.598	0.361	0.091	0.155	0.203	0.265	0.058	0.035	2.436	0.041	0.014	0.096	0.169	0.034

	Cl^- [mg/l]																						
Sample	Z	R	B	BW	P	PG	V	D	C	TA	TB	BH	ST	F	ZE	S	SR	L	M	K	KA	BAA	BA	J
Mean	1.912	1.670	1.139	1.569	1.794	1.927	9.120	5.629	17.522	0.956	0.844	1.657	1.868	1.064	1.209	2.473	0.779	0.470	13.657	0.565	0.469	3.586	8.137	3.177
Median	1.570	1.659	1.140	1.569	1.710	1.927	9.120	5.574	1.166	0.976	0.844	1.676	1.735	1.064	1.205	1.717	0.779	0.496	14.020	0.604	0.469	3.512	3.581	3.177
Std	0.812	0.257	0.215	-	0.223	-	-	0.851	33.016	0.276	0.419	0.164	0.235	0.006	0.403	1.297	0.105	0.063	2.539	0.109	-	0.149	9.608	0.339
Min	1.430	1.430	0.834	1.569	1.516	1.927	9.120	4.560	0.712	0.642	0.548	1.485	1.730	1.060	0.773	1.462	0.704	0.399	10.260	0.442	0.469	3.489	2.850	2.937
Max	3.752	2.154	1.430	1.569	2.134	1.927	9.120	6.936	67.044	1.229	1.140	1.811	2.140	1.068	1.652	4.280	0.853	0.516	16.327	0.649	0.469	3.757	22.537	3.416
Q0.25	1.430	1.430	1.051	1.569	1.676	1.927	9.120	5.420	0.855	0.770	0.696	1.581	1.733	1.062	0.928	1.485	0.741	0.448	12.743	0.523	0.469	3.501	3.242	3.057
Q0.75	1.891	1.755	1.213	1.569	2.000	1.927	9.120	5.655	17.834	1.162	0.992	1.744	1.938	1.066	1.486	3.420	0.816	0.506	14.934	0.627	0.469	3.635	8.475	3.296

	Br^- [mg/l]																						
Sample	Z	R	B	BW	P	PG	V	D	C	TA	TB	BH	ST	F	ZE	S	SR	L	M	K	KA	BAA	BA	J
Mean	0.546	0.397	0.456	1.306	0.432	1.396	-	0.372	0.283	0.336	0.000	1.241	0.418	0.000	0.445	0.477	0.490	0.278	2.853	0.287	0.000	0.330	0.507	0.000
Median	0.000	0.000	0.000	1.306	0.000	1.396	-	0.000	0.000	0.000	0.000	0.000	0.000	0.000	0.000	0.000	0.490	0.000	0.000	0.000	0.000	0.000	0.000	0.000
Std	0.946	0.688	0.790	-	0.748	-	-	0.644	0.491	0.581	-	2.149	0.723	0.000	0.770	0.826	0.693	0.481	4.942	0.498	-	0.571	0.878	0.000
Min	0.000	0.000	0.000	1.306	0.000	1.396	-	0.000	0.000	0.000	0.000	0.000	0.000	0.000	0.000	0.000	0.000	0.000	0.000	0.000	0.000	0.000	0.000	0.000
Max	1.638	1.192	1.368	1.306	1.296	1.396	-	1.116	0.850	1.007	0.000	3.723	1.253	0.000	1.334	1.430	0.980	0.833	8.559	0.862	0.000	0.989	1.521	0.000
Q0.25	0.000	0.000	0.000	1.306	0.000	1.396	-	0.000	0.000	0.000	0.000	0.000	0.000	0.000	0.000	0.000	0.245	0.000	0.000	0.000	0.000	0.000	0.000	0.000
Q0.75	0.819	0.596	0.684	1.306	0.648	1.396	-	0.558	0.425	0.504	0.000	1.862	0.627	0.000	0.667	0.715	0.735	0.417	4.280	0.431	0.000	0.495	0.761	0.000

	NO_2^- [mg/l]																						
Sample	Z	R	B	BW	P	PG	V	D	C	TA	TB	BH	ST	F	ZE	S	SR	L	M	K	KA	BAA	BA	J
Mean	b. d.	b. d.	0.001	b. d.	0.001	b. d.	-	0.103	0.002	b. d.	b. d.	b. d.	b. d.	b. d.	0.004	b. d.	0.079	0.040	b. d.	0.000	0.012	0.003	0.009	0.017
Median	b. d.	b. d.	0.000	b. d.	0.000	b. d.	-	0.000	0.000	b. d.	b. d.	b. d.	b. d.	b. d.	0.000	b. d.	0.079	0.016	b. d.	0.000	0.012	0.000	0.000	0.017
Std	b. d.	b. d.	0.002	b. d.	0.002	b. d.	-	0.179	0.003	b. d.	b. d.	b. d.	b. d.	b. d.	0.007	b. d.	0.076	0.055	b. d.	0.001	-	0.006	0.016	0.023
Min	b. d.	b. d.	0.000	b. d.	0.000	b. d.	-	0.000	0.000	b. d.	b. d.	b. d.	b. d.	b. d.	0.000	b. d.	0.025	0.000	b. d.	0.000	0.012	0.000	0.000	0.000
Max	b. d.	b. d.	0.003	b. d.	0.004	b. d.	-	0.310	0.006	b. d.	b. d.	b. d.	b. d.	b. d.	0.012	b. d.	0.133	0.103	b. d.	0.001	0.012	0.010	0.027	0.033
Q0.25	b. d.	b. d.	0.000	b. d.	0.000	b. d.	-	0.000	0.000	b. d.	b. d.	b. d.	b. d.	b. d.	0.000	b. d.	0.052	0.008	b. d.	0.000	0.012	0.000	0.000	0.008
Q0.75	b. d.	b. d.	0.002	b. d.	0.002	b. d.	-	0.155	0.003	b. d.	b. d.	b. d.	b. d.	b. d.	0.006	b. d.	0.106	0.060	b. d.	0.001	0.012	0.005	0.014	0.025

	NO_3^- [mg/l]																						
Sample	Z	R	B	BW	P	PG	V	D	C	TA	TB	BH	ST	F	ZE	S	SR	L	M	K	KA	BAA	BA	J
Mean	0.256	0.117	0.112	3.177	3.483	4.127	5.729	6.349	0.067	1.787	0.444	0.809	4.438	1.113	2.452	0.583	3.360	1.938	0.548	2.539	2.172	1.451	1.059	3.902
Median	0.227	0.090	0.096	3.177	3.290	4.127	5.729	6.233	0.046	1.804	0.444	0.723	4.345	1.113	2.370	0.355	3.360	1.780	0.273	2.405	2.172	1.358	1.034	3.902
Std	0.190	0.084	0.075	-	0.542	-	-	1.567	0.054	0.046	0.047	0.482	0.178	0.035	0.287	0.565	0.006	0.351	0.683	0.268	-	0.216	0.118	1.543
Min	0.007	0.020	0.026	3.177	2.874	4.127	5.729	4.293	0.030	1.719	0.411	0.375	4.326	1.088	2.213	0.118	3.356	1.693	0.084	2.364	2.172	1.297	0.948	2.811
Max	0.635	0.288	0.214	3.177	4.488	4.127	5.729	7.945	0.146	1.823	0.477	1.328	4.643	1.138	2.857	1.506	3.364	2.340	1.564	2.848	2.172	1.697	1.221	4.993
Q0.25	0.143	0.068	0.052	3.177	3.120	4.127	5.729	5.439	0.033	1.781	0.428	0.549	4.336	1.101	2.271	0.211	3.358	1.737	0.222	2.385	2.172	1.328	0.990	3.357
Q0.75	0.330	0.154	0.184	3.177	3.761	4.127	5.729	7.835	0.081	1.810	0.461	1.026	4.494	1.126	2.552	0.723	3.362	2.060	0.599	2.627	2.172	1.528	1.104	4.448

	PO_4^{3-} [mg/l]																						
Sample	Z	R	B	BW	P	PG	V	D	C	TA	TB	BH	ST	F	ZE	S	SR	L	M	K	KA	BAA	BA	J
Mean	0.003	0.003	0.007	b. d.	0.010	0.008	0.127	0.041	b. d.	0.009	b. d.	b. d.	b. d.	b. d.	0.005	0.052	b. d.	b. d.	0.052	b. d.	b. d.	b. d.	0.007	b. d.
Median	0.001	0.000	0.002	b. d.	0.000	0.008	0.127	0.000	b. d.	0.000	b. d.	b. d.	b. d.	b. d.	0.000	0.000	b. d.	b. d.	0.000	b. d.	b. d.	b. d.	0.005	b. d.
Std	0.004	0.006	0.011	b. d.	0.015	-	-	0.058	b. d.	0.019	b. d.	b. d.	b. d.	b. d.	0.010	0.072	b. d.	b. d.	0.104	b. d.	b. d.	b. d.	0.008	b. d.
Min	0.000	0.000	0.000	b. d.	0.000	0.008	0.127	0.000	b. d.	0.000	b. d.	b. d.	b. d.	b. d.	0.000	0.000	b. d.	b. d.	0.000	b. d.	b. d.	b. d.	0.000	b. d.
Max	0.010	0.017	0.031	b. d.	0.033	0.008	0.127	0.122	b. d.	0.037	b. d.	b. d.	b. d.	b. d.	0.019	0.148	b. d.	b. d.	0.209	b. d.	b. d.	b. d.	0.016	b. d.
Q0.25	0.000	0.000	0.000	b. d.	0.000	0.008	0.127	0.000	b. d.	0.000	b. d.	b. d.	b. d.	b. d.	0.000	0.000	b. d.	b. d.	0.000	b. d.	b. d.	b. d.	0.000	b. d.
Q0.75	0.005	0.002	0.009	b. d.	0.025	0.008	0.127	0.084	b. d.	0.009	b. d.	b. d.	b. d.	b. d.	0.005	0.112	b. d.	b. d.	0.052	b. d.	b. d.	b. d.	0.012	b. d.

	SO_4^{2-} [mg/l]																							
Sample	Z	R	B	BW	P	PG	V	D	C	TA	TB	BH	ST	F	ZE	S	SR	L	M	K	KA	BAA	BA	J
Mean	740.6	273.3	68.5	4.8	3.3	5.2	5.5	3.9	13.3	11.5	19.9	29.5	4.5	25.6	1.9	12.7	3.2	1.9	258.3	2.5	2.1	8.3	16.3	2.6
Median	754.4	265.2	61.4	4.8	3.2	5.2	5.5	4.0	13.4	11.3	19.9	27.4	4.3	25.6	2.3	9.7	3.2	1.8	249.0	2.4	2.1	8.6	15.7	2.6
Std	65.2	21.3	28.4	-	1.0	-	-	0.8	0.8	0.6	0.7	4.1	0.5	6.1	1.3	8.2	0.3	0.5	33.7	0.4	-	1.7	3.0	0.1
Min	662.5	247.9	47.6	4.8	2.3	5.2	5.5	2.7	12.3	10.9	19.4	26.9	4.3	21.3	0.0	6.2	3.0	1.4	231.7	2.2	2.1	6.5	13.7	2.5
Max	826.1	309.4	134.1	4.8	5.3	5.2	5.5	4.9	14.3	12.4	20.4	34.2	5.1	29.9	2.8	26.9	3.4	2.5	303.5	3.0	2.1	9.8	19.9	2.6
Q0.25	675.3	260.0	49.4	4.8	2.7	5.2	5.5	3.5	13.1	11.1	19.7	27.1	4.3	23.4	1.7	9.0	3.1	1.6	233.1	2.3	2.1	7.6	13.8	2.6
Q0.75	787.5	284.6	72.0	4.8	3.7	5.2	5.5	4.3	13.6	11.7	20.1	30.8	4.7	27.7	2.5	11.9	3.3	2.1	274.1	2.7	2.1	9.2	18.2	2.6

	HCO_3^- [mg/l]																							
Sample	Z	R	B	BW	P	PG	V	D	C	TA	TB	BH	ST	F	ZE	S	SR	L	M	K	KA	BAA	BA	J
Mean	180.8	163.6	235.2	236.7	233.8	241.6	270.2	199.2	144.5	182.7	176.8	553.9	212.3	254.4	251.9	257.1	180.0	160.2	1064.5	151.3	161.0	179.8	268.6	166.5
Median	180.6	168.2	239.4	236.7	242.7	241.6	270.2	202.5	150.0	187.9	176.8	568.5	212.3	254.4	251.2	251.3	180.0	156.2	1059.0	153.7	161.0	178.1	268.8	166.5
Std	6.8	7.7	9.1	-	27.9	-	-	11.2	13.8	13.1	5.1	38.7	2.5	19.9	13.5	16.4	2.6	13.9	24.6	6.4	-	12.3	10.2	20.0
Min	168.4	151.3	214.7	236.7	188.0	241.6	270.2	183.0	124.4	163.5	173.2	510.0	209.8	240.3	239.1	239.1	178.1	148.8	1041.9	144.0	161.0	168.4	256.2	152.3
Max	193.7	169.1	241.9	236.7	259.1	241.6	270.2	212.3	153.7	191.5	180.4	583.2	214.7	268.4	266.0	276.1	181.8	175.7	1098.3	156.2	161.0	192.8	280.6	180.6
Q0.25	180.1	159.2	232.6	236.7	213.5	241.6	270.2	194.0	140.9	180.0	175.0	539.3	211.0	247.3	241.0	246.4	179.0	152.5	1049.2	148.9	161.0	173.2	263.6	159.4
Q0.75	181.4	169.0	240.6	236.7	258.8	241.6	270.2	204.4	153.6	190.6	178.6	575.8	213.5	261.4	262.0	272.7	180.9	165.9	1074.3	154.9	161.0	185.5	273.9	173.5

	$\delta^{18}O$ [‰]																							
Sample	Z	R	B	BW	P	PG	V	D	C	TA	TB	BH	ST	F	ZE	S	SR	L	M	K	KA	BAA	BA	J
Mean	-9.57	-9.66	-9.27	-9.00	-9.44	-9.35	-10.20	-9.50	-10.27	-9.71	-9.38	-11.77	-11.29	-9.57	-9.04	-8.97	-9.25	-11.15	-10.48	-9.73	-9.76	-9.65	-10.45	-8.83
Median	-9.58	-9.60	-9.13	-9.00	-9.47	-9.35	-10.20	-9.51	-10.26	-9.52	-9.38	-10.23	-9.69	-9.57	-9.05	-8.83	-9.25	-10.22	-10.36	-9.60	-9.76	-9.38	-10.08	-8.83
Std	0.10	0.18	0.32	0.28	0.39	-	-	0.27	1.02	0.47	0.54	2.72	2.86	0.07	0.30	0.52	0.97	2.15	0.36	0.31	-	1.04	1.65	0.63
Min	-9.73	-10.02	-9.75	-9.19	-9.89	-9.35	-10.20	-9.83	-11.24	-10.40	-9.77	-14.90	-14.60	-9.62	-9.40	-9.65	-9.94	-13.60	-11.00	-10.08	-9.76	-10.80	-12.60	-9.28
Max	-9.45	-9.45	-8.95	-8.80	-8.93	-9.35	-10.20	-9.13	-9.32	-9.40	-9.00	-10.16	-9.59	-9.52	-8.67	-8.40	-8.56	-9.62	-10.20	-9.50	-9.76	-8.76	-9.04	-8.38
Q0.25	-9.63	-9.69	-9.51	-9.10	-9.73	-9.35	-10.20	-9.64	-11.10	-9.79	-9.57	-12.57	-12.15	-9.59	-9.18	-9.36	-9.60	-11.91	-10.58	-9.84	-9.76	-10.09	-11.33	-9.05
Q0.75	-9.49	-9.59	-9.01	-8.90	-9.17	-9.35	-10.20	-9.37	-9.44	-9.44	-9.19	-10.20	-9.64	-9.54	-8.91	-8.61	-8.91	-9.92	-10.25	-9.55	-9.76	-9.07	-9.21	-8.61

	$\delta^{2}H$ [‰]																							
Sample	Z	R	B	BW	P	PG	V	D	C	TA	TB	BH	ST	F	ZE	S	SR	L	M	K	KA	BAA	BA	J
Mean	-59.85	-62.23	-59.53	-57.48	-61.45	-59.70	-67.30	-61.80	-60.78	-60.45	-60.84	-67.46	-63.68	-60.73	-55.34	-54.02	-54.67	-66.08	-67.63	-62.86	-61.83	-59.35	-60.91	-54.75
Median	-59.70	-62.31	-59.43	-59.70	-60.05	-59.70	-67.30	-61.94	-60.81	-59.89	-60.84	-65.22	-61.44	-60.73	-55.34	-54.17	-54.67	-65.46	-67.51	-62.60	-61.83	-60.13	-60.52	-54.75
Std	0.34	0.36	0.66	3.76	3.50	-	-	0.84	1.59	1.24	0.91	4.02	4.27	0.20	0.24	1.42	3.73	5.43	0.73	0.57	-	2.93	2.95	3.75
Min	-60.27	-62.76	-60.58	-67.70	-67.70	-59.70	-67.30	-62.91	-62.20	-62.30	-61.49	-72.10	-68.60	-60.87	-55.60	-55.59	-57.31	-71.80	-68.60	-63.51	-61.83	-61.80	-64.50	-57.40
Max	-59.36	-61.63	-58.74	-56.90	-58.68	-59.70	-67.30	-60.79	-59.32	-59.72	-60.20	-65.05	-61.00	-60.59	-55.08	-52.35	-52.03	-60.99	-66.90	-62.46	-61.83	-56.11	-58.08	-52.10
Q0.25	-60.14	-62.38	-59.94	-65.40	-62.76	-59.70	-67.30	-62.19	-62.14	-60.58	-61.16	-68.66	-65.02	-60.80	-55.50	-55.19	-55.99	-68.63	-67.94	-63.06	-61.83	-60.97	-62.70	-56.07
Q0.75	-59.66	-62.09	-59.02	-58.79	-59.11	-59.70	-67.30	-61.19	-59.46	-59.77	-60.52	-65.13	-61.22	-60.66	-55.17	-52.82	-53.35	-63.23	-67.20	-62.53	-61.83	-58.12	-58.73	-53.42

	SI anhydrite																							
Sample	Z	R	B	BW	P	PG	V	D	C	TA	TB	BH	ST	F	ZE	S	SR	L	M	K	KA	BAA	BA	J
Mean	-0.70	-1.35	-2.10	-3.27	-3.41	-3.21	-3.04	-3.26	-2.95	-2.98	-2.74	-2.19	-3.32	-2.55	-3.56	-2.93	-3.53	-3.65	-1.09	-3.54	-3.63	-2.99	-2.64	-3.56
Median	-0.70	-1.37	-2.16	-3.27	-3.42	-3.21	-3.04	-3.25	-2.95	-2.98	-2.74	-2.22	-3.34	-2.55	-3.57	-2.98	-3.53	-3.68	-1.09	-3.55	-3.63	-2.96	-2.65	-3.56
Std	0.03	0.03	0.15	-	0.12	-	-	0.10	0.03	0.04	0.04	0.06	0.04	0.09	0.05	0.23	0.04	0.15	0.06	0.08	-	0.11	0.08	0.06
Min	-0.75	-1.39	-2.24	-3.27	-3.56	-3.21	-3.04	-3.41	-2.99	-3.03	-2.77	-2.22	-3.35	-2.61	-3.60	-3.18	-3.55	-3.78	-1.14	-3.61	-3.63	-3.12	-2.72	-3.60
Max	-0.65	-1.31	-1.75	-3.27	-3.19	-3.21	-3.04	-3.14	-2.91	-2.93	-2.71	-2.12	-3.27	-2.48	-3.51	-2.55	-3.50	-3.49	-1.02	-3.45	-3.63	-2.90	-2.54	-3.52
Q0.25	-0.72	-1.37	-2.17	-3.27	-3.52	-3.21	-3.04	-3.30	-2.97	-3.01	-2.76	-2.22	-3.35	-2.58	-3.59	-3.02	-3.54	-3.73	-1.13	-3.58	-3.63	-3.04	-2.71	-3.58
Q0.75	-0.68	-1.33	-2.07	-3.27	-3.35	-3.21	-3.04	-3.20	-2.93	-2.95	-2.73	-2.17	-3.31	-2.51	-3.54	-2.92	-3.51	-3.59	-1.05	-3.50	-3.63	-2.93	-2.59	-3.54

	SI gypsum																							
Sample	Z	R	B	BW	P	PG	V	D	C	TA	TB	BH	ST	F	ZE	S	SR	L	M	K	KA	BAA	BA	J
Mean	-0.45	-1.10	-1.84	-3.02	-3.16	-2.96	-2.78	-3.00	-2.73	-2.74	-2.52	-1.96	-3.08	-2.32	-3.31	-2.67	-3.28	-3.39	-0.84	-3.28	-3.37	-2.73	-2.39	-3.30
Median	-0.44	-1.11	-1.91	-3.02	-3.16	-2.96	-2.78	-3.00	-2.74	-2.75	-2.52	-1.99	-3.10	-2.32	-3.32	-2.72	-3.28	-3.42	-0.85	-3.30	-3.37	-2.70	-2.40	-3.30
Std	0.03	0.03	0.15	-	0.12	-	-	0.10	0.03	0.05	0.04	0.06	0.04	0.10	0.05	0.23	0.03	0.14	0.06	0.08	-	0.11	0.08	0.06
Min	-0.50	-1.13	-1.99	-3.02	-3.31	-2.96	-2.78	-3.15	-2.75	-2.79	-2.55	-2.00	-3.11	-2.39	-3.35	-2.92	-3.30	-3.52	-0.89	-3.35	-3.37	-2.86	-2.47	-3.34
Max	-0.40	-1.06	-1.50	-3.02	-2.94	-2.96	-2.78	-2.88	-2.68	-2.69	-2.49	-1.90	-3.03	-2.25	-3.25	-2.30	-3.26	-3.24	-0.77	-3.19	-3.37	-2.64	-2.30	-3.26
Q0.25	-0.47	-1.12	-1.91	-3.02	-3.26	-2.96	-2.78	-3.04	-2.75	-2.78	-2.54	-2.00	-3.11	-2.36	-3.34	-2.76	-3.29	-3.47	-0.88	-3.33	-3.37	-2.78	-2.46	-3.32
Q0.75	-0.43	-1.08	-1.82	-3.02	-3.09	-2.96	-2.78	-2.95	-2.72	-2.71	-2.51	-1.95	-3.07	-2.29	-3.29	-2.66	-3.27	-3.33	-0.80	-3.25	-3.37	-2.67	-2.34	-3.28

	SI dolomite																							
Sample	Z	R	B	BW	P	PG	V	D	C	TA	TB	BH	ST	F	ZE	S	SR	L	M	K	KA	BAA	BA	J
Mean	-0.31	-0.17	-0.15	1.75	0.19	0.09	0.16	-0.69	0.54	0.04	0.11	0.01	0.07	0.83	-0.42	0.03	1.17	-0.08	-0.79	-0.13	0.23	-0.60	-0.33	0.56
Median	-0.24	-0.22	-0.18	1.75	0.24	0.09	0.16	-0.91	0.57	-0.12	0.11	0.06	0.22	0.83	-0.35	-0.03	1.17	-0.05	-0.81	0.00	0.23	-0.52	-0.19	0.56
Std	0.26	0.23	0.24	-	0.32	-	-	1.14	0.27	0.57	0.57	0.10	0.32	0.17	0.33	0.32	0.11	0.62	0.14	0.34	-	0.49	0.36	0.62
Min	-0.63	-0.45	-0.49	1.75	-0.33	0.09	0.16	-1.55	0.20	-0.41	-0.30	-0.10	-0.30	0.71	-0.88	-0.29	1.09	-0.72	-0.93	-0.52	0.23	-1.13	-0.86	0.12
Max	0.00	0.19	0.15	1.75	0.67	0.09	0.16	1.24	0.81	0.79	0.51	0.08	0.29	0.95	-0.11	0.45	1.24	0.52	-0.60	0.12	0.23	-0.15	-0.08	1.00
Q0.25	-0.57	-0.34	-0.28	1.75	0.10	0.09	0.16	-1.51	0.39	-0.40	-0.10	-0.02	-0.04	0.77	-0.50	-0.26	1.13	-0.39	-0.85	-0.26	0.23	-0.83	-0.40	0.34
Q0.75	-0.09	0.00	0.04	1.75	0.31	0.09	0.16	-0.73	0.72	0.32	0.31	0.07	0.26	0.89	-0.28	0.26	1.20	0.24	-0.75	0.06	0.23	-0.34	-0.11	0.78

	SI dolomite (d)																							
Sample	Z	R	B	BW	P	PG	V	D	C	TA	TB	BH	ST	F	ZE	S	SR	L	M	K	KA	BAA	BA	J
Mean	-0.92	-0.79	-0.76	1.16	-0.43	-0.51	-0.45	-1.31	-0.01	-0.53	-0.46	-0.55	-0.50	0.28	-1.03	-0.59	0.58	-0.71	-1.38	-0.76	-0.40	-1.21	-0.91	-0.06
Median	-0.86	-0.84	-0.79	1.16	-0.37	-0.51	-0.45	-1.53	0.02	-0.69	-0.46	-0.49	-0.35	0.28	-0.96	-0.65	0.58	-0.68	-1.40	-0.63	-0.40	-1.13	-0.77	-0.06
Std	0.26	0.23	0.24	-	0.32	-	-	1.14	0.28	0.57	0.57	0.11	0.32	0.17	0.33	0.32	0.08	0.62	0.14	0.33	-	0.50	0.36	0.62
Min	-1.24	-1.06	-1.11	1.16	-0.95	-0.51	-0.45	-2.17	-0.37	-0.98	-0.86	-0.67	-0.87	0.16	-1.49	-0.90	0.52	-1.34	-1.52	-1.14	-0.40	-1.74	-1.44	-0.50
Max	-0.61	-0.42	-0.46	1.16	0.05	-0.51	-0.45	0.62	0.27	0.22	-0.05	-0.48	-0.28	0.40	-0.72	-0.16	0.64	-0.11	-1.19	-0.51	-0.40	-0.75	-0.67	0.38
Q0.25	-1.18	-0.96	-0.89	1.16	-0.52	-0.51	-0.45	-2.13	-0.17	-0.97	-0.66	-0.58	-0.61	0.22	-1.11	-0.87	0.55	-1.01	-1.44	-0.89	-0.40	-1.44	-0.99	-0.28
Q0.75	-0.71	-0.62	-0.57	1.16	-0.31	-0.51	-0.45	-1.35	0.17	-0.25	-0.25	-0.49	-0.32	0.34	-0.89	-0.35	0.61	-0.40	-1.34	-0.57	-0.40	-0.94	-0.69	0.16

	SI calcite																							
Sample	Z	R	B	BW	P	PG	V	D	C	TA	TB	BH	ST	F	ZE	S	SR	L	M	K	KA	BAA	BA	J
Mean	0.10	0.06	0.02	0.92	0.25	0.13	0.47	-0.02	0.24	0.01	0.03	0.13	0.06	0.38	-0.15	0.08	0.63	0.35	-0.10	0.22	0.44	-0.02	0.02	0.48
Median	0.14	0.04	0.02	0.92	0.26	0.13	0.47	-0.11	0.25	-0.07	0.03	0.14	0.14	0.38	-0.11	0.06	0.63	0.40	-0.10	0.28	0.44	0.01	0.09	0.48
Std	0.14	0.11	0.11	-	0.13	-	-	0.56	0.12	0.28	0.28	0.04	0.17	0.08	0.17	0.16	0.09	0.32	0.07	0.19	-	0.27	0.19	0.29
Min	-0.06	-0.08	-0.15	0.92	0.07	0.13	0.47	-0.44	0.09	-0.21	-0.17	0.08	-0.13	0.32	-0.38	-0.07	0.56	0.01	-0.18	0.00	0.44	-0.30	-0.26	0.27
Max	0.26	0.22	0.20	0.92	0.47	0.13	0.47	0.93	0.36	0.38	0.22	0.16	0.17	0.44	0.01	0.30	0.69	0.65	0.00	0.37	0.44	0.23	0.15	0.68
Q0.25	-0.02	-0.02	-0.04	0.92	0.18	0.13	0.47	-0.44	0.17	-0.20	-0.07	0.11	0.01	0.35	-0.19	-0.07	0.59	0.21	-0.13	0.14	0.44	-0.15	-0.01	0.37
Q0.75	0.21	0.14	0.09	0.92	0.30	0.13	0.47	-0.05	0.31	0.14	0.12	0.15	0.16	0.41	-0.07	0.20	0.66	0.53	-0.07	0.33	0.44	0.12	0.11	0.58

	SI CO_2																							
Sample	Z	R	B	BW	P	PG	V	D	C	TA	TB	BH	ST	F	ZE	S	SR	L	M	K	KA	BAA	BA	J
Mean	-2.19	-2.54	-2.31	-3.20	-2.60	-2.37	-2.53	-2.41	-2.89	-2.31	-2.34	-1.23	-2.12	-2.39	-2.13	-2.12	-3.11	-2.75	-0.24	-2.85	-2.59	-2.31	-1.94	-3.24
Median	-2.20	-2.54	-2.30	-3.20	-2.56	-2.37	-2.53	-2.29	-2.90	-2.29	-2.34	-1.19	-2.05	-2.39	-2.16	-2.11	-3.11	-2.79	-0.24	-2.85	-2.59	-2.27	-1.98	-3.24
Std	0.14	0.13	0.11	-	0.16	-	-	0.60	0.10	0.12	0.16	0.17	0.22	0.15	0.19	0.11	0.28	0.12	0.10	0.24	-	0.19	0.16	0.49
Min	-2.37	-2.72	-2.48	-3.20	-2.82	-2.37	-2.53	-3.44	-3.00	-2.47	-2.45	-1.41	-2.37	-2.49	-2.33	-2.24	-3.30	-2.85	-0.36	-3.09	-2.59	-2.52	-2.08	-3.59
Max	-2.01	-2.39	-2.13	-3.20	-2.36	-2.37	-2.53	-1.96	-2.76	-2.19	-2.23	-1.08	-1.95	-2.28	-1.88	-1.98	-2.91	-2.61	-0.12	-2.61	-2.59	-2.14	-1.71	-2.89
Q0.25	-2.29	-2.64	-2.40	-3.20	-2.69	-2.37	-2.53	-2.31	-2.95	-2.36	-2.40	-1.30	-2.21	-2.44	-2.23	-2.20	-3.20	-2.82	-0.29	-2.97	-2.59	-2.40	-2.03	-3.42
Q0.75	-2.07	-2.42	-2.25	-3.20	-2.51	-2.37	-2.53	-2.04	-2.84	-2.24	-2.29	-1.14	-2.00	-2.33	-2.07	-2.05	-3.01	-2.70	-0.19	-2.73	-2.59	-2.21	-1.89	-3.07

8) Z (Zavčan)

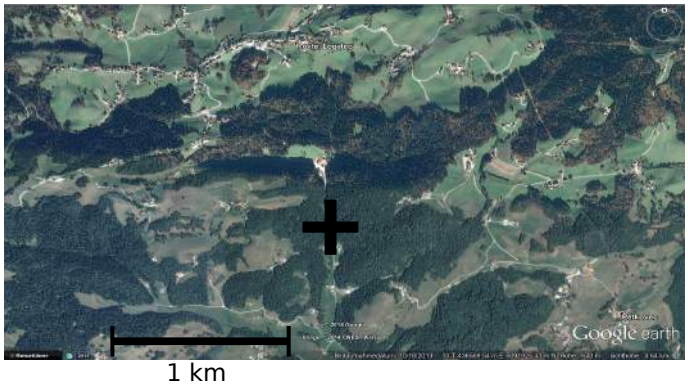

1 km

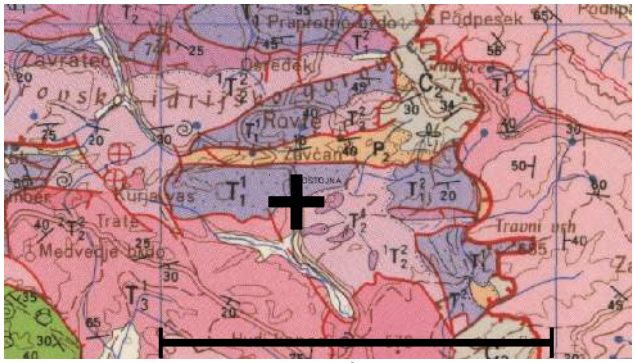

1 km

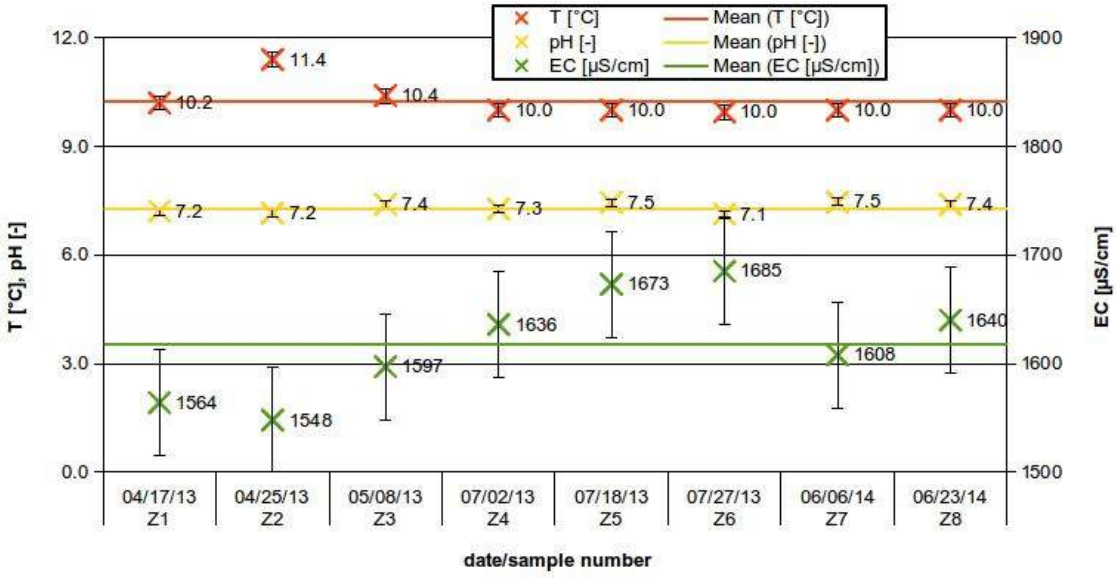

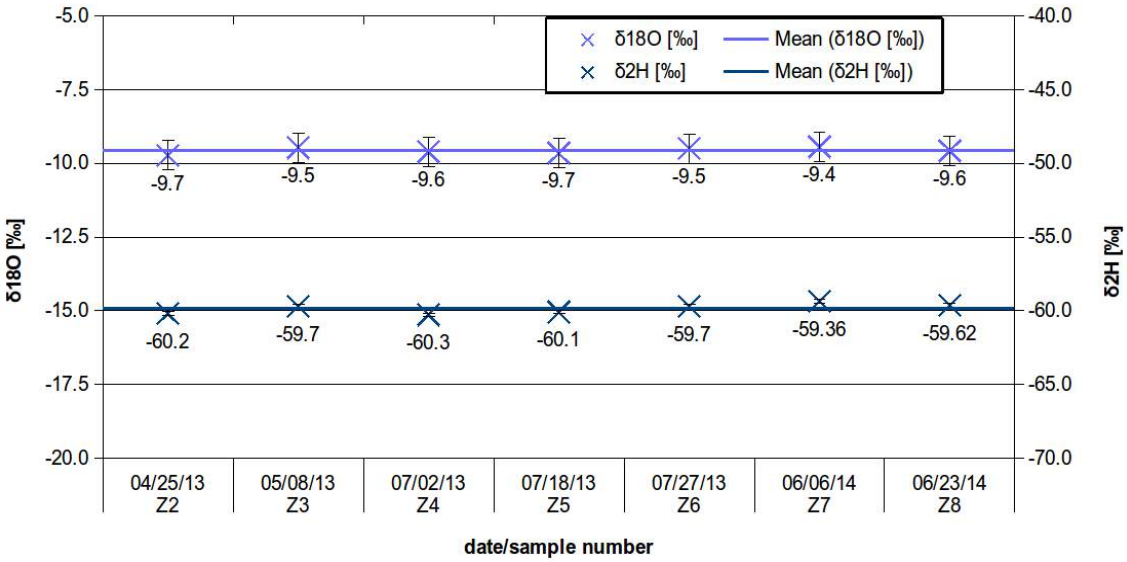

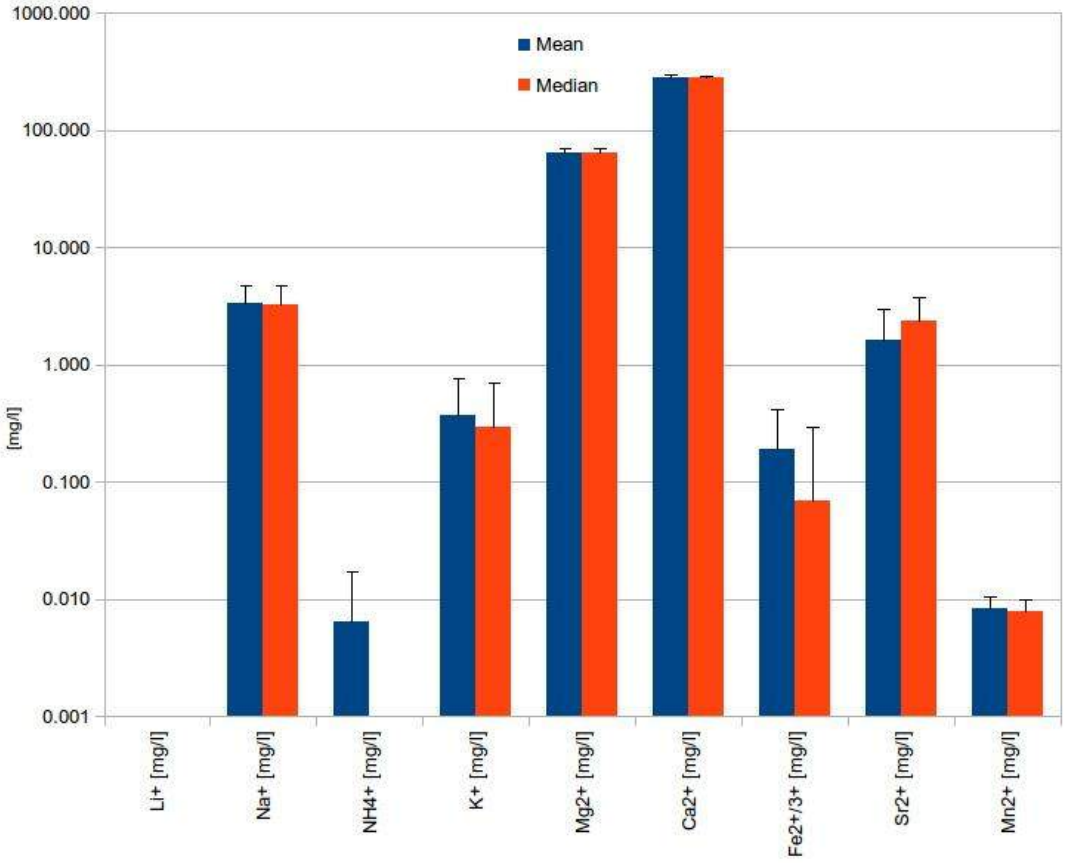

n = 3 n = 3 n = 3 n = 3 n = 8 n = 8 n = 3 n = 3 n = 3

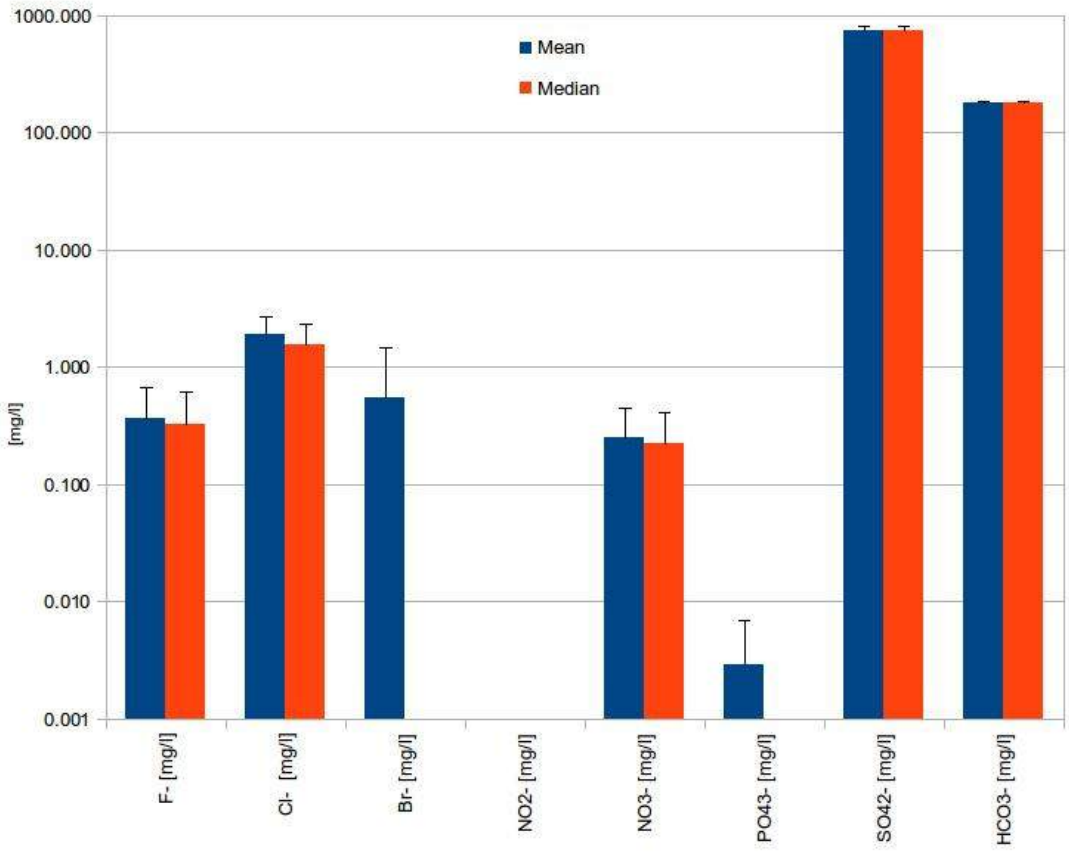

n = 3 n = 8 n = 3 n = 3 n = 8 n = 8 n = 8 n = 8

9) R (Rodofov mlin)

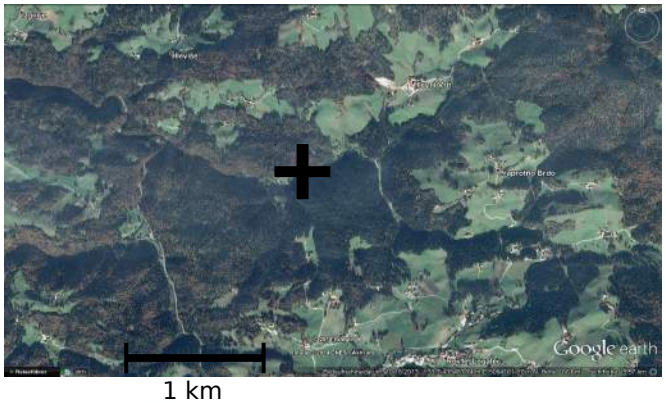

1 km

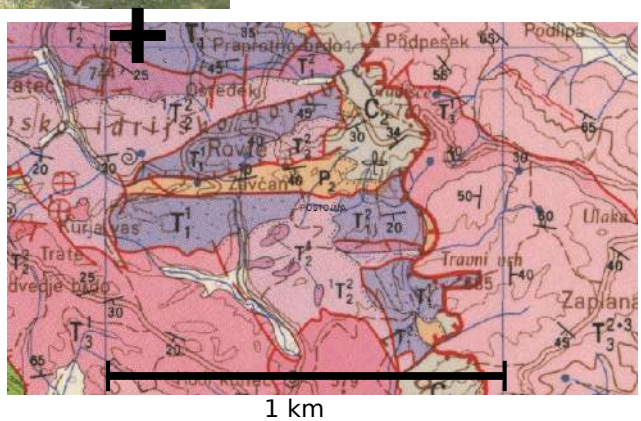

1 km

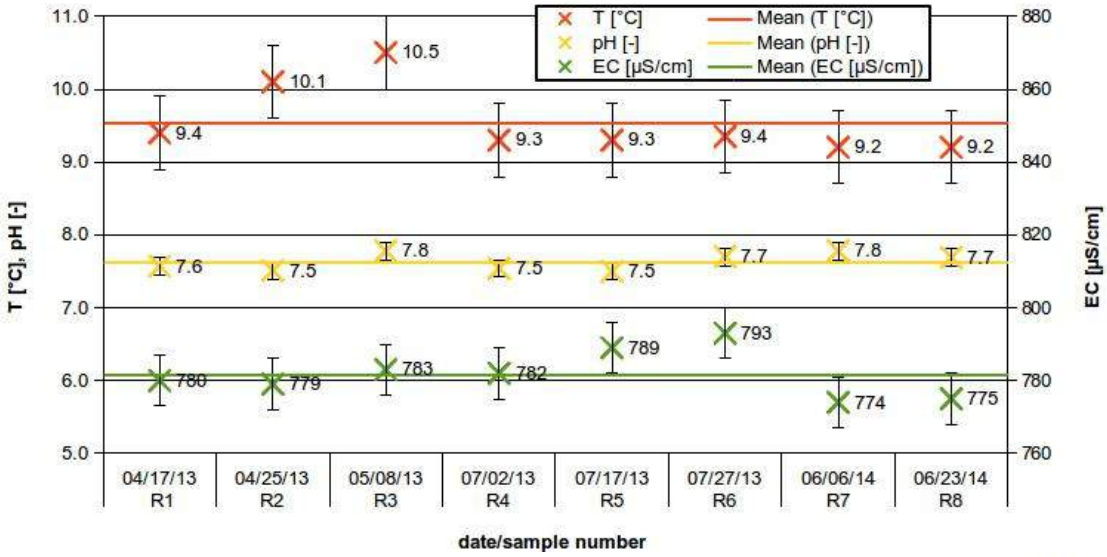

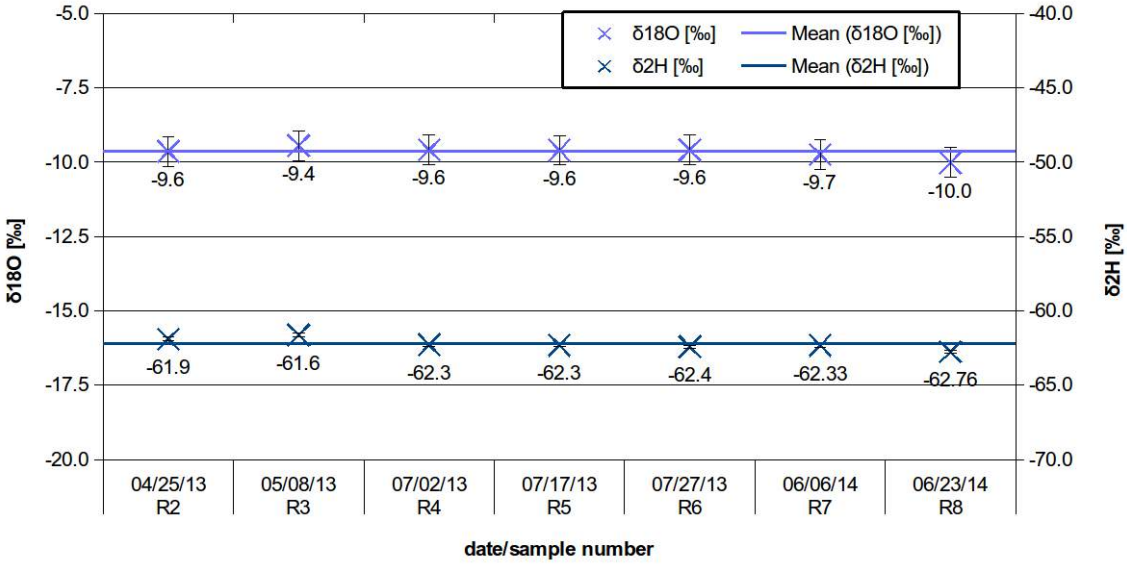

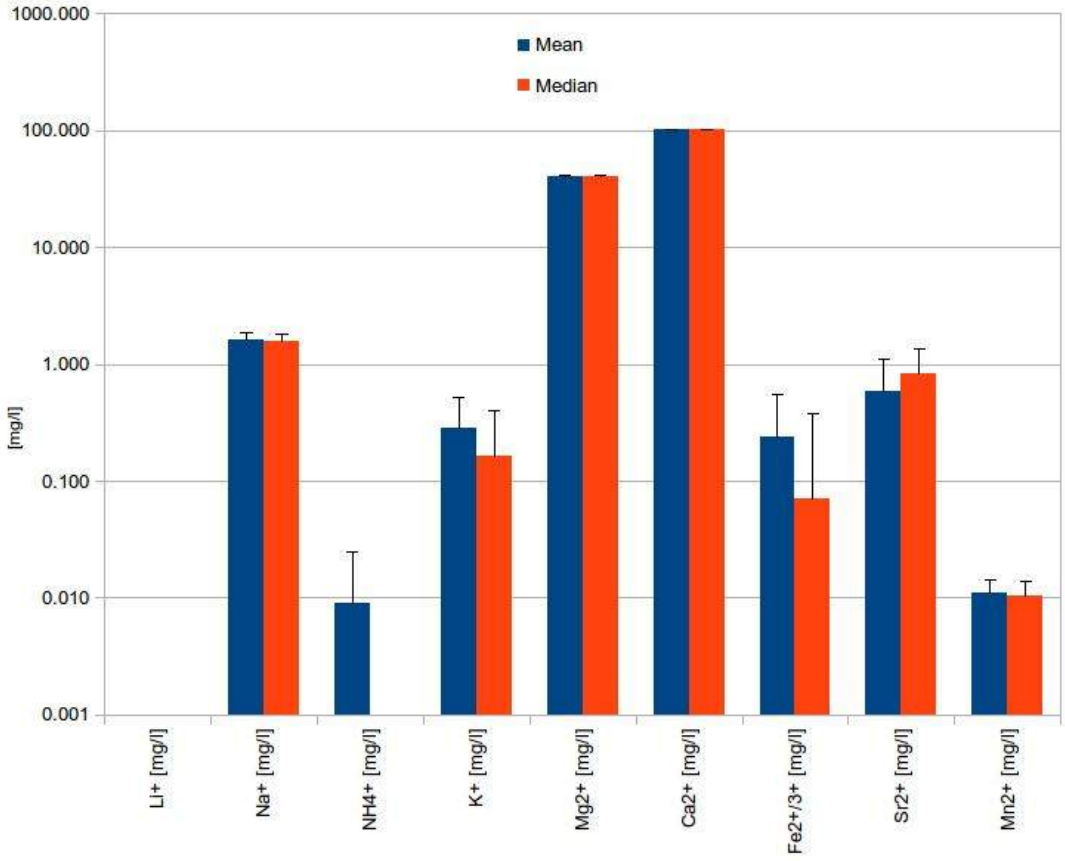

n = 3 n = 3 n = 3 n = 3 n = 8 n = 8 n = 3 n = 3 n = 3

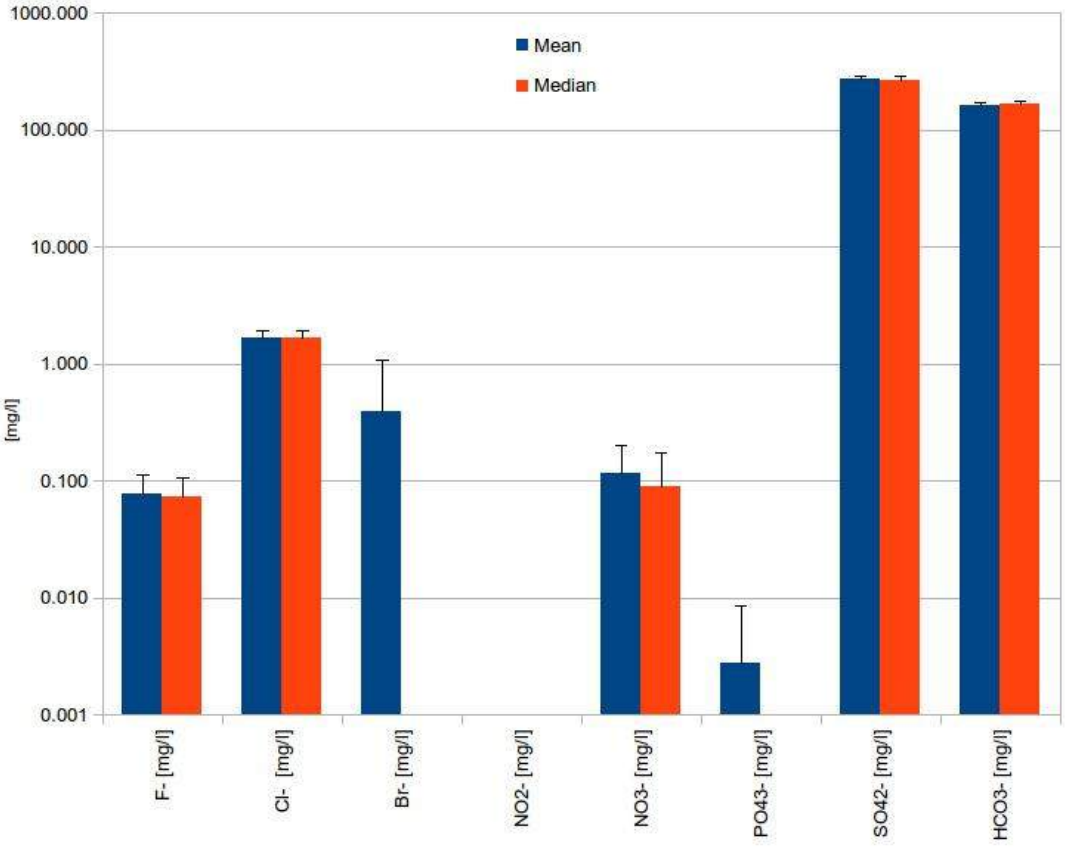

n = 3 n = 8 n = 3 n = 3 n = 8 n = 8 n = 8 n = 8

10) B (Bizjakov mlin)

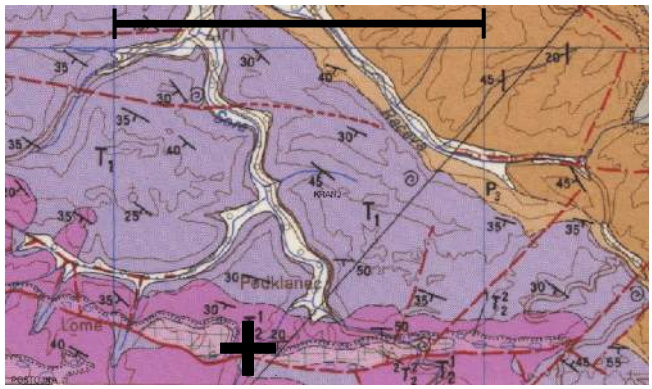

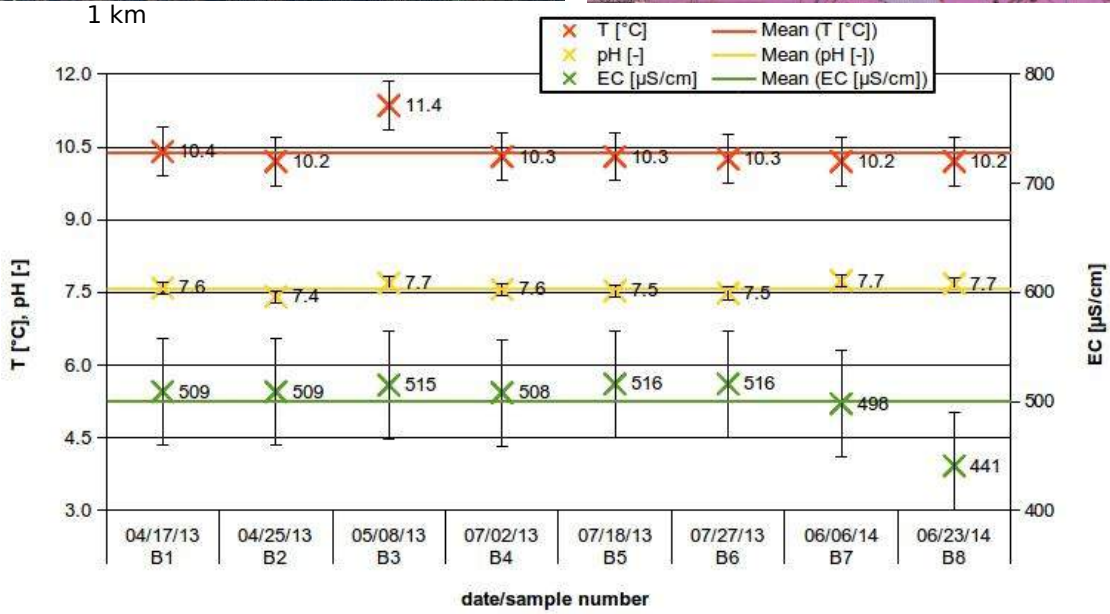

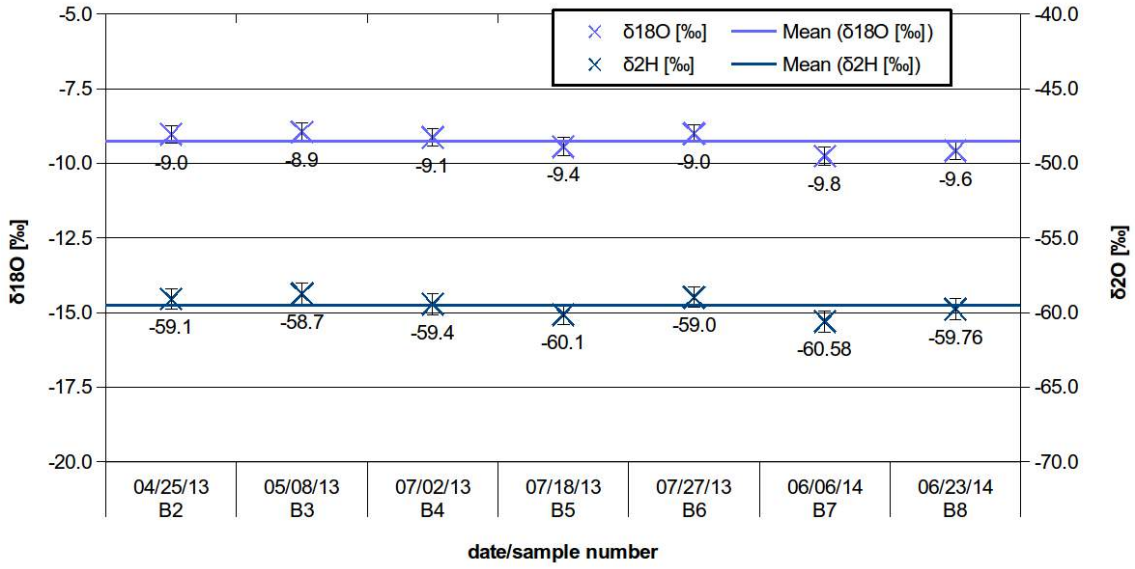

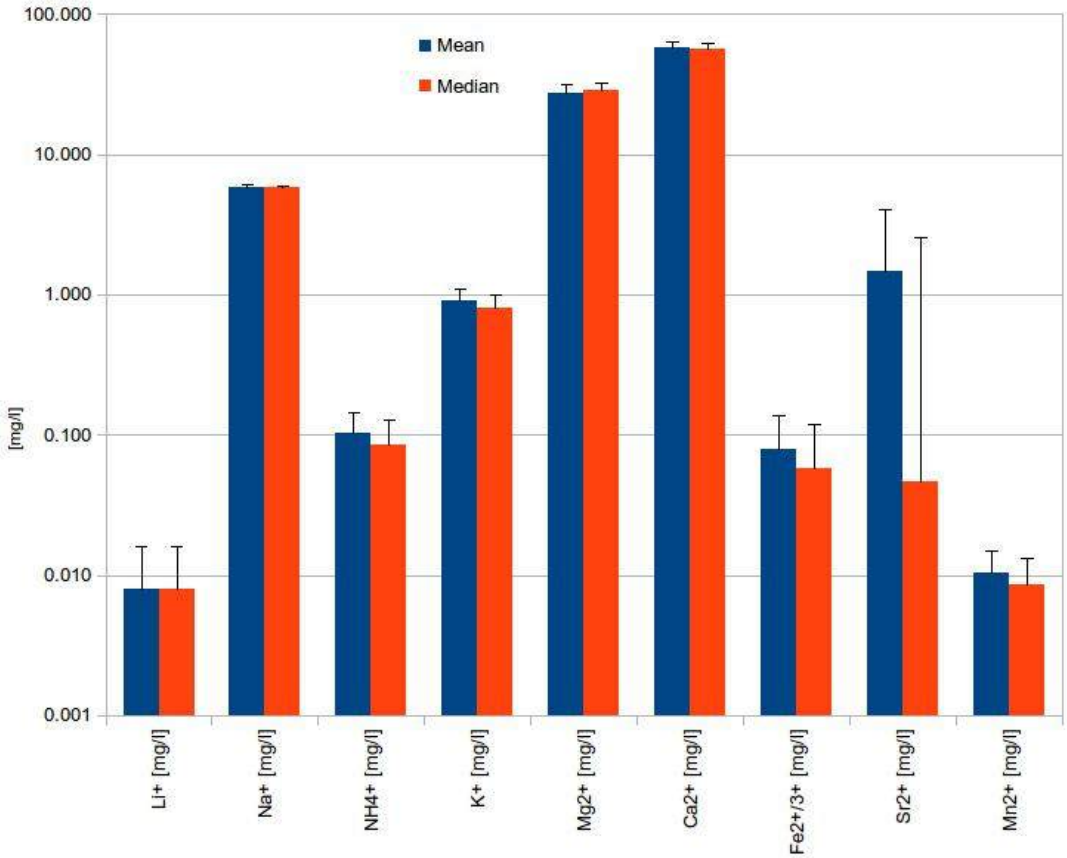

n = 3 n = 3 n = 3 n = 3 n = 8 n = 8 n = 3 n = 3 n = 3

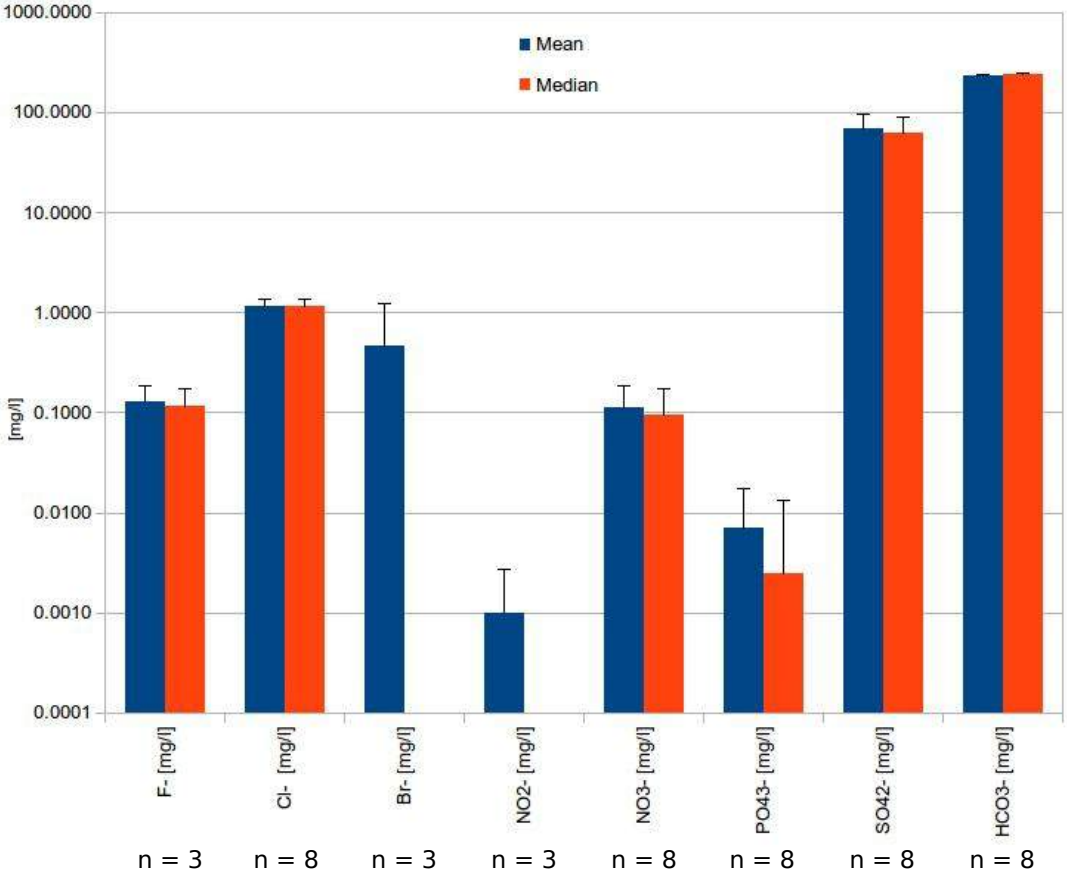

n = 3 n = 8 n = 3 n = 3 n = 8 n = 8 n = 8 n = 8

11) BW (Bizjakov mlin water)

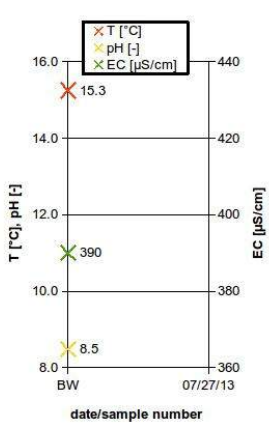

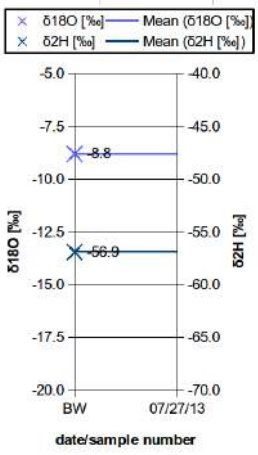

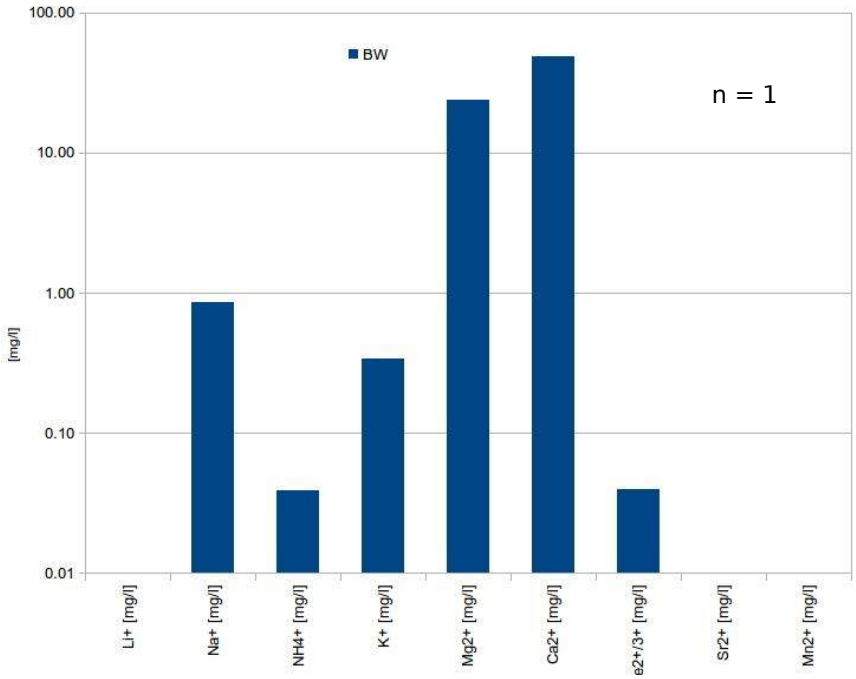

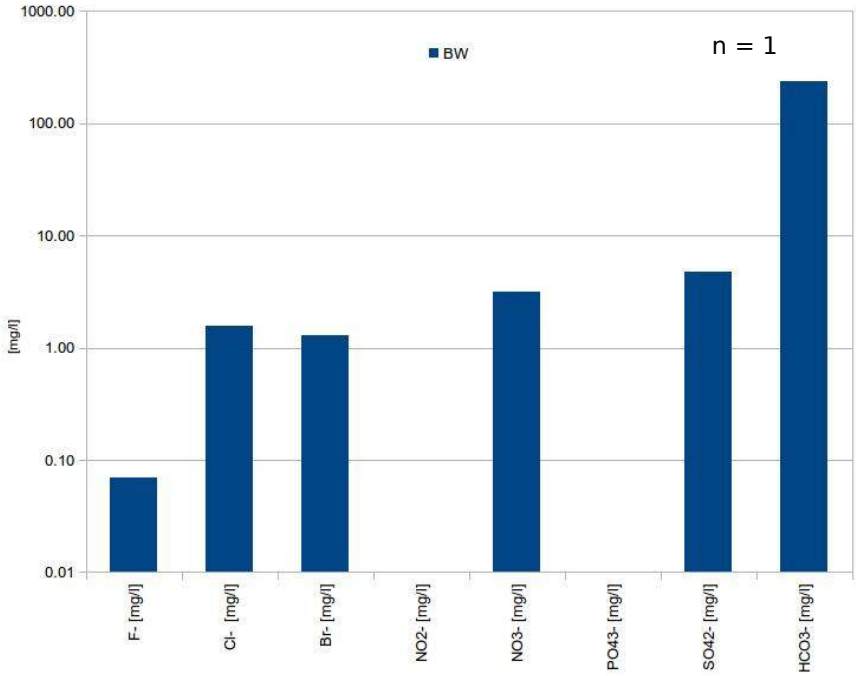

12) P (Podklanec)

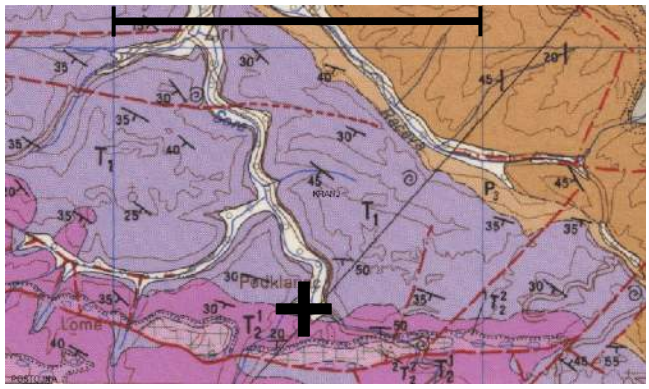

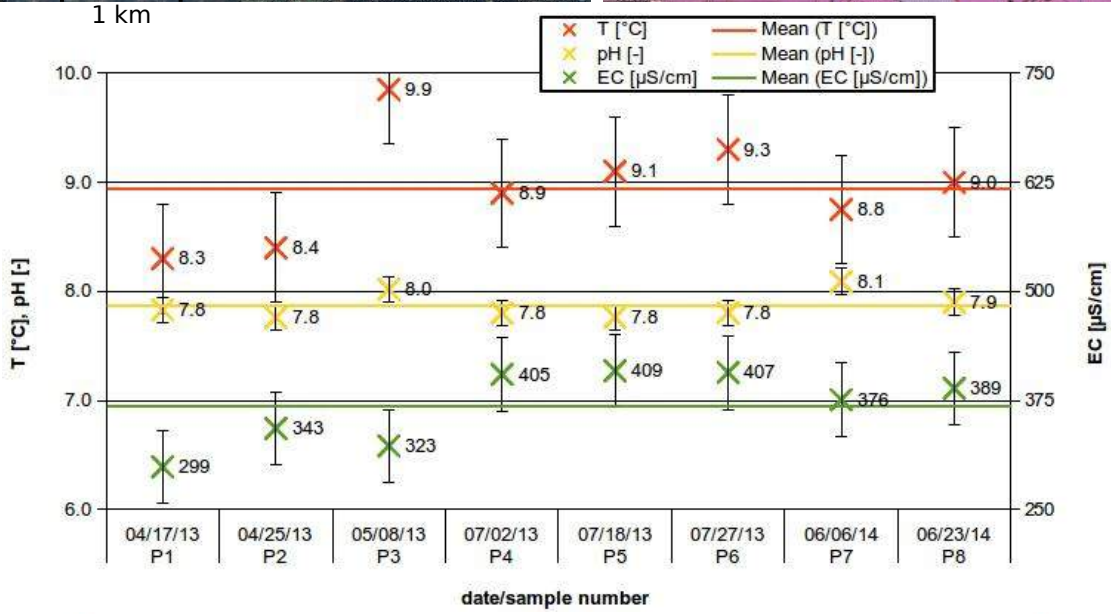

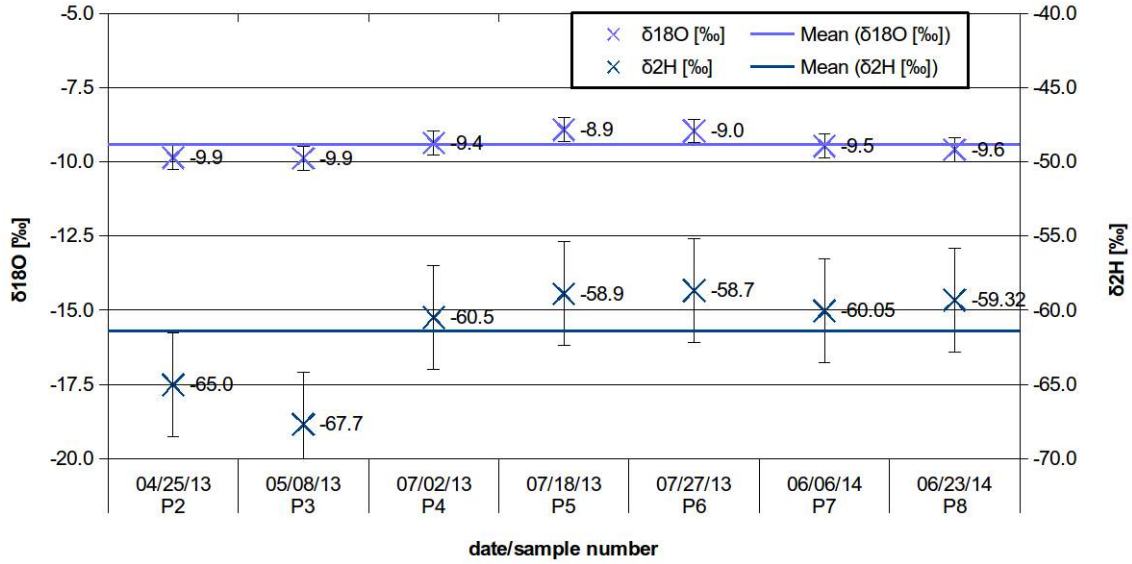

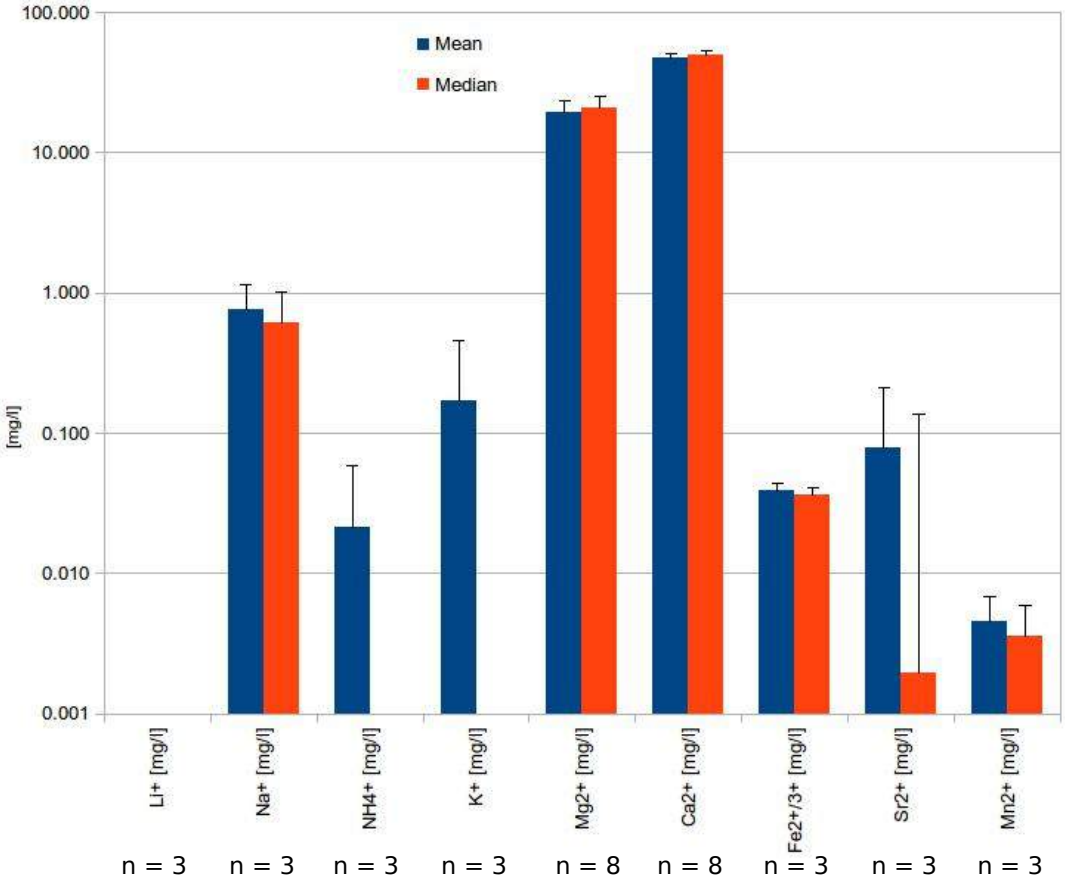

n = 3 n = 3 n = 3 n = 3 n = 8 n = 8 n = 3 n = 3 n = 3

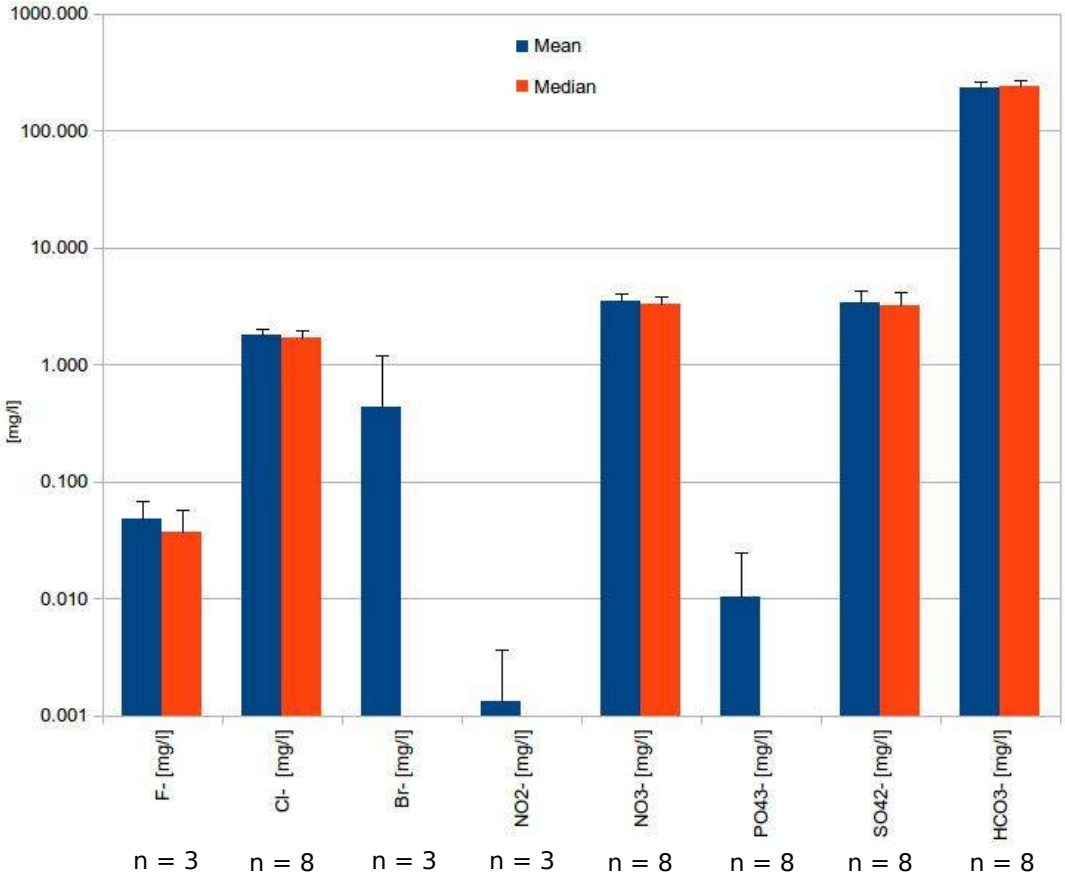

n = 3 n = 8 n = 3 n = 3 n = 8 n = 8 n = 8 n = 8

13) PG (Podklanec G)

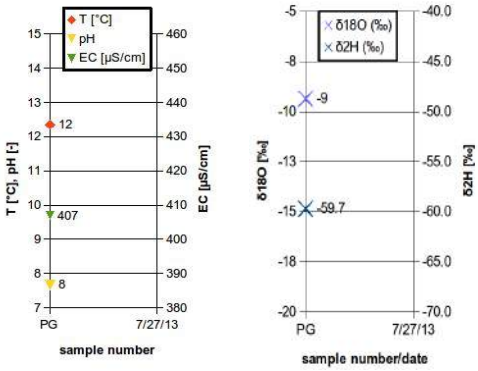

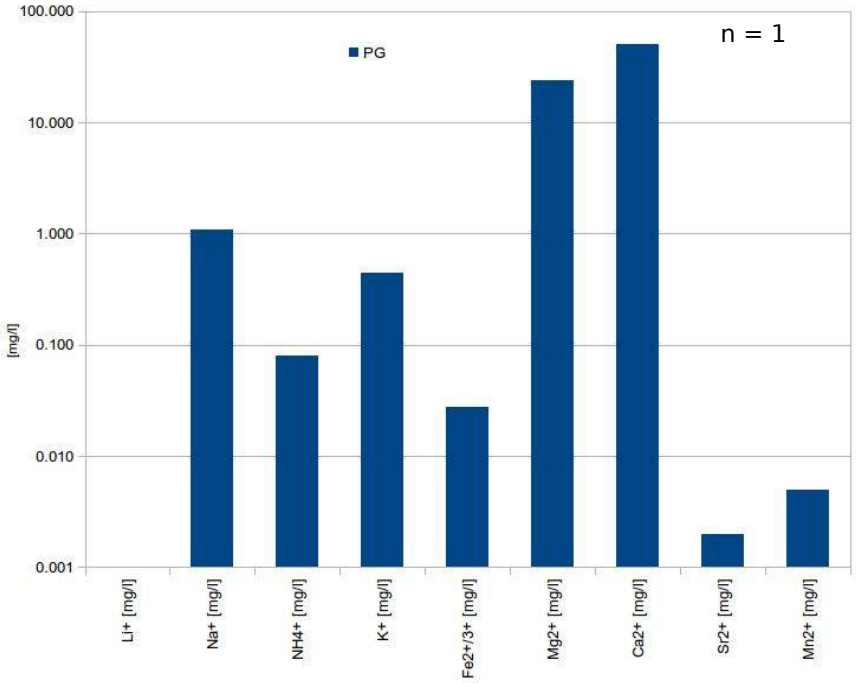

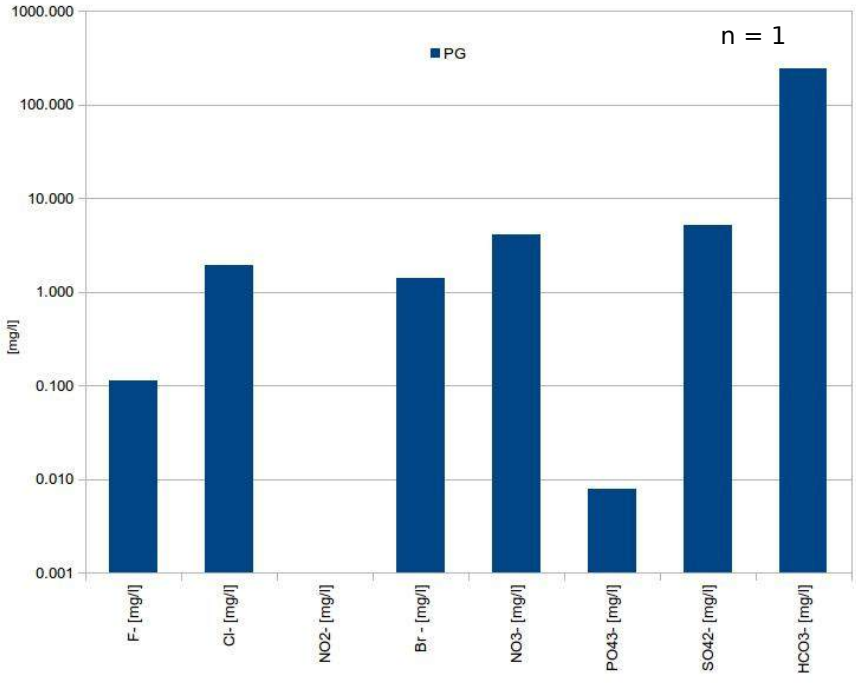

14) V (Vrh)

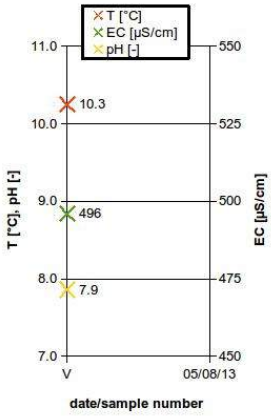
T [°C]
EC [µS/cm]
pH [-]
11.0
10.0
9.0
8.0
7.0
550
525
500
475
450
10.3
496
7.9
V
05/08/13
T [°C], pH [-]
EC [µS/cm]
date/sample number

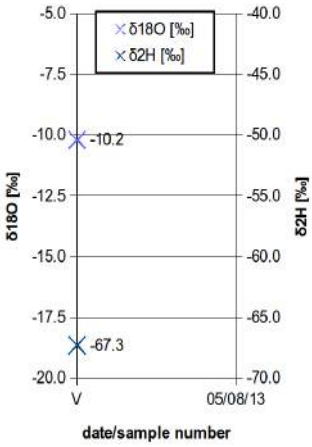
δ18O [‰]
δ2H [‰]
-5.0
-7.5
-10.0
-12.5
-15.0
-17.5
-20.0
-40.0
-45.0
-50.0
-55.0
-60.0
-65.0
-70.0
-10.2
-67.3
V
05/08/13
δ18O [‰]
δ2H [‰]
date/sample number


Google earth

1 km

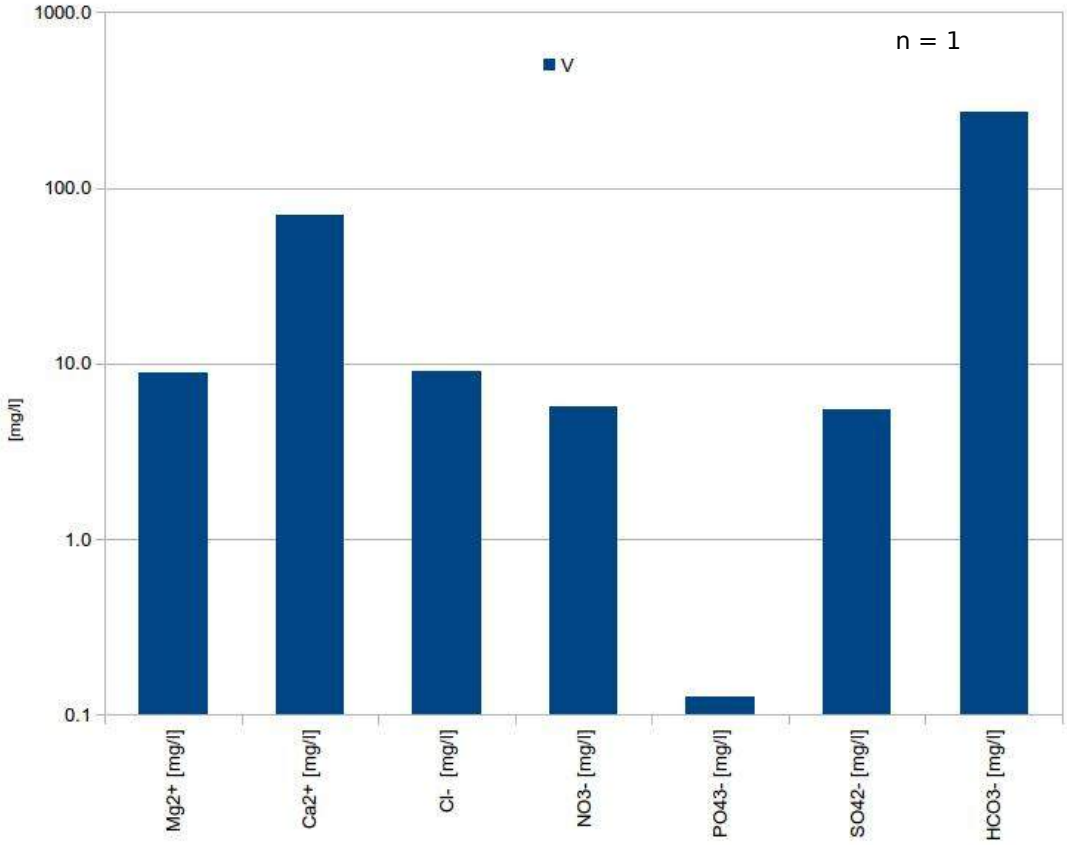
1000.0
100.0
10.0
1.0
0.1
[mg/l]
n = 1
V
Mg2+ [mg/l]
Ca2+ [mg/l]
Cl- [mg/l]
NO3- [mg/l]
PO43- [mg/l]
SO42- [mg/l]
HCO3- [mg/l]

15) D (Dolini)

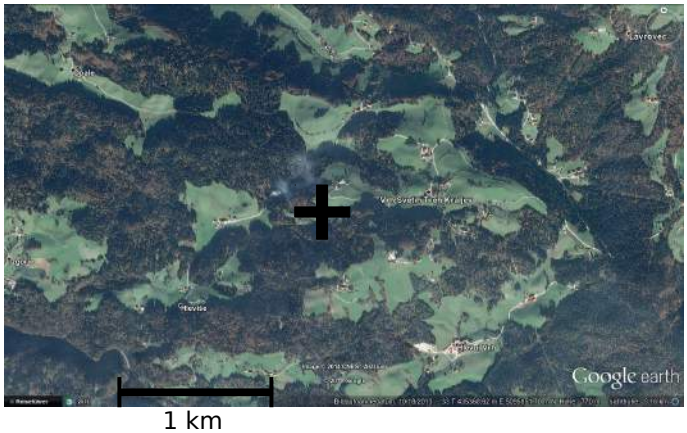
Google earth
1 km

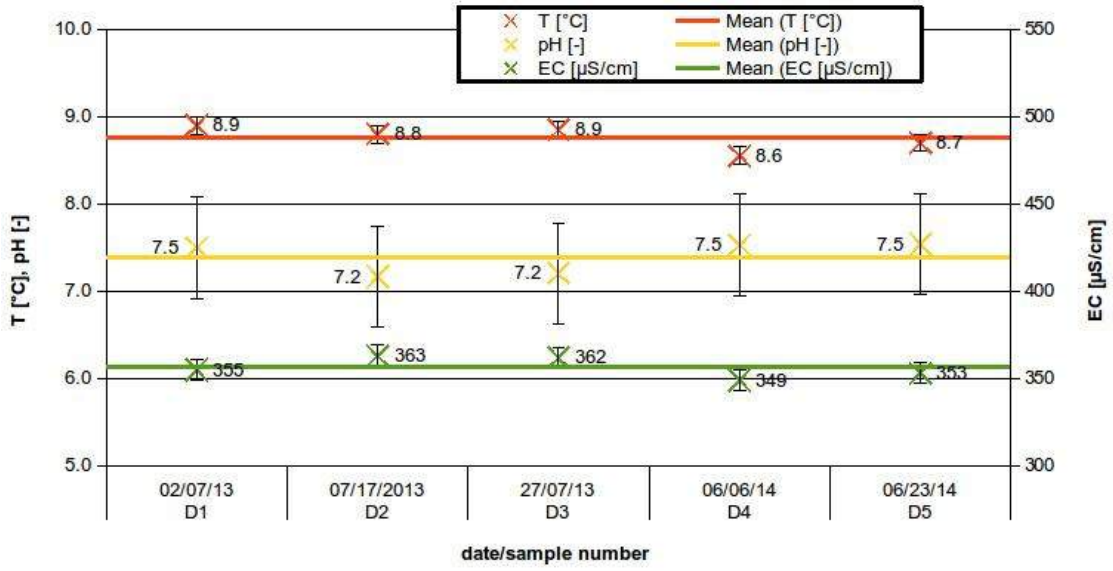
T [°C]
pH [-]
EC [µS/cm]
Mean (T [°C])
Mean (pH [-])
Mean (EC [µS/cm])
T [°C], pH [-]
EC [µS/cm]
8.9
8.8
8.9
8.6
8.7
7.5
7.2
7.2
7.5
7.5
355
363
362
349
353
02/07/13 D1
07/17/2013 D2
27/07/13 D3
06/06/14 D4
06/23/14 D5
date/sample number

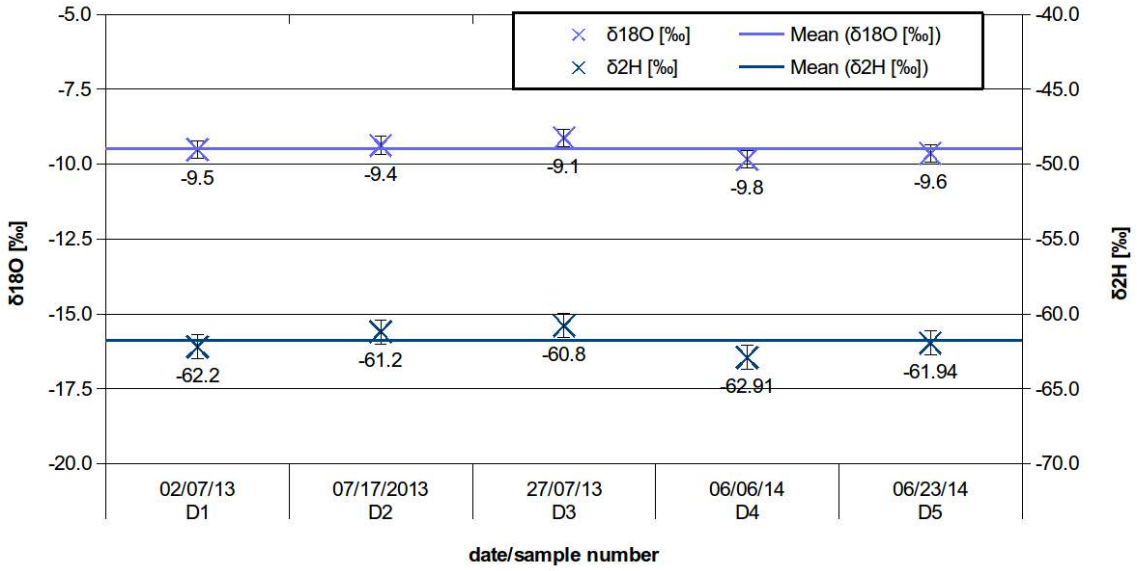
δ18O [‰]
δ2H [‰]
Mean (δ18O [‰])
Mean (δ2H [‰])
δ18O [‰]
δ2H [‰]
-9.5
-9.4
-9.1
-9.8
-9.6
-62.2
-61.2
-60.8
-62.91
-61.94
02/07/13 D1
07/17/2013 D2
27/07/13 D3
06/06/14 D4
06/23/14 D5
date/sample number

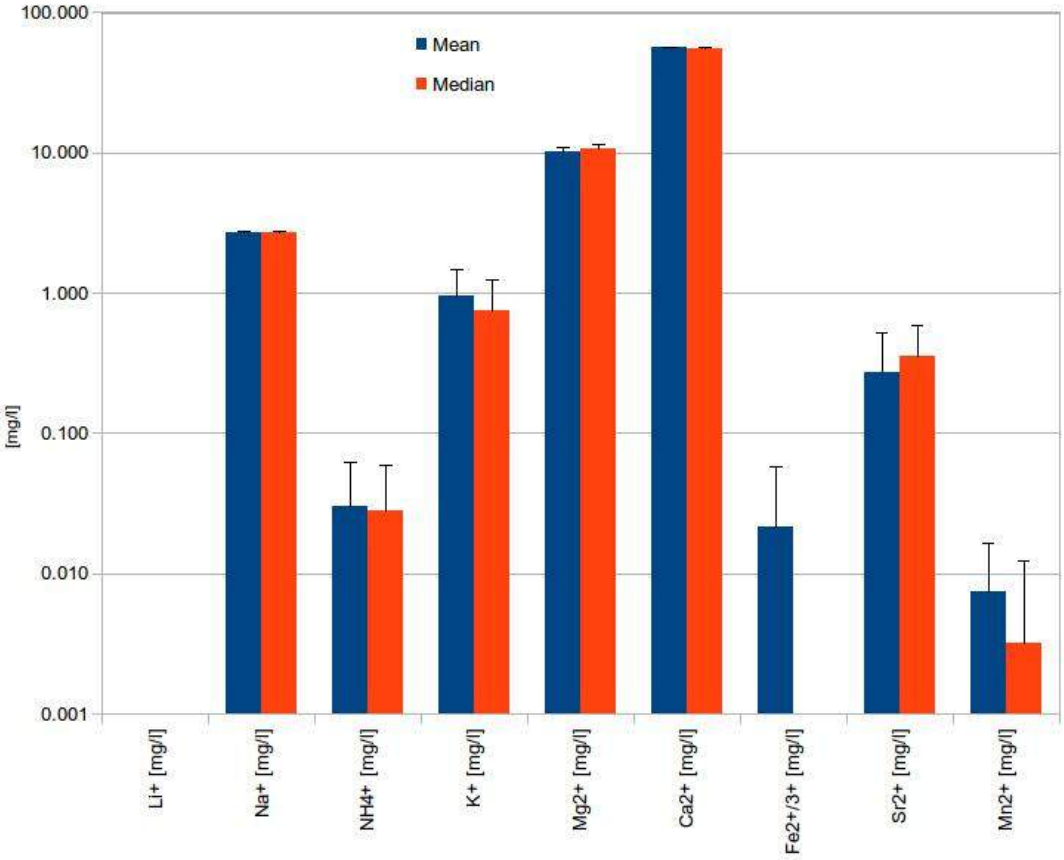

n = 3 n = 3 n = 3 n = 3 n = 5 n = 5 n = 3 n = 3 n = 3

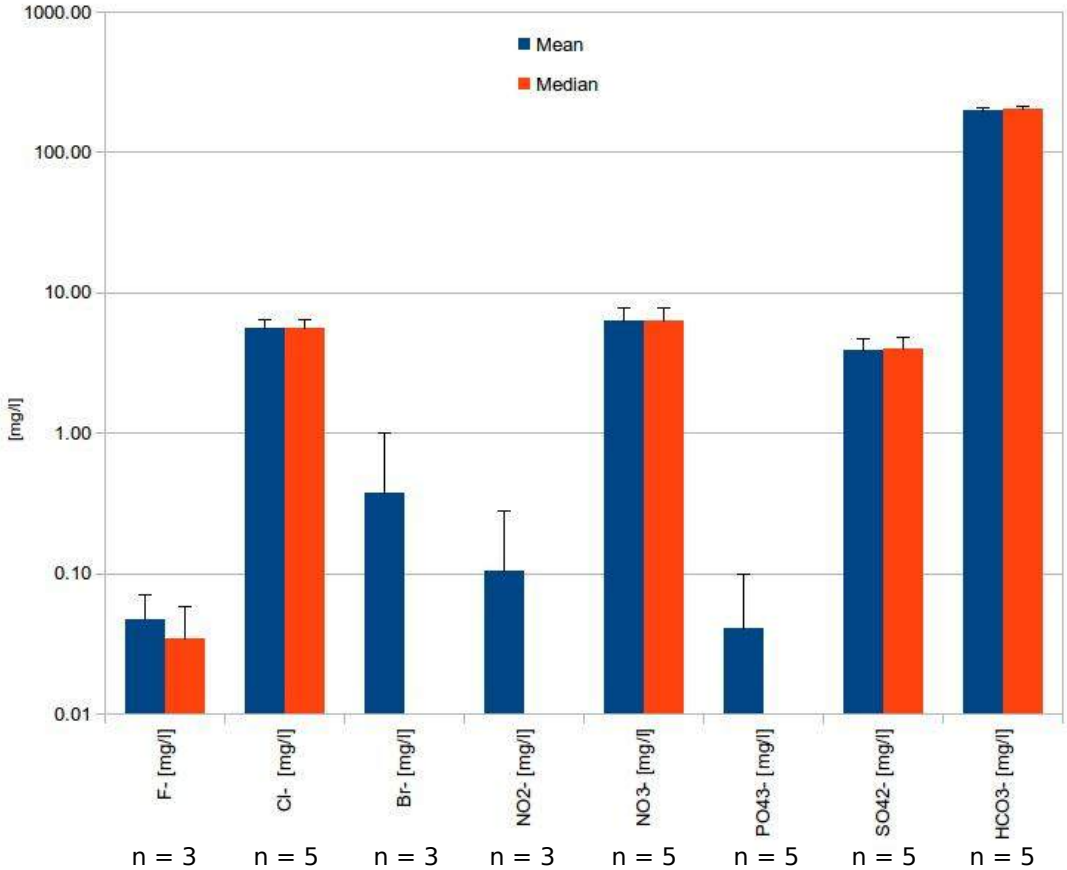

n = 3 n = 5 n = 3 n = 3 n = 5 n = 5 n = 5 n = 5

16) C (Cerkno Hotel)

1 km

1 km

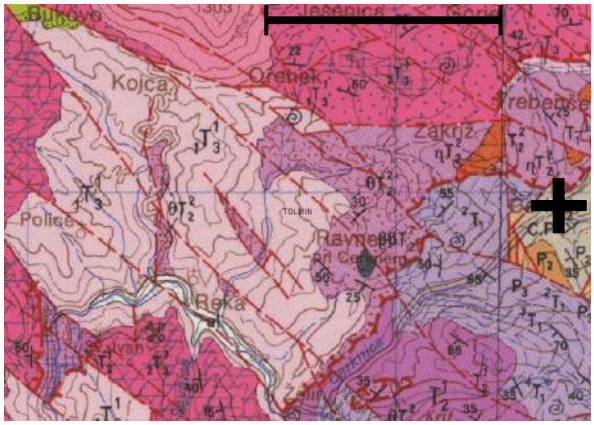

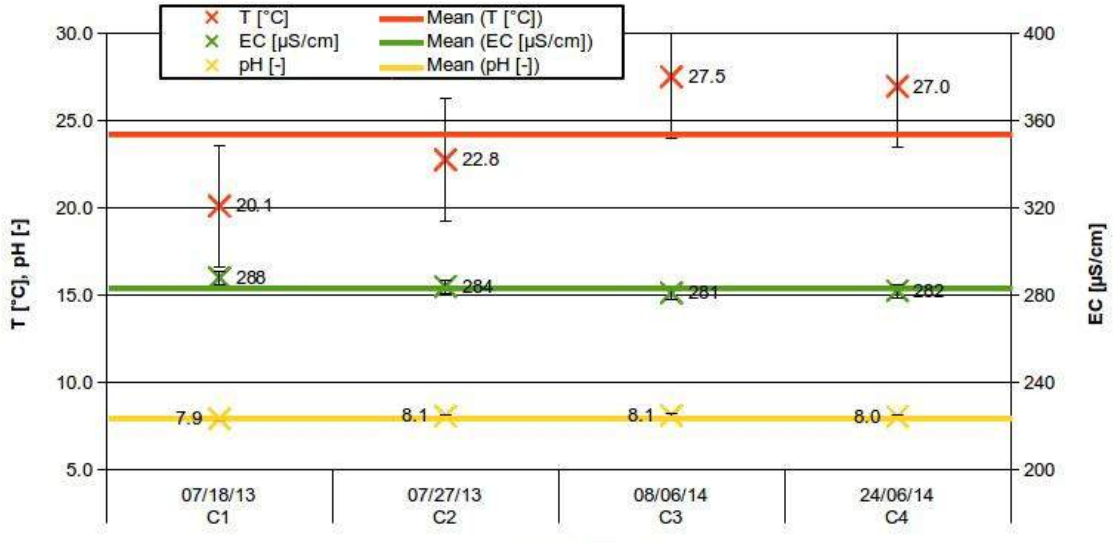

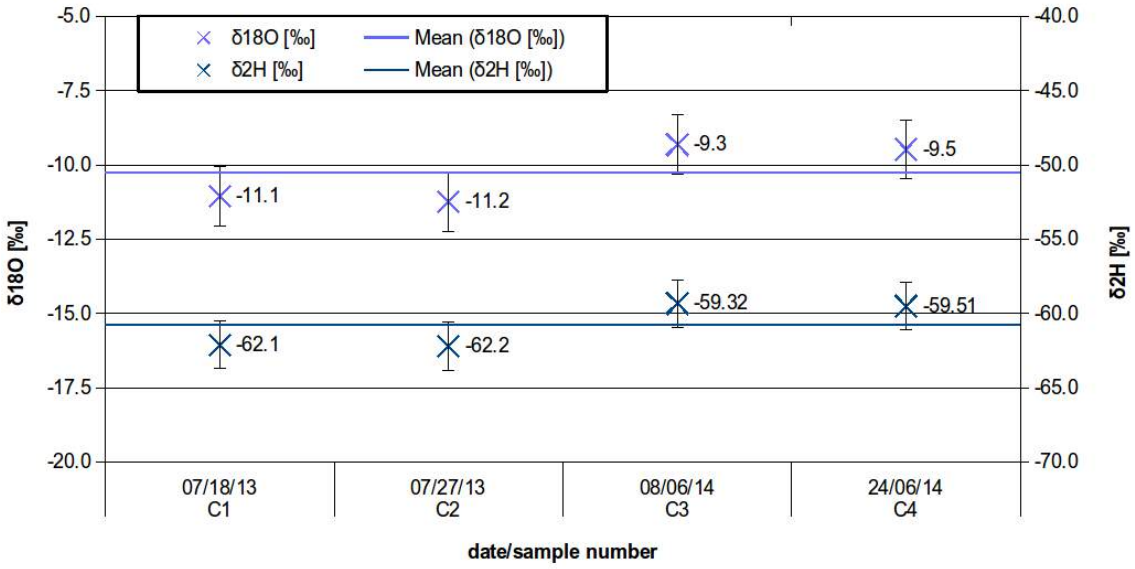

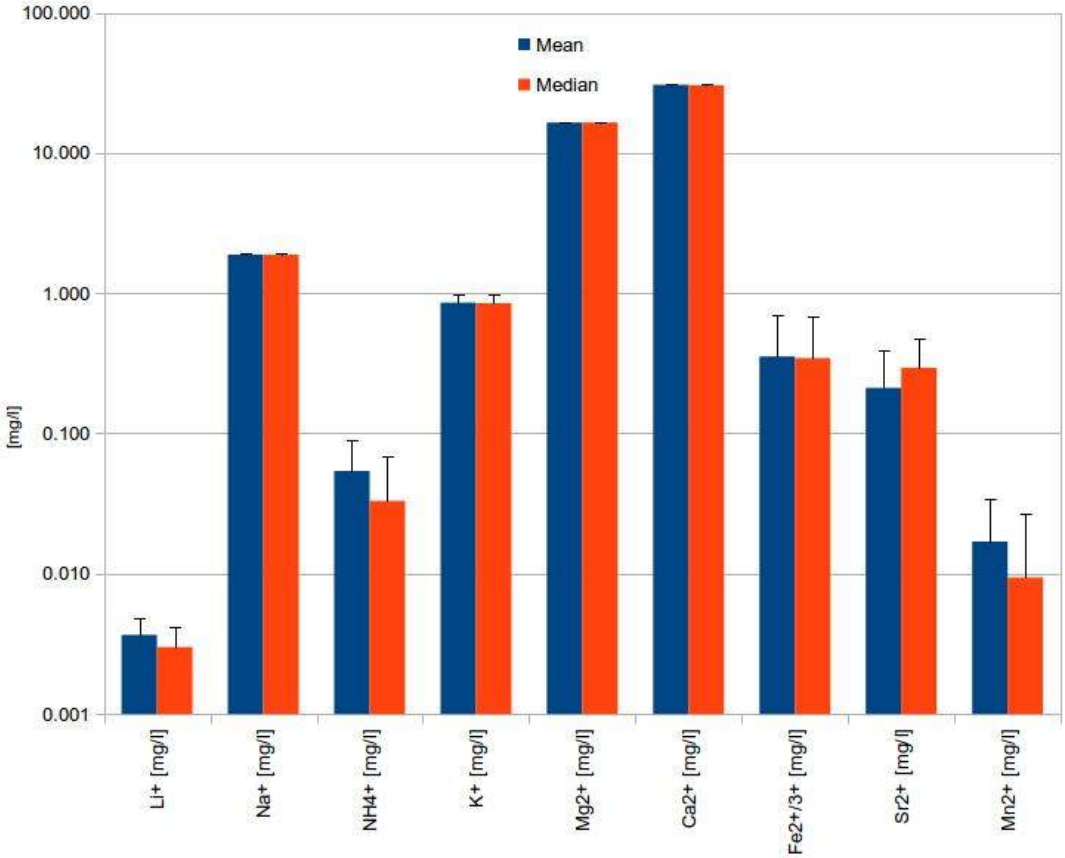

n = 3 n = 3 n = 3 n = 3 n = 4 n = 4 n = 3 n = 3 n = 3

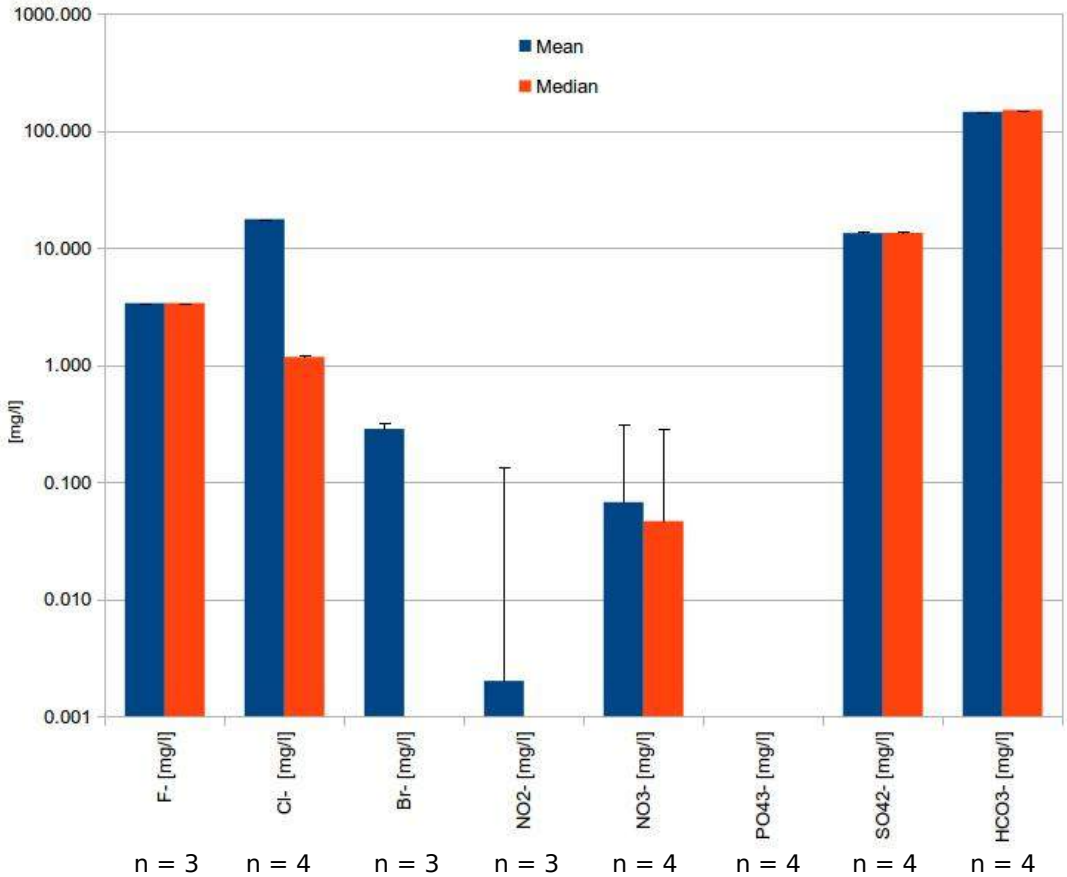

n = 3 n = 4 n = 3 n = 3 n = 4 n = 4 n = 4 n = 4

17) T (Toplice Hotavlje)

TA

TB

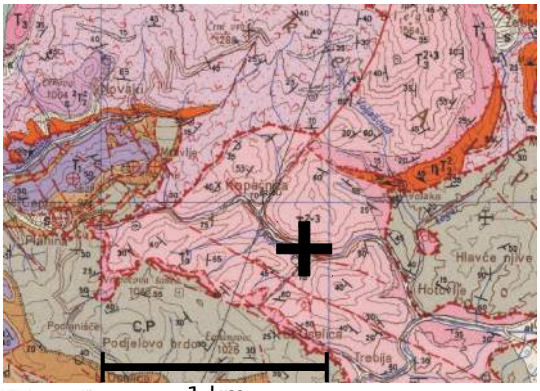

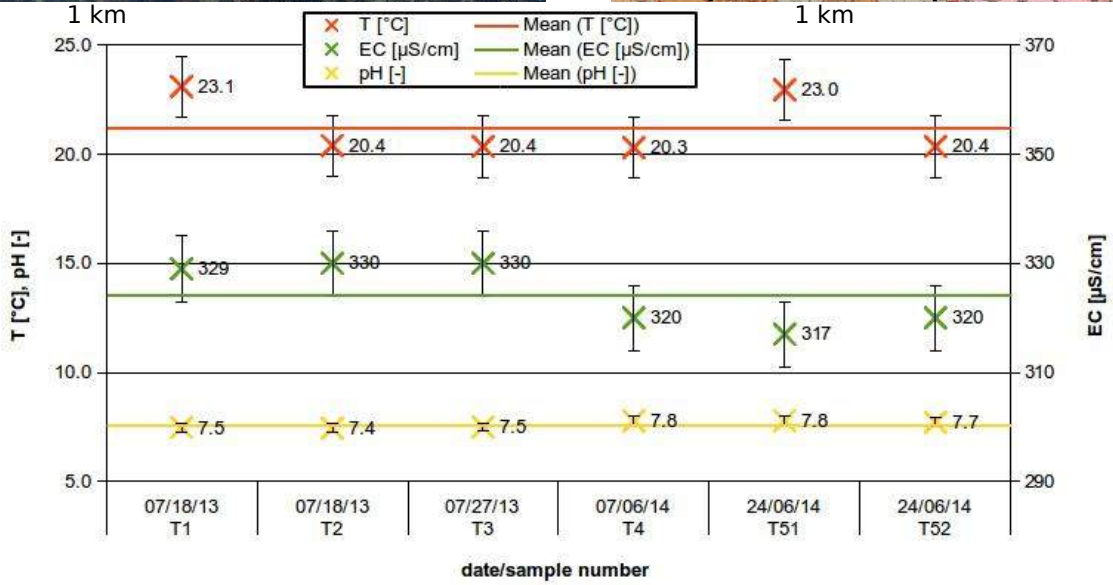

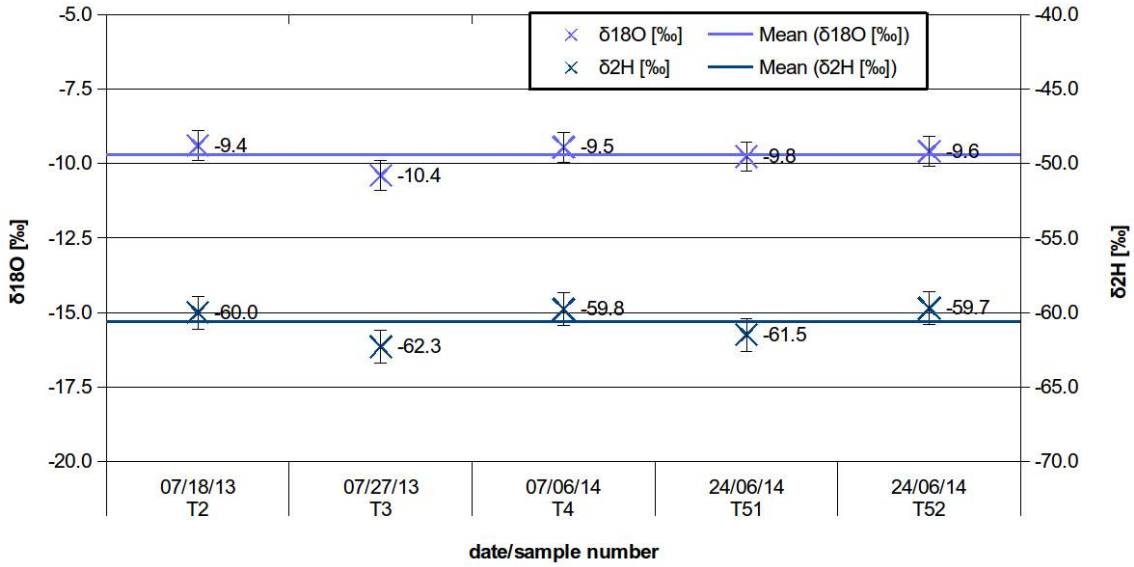

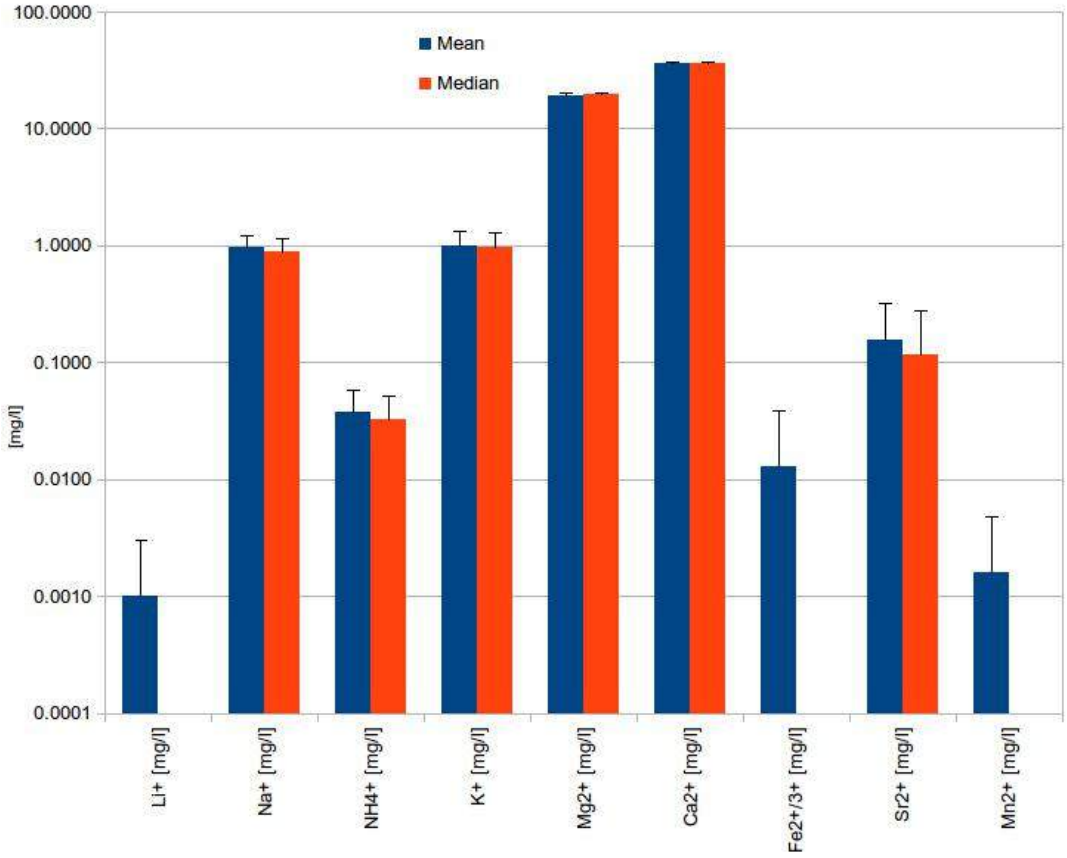

n = 4 n = 4 n = 4 n = 4 n = 6 n = 6 n = 4 n = 4 n = 4

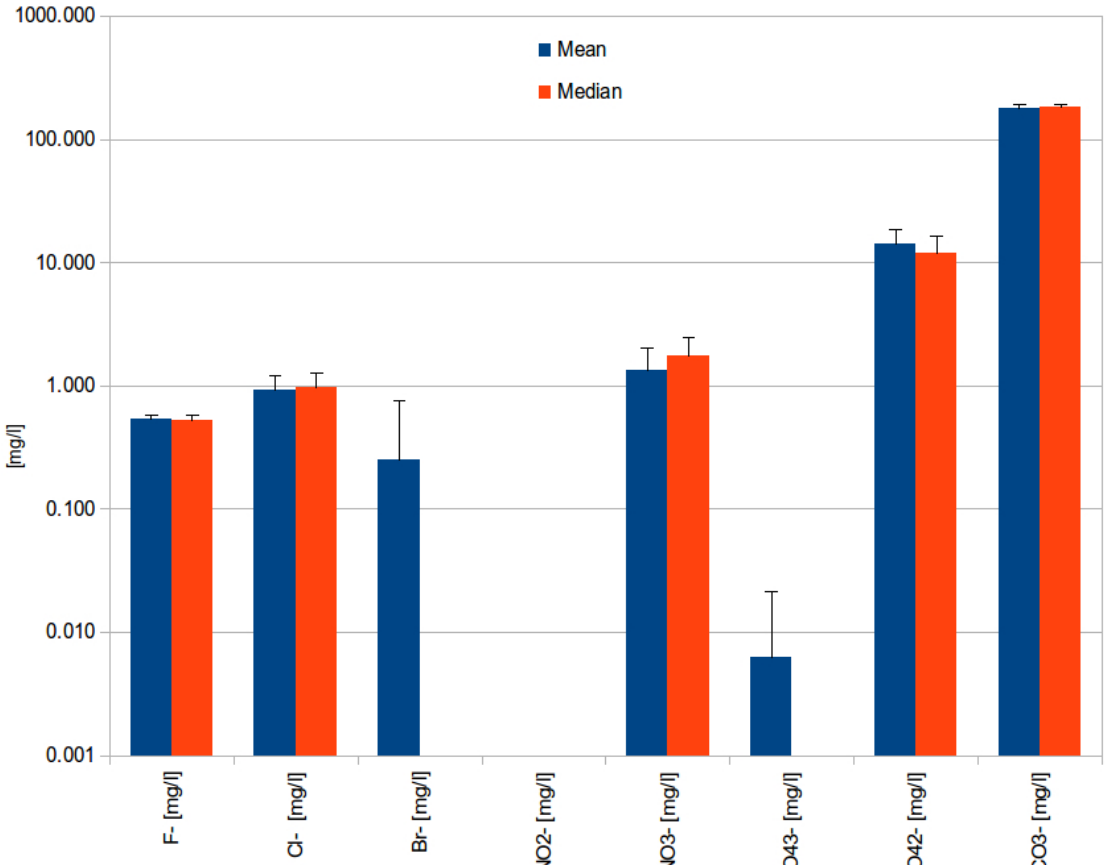

n = 4 n = 6 n = 4 n = 4 n = 6 n = 6 n = 6 n = 6

18) BH (Bled Hotel)

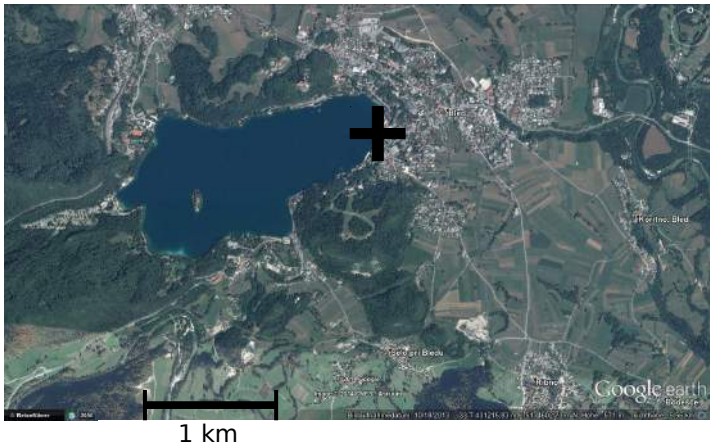

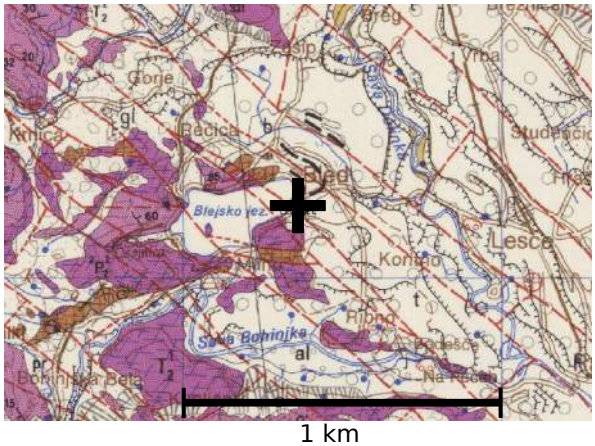

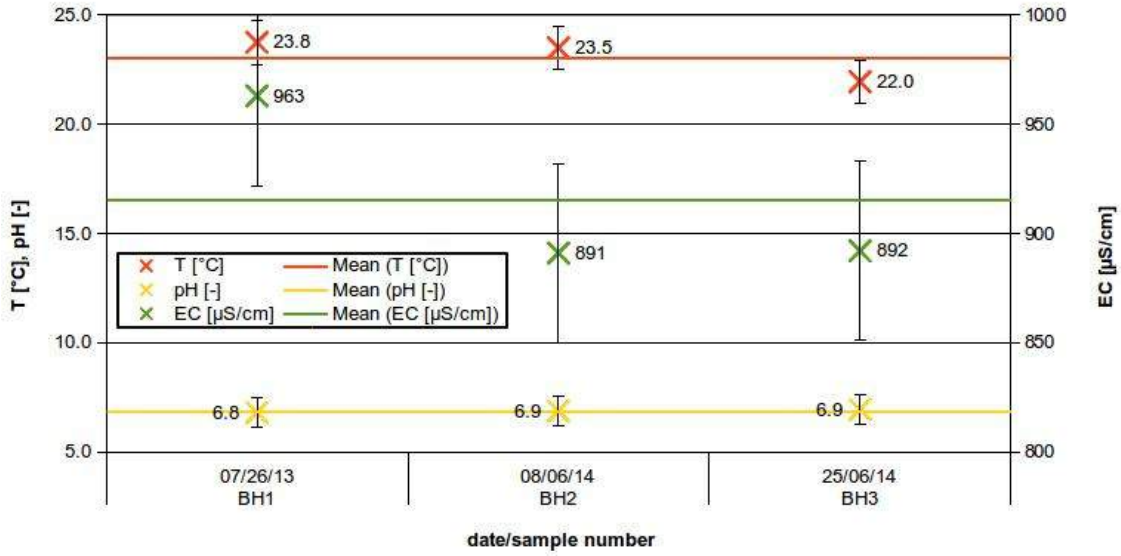

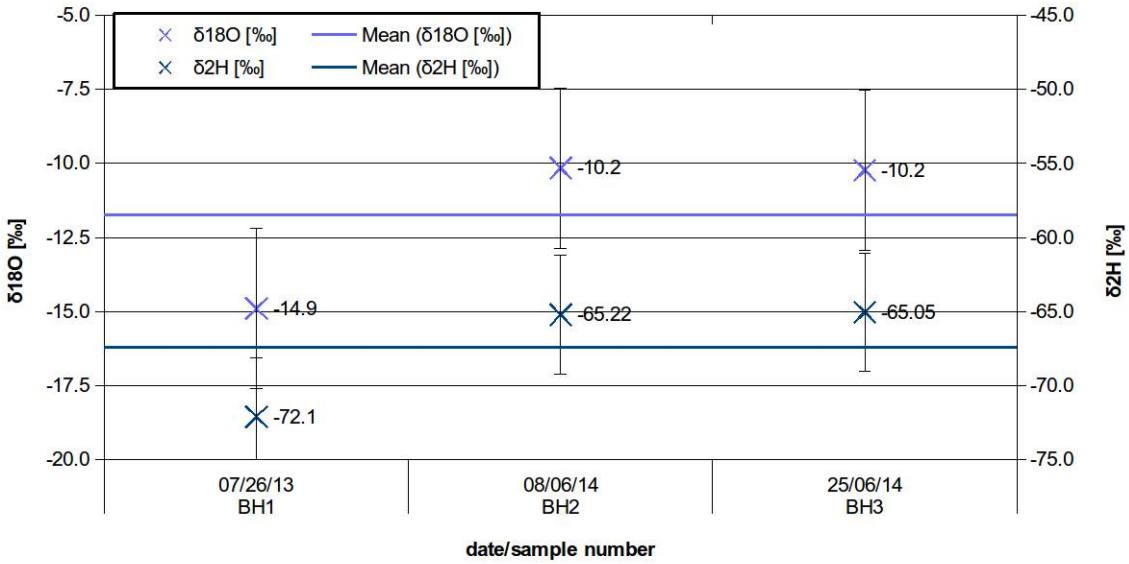

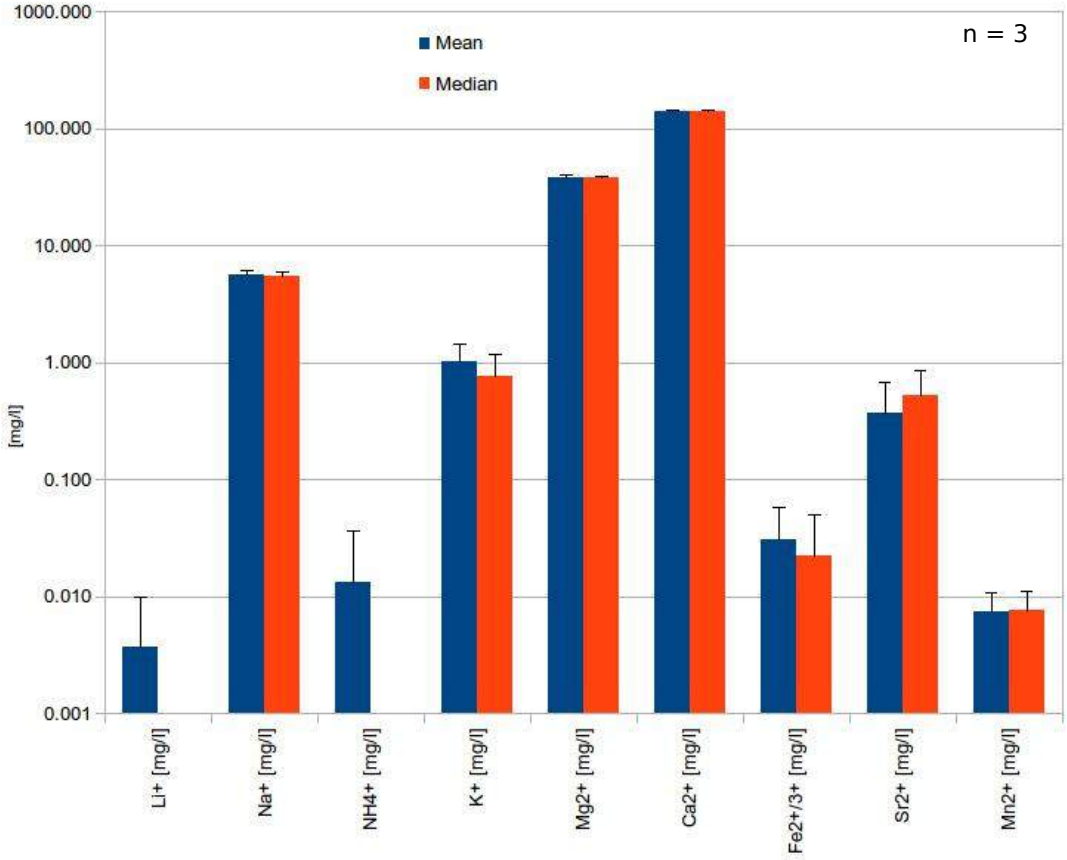
n = 3
Mean
Median
1000.000
100.000
10.000
1.000
0.100
0.010
0.001
[mg/l]
Li+ [mg/l]
Na+ [mg/l]
NH4+ [mg/l]
K+ [mg/l]
Mg2+ [mg/l]
Ca2+ [mg/l]
Fe2+/3+ [mg/l]
Sr2+ [mg/l]
Mn2+ [mg/l]

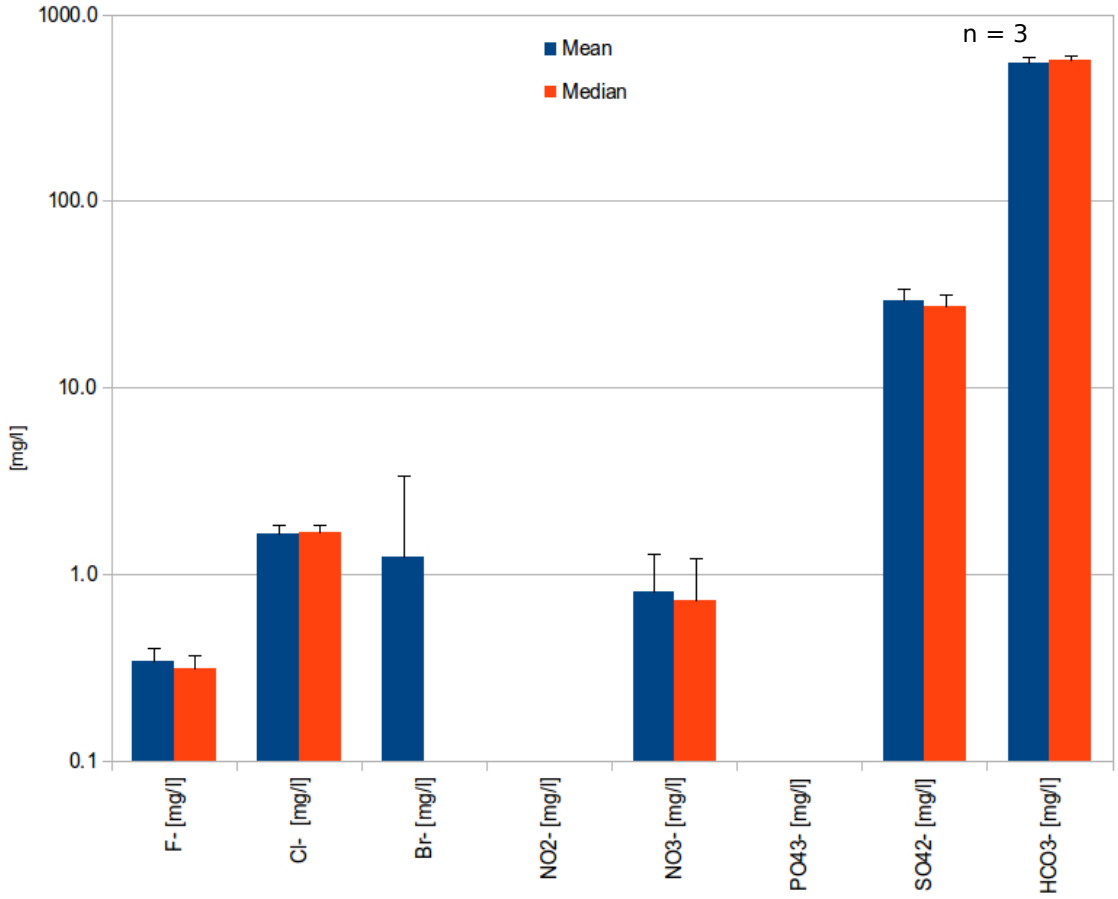
n = 3
Mean
Median
1000.0
100.0
10.0
1.0
0.1
[mg/l]
F- [mg/l]
Cl- [mg/l]
Br- [mg/l]
NO2- [mg/l]
NO3- [mg/l]
PO43- [mg/l]
SO42- [mg/l]
HCO3- [mg/l]

19) ST (Straza spodnje Pirniče)

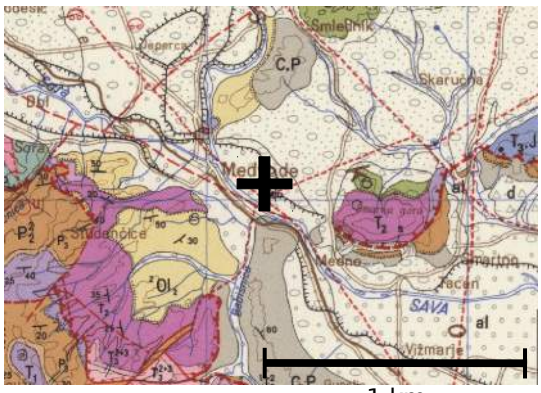

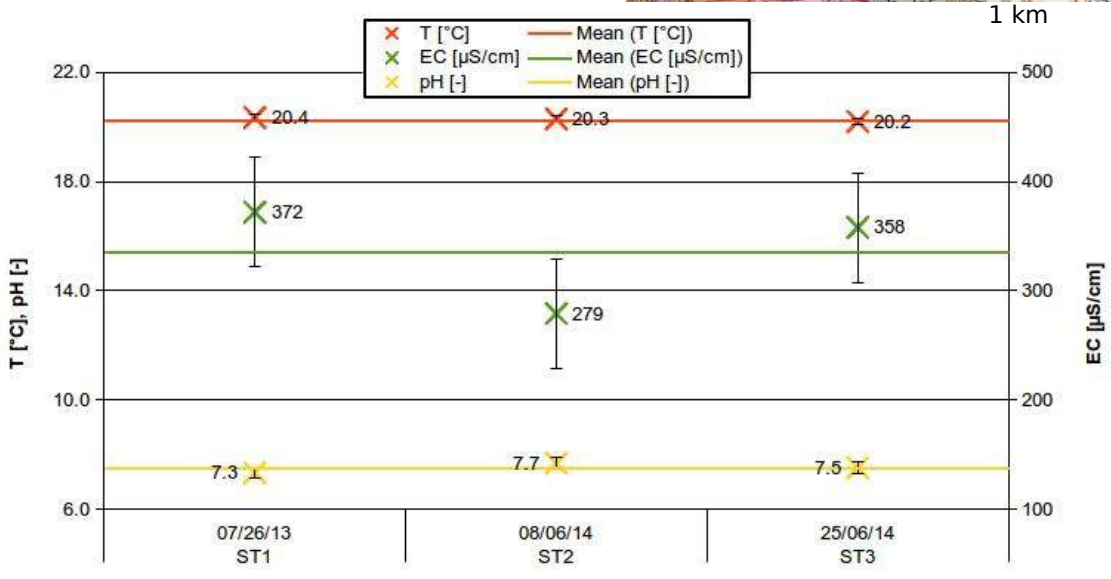

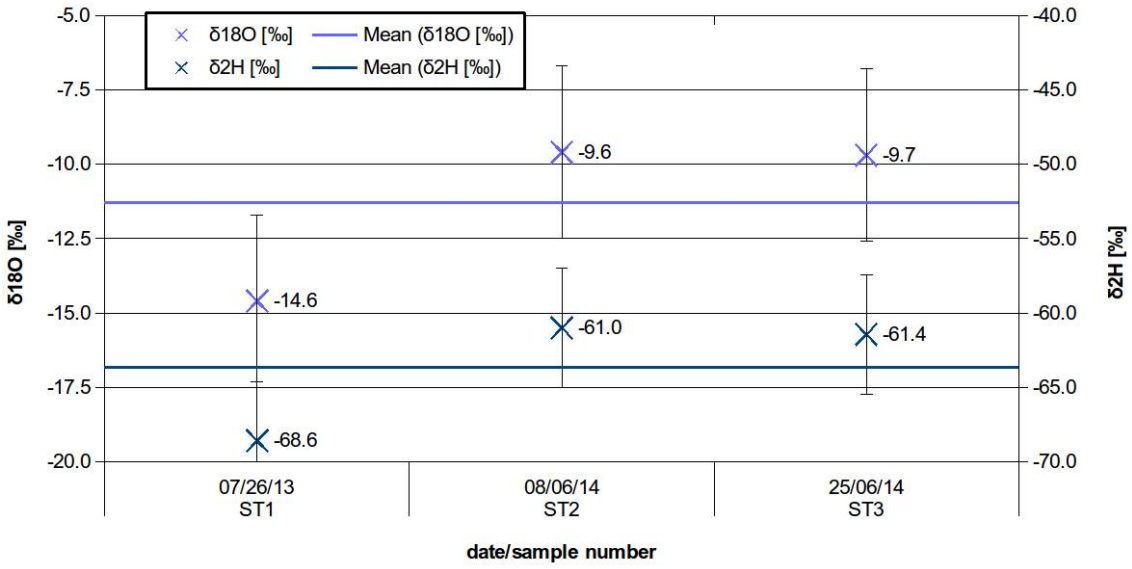

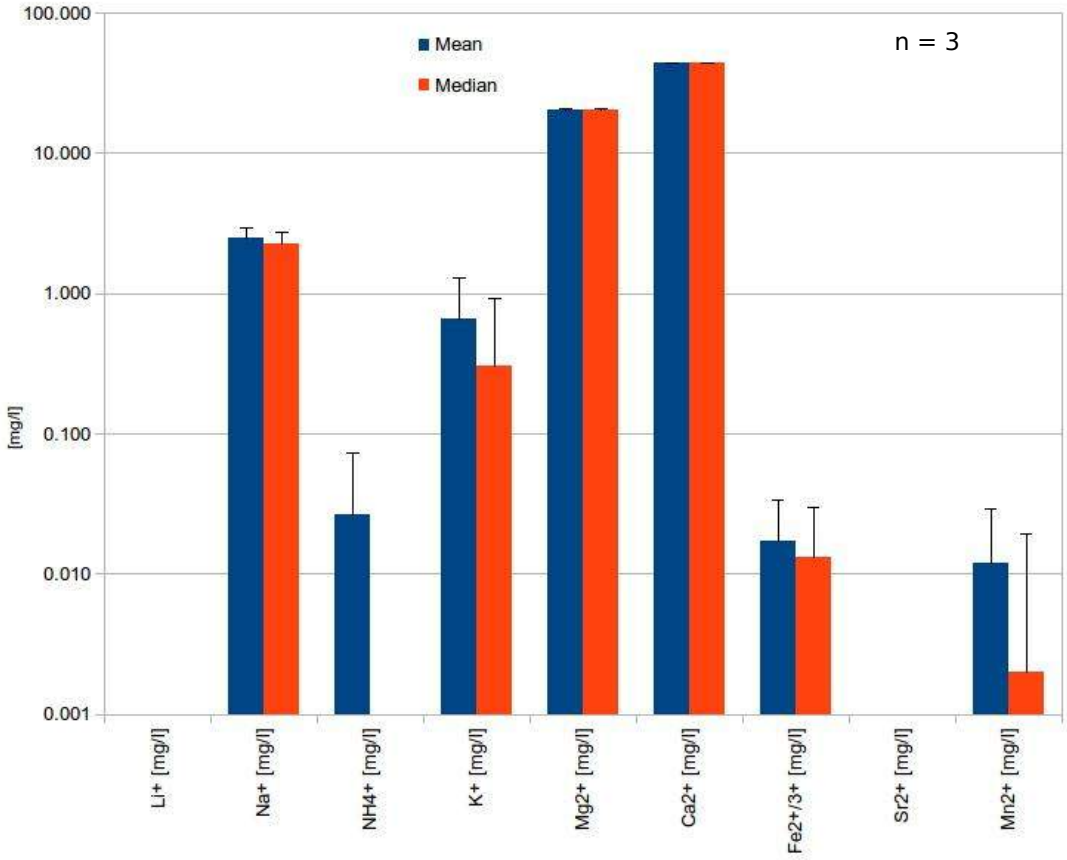
100.000
10.000
1.000
0.100
0.010
0.001
[mg/l]
Mean
Median
n = 3
Li+ [mg/l]
Na+ [mg/l]
NH4+ [mg/l]
K+ [mg/l]
Mg2+ [mg/l]
Ca2+ [mg/l]
Fe2+/3+ [mg/l]
Sr2+ [mg/l]
Mn2+ [mg/l]

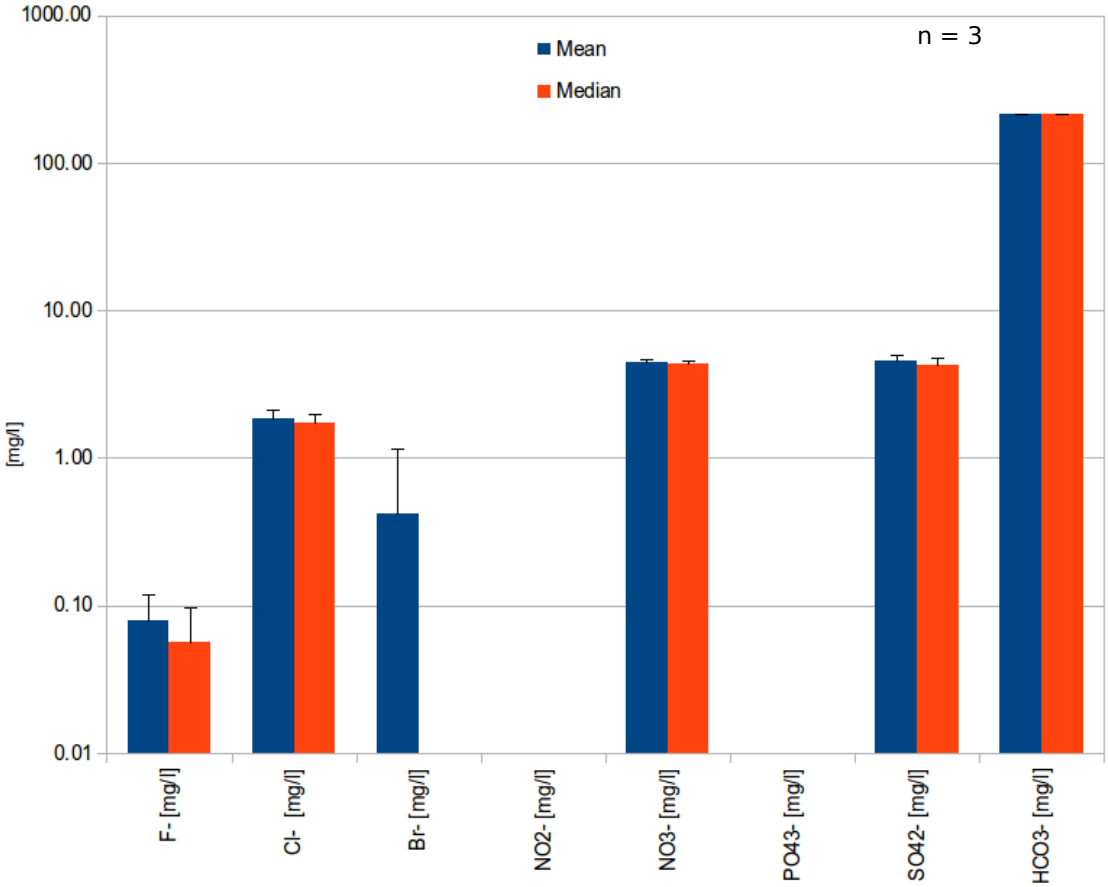
1000.00
100.00
10.00
1.00
0.10
0.01
[mg/l]
Mean
Median
n = 3
F- [mg/l]
Cl- [mg/l]
Br- [mg/l]
NO2- [mg/l]
NO3- [mg/l]
PO43- [mg/l]
SO42- [mg/l]
HCO3- [mg/l]

20) F (Furnalove Toplice)

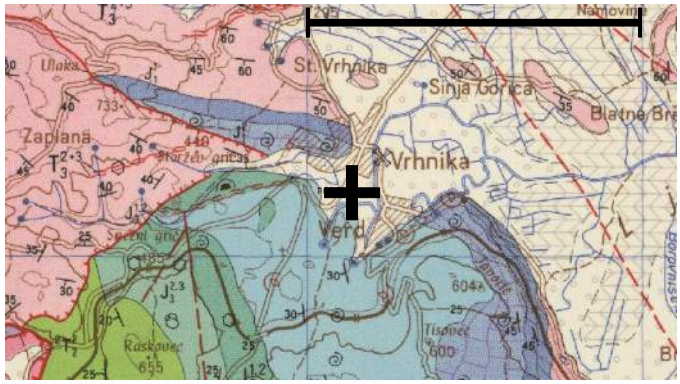

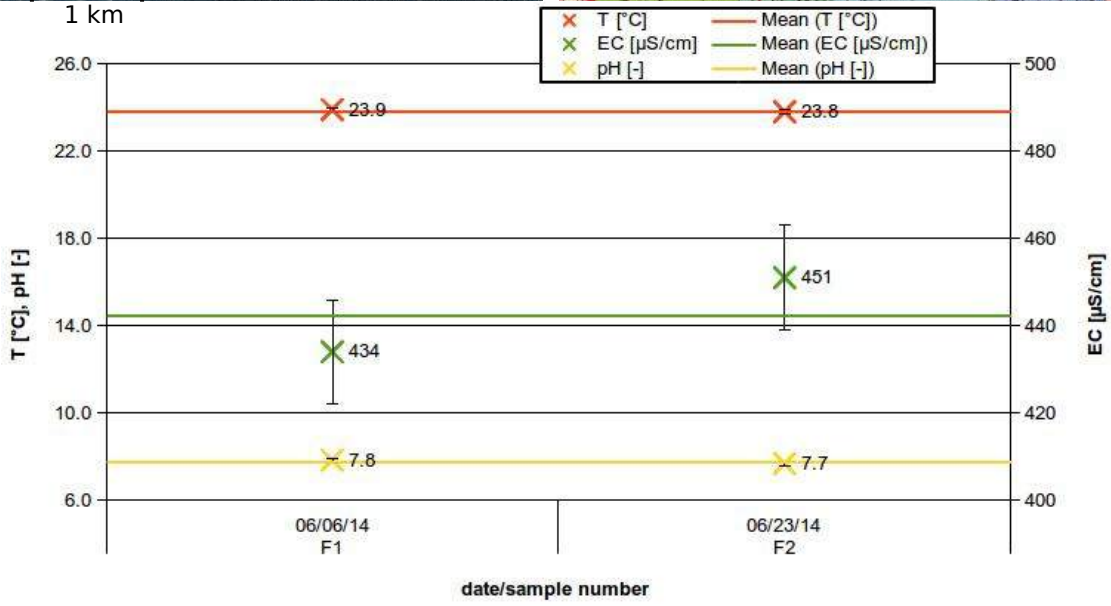

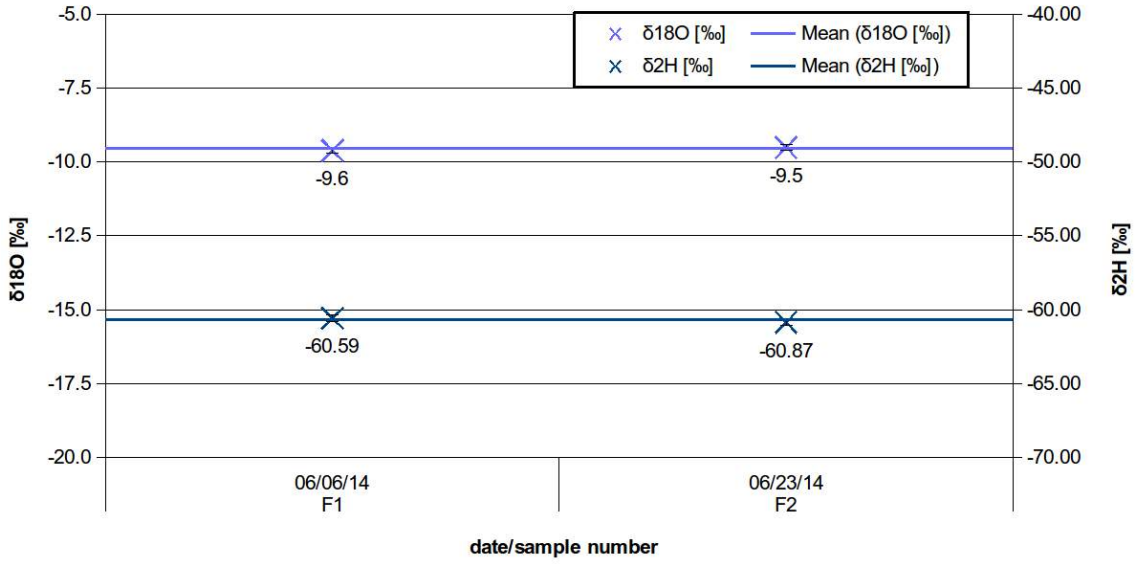

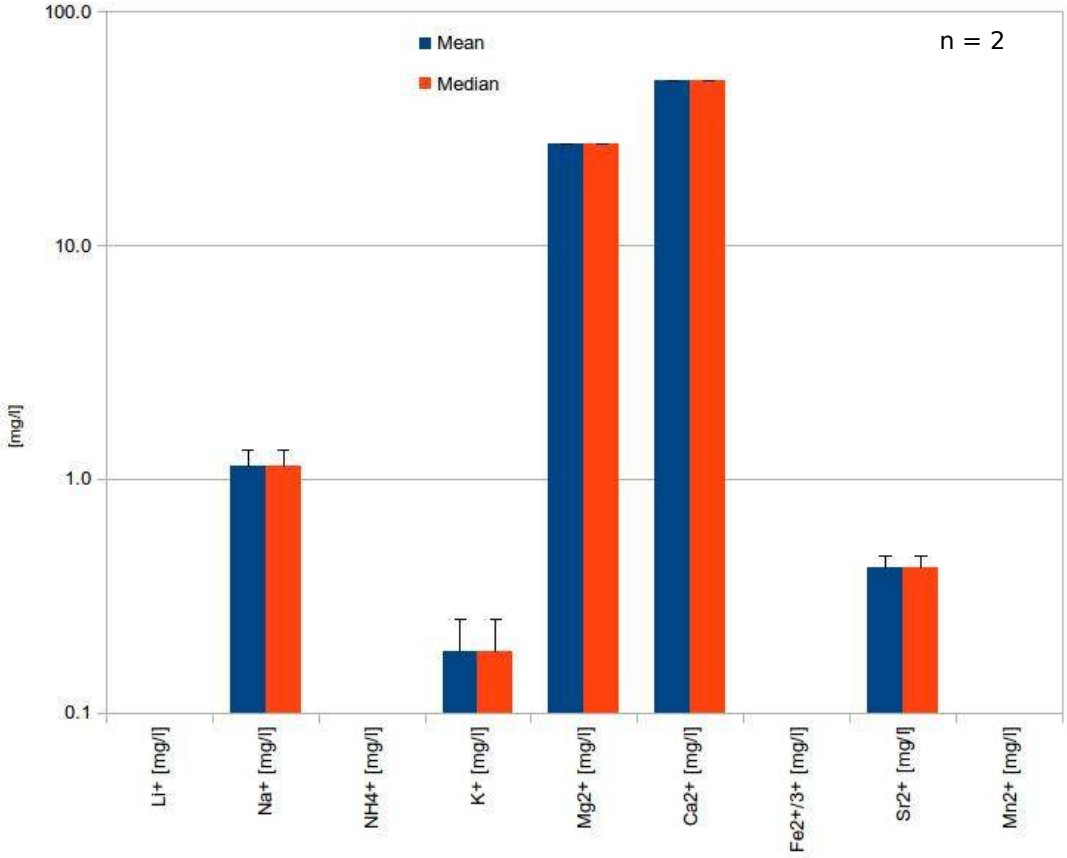
100.0
10.0
1.0
0.1
[mg/l]
Mean
Median
n = 2
Li+ [mg/l]
Na+ [mg/l]
NH4+ [mg/l]
K+ [mg/l]
Mg2+ [mg/l]
Ca2+ [mg/l]
Fe2+/3+ [mg/l]
Sr2+ [mg/l]
Mn2+ [mg/l]

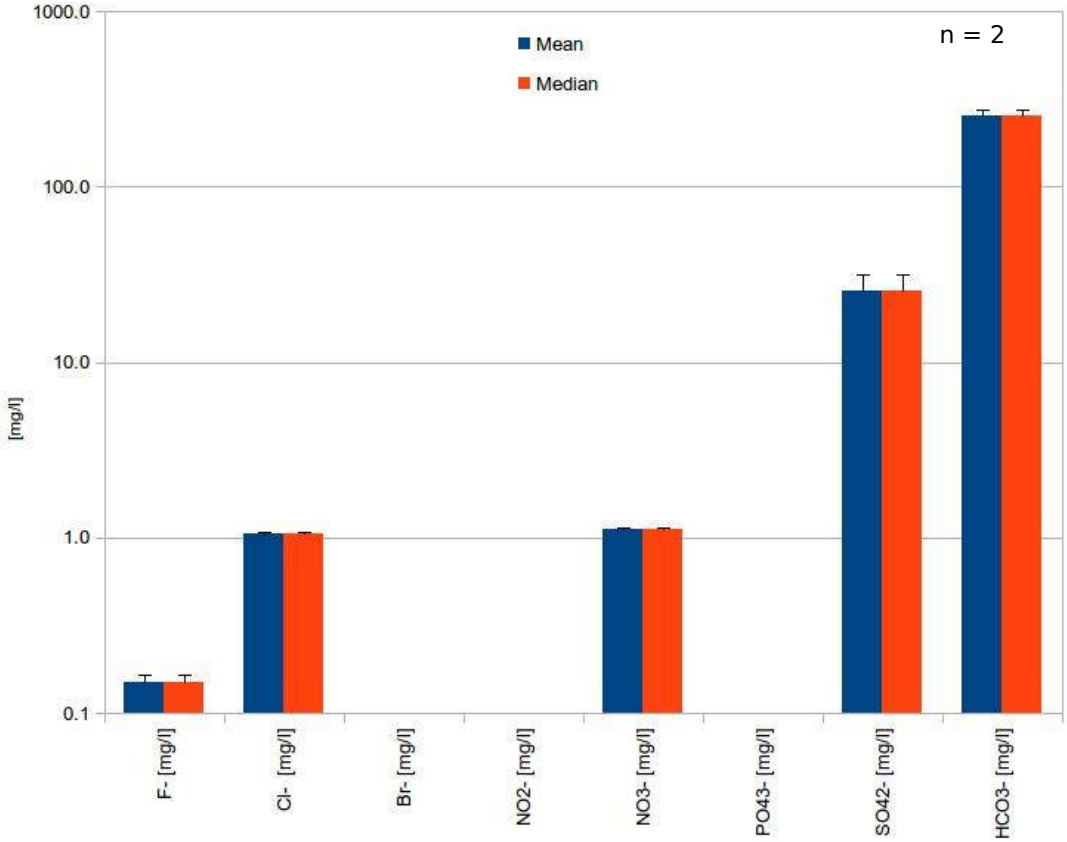
1000.0
100.0
10.0
1.0
0.1
[mg/l]
Mean
Median
n = 2
F- [mg/l]
Cl- [mg/l]
Br- [mg/l]
NO2- [mg/l]
NO3- [mg/l]
PO43- [mg/l]
SO42- [mg/l]
HCO3- [mg/l]

21) ZE (above Zeplinica)

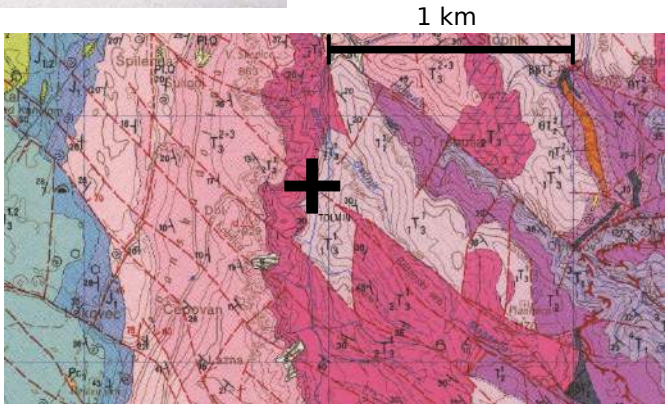

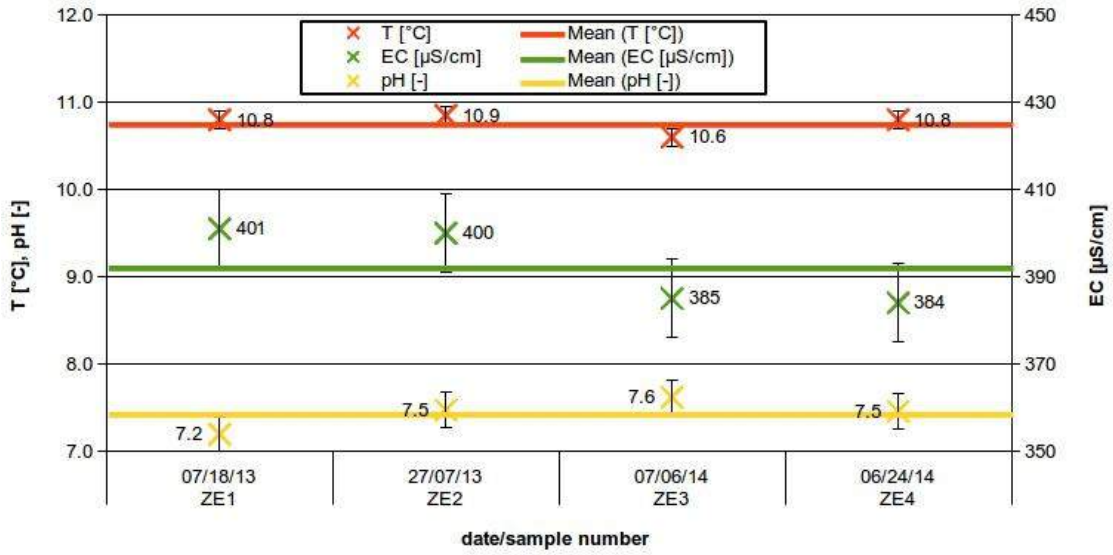

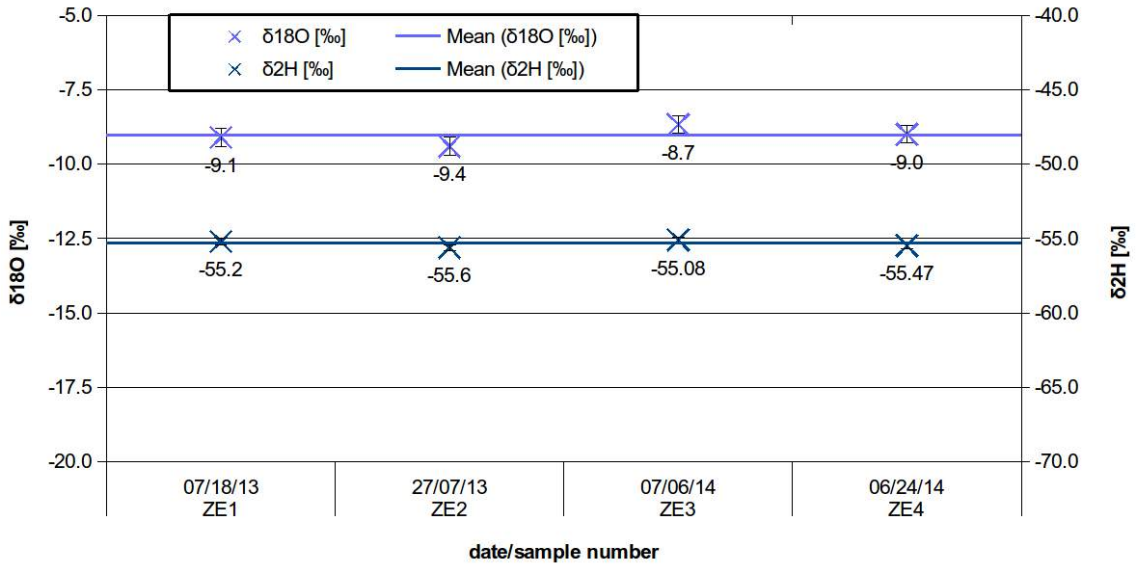

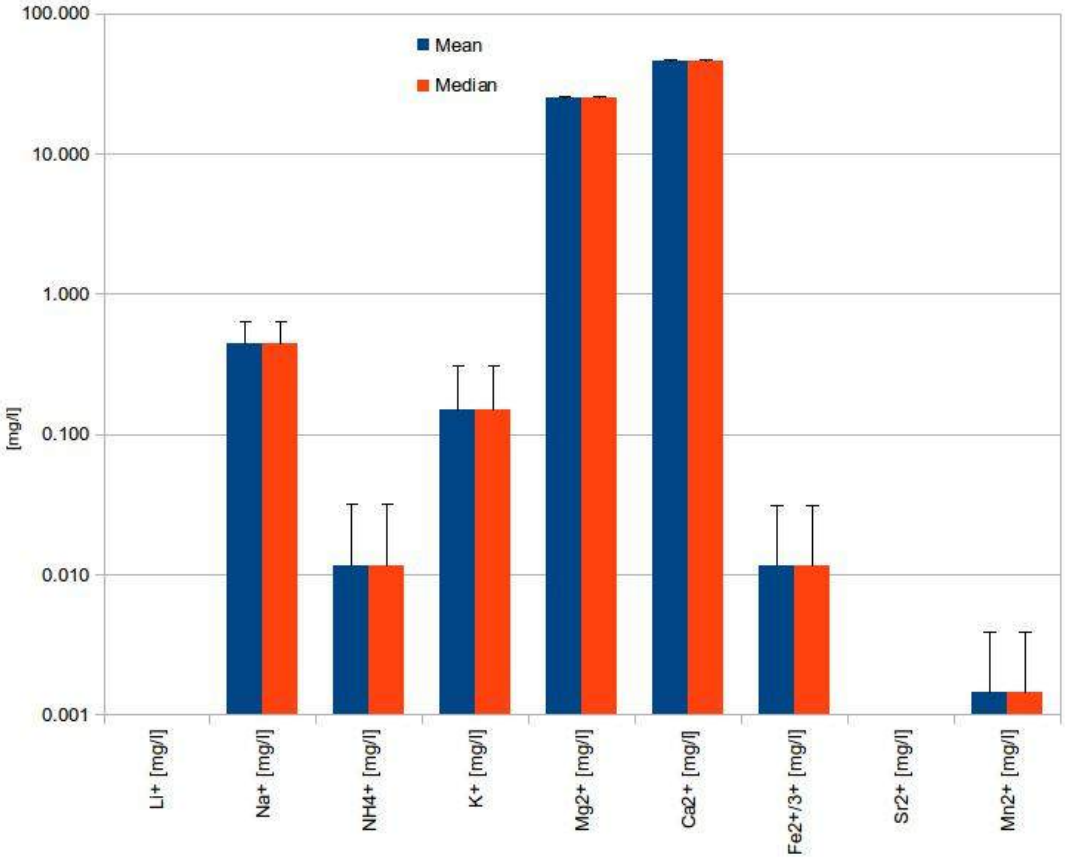

n = 3 n = 3 n = 3 n = 3 n = 4 n = 4 n = 3 n = 3 n = 3

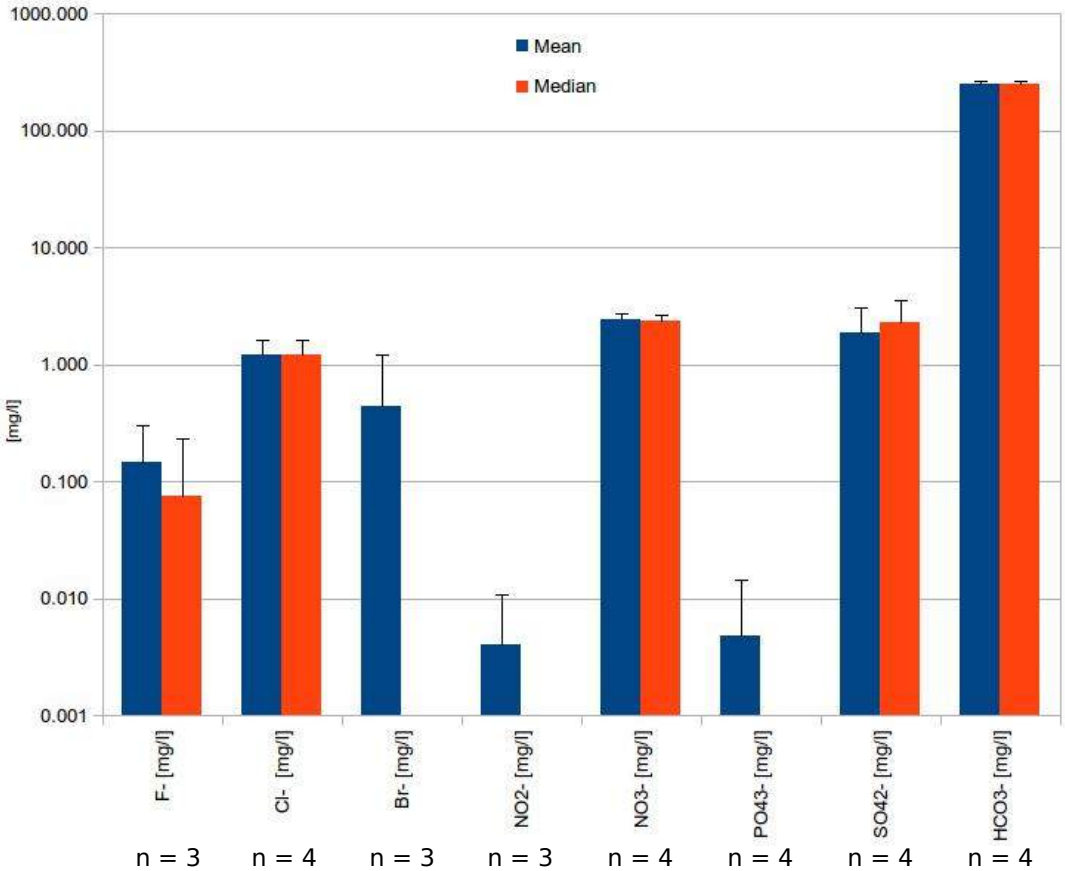

n = 3 n = 4 n = 3 n = 3 n = 4 n = 4 n = 4 n = 4

22) S (Zeplinica)

1 km

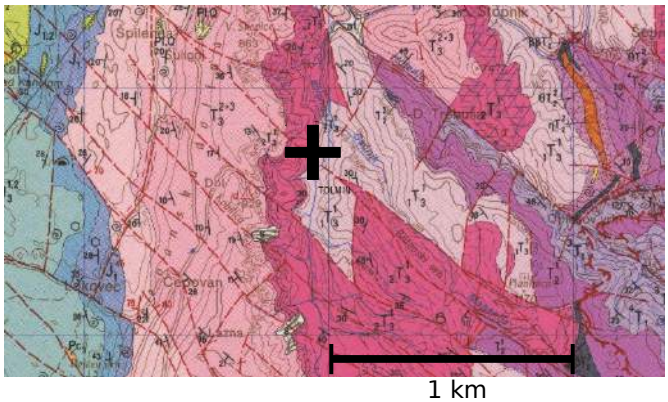

1 km

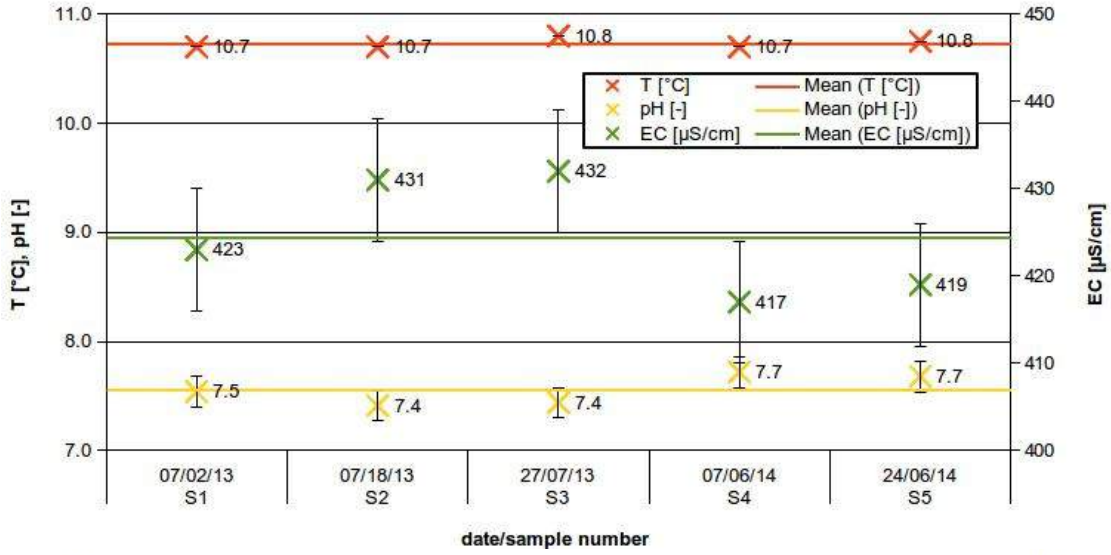

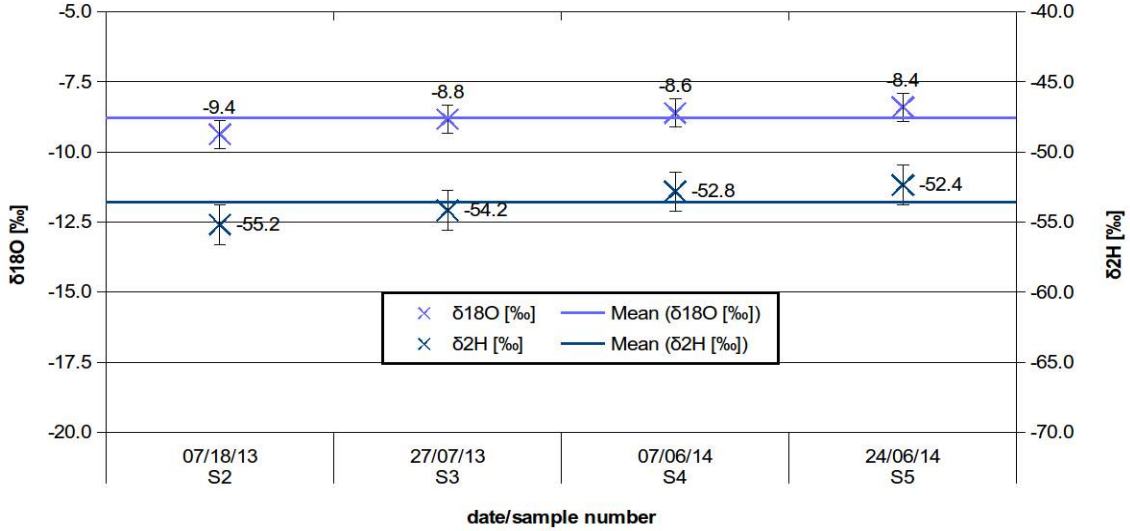

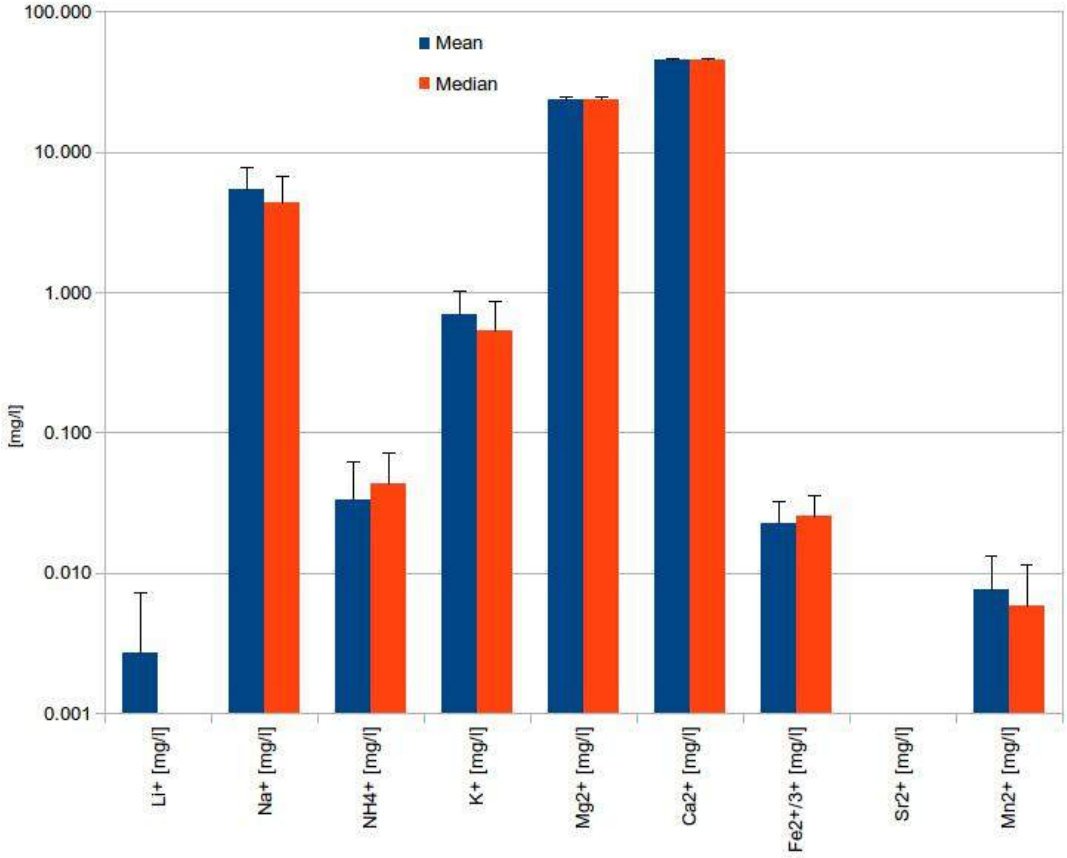
100.000
10.000
1.000
0.100
0.010
0.001
[mg/l]
Mean
Median
Li+ [mg/l]
Na+ [mg/l]
NH4+ [mg/l]
K+ [mg/l]
Mg2+ [mg/l]
Ca2+ [mg/l]
Fe2+/3+ [mg/l]
Sr2+ [mg/l]
Mn2+ [mg/l]
n = 3 n = 3 n = 3 n = 3 n = 5 n = 5 n = 3 n = 3 n = 3

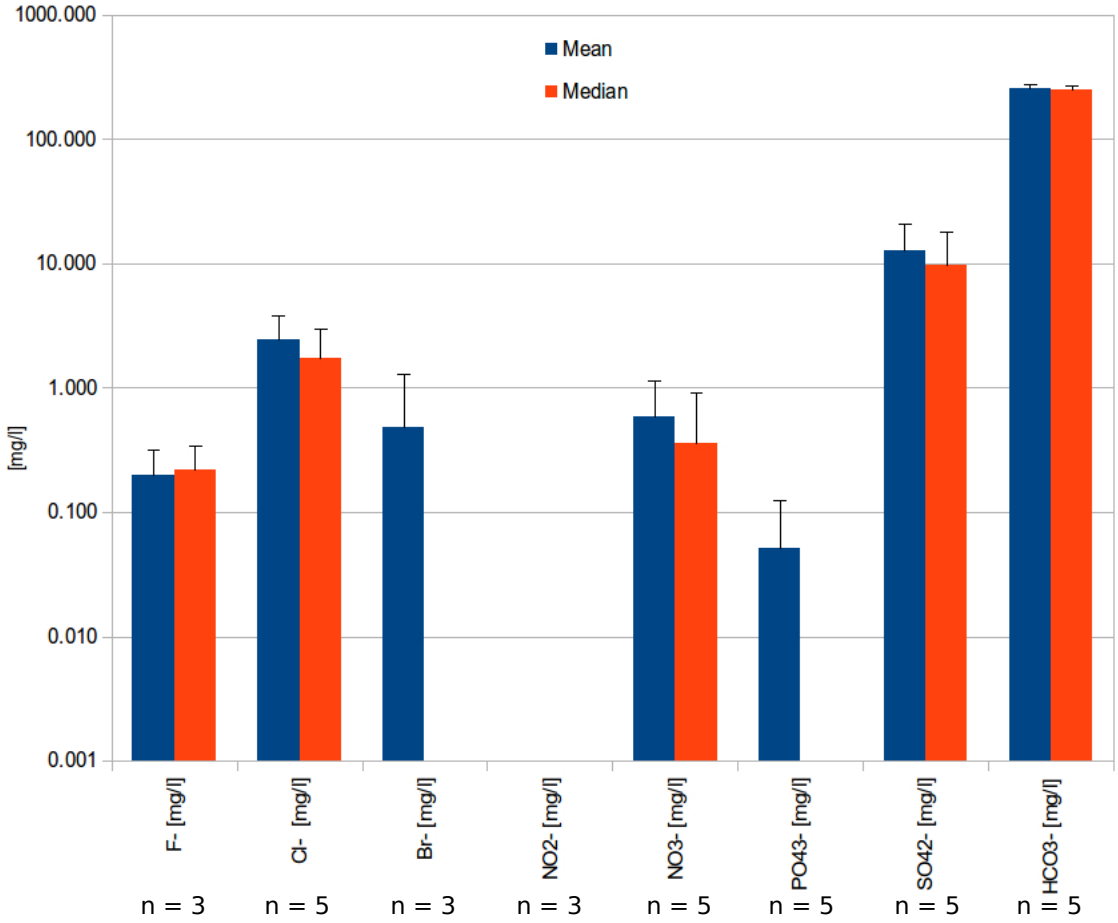
1000.000
100.000
10.000
1.000
0.100
0.010
0.001
[mg/l]
Mean
Median
F- [mg/l]
Cl- [mg/l]
Br- [mg/l]
NO2- [mg/l]
NO3- [mg/l]
PO43- [mg/l]
SO42- [mg/l]
HCO3- [mg/l]
n = 3 n = 5 n = 3 n = 3 n = 5 n = 5 n = 5 n = 5

23) SR (Zeplinica river)

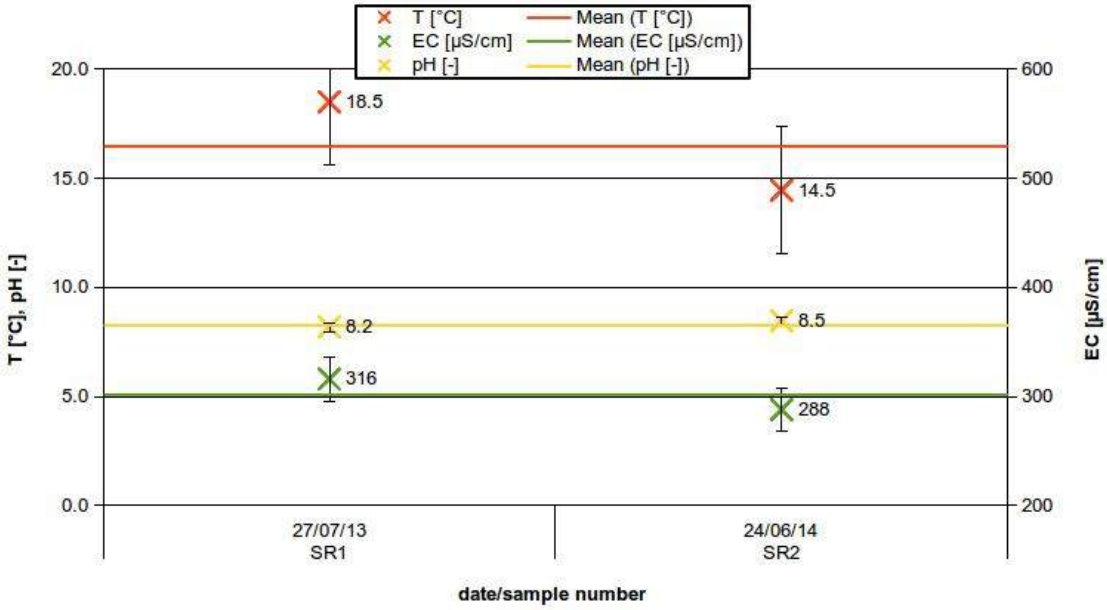

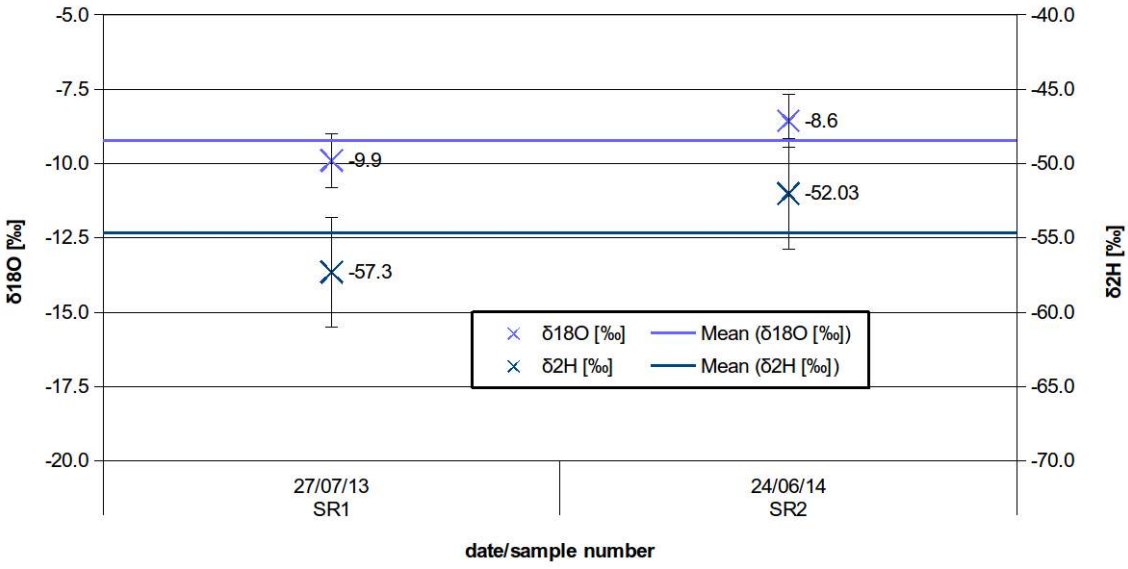

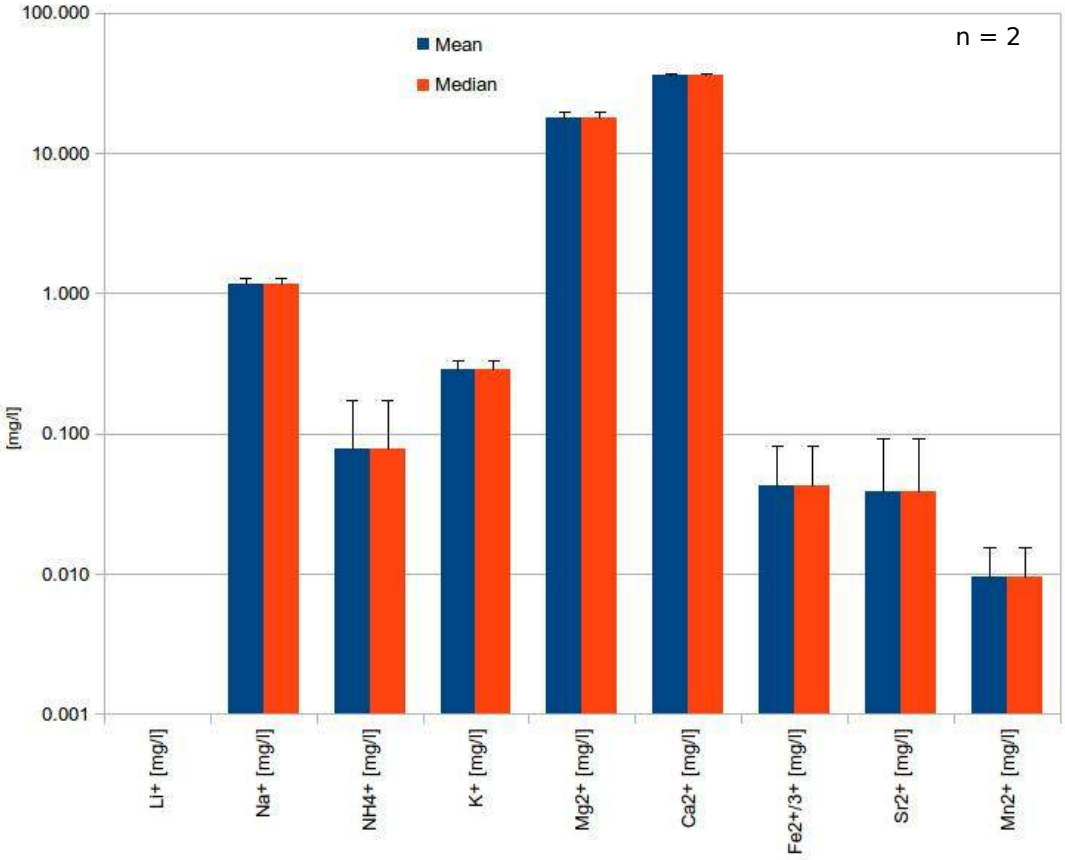
n = 2
Mean
Median
100.000
10.000
1.000
0.100
0.010
0.001
[mg/l]
Li+ [mg/l]
Na+ [mg/l]
NH4+ [mg/l]
K+ [mg/l]
Mg2+ [mg/l]
Ca2+ [mg/l]
Fe2+/3+ [mg/l]
Sr2+ [mg/l]
Mn2+ [mg/l]

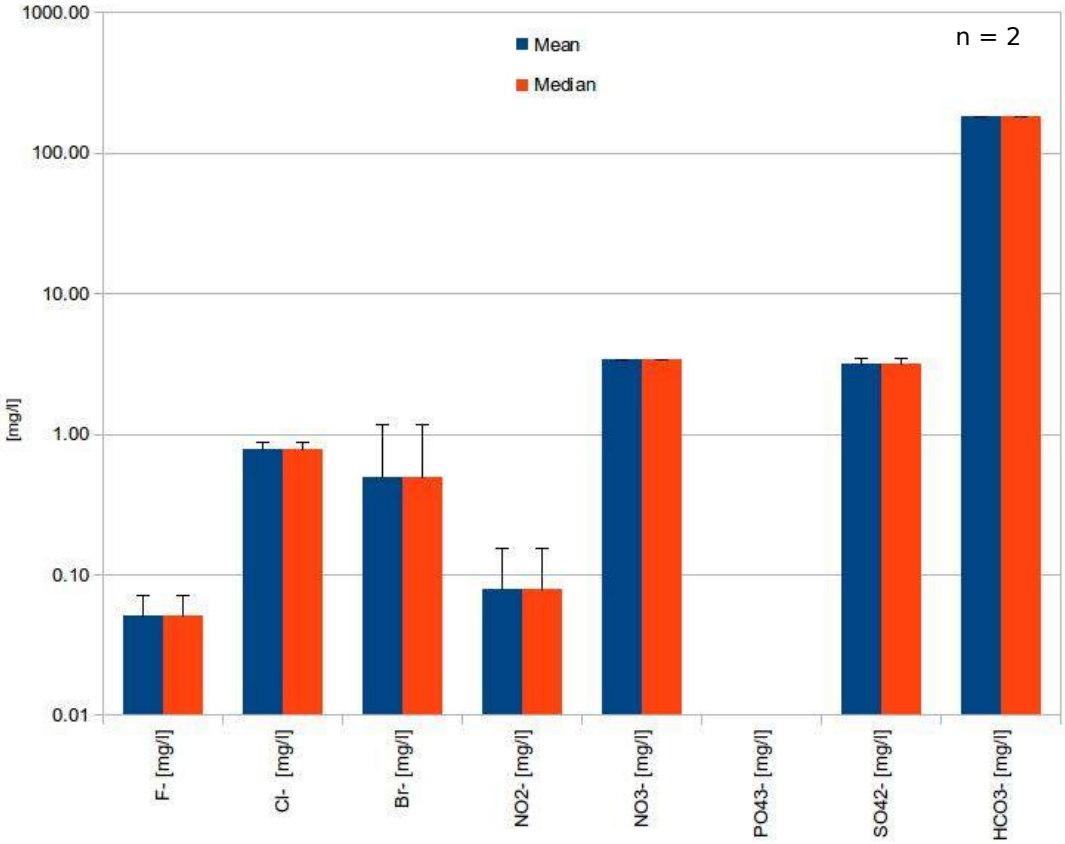
n = 2
Mean
Median
1000.00
100.00
10.00
1.00
0.10
0.01
[mg/l]
F- [mg/l]
Cl- [mg/l]
Br- [mg/l]
NO2- [mg/l]
NO3- [mg/l]
PO43- [mg/l]
SO42- [mg/l]
HCO3- [mg/l]

24) L (Lipnica)

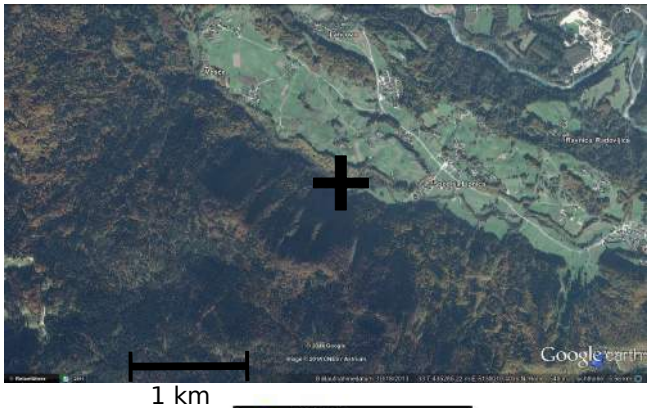

1 km

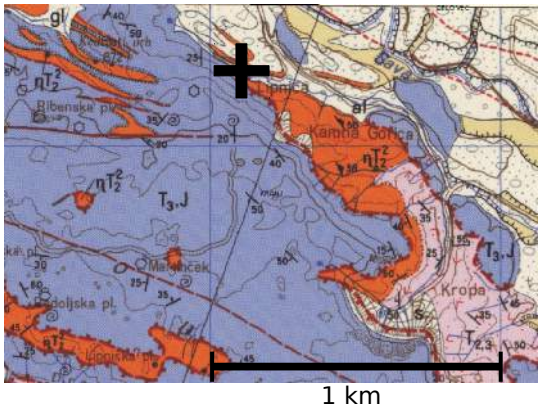

1 km

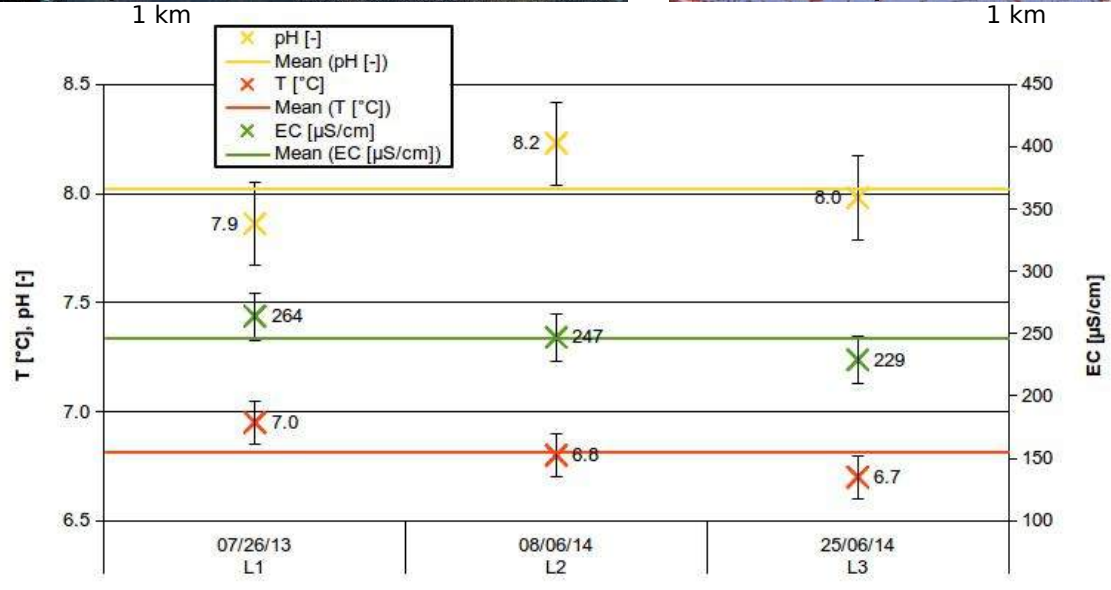

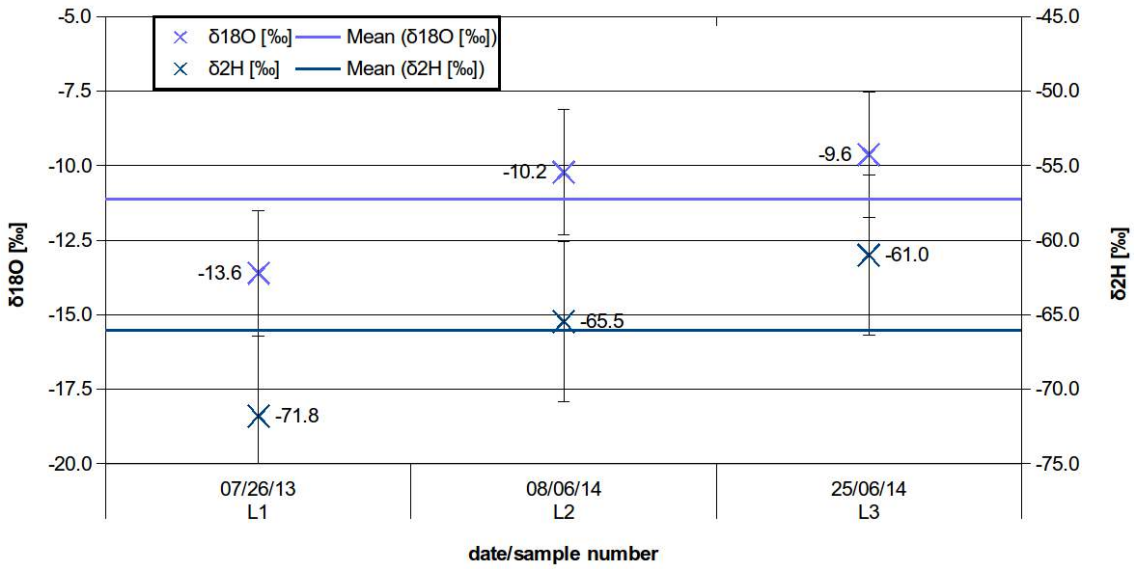

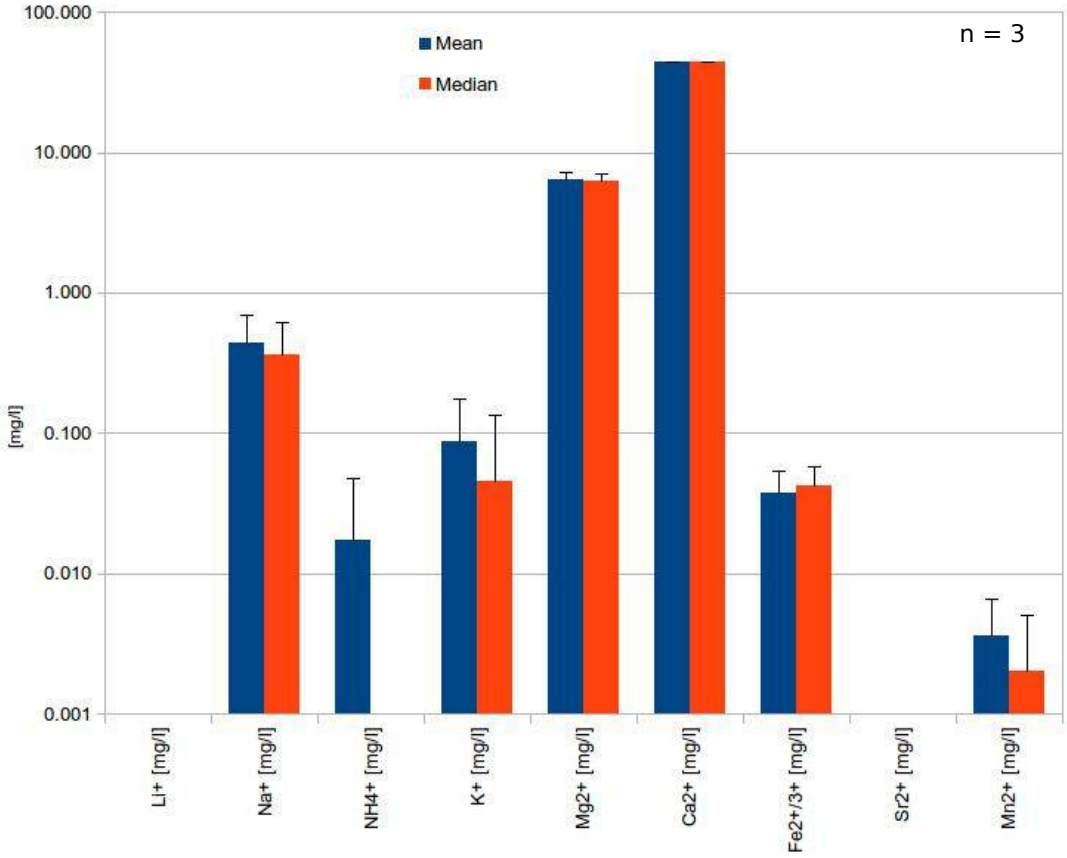
n = 3
Mean
Median
100.000
10.000
1.000
0.100
0.010
0.001
[mg/l]
Li+ [mg/l]
Na+ [mg/l]
NH4+ [mg/l]
K+ [mg/l]
Mg2+ [mg/l]
Ca2+ [mg/l]
Fe2+/3+ [mg/l]
Sr2+ [mg/l]
Mn2+ [mg/l]

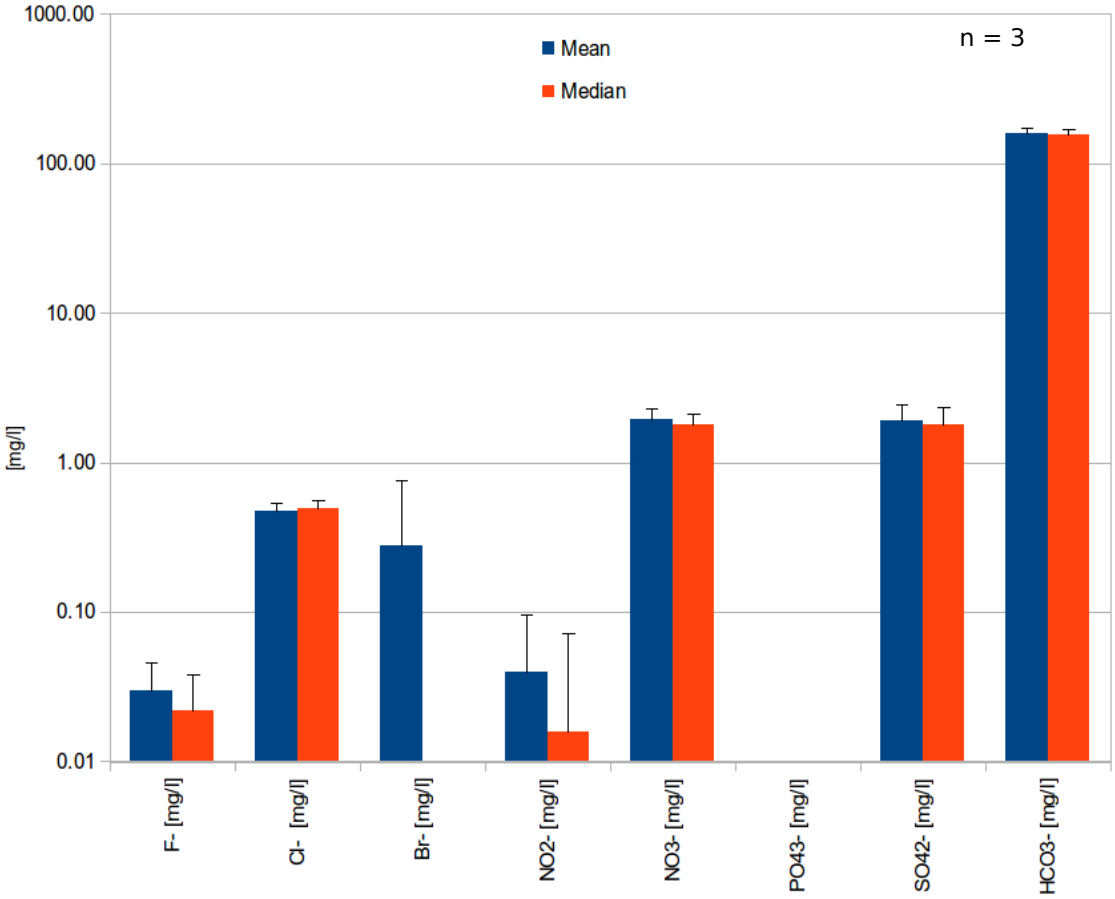
n = 3
Mean
Median
1000.00
100.00
10.00
1.00
0.10
0.01
[mg/l]
F- [mg/l]
Cl- [mg/l]
Br- [mg/l]
NO2- [mg/l]
NO3- [mg/l]
PO43- [mg/l]
SO42- [mg/l]
HCO3- [mg/l]

25) M (Mans power)

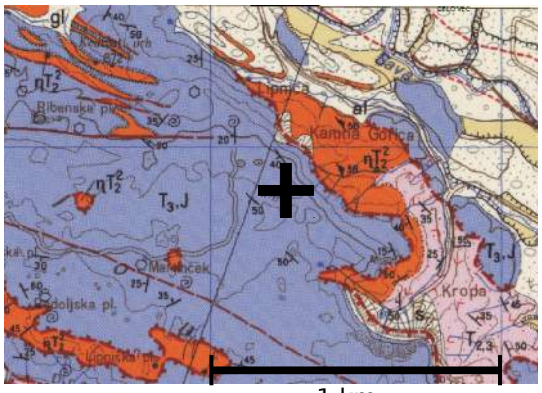

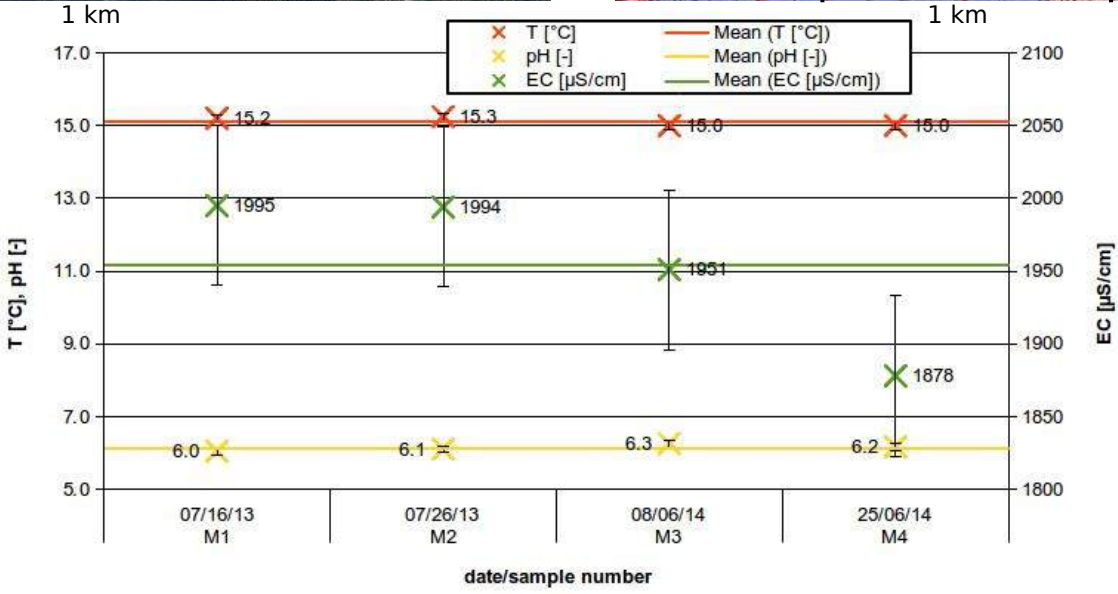

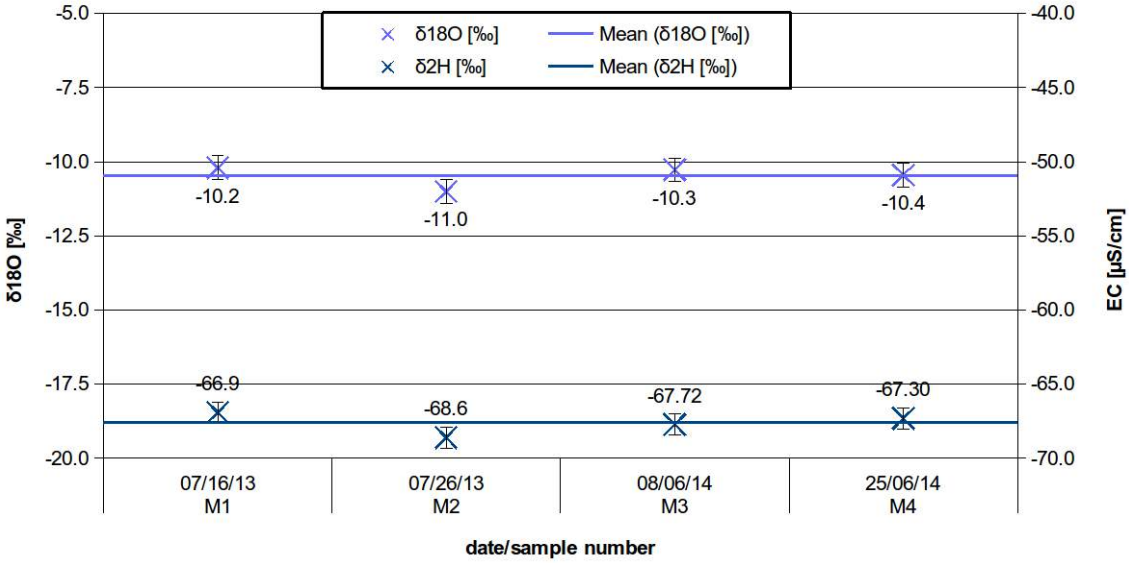

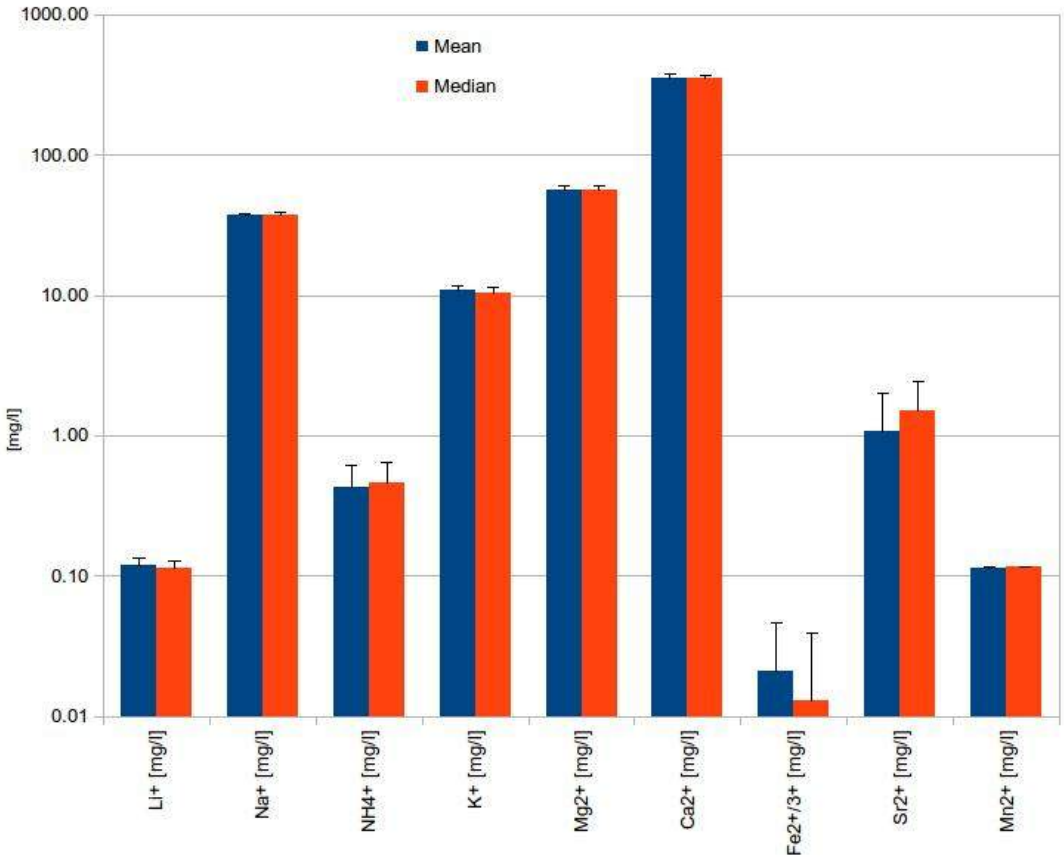

n = 3 n = 3 n = 3 n = 3 n = 4 n = 4 n = 3 n = 3 n = 3

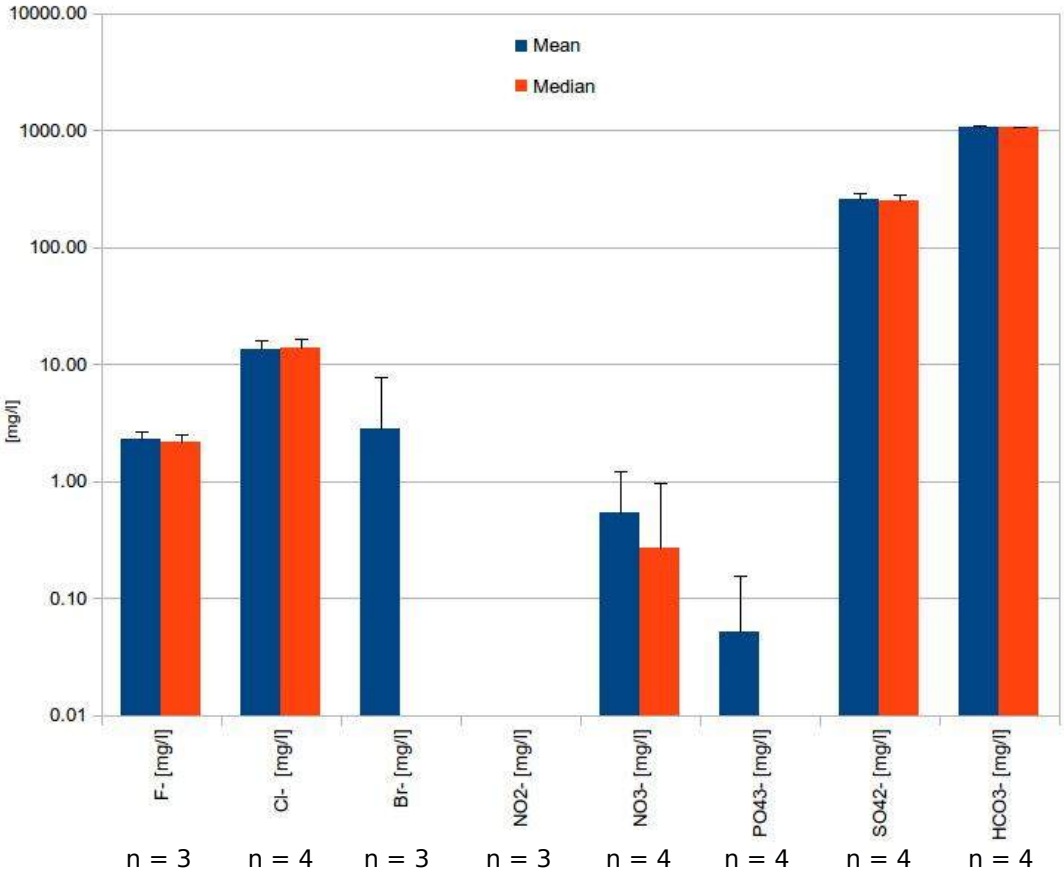

n = 3 n = 4 n = 3 n = 3 n = 4 n = 4 n = 4 n = 4

26) K (Izvir Kroparice) and KA (above Kroparice)

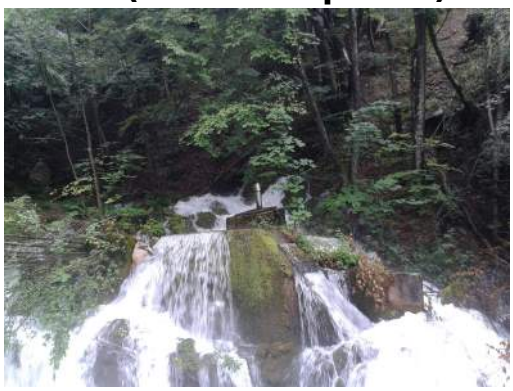

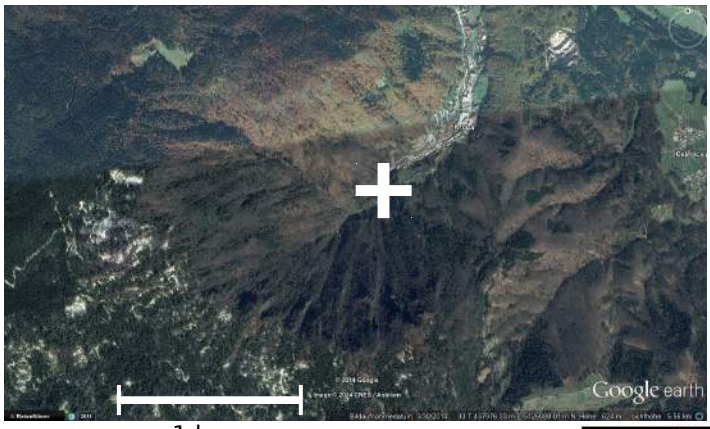

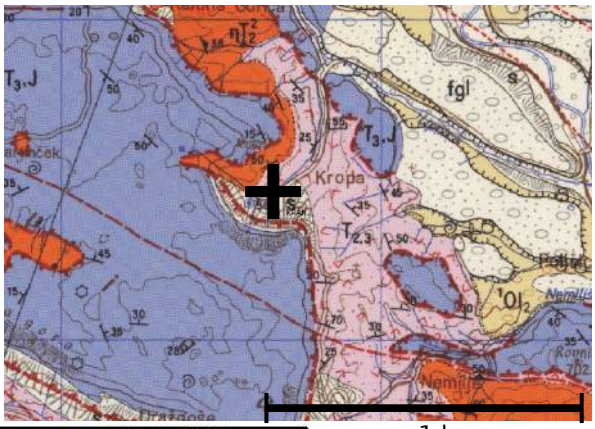

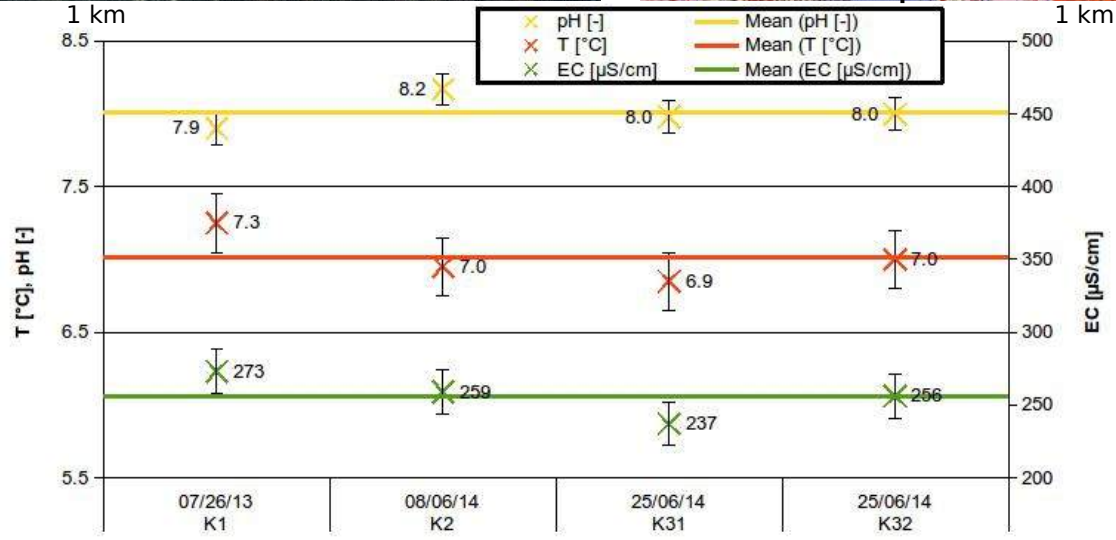

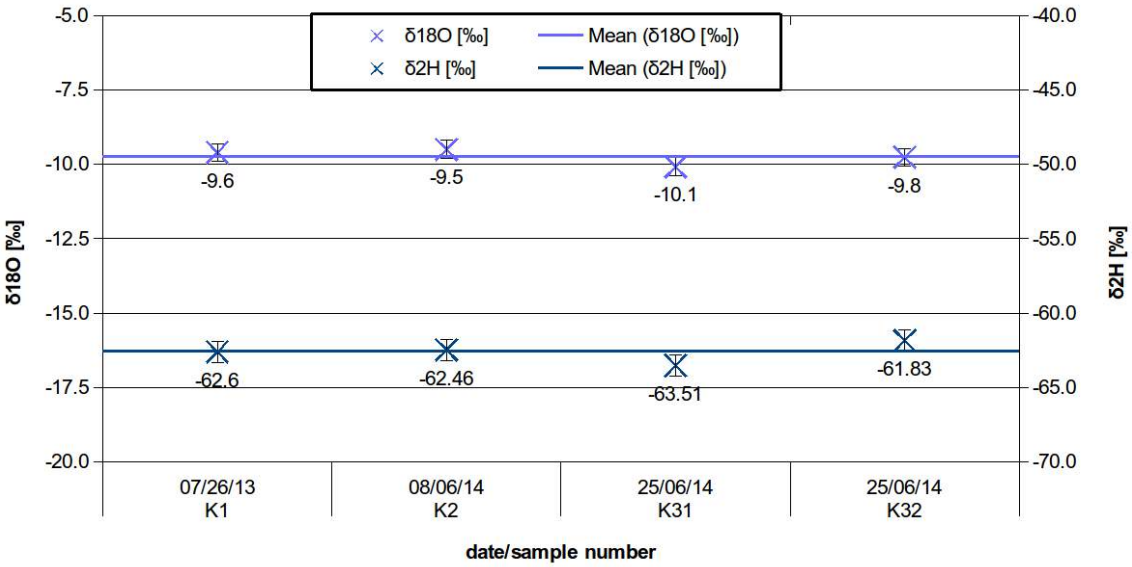

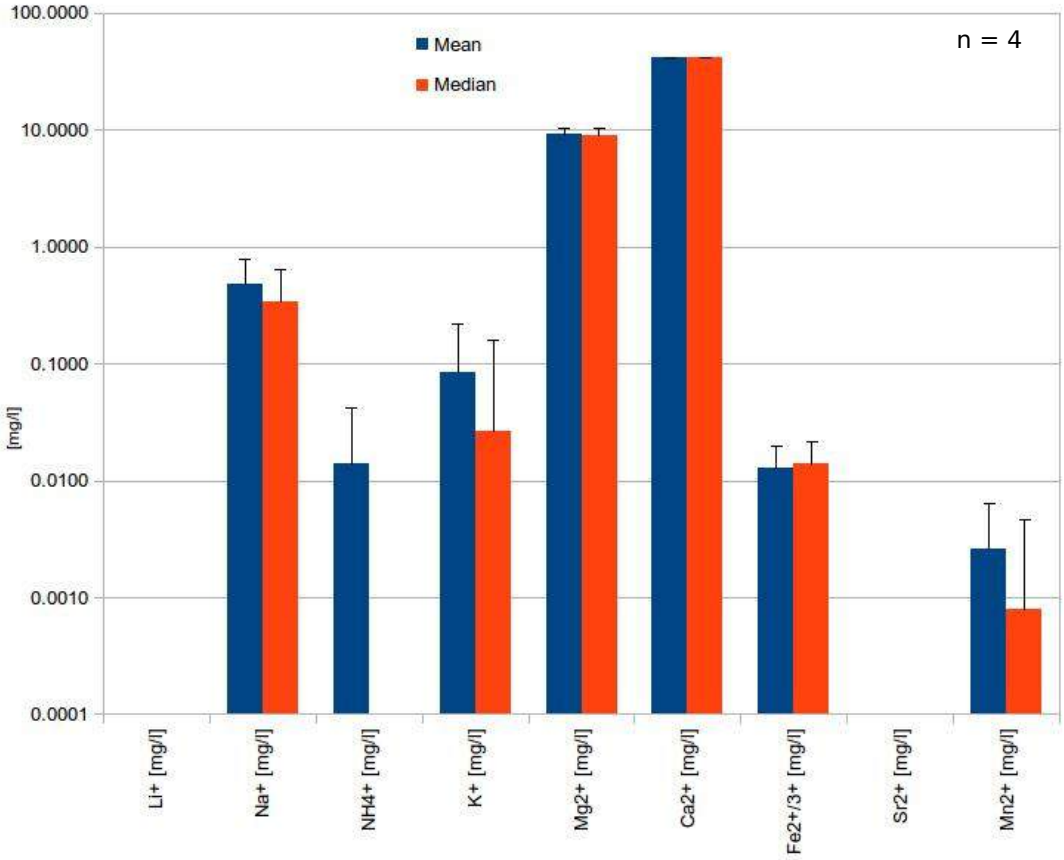
n = 4
Mean
Median
100.0000
10.0000
1.0000
0.1000
0.0100
0.0010
0.0001
[mg/l]
Li+ [mg/l]
Na+ [mg/l]
NH4+ [mg/l]
K+ [mg/l]
Mg2+ [mg/l]
Ca2+ [mg/l]
Fe2+/3+ [mg/l]
Sr2+ [mg/l]
Mn2+ [mg/l]

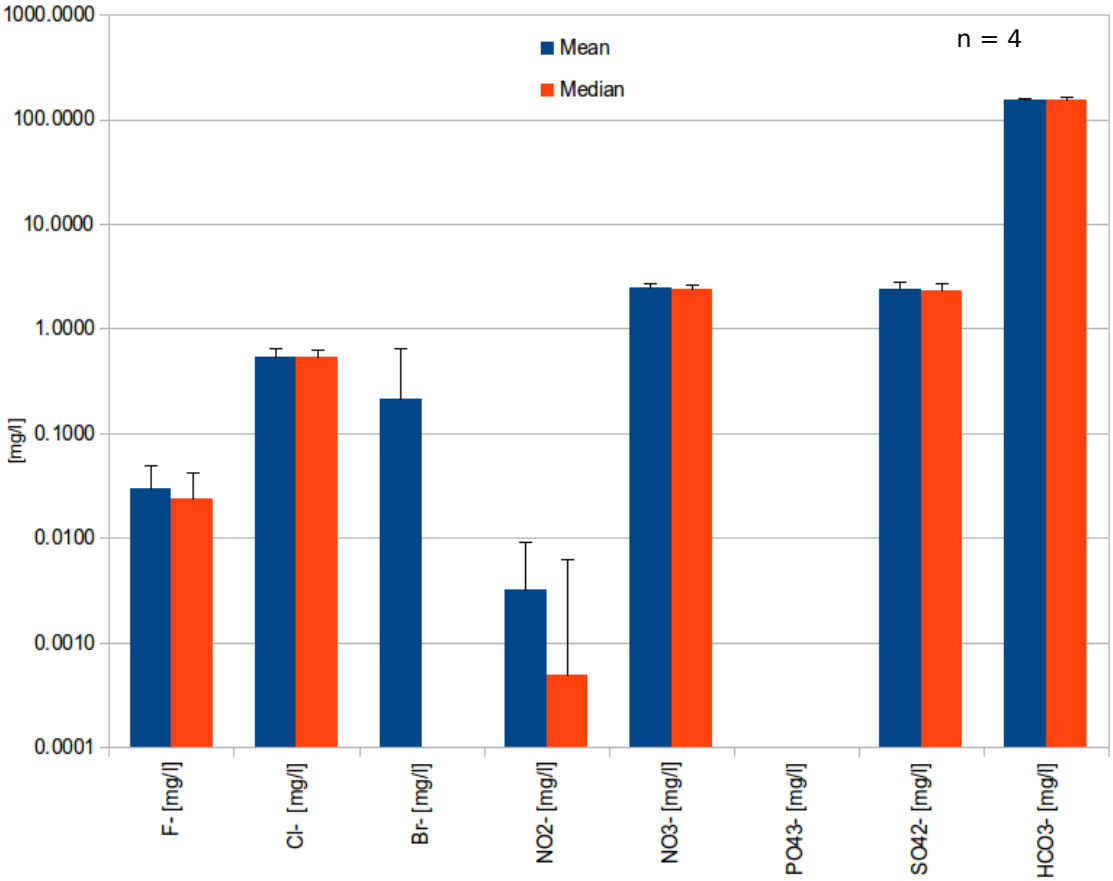
n = 4
Mean
Median
1000.0000
100.0000
10.0000
1.0000
0.1000
0.0100
0.0010
0.0001
[mg/l]
F- [mg/l]
Cl- [mg/l]
Br- [mg/l]
NO2- [mg/l]
NO3- [mg/l]
PO43- [mg/l]
SO42- [mg/l]
HCO3- [mg/l]

27) BAA (Zgornja Besnica A)

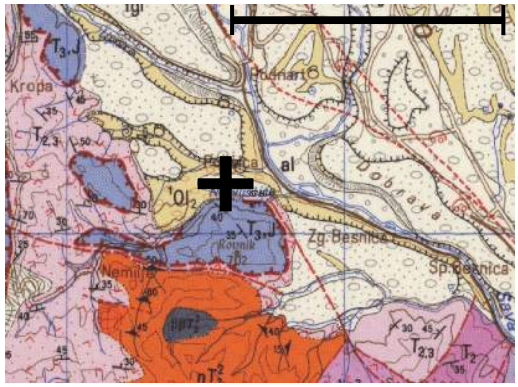

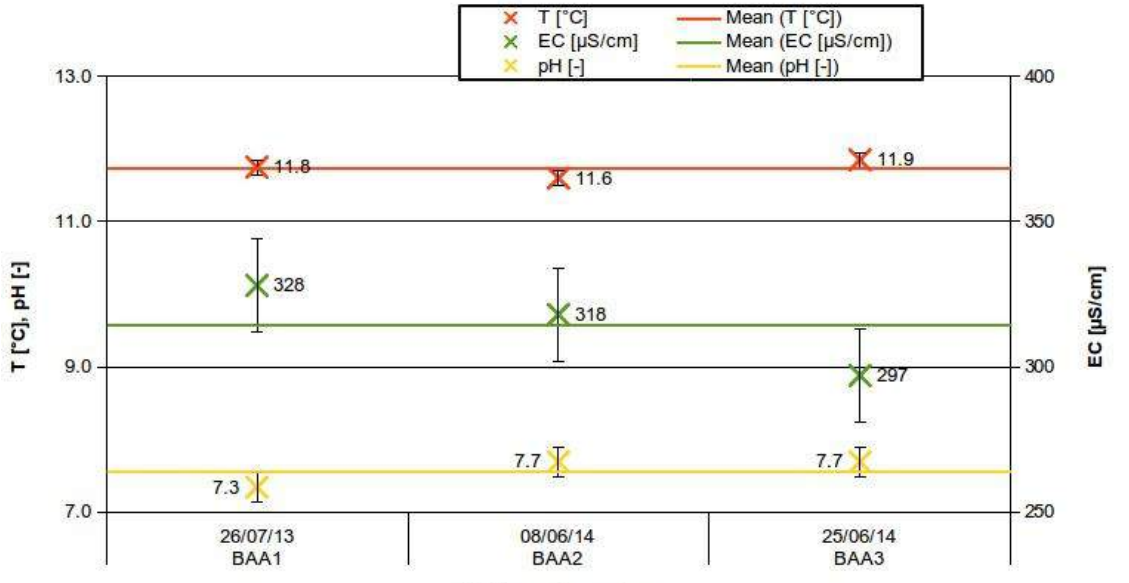

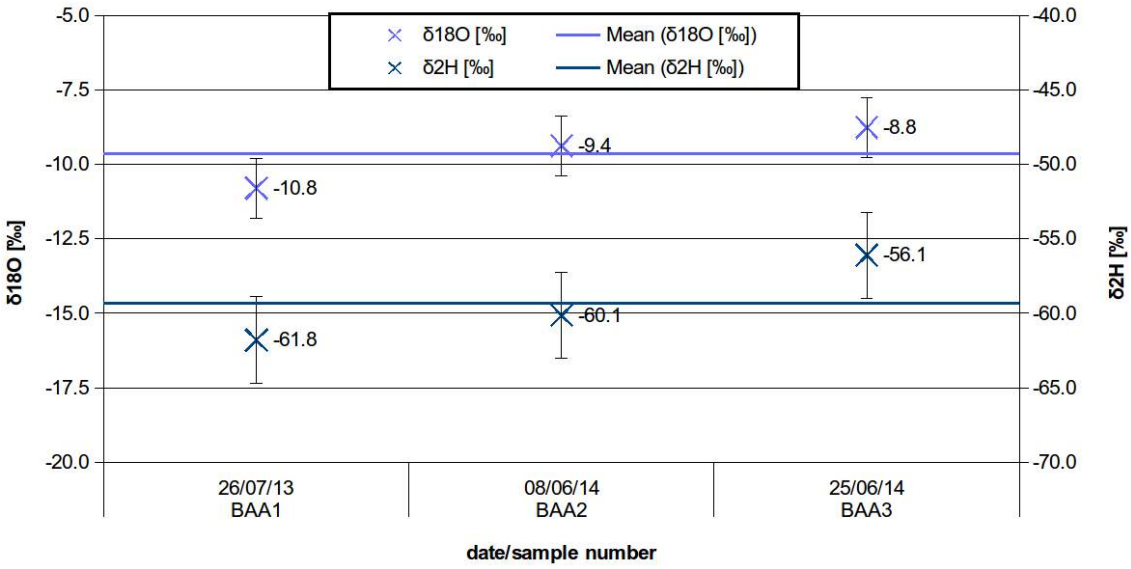

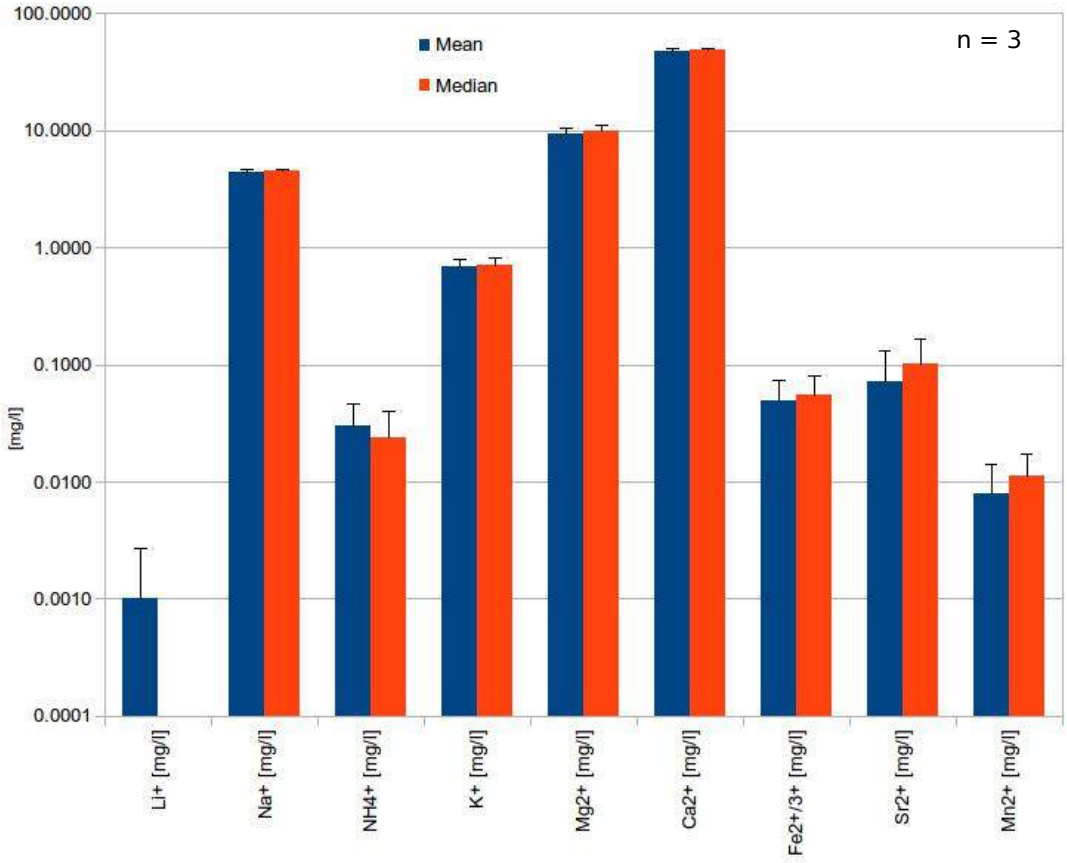
100.0000
10.0000
1.0000
0.1000
0.0100
0.0010
0.0001
[mg/l]
Mean
Median
n = 3
Li+ [mg/l]
Na+ [mg/l]
NH4+ [mg/l]
K+ [mg/l]
Mg2+ [mg/l]
Ca2+ [mg/l]
Fe2+/3+ [mg/l]
Sr2+ [mg/l]
Mn2+ [mg/l]

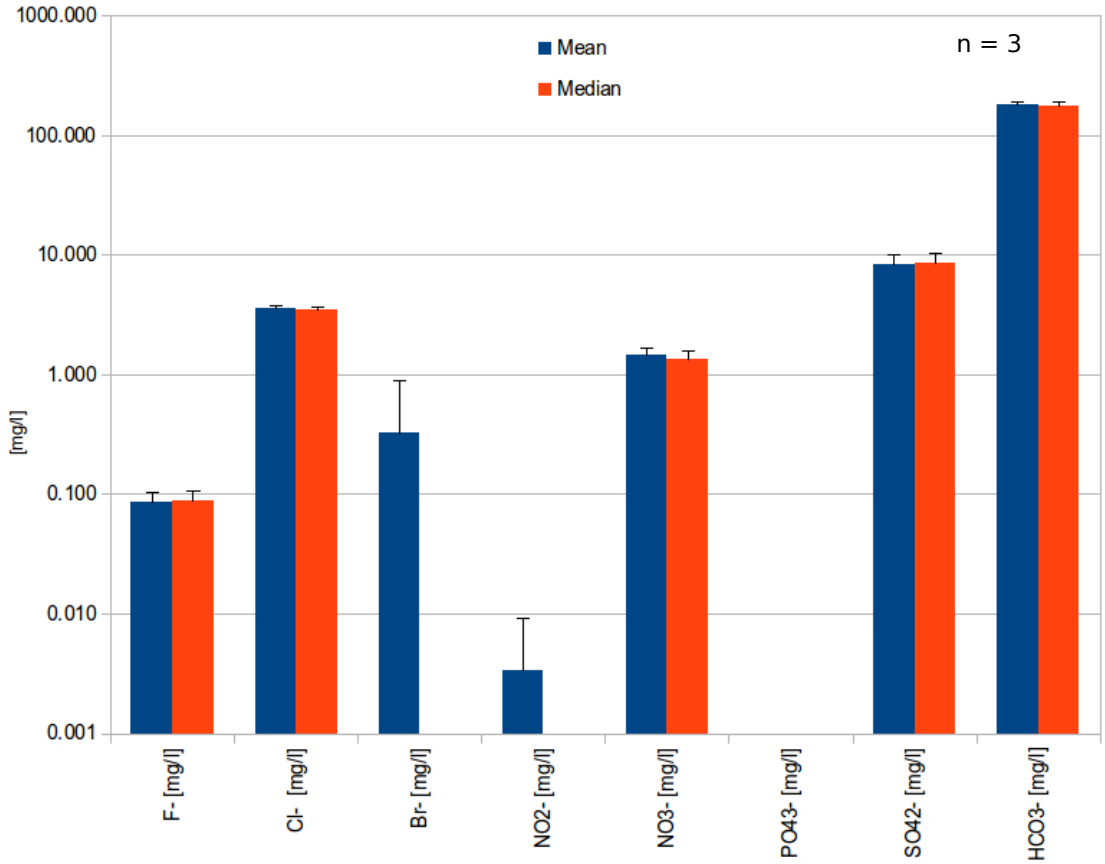
1000.000
100.000
10.000
1.000
0.100
0.010
0.001
[mg/l]
Mean
Median
n = 3
F- [mg/l]
Cl- [mg/l]
Br- [mg/l]
NO2- [mg/l]
NO3- [mg/l]
PO43- [mg/l]
SO42- [mg/l]
HCO3- [mg/l]

28) BA (Zgornja Besnica)

1 km

1 km

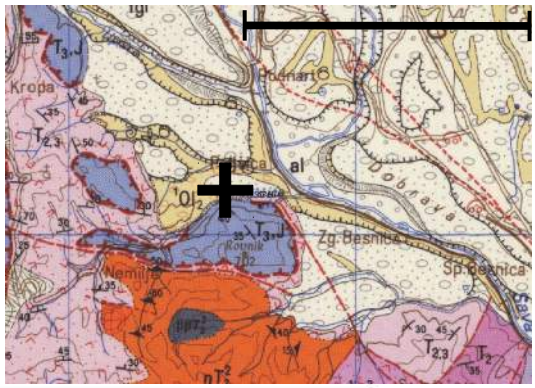

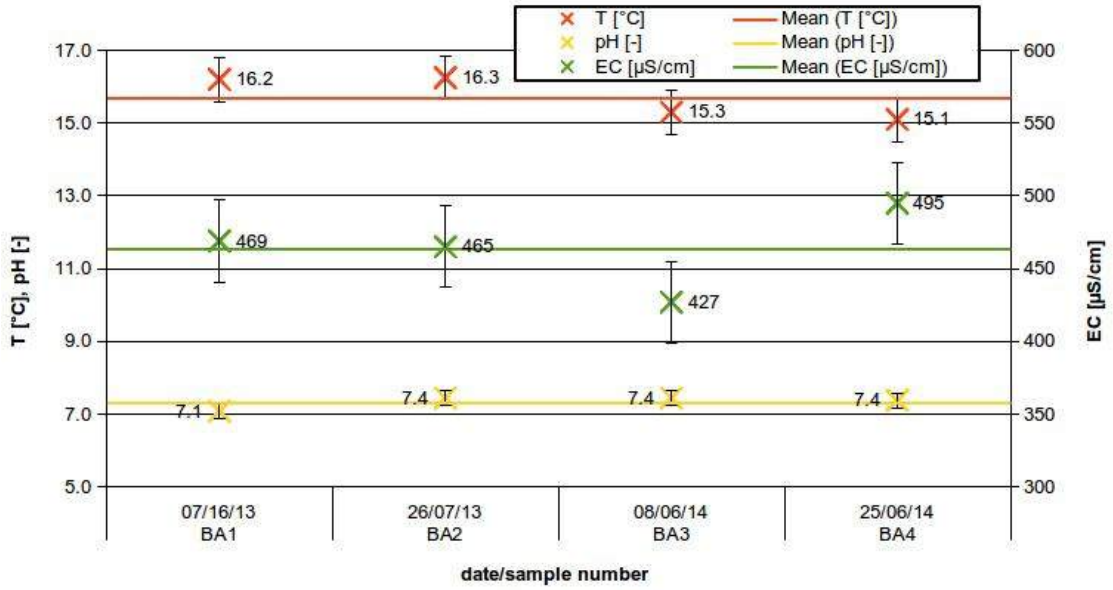

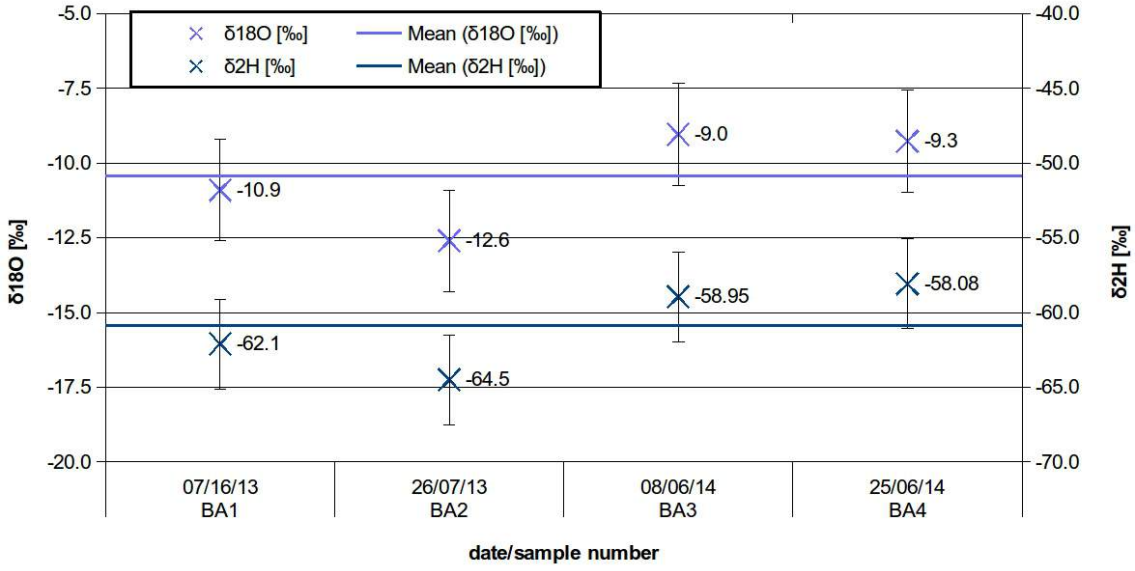

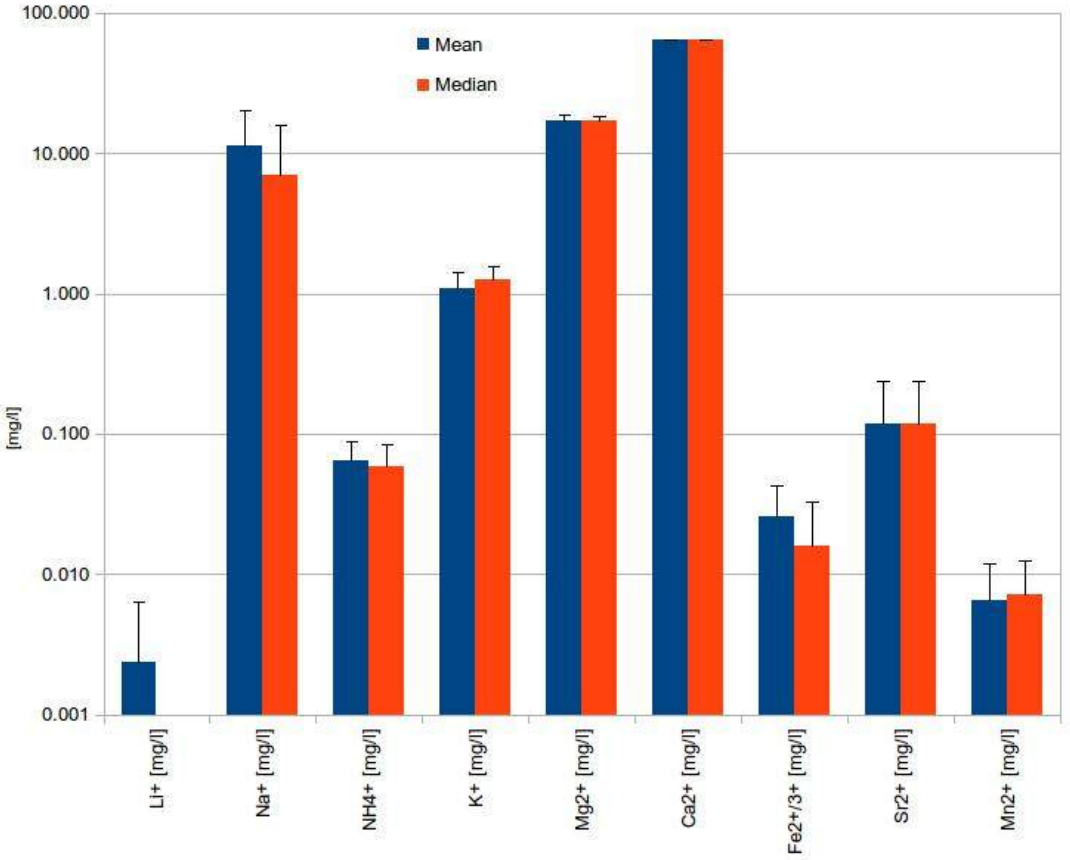

n = 3 n = 3 n = 3 n = 3 n = 4 n = 4 n = 3 n = 3 n = 3

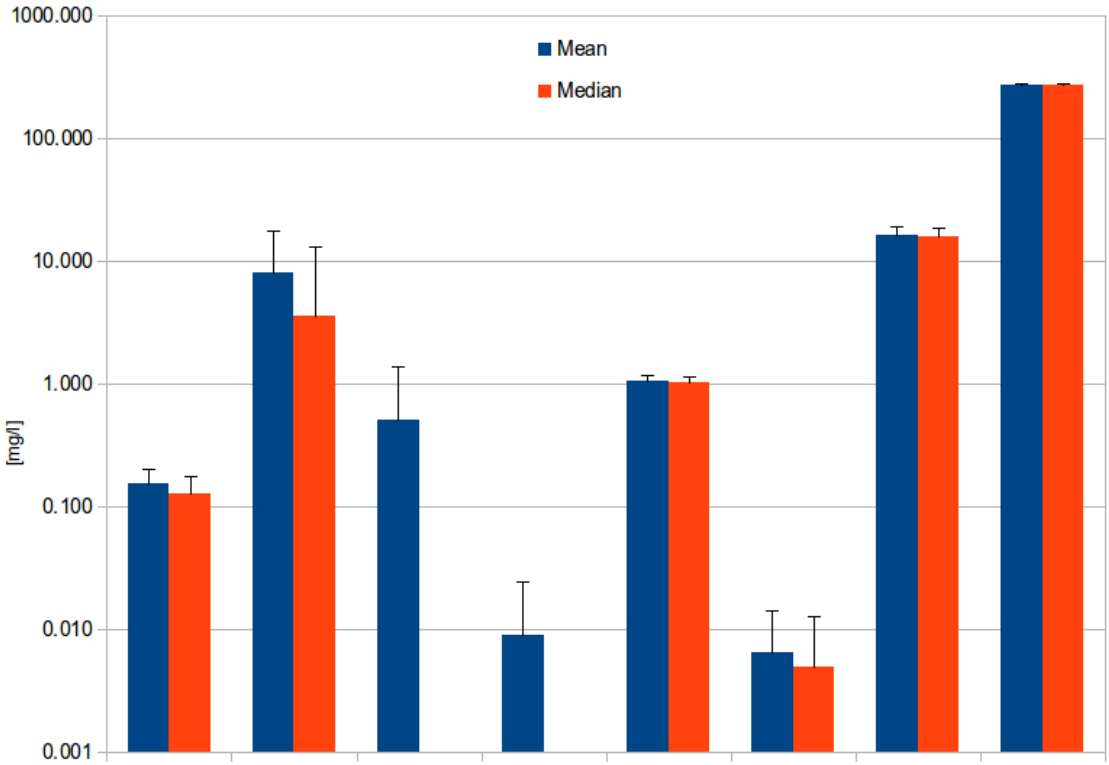

n = 3 n = 4 n = 3 n = 3 n = 4 n = 4 n = 4 n = 4

29) J (Divje Jezero)

1 km

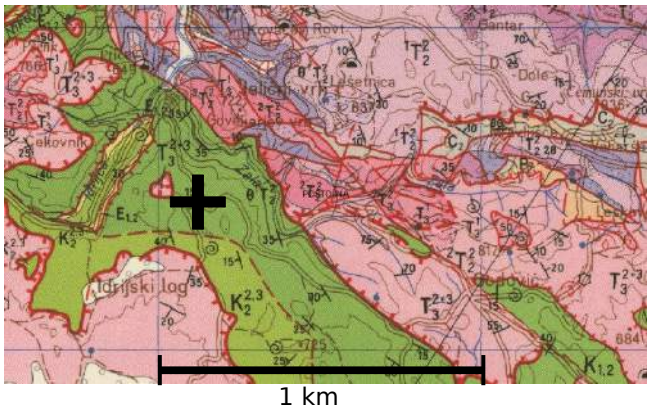

1 km

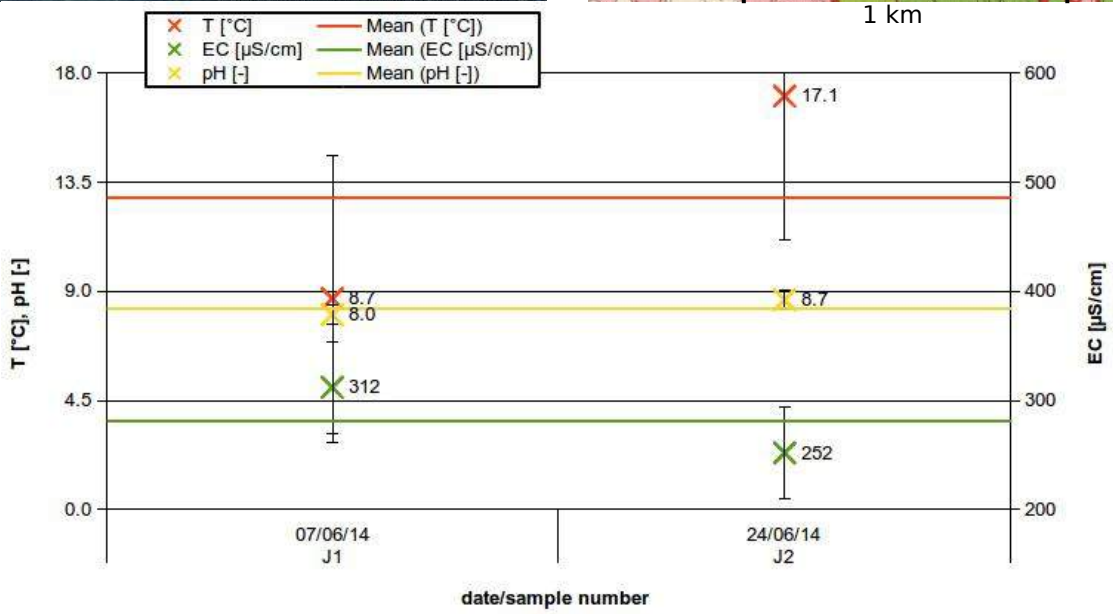

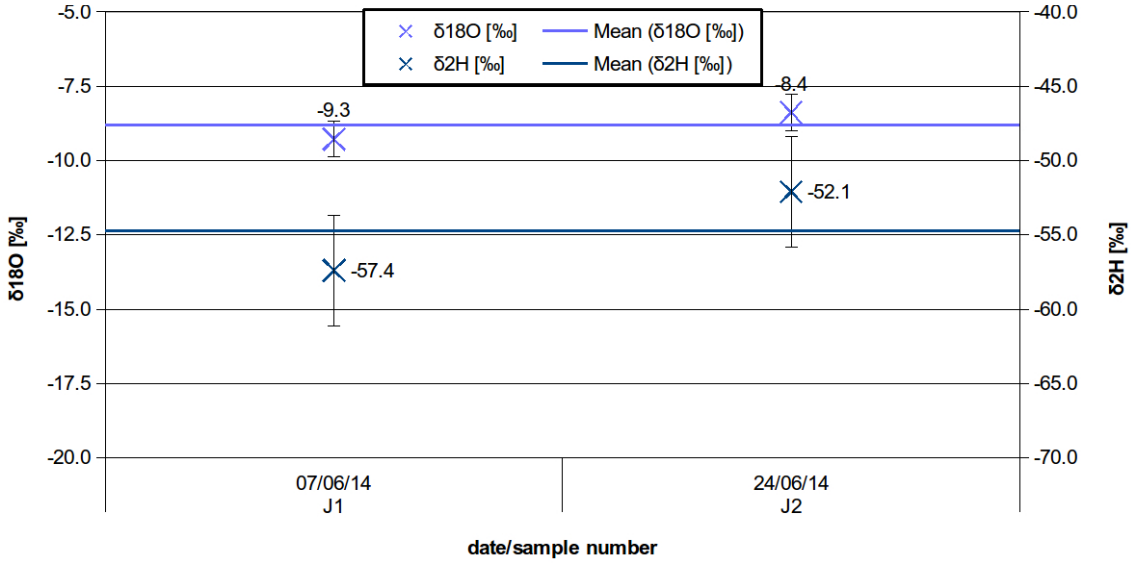

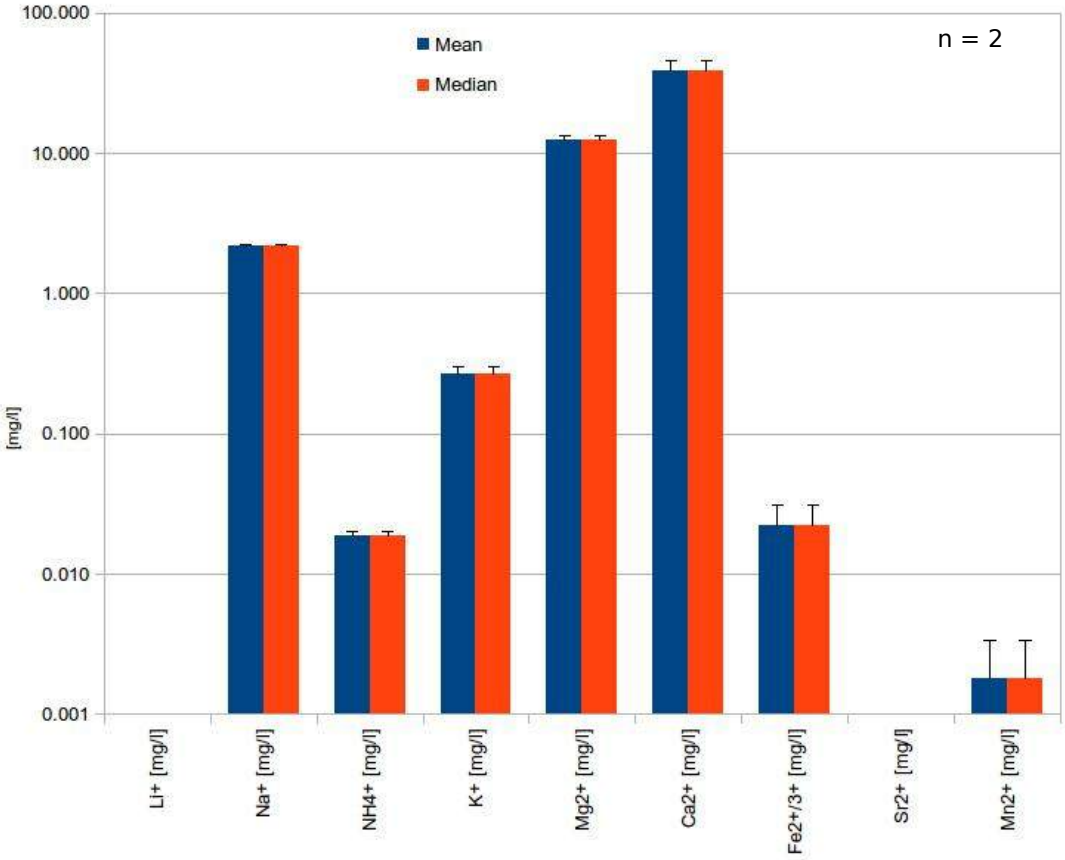
100.000
10.000
1.000
0.100
0.010
0.001
[mg/l]
Mean
Median
n = 2
Li+ [mg/l]
Na+ [mg/l]
NH4+ [mg/l]
K+ [mg/l]
Mg2+ [mg/l]
Ca2+ [mg/l]
Fe2+/3+ [mg/l]
Sr2+ [mg/l]
Mn2+ [mg/l]

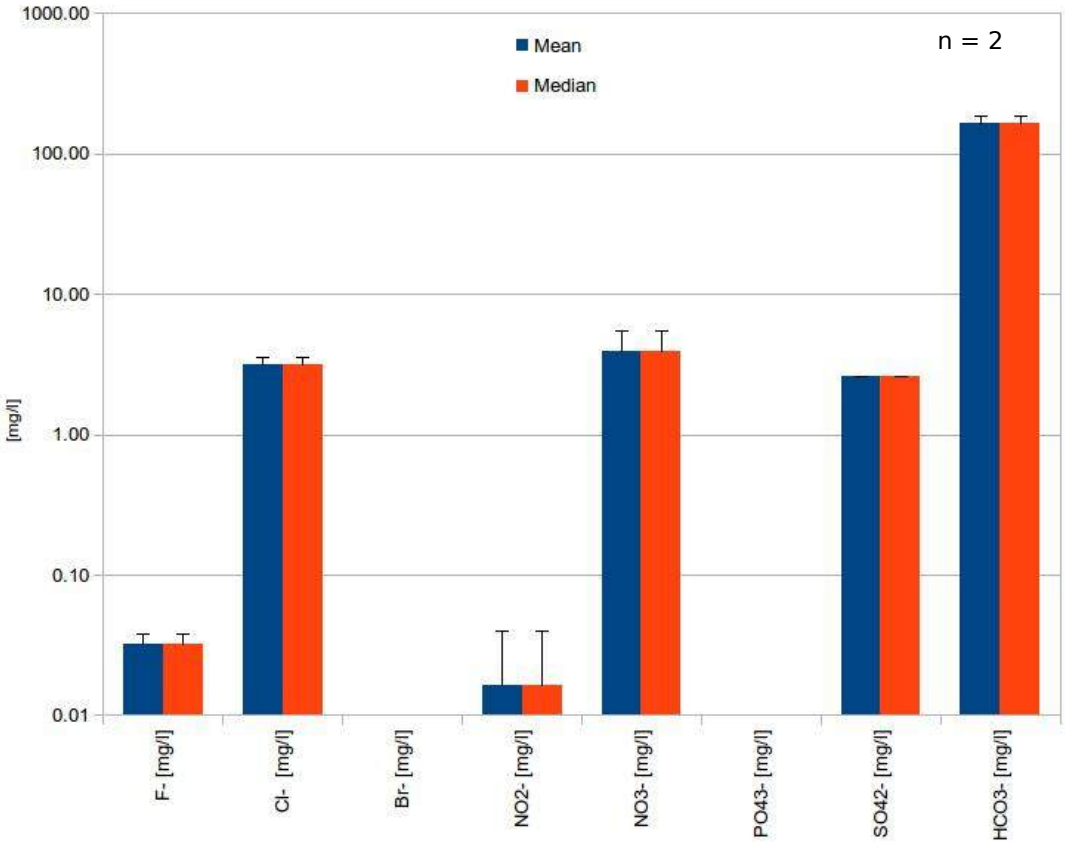
1000.00
100.00
10.00
1.00
0.10
0.01
[mg/l]
Mean
Median
n = 2
F- [mg/l]
Cl- [mg/l]
Br- [mg/l]
NO2- [mg/l]
NO3- [mg/l]
PO43- [mg/l]
SO42- [mg/l]
HCO3- [mg/l]